POLITECHNIKA ŚWIĘTOKRZYSKA

WYDZIAŁ INŻYNIERII ŚRODOWISKA, GEODEZJI I ENERGETYKI ODNAWIALNEJ

ROZPRAWA DOKTORSKA

Zintegrowany model obliczeniowy do oceny i poprawy działania sieci kanalizacji deszczowej w zlewniach miejskich, w kontekście planowania przestrzennego

Integrated computational model for assessing and improving the performance of the stormwater system in urban catchments, in the context of spatial planning

mgr inż. Anita Marlena Białek

Praca napisana pod kierunkiem:

prof. dr hab. inż. Bartosz Szeląg

Kielce 2025

„Nie ten jest mądry, kto wiele wie, lecz ten, kto zrozumiał istotę rzeczy.”
— platoński aforyzm

Ta rozprawa nie powstałaby bez obecności tych, którzy dzielili się wiedzą,

czasem i zrozumieniem.

Wszystkim, którzy byli obok – dziękuję.

Spis treści

Streszczenie

Postępująca urbanizacja oraz zmiany klimatyczne znacząco intensyfikują presję na systemy kanalizacji deszczowej, obniżając ich niezawodność oraz ograniczając możliwości skutecznego prognozowania. Wzrost udziału powierzchni nieprzepuszczalnych, w połączeniu z rosnącą częstotliwością występowania opadów ekstremalnych, prowadzi do przeciążeń sieci odwodnieniowej. W efekcie niezbędne staje się wdrażanie nowoczesnych narzędzi analitycznych wspierających procesy planowania i optymalizacji tego typu infrastruktury.

Celem niniejszej rozprawy było opracowanie zintegrowanego modelu obliczeniowego umożliwiającego ocenę i usprawnienie funkcjonowania sieci kanalizacji deszczowej w warunkach zlewni miejskich, z uwzględnieniem uwarunkowań planistycznych i przestrzennych. Zastosowano podejście holistyczne, łączące modelowanie hydrodynamiczne z technikami uczenia maszynowego.

W wyniku przeprowadzonych badań powstała autorska aplikacja obliczeniowa wspomagająca projektowanie elementów zielonej infrastruktury, takich jak ogrody deszczowe, rowy infiltracyjne oraz zbiorniki retencyjne z możliwością regulacji odpływu. Narzędzie zostało zaprojektowane z myślą o małych zlewniach miejskich, w których lokalne uwarunkowania topograficzne oraz sposób zagospodarowania terenu mają istotny wpływ na efektywność gospodarowania wodami opadowymi. Aplikacja umożliwia szybkie przeprowadzanie analiz z uwzględnieniem kluczowych danych fizyczno-geograficznych, tym samym wspierając procesy decyzyjne na etapie projektowania i modernizacji systemów odwodnieniowych.

Jako rozszerzenie podjętej tematyki badawczej opracowano uproszczone modele predykcyjne do identyfikacji wylania ścieków i prognozy przepływu maksymalnego w małej niehomogenicznej zlewni miejskiej wykorzystując techniki uczenia maszynowego. Opracowane narzędzia umożliwiają identyfikację działania sieci kanalizacyjnej w oparciu o dane opadowe, topologię sieci kanalizacyjnej, retencję terenową i kanałową, jako rozwiązania alternatywne do powszechnie stosowanych modeli mechanistycznych – SWMM (Storm Water Management Model).

Rozprawa wnosi istotny wkład w rozwój metod planowania i zarządzania systemami odwodnienia w środowisku zurbanizowanym. Zastosowane podejście stanowi podstawę do projektowania infrastruktury odpornej na skutki zmian klimatycznych oraz zgodnej z zasadami zrównoważonego rozwoju przestrzennego.

Abstract

Progressive urbanization and climate change are exerting increasing pressure on stormwater systems, reducing their reliability and limiting the capacity for effective performance forecasting. The growing extent of impervious surfaces, combined with the rising frequency of extreme rainfall events, often results in the overloading of drainage networks. Consequently, there is a pressing need to implement advanced analytical tools that can support the planning, design, and optimization of such infrastructure.

The objective of this dissertation was to develop an integrated computational model for evaluating and enhancing the performance of stormwater systems in urban catchments, with explicit consideration of spatial planning conditions. A holistic approach was adopted, integrating hydrodynamic modelling with machine learning techniques.

The research resulted in the development of an original computational application designed to support the planning and design of green infrastructure elements, including rain gardens, infiltration trenches, and retention tanks with controlled outflow. The tool is particularly suited to small urban catchments, where local topographic characteristics and land-use patterns exert a significant influence on stormwater management efficiency. By incorporating key physical and geographical data, the application enables rapid analysis and facilitates informed decision-making in the design and modernization of stormwater systems.

As an extension of this research, simplified predictive models were developed to identify sewer overflows and forecast peak flows in small, heterogeneous urban catchments using machine learning methods. These models allow the assessment of stormwater system performance based on rainfall data, sewer network topology, and both surface and channel retention, providing an alternative to commonly used mechanistic approaches such as the Storm Water Management Model (SWMM).

This dissertation makes a substantive contribution to the advancement of planning and management methodologies for stormwater systems in urbanized environments. The proposed approach lays the groundwork for designing infrastructure that is both resilient to the impacts of climate change and aligned with the principles of sustainable spatial development.

Wykaz publikacji wchodzących w skład rozprawy doktorskiej

Nr	Autorzy i tytuł publikacji	Impact Factor *	Punktacja MNiSW**
A1	**Białek, A.**, Musz-Pomorska, A. (2025). Development of a computational tool for stormwater management in small urban catchments. Journal of Ecological Engineering, 26(6), 410-423. *https://doi.org/10.12911/22998993/202322*	1,5	70
A2	**Białek, A.**, Łagód, G. (2025). The impact of physical-geographical conditions on the sizing of rain gardens: A spatial case of Poland. Journal of Ecological Engineering, 26(10), 460-476. *https://doi.org/10.*12911*/22998993/207167*	1,5	70
A3	Szeląg, B., Fatone, F., Kiczko, A., Majerek, D., **Białek, A**., Łagód, G., Piotrowicz, A., and Dąbek, L. (2024). Extended Evaluation of the Impact of Rainfall, Sewer Network and Land Use Retention on Drainage System Performance in a Multi-Criteria Approach – Modeling, Sensitivity Analysis. Advances in Science and Technology Research Journal, 18(6), pp.291-303. https://doi.org/10.12913/22998624/192023	1,3	100
A4	Szeląg, B., Kowal, P., Kiczko, A., **Białek, A.**, Wałek, G., Majerek, D., Siwicki, P., Fatone, F., & Boczkaj, G. (2023). Integrated model for the fast assessment of flood volume: Modelling – management, uncertainty and sensitivity analysis. Journal of Hydrology, 625, 129967. *https://doi.org/10.1016/j.jhydrol.2023.129967*	5,9	140
A5	Barbusiński, K., Szeląg, B., **Białek, A**., Kalenik, M., & Bakalár, T. (2025). An innovative method of predicting the maximum flow in stormwater sewage systems using soft-sensors. Archives of Environmental Protection, 51(3), 54–73. *https://doi.org/10.24425/aep.2025.156009*	1,4	100
	Suma	**11,6**	**480**

* Impact Factor (IF) wg bazy Journal Citation Reports (JCR) w roku wydania

** Liczba punktów wg listy MNiSW zgodna z rokiem ukazania się prac

Wykaz skrótów i symboli stosowanych w autoreferacie

Skrót / Symbol	Opis / Nazwa pełna	Jednostka
SWMM	Storm Water Management Model - Model hydrodynamiczny kanalizacji deszczowej	–
MIKE URBAN	Modelling Integrated Urban Drainage and Water Distribution System - Modelowanie zintegrowanego systemu odwodnienia miejskiego i dystrybucji wody	–
MIKE FLOOD	Integrated Flood Modeling System – Zintegrowany system modelowania powodzi	
InfoWorks ICM	Integrated Catchment Modeling – Zintegrowane modelowanie zlewni	
HEC-RAS	Hydrologic Engineering Center – River Analysis System - System Analizy Rzecznej Centrum Inżynierii Hydrologicznej	–
GIS	Geographic Information Systems – Systemy informacji geograficznej	–
AI	Artificial Intelligence – Sztuczna Inteligencja	–
ML	Machine Learning – Uczenie Maszynowe	–
LID	Low Impact Development – Niskoemisyjny rozwój urbanistyczny lub Rozwój o niskim wpływie na środowisko	–
GSA	Global Sensitivity Analysis -Globalna Analiza Wrażliwości	
LSTM	Long Short-Term Memory – Sieć Neuronowa Pamięci Długiej	–
MLP	Multi-Layer Perceptron – Wielowarstwowy perceptron	
SVM	Support Vector Machines – Maszyny wektorów nośnych	
CNN	Convolutional Neural Network – Splotowa Sieć Neuronowa	–
XGBoost	Extreme Gradient Boosting – Metoda Wzmacniania Gradientowego	–
PSO	Particle Swarm Optimization – Optymalizacja Rojem Cząstek	–
RF	Random Forest - Metoda Lasów Losowych	–
RNN	Recurrent Neural Networks – Rekurencyjne sieci neuronowe	
MARS	Multivariate Adaptive Regression Splines – Adaptacyjne Regresje Splajnów	–
GI	Green Infrastructure – Zielona Infrastruktura	–
PN-EN 752	Norma: Systemy kanalizacyjne	–
PN-EN 16933	Norma: Systemy kanalizacyjne	–
RLM	Równoważna Liczba Mieszkańców	–
IMGW	Instytut Meteorologii i Gospodarki Wodnej	
NSE	Nash–Sutcliffe Efficiency – Wskaźnik Dopasowania Modeli Hydrologicznych	–
NBS	Nature-Based Solutions - Rozwiązania oparte na przyrodzie	–
R^2	Coefficient of Determination – Współczynnik Determinacji	–
MAE	Mean Absolute Error – Średni Błąd Bezwzględny	–
RMSE	Root Mean Square Error – Pierwiastek Średniego Błędu Kwadratowego	–
i, i_0	Natężenie opadu	mm/hr
t_d	Czas trwania opadu	min
a_0, a_1, a_2	Współczynniki empiryczne	–
S_f, S_0	Spadek hydrauliczny	–
R_h /R	Promień hydrauliczny	m
f_d	Współczynnik oporu tarcia	–
V	Średnia prędkość przepływu	m/s
C	Współczynnik oporu przepływu laminarnego	–
A	Pole powierzchni przekroju poprzecznego	m^2
Re	Liczba Reynoldsa	–

υ	Współczynnik lepkości kinematycznej	m^2/s
n	Współczynnik szorstkości wg Manninga	$m^{-1/3} \cdot s$
p_s	Wskaźnik wrażliwości	–
λ_1	Jednostkowa objętość wylania	$m^3 \cdot ha^{-1}$
λ_2	Stopień wylania	–
κ	Wskaźnik objętości odpływu jednostkowego z danego epizodu opadowego	$m^3 \cdot ha^{-1}$
F	Powierzchnia zlewni	ha
F_{imp}	Udział powierzchni przepuszczalnych	–
Imp	Udział powierzchni nieprzepuszczalnych	–
α	Współczynnik regresji	–
γ	Współczynnik korekcyjny	–
β	Współczynnik nachylenia	–
D_{imp}	Głębokość retencji dla powierzchni nieprzepuszczalnych	mm
D_{per}	Głębokość retencji dla powierzchni przepuszczalnych	mm
n_{sew}	Współczynnik szorstkości Manninga dla kanałów	$s \cdot m^{-1/3}$
n_{imp}	Współczynnik szorstkości Manninga dla powierzchni nieprzepuszczalnych	$s \cdot m^{-1/3}$
d_{imp}	Głębokość retencji powierzchniowej na terenach nieprzepuszczalnych	mm
d_{ret}	Głębokość retencji początkowej	mm
S	Spadek terenu / dna kanału	–
q_L	Ilość wody na jednostkę szerokości	mm/hr*m
y_L	Głębokość przepływu	m
g	Przyspieszenie ziemskie	m/s^2
t, t_r, t_d, t_e, t_p	Czas: ogólny / trwania opadu / czas trwania deszczu / czas szczytowego natężenia / czas do osiągnięcia maksymalnego przepływu	s, min
q	Jednostkowe natężenie przepływu	$m^3/s \cdot m$
Q_{dmax}	Maksymalny dopływ do rowu rozsączającego	m^3/s
λ	Współczynnik oporów liniowych	–
Q	Natężenie przepływu	m^3/s
Q_m	Przepływ maksymalny	m^3/s
Vk	Objętość kanałów/kolektora	m^3
Vkp	Objętość przewodu przed zamknięciem zlewni	m^3
Vrd/Vkd	Współczynnik retencji (udział retencji do objętości sieci)	–
FD	Wymiar fraktalny sieci kanalizacyjnej	–
Gk	Długość kolektora na jednostkę powierzchni nieprzepuszczalnej	$m \cdot ha^{-1}$
Jkp	Współczynnik retencji	–
Gkd	Spadek dna kanału	$m \cdot ha^{-1}$
$Vrd \cdot Vkd^{-1}$	Objętość sieci kanalizacyjnej w dolnym biegu na objętość sieci całkowitą	–
R.t.	Różnica rzędnych przewodu kanalizacyjnego	m
f_c	Współczynnik frakcji opóźnienia odpływu	mm/h
ε	Efektywna porowatość złoża	–
μ	Współczynnik przepływu przelewu	–
B, L, h, H	Szerokość, długość, głębokość, wysokość zwierciadła wody	m
C_w, C_d	Współczynnik wypływu (dla przelewu swobodnego i przez otwór)	–
A_{pipe}	Pole przekroju przewodu	m^2
Θ_{agg}	Porowatość złoża	–
CL	Współczynnik oporów miejscowych	–

1. WPROWADZENIE

Współczesne miasta coraz częściej zmagają się z narastającymi zagrożeniami hydrologicznymi, wynikającymi z jednoczesnego oddziaływania dwóch kluczowych czynników: zmian klimatycznych oraz intensywnej urbanizacji (Ruan i in., 2024; Long & Duan, 2025). Z jednej strony obserwuje się wzrost częstotliwości i intensywności opadów ekstremalnych, z drugiej – systematyczne zwiększanie udziału powierzchni nieprzepuszczalnych, związane z rozwojem infrastruktury miejskiej. Synergia tych zjawisk ogranicza możliwości infiltracji i retencji wód opadowych, zwiększając objętość spływu powierzchniowego i prowadząc do przeciążenia systemów kanalizacji deszczowej (Miller i in., 2017).

W konsekwencji rośnie ryzyko występowania powodzi miejskich i lokalnych podtopień, niosących ze sobą straty ekonomiczne, zagrożenia dla zdrowia publicznego oraz zakłócenia w funkcjonowaniu infrastruktury krytycznej (European Commission, 2015; Cea i Costable, 2022). Zmiany w pokryciu terenu, szczególnie związane z procesami urbanizacyjnymi, mogą odpowiadać za znaczną część wzrostu spływu powierzchniowego – w niektórych przypadkach ich wpływ przewyższa znaczenie czynników klimatycznych. Dodatkowo, nasilone zrzuty burzowe oraz związany z nimi transport zanieczyszczeń przyczyniają się do pogorszenia jakości wód powierzchniowych (Fletcher i in., 2015; Kumar i in., 2024).

W odpowiedzi na rosnące wyzwania hydrologiczne projektowanie systemów kanalizacji deszczowej skupia się na efektywnym odprowadzaniu wód opadowych oraz minimalizacji ryzyka przeciążeń hydraulicznych, szczególnie podczas intensywnych opadów. Kluczowym elementem tego procesu jest analiza hydrologiczno-hydrauliczna zlewni, uwzględniająca takie parametry jak: powierzchnia czynna, stopień uszczelnienia, współczynnik spływu, intensywność opadu miarodajnego oraz czas koncentracji. W Polsce projektowanie odbywa się zgodnie z normami PN-EN 752 i PN-EN 16933, z wykorzystaniem danych opadowych Instytutu Meteorologii i Gospodarki Wodnej (IMGW).

Weryfikacja działania systemów kanalizacji deszczowej prowadzona jest z zastosowaniem dynamicznych modeli numerycznych, takich jak: SWMM (Storm Water Management Model), MIKE URBAN (Modeling Integrated Urban Water Systems), MIKE FLOOD (Integrated 1D and 2D Flood Modeling System), InfoWorks ICM (Integrated Catchment Modeling) oraz HEC-HMS (Hydrologic Engineering Center – Hydrologic

Modeling System). Narzędzia te umożliwiają symulację przepływów, procesów retencji i infiltracji, a także ocenę ryzyka wystąpienia lokalnych podtopień (Guo i in., 2021; Zhang i in., 2022). Mimo to modele te są złożone i wymagają wielu szczegółowych danych, których pozyskanie jest kosztowne, czasochłonne i nie zawsze możliwe z odpowiednią dokładnością. Prowadzi to do spadku wiarygodności prognoz oraz trudności w podejmowaniu decyzji w warunkach niepewności. Dlatego istnieje potrzeba tworzenia inżynierskich aplikacji obliczeniowych wspierających prognozowanie zjawisk odpływu oraz projektowanie obiektów opartych na rozwiązaniach opartych na przyrodzie (Nature-Based Solutions).

Aby zminimalizować negatywny wpływ intensyfikującej się urbanizacji oraz zmieniających się warunków klimatycznych, współczesne systemy kanalizacji deszczowej coraz częściej integrują tradycyjne rozwiązania inżynieryjne – takie jak osadniki, separatory czy piaskowniki – z elementami zielonej infrastruktury (Green Infrastructure, GI), obejmującymi m.in. ogrody deszczowe, rowy infiltracyjne oraz zbiorniki retencyjno-infiltracyjne. Zintegrowane podejście projektowe, zgodne z wytycznymi CIRIA (2015) i US EPA (2021), łączy konwencjonalne systemy kanalizacyjne z rozproszonymi formami retencji, co przyczynia się do zwiększenia odporności infrastruktury, poprawy bilansu wodnego zlewni oraz podniesienia jakości odpływów (Chan i in., 2018; Jiang i in., 2018; Boogaard i in., 2024).

Coraz większe znaczenie zyskują zintegrowane podejścia obliczeniowe, które łączą klasyczne modele hydrodynamiczne, takie jak SWMM (Storm Water Management Model), z narzędziami sztucznej inteligencji AI (Artificial Intelligence), metodami statystycznymi oraz systemami informacji geograficznej GIS (Geographic Information Systems) (Jato-Espino i in., 2018; Li i Willems, 2020; Perdikaki i in., 2022; Addison-Atkinson i in., 2022; Amiri i in., 2022; Rodríguez i in., 2024). Szczególne znaczenie zyskują modele hybrydowe, integrujące deterministyczne podejścia hydrologiczne z algorytmami uczenia maszynowego (Machine Learning, ML), takimi jak sieci neuronowe, drzewa regresyjne oraz ich zaawansowane modyfikacje, w tym LSTM (Long Short-Term Memory), CNN (Convolutional Neural Networks) i XGBoost (Extreme Gradient Boosting). Przykładowo, model LSTM – SWMM osiągnął bardzo wysoką dokładność predykcji przepływów (R^2 = 0,969; NSE = 0,967) (Yang i Chui, 2020), a system CNN – LSTM, wdrożony w mieście Zhoukou, pozwala na błyskawiczne prognozowanie głębokości zalewania przy średnim błędzie poniżej 6,5% (Chen i in., 2023).

Tego rodzaju podejścia zwiększają skuteczność prognoz oraz wspierają adaptacyjne planowanie przestrzenne w kontekście zrównoważonego zarządzania wodami opadowymi. Pomimo dynamicznego rozwoju technologii, wiele proponowanych rozwiązań nadal pozostaje dostosowanych do pojedynczych zlewni, co ogranicza ich uniwersalność i wymaga czasochłonnej kalibracji. Opracowanie skalowalnych, uniwersalnych narzędzi, możliwych do łatwego wdrożenia w różnych warunkach hydrologicznych i urbanistycznych, stanowi istotne wyzwanie. Integracja modelowania hydrodynamicznego z technikami uczenia maszynowego w ramach spójnego środowiska obliczeniowego otwiera nowe perspektywy dla projektowania odpornych systemów kanalizacji deszczowej, zgodnych z zasadami zrównoważonego rozwoju i adaptacji do zmian klimatu.

2. CEL I ZAKRES ROZPRAWY

Głównym celem niniejszej rozprawy było opracowanie uniwersalnego, skalowalnego narzędzia obliczeniowego umożliwiającego kompleksową ocenę oraz optymalizację funkcjonowania systemów kanalizacji deszczowej w małoskalowych zlewniach miejskich, z uwzględnieniem zmiennych warunków klimatycznych, urbanistycznych i przestrzennych, w kontekście zrównoważonego planowania przestrzennego.

Zakres badań obejmował analizę mechanizmów prowadzących do przeciążeń hydraulicznych w systemach kanalizacyjnych, w tym procesów spływu powierzchniowego, retencji powierzchniowej i kanałowej, a także ich wzajemnych interakcji, które w warunkach intensywnych opadów mogą skutkować kumulacją zjawisk krytycznych. W tym kontekście przeprowadzono ocenę skuteczności rozwiązań opartych na przyrodzie (NBS), mających na celu zwiększenie retencji i infiltracji (Pons i in., 2023). Implementacja takich rozwiązań przyczynia się do ograniczenia obciążenia sieci kanalizacji deszczowej w czasie opadów nawalnych.

Zaproponowane w pracy podejście obejmuje dwa niezależne modele:

(i) model mechanistyczny, wykorzystany do prognozowania przepływów oraz oceny efektywności zastosowania elementów zielonej infrastruktury w zlewniach miejskich. Został zaimplementowany w formie aplikacji obliczeniowej, umożliwiającej zarówno prognozowanie przepływów, jak i ocenę skutków wdrażania rozproszonych form retencji w warunkach małych zlewni miejskich;

(ii) model oparty na technikach uczenia maszynowego, zastosowany do analizy zależności opad – odpływ oraz predykcji zachowania systemów kanalizacji

deszczowej na podstawie danych opadowych i fizyczno-geograficznych cech zlewni. W ramach tego modelu przeanalizowano wpływ wysokości retencji terenowej i kanałowej, współczynnika szorstkości Manninga, udziału powierzchni nieprzepuszczalnych oraz parametrów kanałów deszczowych. Analiza została przeprowadzona z pominięciem danych wysokościowych dotyczących sieci kanalizacyjnej oraz przestrzennego zróżnicowania zagospodarowania terenu.

Realizacja głównego celu rozprawy została osiągnięta poprzez opracowanie:

(1) aplikacji obliczeniowej stanowiącej narzędzie inżynierskie wspomagające projektowanie systemów retencyjnych z wykorzystaniem elementów zielonej infrastruktury (GI);

(2) zintegrowanego modelu obejmującego ocenę zastosowania modeli uczenia maszynowego do identyfikacji działania sieci kanalizacyjnej w warunkach przeciążenia hydraulicznego (wylania) oraz prognozy przepływu maksymalnego w kontekście analizy przepustowości istniejących i projektowanych kanałów deszczowych, z możliwością adaptacji do zmian klimatycznych.

W ramach realizacji celu (1) wykonano następujące zadania:

- Opracowano aplikację obliczeniową Calculator_NBS, wspierającą projektowanie i analizę rozwiązań opartych na zielonej infrastrukturze, takich jak ogrody deszczowe i rowy rozsączające. Narzędzie zostało dostosowane do specyfiki małych zlewni miejskich oraz zmieniających się warunków opadowych, w tym okresów bezdeszczowych. Umożliwia ocenę działania istniejących systemów odwodnienia oraz wspomaga proces ich projektowania i modernizacji. Aplikację wykorzystano także do analizy regionalnych uwarunkowań retencyjnych na obszarze Polski.
- Podjęto próby sformułowania wytycznych projektowych do wymiarowania ogrodów deszczowych, uwzględniających dobór lokalizacji, określenie wymaganej objętości złoża oraz zaprojektowanie systemu regulacji odpływu z warstwy infiltracyjnej.
- Przeprowadzono regionalizację warunków hydrologicznych w Polsce na podstawie danych opadowych oraz objętości złoża infiltracyjnego rowów rozsączających, wykorzystując nienadzorowaną analizę skupień (k - means clustering) wykorzystując wyniki obliczeń uzyskane dla 21 miast na terenie Polski za pomocą aplikacji Calculator_NBS. Analiza umożliwiła pogrupowanie obszarów w klastry o zbliżonych parametrach opadowych i retencyjnych, co pozwoliło na

wyodrębnienie jednorodnych regionów pod względem statystycznych właściwości opadu (średnia, wariancja) oraz zdolności retencyjnej podłoża. W celu identyfikacji zależności przestrzennych pomiędzy zmiennymi geograficznymi (np. długością geograficzną) a objętością retencji obliczono współczynniki korelacji Pearsona.

W ramach celu (2) zrealizowano następujące zadania:

- Opracowano modele regresji logistycznej do identyfikacji przeciążenia kanalizacji deszczowej uwzględniając jednostkową objętość wylania ścieków i udział studni przepełnionych na bazie danych opadowych, wysokości retencji terenowej i kanałowej odnosząc się do granicznych wartości podanych przez Siekmann i Pinnekamp (2011).
- Opracowano uniwersalny zintegrowany model do identyfikacji objętości wylania i kalibracji modelu w systemach kanalizacji deszczowej, bazujący na analizie struktury geometrycznej i topologicznej sieci oraz parametrach: długości kolektora głównego, objętości kanałów, spadkach podłużnych, różnicy rzędnych dna i stosunku objętości retencji do objętości sieci.
- Opracowano modele predykcyjne przepływów maksymalnych, opracowane z wykorzystaniem metody MARS (Multivariate Adaptive Regression Splines), uwzględniające topologię sieci kanalizacyjnej oraz zmienne morfologiczne i hydrauliczne małej zlewni miejskiej. W modelach uwzględniono m.in. sposób zagospodarowania terenu (powierzchnie przepuszczalne i nieprzepuszczalne), retencję kanałową, retencję terenową oraz topologię sieci kanalizacyjnej.
- Opracowano analizę ryzyka działania kanałów deszczowych, opartą na zaproponowanym współczynniku rezerwy przepustowości. Analiza ta miała na celu ocenę możliwości poprawy funkcjonowania systemu w warunkach niepewności związanych ze zmianami klimatu oraz ograniczoną dostępnością i wiarygodnością danych pomiarowych.

3. PROBLEM BADAWCZY I HIPOTEZA

W niniejszej rozprawie postawiono hipotezę:

Integracja modeli mechanistycznych dla małych zlewni miejskich wspomaganych modelami uczenia maszynowego dostarcza niezawodnych narzędzi do oceny działania i projektowania sieciami kanalizacyjnymi w warunkach niepewności obejmujących zróżnicowane warunki opadowe, zmiany klimatyczne, urbanizację i wiarygodność danych pomiarowych.

Weryfikacja tej hipotezy opierała się na podejściu wieloskalowym (Tabela 1) – obejmującym modelowanie hydrodynamiczne w skali całej zlewni miejskiej oraz szczegółową analizę wybranej zlewni cząstkowej. Tabela 1 zestawia główne zagadnienia badawcze i odpowiadające im założenia, podkreślając złożoność i interdyscyplinarny charakter badań.

Tabela 1 Problemy badawcze i założenia

Nr	Autorzy (rok)	Problem badawczy	Założenia
A1	Białek A. i Musz-Pomorska A. (2025)	Brakuje dedykowanego narzędzia obliczeniowego wspierającego projektowanie systemów odwodnienia w małych zlewniach miejskich, uwzględniającego lokalne uwarunkowania opadowe, przestrzenne i hydrologiczne.	Narzędzie obliczeniowe uwzględniające lokalne warunki opadowe, topograficzne i użytkowanie terenu umożliwia projektowanie systemów odwodnienia w małych zlewniach miejskich.
A2	Białek A. i Łagód G. (2025)	Brak uwzględnienia regionalnego zróżnicowania warunków fizycznogeograficznych w projektowaniu ogrodów deszczowych.	Warunki fizycznogeograficzne istotnie wpływają na wymiarowanie ogrodów deszczowych.
A3	Szeląg B. i in. (2024)	Kompleksowa ocena możliwości opracowania narzędzi do szybkiej identyfikacji wylania ścieków w zlewni.	W warunkach miejskich retencja terenu, zwłaszcza z obszarów przepuszczalnych, ma dominujący wpływ na ograniczenie przeciążeń sieci kanalizacyjnej i objętości wylań.
A4	Szeląg B. i in. (2023)	Brak uniwersalnego narzędzia umożliwiającego szybkie i wiarygodne oszacowanie objętości powodziowej w zlewniach miejskich przy ograniczonej ilości danych wejściowych, z uwzględnieniem topologii sieci kanalizacyjnej.	Uproszczony model obliczeniowy obejmujący dane retencji terenowej, kanałowej i topologii sieci kanalizacyjnej umożliwia wiarygodną prognozę osiągając dokładność porównywalną z modelem SWMM.
A5	Barbusiński K. i in. (2025)	Brak uniwersalnych metod analizy ryzyka wykorzystujących przepływy maksymalne w systemach kanalizacji deszczowej.	Możliwe jest zarządzanie i projektowanie sieci kanalizacyjnych w warunkach niepewności retencji kanałowej i terenowej.

Weryfikacja hipotezy przebiegała w trzech etapach, realizowanych w układzie przyczynowo - skutkowym.

Etap 1 *– Uniwersalna aplikacja inżynierska*

Opracowano autorską aplikację obliczeniową do projektowania i optymalizacji obiektów zielonej infrastruktury w rzeczywistych warunkach eksploatacyjnych. Aplikacja opiera się na równaniu fali kinematycznej, bilansie objętości oraz modelach przepływu (Darcy–Weisbach, Manning) – szczegółowo opisanych w rozdziale 4.1.1 – i może być

stosowana na różnych etapach procesu inwestycyjnego: od koncepcji, przez projekt, aż po jego weryfikację. Moduły obliczeniowe umożliwiają dobór geometrii i pojemności dla ogrodów deszczowych, niecek infiltracyjnych, rowów rozsączających oraz zbiorników detencyjnych. Walidacja aplikacji, oparta na danych z miast w Polsce, potwierdziła zarówno wysoką dokładność odwzorowania procesów odpływu, jak i dużą wydajność obliczeniową.

Etap 2 *– Studium przypadku: przepływy maksymalne i zjawiska wylania*

W drugim etapie, mającym charakter studium przypadku, oceniono możliwość wiarygodnego odwzorowania przepływów i zjawisk wylania w rzeczywistej sieci kanalizacyjnej przy ograniczonym dostępie do danych wejściowych. Wykorzystano uproszczone modele hydrauliczne, dane przestrzenne z GIS, informacje o zagospodarowaniu terenu, wskaźniki uszczelnienia oraz dane opadowe z punktowych stacji meteorologicznych. Opracowano dwa komplementarne narzędzia:

(i) model logitowy oparty na regresji logistycznej, uwzględniający charakterystyki opadów oraz parametry morfologiczne i hydrauliczne zlewni;

(ii) skalibrowany model SWMM, oparty m.in. na wysokości retencji, współczynnikach szorstkości Manninga i wskaźnikach topologicznych sieci. Dla oceny funkcjonowania systemu zastosowano wskaźniki λ_1 (jednostkowa objętość wylania) i λ_2 (udział przepełnionych studni w sieci kanalizacyjnej), dla których określono progi krytyczne.

Etap 3 *– System do kalibracji i uniwersalne narzędzie do szybkiej identyfikacji przeciążeń hydraulicznych*

W trzecim etapie opracowano narzędzie do szybkiej identyfikacji przeciążeń hydraulicznych, definiowanych jako przekroczenie jednostkowej objętości wylania ($\kappa \geq 13$ m^3/ha), bez konieczności przeprowadzania pełnych symulacji w środowisku SWMM. Zastosowano podejście hybrydowe:

(i) opracowano model regresji logistycznej (Etap 2);

(ii) stosując techniki uczenia maszynowego RF (Random Forest) opracowano symulator w celu redukcji niepewności prognoz odpływu i wylań ze zlewni, optymalizacji doboru parametrów kalibracyjnych oraz identyfikacji najistotniejszych zmiennych.

3.1. Aktualny stan wiedzy i luka badawcza

Miejskie systemy odwodnienia coraz częściej ulegają przeciążeniom hydraulicznym, co skutkuje lokalnymi podtopieniami oraz pogorszeniem jakości wód odbiorników. Zjawiska te są wynikiem intensyfikacji zjawisk opadowych, obserwowanych w związku ze zmianami klimatycznymi, oraz wzrostu udziału powierzchni nieprzepuszczalnych w zurbanizowanej przestrzeni miejskiej.

W odpowiedzi na te wyzwania w inżynierii wodnej szeroko stosowane są deterministyczne modele hydrodynamiczne, takie jak SWMM (Storm Water Management Model), MIKE URBAN (Modelling Integrated Urban Drainage and Water Distribution System) oraz HEC-RAS (Hydrologic Engineering Center – River Analysis System) (Barco i in., 2008; De Martino i in., 2010; Pons i in., 2023). Modele te, bazujące na uproszczonych formach równań Saint-Venanta, umożliwiają szczegółowe odwzorowanie transformacji opadu w odpływ oraz analizę przepływów w kanałach otwartych i zamkniętych. Pomimo wysokiej dokładności, ich stosowanie wymaga pełnych danych wejściowych, precyzyjnej kalibracji oraz dostępu do infrastruktury monitorującej. W warunkach ograniczonej dostępności danych ich zastosowanie może być istotnie utrudnione (Barco i in., 2008; Szeląg i in., 2024).

Modelowanie obiektów typu NBS, takich jak ogrody deszczowe, zbiorniki infiltracyjne, zielone dachy czy nawierzchnie przepuszczalne, wiąże się ze szczególnymi trudnościami (CIRIA, 2015; Chan i in., 2018; Boogaard i Kondratenko, 2024; Rodríguez i in., 2024). Ich implementacja w modelach hydrologicznych wymaga szczegółowej parametryzacji szerokiego zakresu zmiennych: intensywność i czas trwania opadu, przewodność hydrauliczną gruntu w stanie nasycenia, efektywną pojemność retencyjną, współczynnik szorstkości hydraulicznej, czas koncentracji oraz wilgotność początkową podłoża. Znaczna liczba parametrów, a także ich przestrzenna i czasowa zmienność, przekładają się na wysoki poziom niepewności obliczeniowej oraz znaczące utrudnienia w procesie kalibracji modeli (Beven i Binley, 2014; Fraga i in., 2016).

Model SWMM, mimo że zawiera komponenty LID (Low Impact Development), został zaprojektowany do analizy zlewni cząstkowych o jednorodnych warunkach fizycznych i hydraulicznych. Ogranicza to jego zdolność do odwzorowania wpływu pojedynczych obiektów NBS na odpływ całkowity z większych, niejednorodnych przestrzennie zlewni miejskich. Konieczność agregacji parametrów i uproszczeń przestrzennych skutkuje spadkiem dokładności wyników oraz utrudnia wykorzystanie tych narzędzi do planowania strategicznego (Barco i in., 2008; Zhang i in., 2022).

W kontekście powyższych ograniczeń ujawnia się wyraźna luka badawcza. Obecnie dostępne modele są zoptymalizowane głównie do zastosowań w skali makro – systemów kanalizacyjnych obejmujących całe dzielnice lub miasta. Brakuje natomiast narzędzi dedykowanych do modelowania w skali mikro (<1 ha), obejmującej lokalne układy retencyjne (Akan, 1993; Pons i in., 2023). W takich przypadkach stosowanie zaawansowanych modeli hydrodynamicznych, takich jak SWMM, jest nieefektywne, gdyż wymaga wysokiej jakości danych wejściowych oraz zaawansowanej wiedzy z zakresu hydrologii i hydrauliki, która nie jest niezbędna w tak ograniczonej skali.

Alternatywę dla klasycznych modeli deterministycznych stanowią metody ML (Machine Learning), które umożliwiają modelowanie nieliniowych zależności bez konieczności bezpośredniego odwzorowania mechanizmów fizycznych (Friedman, 1991; Breiman, 2001; Fisher i in., 2019). W literaturze wykazano skuteczność wielu algorytmów uczenia maszynowego, w tym: RF (Random Forest), XGBoost, MLP (Multi-Layer Perceptron), SVM (Support Vector Machines), MARS (Multivariate Adaptive Regression Splines) oraz LSTM (Long Short-Term Memory). Szczególnie sieci LSTM, należące do klasy RNN (Recurrent Neural Networks), wykazują wysoką skuteczność w krótkoterminowym prognozowaniu zmiennych hydrologicznych na podstawie danych szeregów czasowych (Kratzert i in., 2019; Yang i Chui, 2020; Palmitessa i in., 2022; Zhang i in., 2022; Zhao i in., 2023).

Badania Teweldebrhana i in. (2020) oraz Wolfs i Willemsa (2016) opisują podejścia hybrydowe, w których modele ML pełnią funkcję emulatorów wyników analiz Monte Carlo, opartych na ograniczonej liczbie symulacji deterministycznych. Rozwiązanie to znacząco obniża koszty obliczeniowe, umożliwiając efektywną analizę niepewności bez konieczności wielokrotnego uruchamiania złożonych modeli.

Pomimo rosnącej dostępności narzędzi opartych na ML oraz postępu technologicznego w modelowaniu hydrologicznym, luka badawcza wciąż pozostaje otwarta. Brakuje zintegrowanych modeli obliczeniowych umożliwiających ocenę skuteczności obiektów NBS w warunkach ograniczonej dostępności danych, wysokiej zmienności przestrzennej oraz strukturalnej złożoności miejskich systemów odwodnienia. Istniejące narzędzia rzadko integrują dane czasowe z informacjami przestrzennymi i topologicznymi, takimi jak struktura sieci kanalizacyjnej czy rozmieszczenie obiektów retencyjnych (Gires i in., 2017; Ichiba i in., 2018; Guo i in., 2021; Li i Willems, 2020).

Nowelizacja Dyrektywy UE 2024/3019, wprowadzająca obowiązek monitorowania i redukcji zrzutów burzowych w aglomeracjach powyżej 10 000 RLM (równoważna liczba

mieszkańców), jednoznacznie wskazuje na konieczność rozwoju narzędzi modelowych, które będą skalowalne, obliczeniowo efektywne i możliwe do praktycznego wykorzystania również w małej skali (PN-EN 752:2017; PN-EN 16933-1:2022; Zhou, 2014).

Zidentyfikowana luka badawcza odnosi się do ograniczonej użyteczności dostępnych narzędzi modelowych w kontekście analiz prowadzonych w skali lokalnej. Większość istniejących modeli charakteryzuje się wysokim zapotrzebowaniem na dane wejściowe i zasoby obliczeniowe, co znacząco utrudnia ich zastosowanie w praktyce, zwłaszcza przy projektowaniu i ocenie rozwiązań opartych na przyrodzie. Ponadto, modele te często nie uwzględniają zmienności lokalnych warunków środowiskowych ani specyfiki małych zlewni miejskich. W związku z tym istnieje potrzeba opracowania narzędzi o uproszczonej strukturze, wysokiej elastyczności adaptacyjnej oraz możliwości operacyjnego wykorzystania w warunkach ograniczonej dostępności danych. Rozwój takich modeli stanowi istotne wyzwanie dla współczesnej inżynierii wodnej i planowania zrównoważonego rozwoju w środowisku zurbanizowanym.

3.2. Struktura rozprawy doktorskiej

Rozprawa została przygotowana w formie cyklu pięciu recenzowanych publikacji naukowych, które są ze sobą ściśle powiązane tematycznie i merytorycznie (Wykaz publikacji wchodzących w skład rozprawy doktorskiej). Każda z publikacji rozwija odrębny, lecz komplementarny komponent badawczy, umożliwiając kompleksową i interdyscyplinarną analizę funkcjonowania systemów kanalizacji deszczowej oraz zielonej infrastruktury w miejskich zlewniach. Cykl ten spełnia formalne wymagania określone w §13 ust. 1 pkt 1 Rozporządzenia Ministra Nauki i Szkolnictwa Wyższego z dnia 22 lutego 2019 r. Szczegółowa analiza wyników badań zawartych w poszczególnych publikacjach została przedstawiona w rozdziale 6.

4. METODYKA BADAŃ

4.1. Aplikacja do wymiarowania obiektów zielonej infrastruktury (założenia hydrologiczno – hydrauliczne)

Na potrzeby niniejszych badań opracowałam dedykowaną aplikację obliczeniową Calculator_NBS, stworzoną w języku C++ z wykorzystaniem środowiska programistycznego *Qt Creator*. Narzędzie to umożliwia wymiarowanie obiektów zielonej infrastruktury z zastosowaniem zaawansowanych algorytmów hydrologiczno-hydraulicznych, opartych na równaniu fali kinematycznej (Akan, 1993) oraz bilansie objętościowym.

Aplikacja została zoptymalizowana pod kątem systemu operacyjnego Windows, co pozwala na jej szerokie wykorzystanie w praktyce inżynierskiej. Interfejs użytkownika oparty jest na głównym oknie programu (Rysunek 1), które stanowi centralny obszar interakcji – umożliwia wprowadzanie danych wejściowych oraz przeprowadzanie obliczeń.

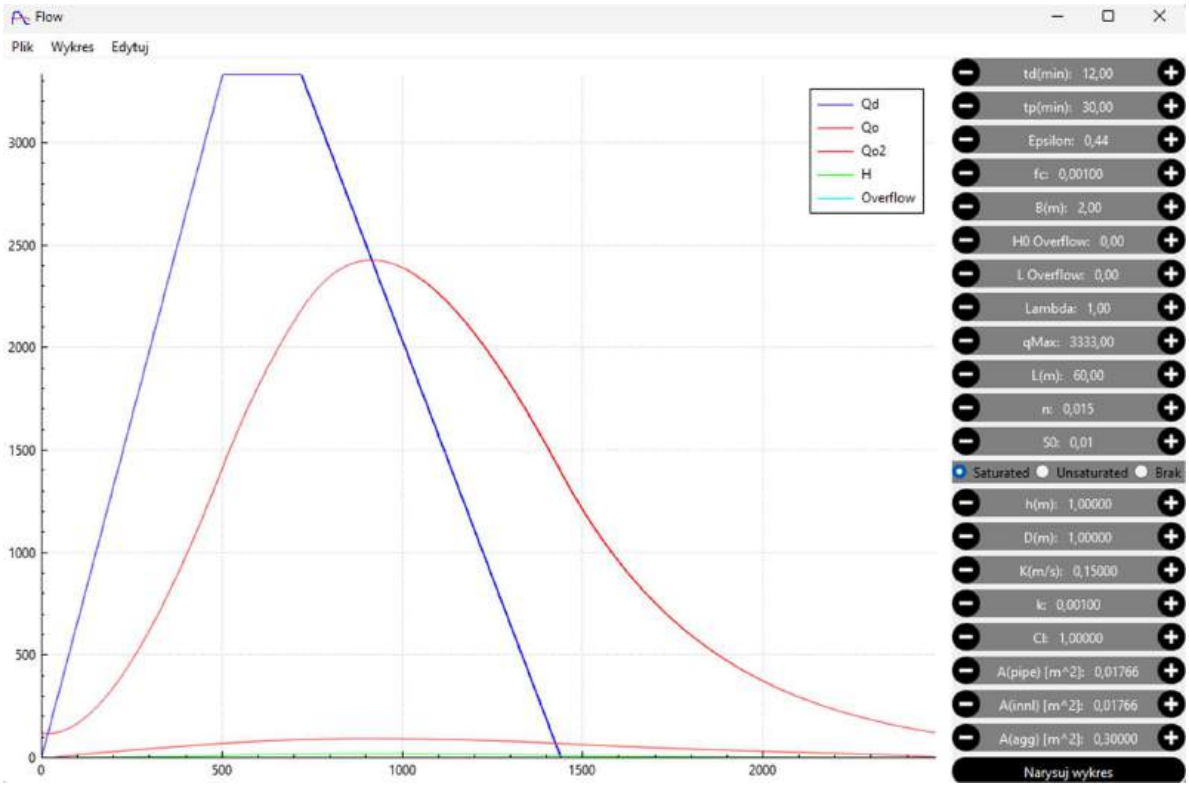

Rysunek 1 Okno główne aplikacji

Interfejs programu podzielony jest na dwa główne obszary:

(1) panel parametrów (lewa strona) – zawiera opcje konfiguracji modelu oraz ustawienia ogólne;

(2) okno robocze (prawa strona) – umożliwia wprowadzanie szczegółowych wartości parametrów i współczynników dla poszczególnych elementów modelu, takich jak rów rozsączający, zlewnia, przelew, złoże gruntowe oraz rurociąg odpływowy.

Taka struktura interfejsu pozwala na elastyczne dostosowanie modelu do specyfiki analizowanego przypadku. Po wprowadzeniu danych użytkownik ma możliwość wygenerowania wykresu wynikowego.

Rysunek 2 przedstawia strukturę funkcjonalną aplikacji, ze szczególnym uwzględnieniem dostępnych funkcji użytkowych. Jednym z kluczowych elementów programu jest generowanie hydrogramu odpływu, zgodnie z metodyką opisaną w rozdziałach 4.1.1 – 4.1.3.

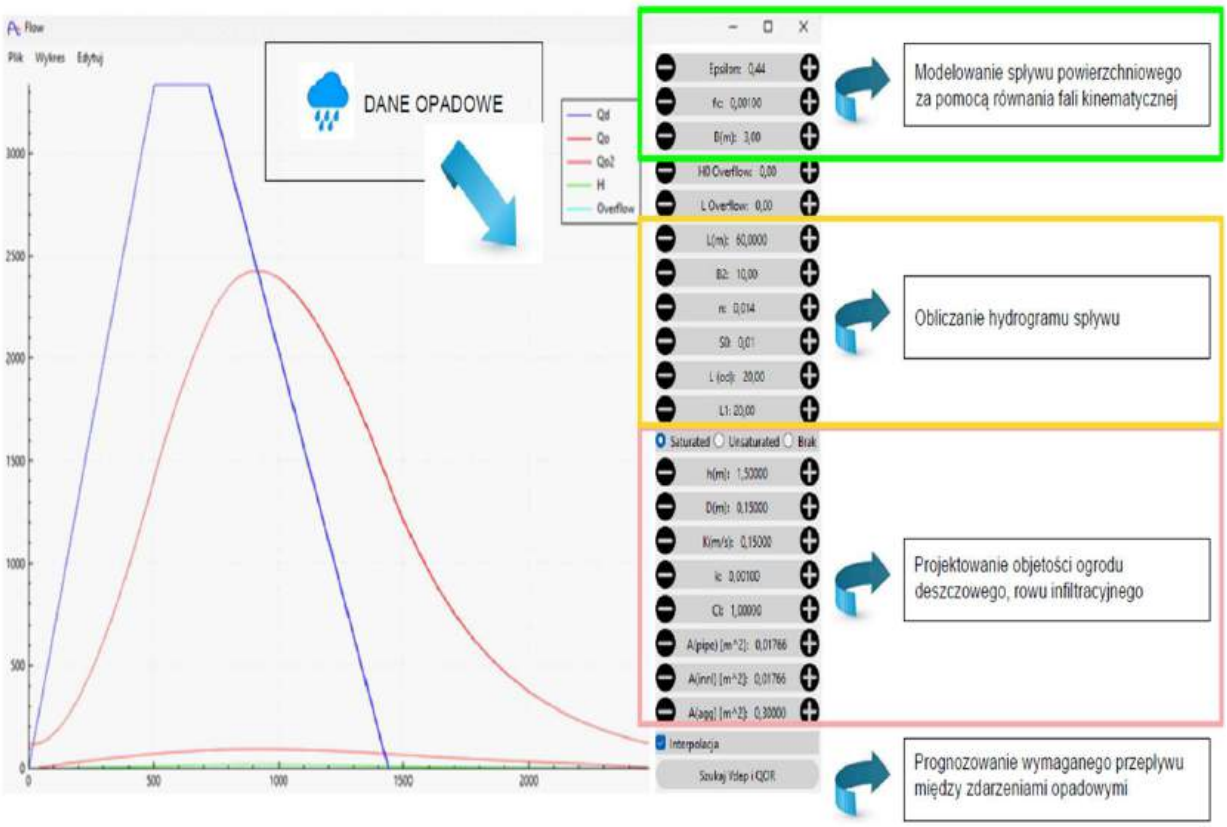

Rysunek 2 Okno dialogowe wyświetlające dostępne funkcje narzędzia

Na podstawie przeprowadzonych obliczeń program generuje hydrogram odpływu oraz wykresy strumienia odpływu, wysokości zwierciadła wody (h) i przepływu przez przelew, z możliwością eksportu wyników do pliku .csv. Dane wejściowe można importować w tym samym formacie (krok czasowy 1 s). Aplikacja umożliwia także symulację wpływu długości i szerokości rowu rozsączającego dla różnych wariantów intensywności opadu początkowego (i_0), które mogą być wprowadzane ręcznie, importowane lub wyznaczane automatycznie na podstawie czasu trwania opadu deszczu - t_d i regionalnych współczynników (a_0, a_1, a_2).

Program pozwala również na analizę odpływu do odbiornika końcowego (kanalizacji deszczowej) oraz generowanie wykresów wynikowych w formacie .pdf i porównanie wariantów obliczeniowych. Głównym celem narzędzia jest określenie zależności między parametrami geometrycznymi i objętościowymi rowu rozsączającego (V złoża).

4.1.1. Model fali kinematycznej

Model odpływu powierzchniowego oparto na równaniu fali kinematycznej (1):

$$\frac{\partial q}{\partial x} + \frac{\partial y}{\partial t} = i - f \qquad (1)$$

gdzie: $\frac{\partial q}{\partial x}$ - gradient przepływu w kierunku przestrzennym, (-); $\frac{\partial y}{\partial t}$ - zmiana wysokości wody w czasie, (-); i - intensywność opadu, (mm/hr); f - rzeczywista szybkość infiltracji, (-).
Przy założeniu $R_h = y$, gdzie y to grubość warstwy wody (m), równanie (1) pozwala na modelowanie odpływu powierzchniowego na terenach płaskich, uwzględniając intensywność opadu i infiltrację.
Zgodnie z równaniem Darcy-Weisbacha spadek hydrauliczny S_f liczony jest zgodnie z równaniem (2) i (3):

$$S_f = \frac{f_d \cdot V^2}{8 \cdot g \cdot R_h} \qquad (2)$$

dla:

$$f_d = \frac{C}{Re} \qquad (3)$$

Spadek hydrauliczny S_f wyznacza się na podstawie empirycznego równania Manninga-Stricklera (4):

$$S_f = \left(\frac{n \cdot Q}{k \cdot A}\right)^2 \cdot \frac{1}{R_h^{4/3}} \qquad (4)$$

gdzie: S_f, S_0 – spadek hydrauliczny, (-); R_h – promień hydrauliczny, (m), f_d – współczynnik oporu tarcia, obliczany ze wzoru (3), (-); V – średnia prędkość przepływu, (m/s); C - współczynnik oporu przepływu laminarnego, (-); g – przyśpieszenie ziemskie, (m/s^2); Re - liczba Reynoldsa, (-); υ - kinematyczny współczynnik lepkości ścieków, (m^2/s); n- współczynnik szorstkości wg Manninga, (m$^{-1/3}$·s); Q – natężenie przepływu, (m^3/s); k - stała jednostkowa $k = 1.0\ m^{1/3}/s$; A – pole powierzchni przekroju poprzecznego, (m^2).

Do obliczeń odpływu ze zlewni wykorzystano równanie (1), zgodnie z równaniem Darcy-Weisbacha i formułą Manninga (5):

$$q = \alpha \cdot y^m \qquad (5)$$

współczynnik α i m zależą od przyjętego wzoru na opór przepływu oraz $S_0 = S_f$.

1) dla przepływu laminarnego m = 3, to $\alpha = \frac{8 \cdot g \cdot S_0}{C \cdot \vartheta}$;
2) dla przepływu turbulentnego $m = \frac{5}{3}$, to $\alpha = \left(\frac{k}{n}\right) \cdot S_0^{1/2}$;

Hydrogram odpływu jest obliczany zgodnie ze wzorem (5), w którym maksymalny spływ ze zlewni jest określony jako równanie (6):

$$t_e = \frac{L^{1/m}}{(\alpha \cdot {i_0}^{m-1})^{1/m}} \qquad (6)$$

gdzie: t_e – czas szczytowego natężenia, (s); t – czas równowagi, (s); t_d – czas trwania opadu deszczu, (s); L – długość odpływu, (m); i_0 – natężenie opadu, (mm/hr); $i_0 = i - f = const.$

Wzór (6) umożliwia wyznaczenie czasu maksymalnego spływu powierzchniowego, uwzględniając parametry oporu przepływu, co pozwala dostosować model do lokalnych warunków hydrologicznych.

Uwzględnienie warunków brzegowych dla rozwiązania równania (1) :

1) $t_e \leq t_d$ i $t \leq t_e$, używamy $q_L = \alpha \cdot (i_0 \cdot t)^m$

3) gdy, $t_e < t < t_d$, używamy $q_L = i_0 \cdot L$

4) gdy, $t \geq t_d$, używamy $t = t_d + \frac{(L|\alpha \cdot y_L^{m-1}) - (y_L|i_0)}{m}$ dla $q_L = \left(\frac{q_L}{\alpha}\right)^{1/m}$

2) $t_e > t_d$ używamy $q_L = \alpha \cdot (i_0 \cdot t_d)^m$, gdzie $t_p = t_d - \left(\frac{t_d}{m}\right) + \frac{L}{m \cdot \alpha \cdot (i_0 \cdot t_d)^{m-1}}$

gdzie: q_L- ilość wody na jednostkę szerokości, (mm/hr·m); y_L- głębokość przepływu, (m).

4.1.2. Równanie bilansu dla obiektów zielonej infrastruktury

Równanie bilansu dla obiektów zielonej infrastruktury można wyrazić jako (7):

$$dV = Q_{dop}(t)dt - Q_{odp}(t)dt - Q_{inf}(t)dt - ET(t)dt \qquad (7)$$

gdzie: dV - zmiana objętości zbiornika w danym okresie czasu, (m^3); $Q_{dop}(t)$ – dopływ wody do obiektu zielonej infrastruktury w czasie t, (m^3/s); $Q_{odp}(t)$ – odpływ ze złoża w czasie t, obejmuje przepływ do gruntu, (m^3/s); w przypadku przekroczenia dopuszczalnej przepustowości hydraulicznej następuje zrzut przelewem (rozdział 4.1.3), $Q_{inf}(t)$ – objętość wody odpływająca do gruntu w jednostce czasu, (m^3/s); ET(t) - ewapotranspiracja z warstwy powierzchniowej, (m^3/s).

Równanie bilansu wodnego (7) stanowi podstawę modelowania przepływu wody w obiektach zielonej infrastruktury, uwzględniając dopływ, odpływ, infiltrację oraz ewapotranspirację. Pozwala ono na analizę zmian objętości retencyjnej w czasie i wspiera planowanie systemów odwodnieniowych w zróżnicowanych warunkach.

Rysunek 3 przedstawia schemat obliczeniowy systemu infiltracji według koncepcji Piazza i Ursino (2022).

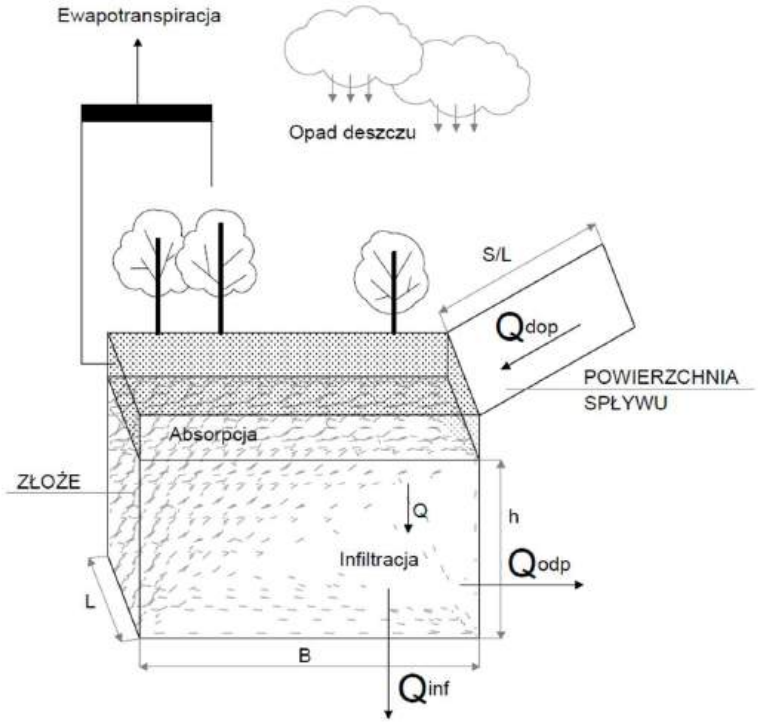

Rysunek 3 Schematyczne przedstawienie systemu infiltracji

Wyjściowa postać równania:

$$Q_{inf} = f_c * (B * L + h(B + L)) \qquad (8)$$

$$Q_{dop} - Q_{odp} = \varepsilon * B * L * \frac{dh}{dt} \qquad (9)$$

Warunki brzegowe (10) i (11) przyjęte w zależności zakresu czasu trwania opadu deszczu:

$$Q_{dop} = Q_{dmax} * \frac{t}{t_p} \quad dla\ t \leq t_p \qquad (10)$$

$$Q_{dop} = Q_{dmax}(1 + \frac{1}{\lambda} - \frac{t}{\lambda * t_p}) \quad dla\ t > t_p \qquad (11)$$

Do obliczeń rowu rozsączającego wykorzystano równania (12) i (13) po odpowiednich przekształceniach:

$$Q_{dmax} * \frac{t}{t_p} - f_c * (B * L + h(B + L)) = \varepsilon * B * L * \frac{dh}{dt} \qquad (12)$$

$$Q_{dmax}\left(1 + \frac{1}{\lambda} - \frac{t}{\lambda * t_p}\right) - f_c * (B * L + h(B + L)) = \varepsilon * B * L * \frac{dh}{dt} \qquad (13)$$

gdzie: Q_{dmax} – maksymalny dopływ do rowu rozsączającego, (m^3/s); f_c – współczynnik frakcji opóźnienia odpływu, (mm/hr); B – szerokość rowu rozsączającego, (m); L – długość rowu rozsączającego, (m); h - głębokość wody w zbiorniku, (m); ε - efektywna porowatość złoża, (-); t – czas trwania opadu deszczu, (min); t_p – czas do osiągnięcia maksymalnego

przepływu, (min); λ – współczynnik oporów liniowych, (-); $\frac{dh}{dt}$ - zmiana głębokości wody w zbiorniku w czasie.

Przyjmując w równaniu (13) wartość ε = 1, zaproponowane narzędzie można wykorzystać do analizy hydrogramu odpływu ze zbiornika retencyjnego oraz niecki rozsączającej.

Warunki brzegowe w równaniu bilansu wodnego (7) zależą od czasu trwania opadu i obejmują: początkowy stan nawodnienia systemu, zmienne w czasie dopływy i odpływy oraz końcowy stan wodny po opadzie. Ich prawidłowe określenie, uwzględniające zmienność warunków atmosferycznych, hydrologicznych i topograficznych, pozwala na dokładniejsze modelowanie funkcjonowania systemów odwodnienia miejskiego.

Równanie bilansu (9) przy założeniach odpływu do rurociągów drenarskich (14):

$$\varepsilon \cdot B \cdot L \cdot \frac{dh}{dt} = Q_{dop}(t) - Q_{odp}(t) \qquad (14)$$

1) dla strefy saturacji odpływ przewodem drenarskim opisują zależności (15) i (16):

$$Q_o = \frac{-\left(\frac{h+D}{L \cdot B \cdot K}\right) + \sqrt{\left(\frac{h+D}{L \cdot W \cdot K}\right)^2 + 4 \cdot N \cdot H}}{2 \cdot N} \qquad (15)$$

$$N = \frac{f \cdot L}{2 \cdot g \cdot A_{pipe}^2 \cdot D} + \frac{1}{2 \cdot g \cdot A_{pipe}^2} + \frac{C_L}{2 \cdot g \cdot A_{inl}^2 \cdot \Theta_{agg}^2} \qquad (16)$$

gdzie: Q_o – odpływ przy saturacji, (m³/s); D – średnica wewnętrzna przewodu drenarskiego, (m); L – długość rowu, (m); B, W – szerokości warstw złoża, (m); K – konduktywność hydrauliczna, (m/s); N – współczynnik przepływu przez rury, (m²/s); H – grubość zwierciadła wody w złożu, (m); h – grubość złoża nad wierzchołkiem przewodu, (m); A_{pipe} – pole przekroju poprzecznego przewodu, (m²); Θ_{agg} – porowatość złoża, (-); CL – współczynnik oporów miejscowych, (-); g – przyspieszenie ziemskie, (m/s²); $\boldsymbol{\lambda}$ – współczynnik oporów liniowych, (-); obliczany ze wzoru (17):

$$\lambda = \frac{1}{\left(-2 \cdot log\left(\frac{k}{3.71 \cdot D}\right)\right)^2} \qquad (17)$$

w którym: k – chropowatość przewodu, (m); D – średnica wewnętrzna przewodu, (m).

2) odpływ rurociągiem drenarskim zakładając brak saturacji złoża:

$$Q_{odp} = \frac{-\left(\frac{L}{\left(H+\frac{D}{2}\right) \cdot K}\right) + \sqrt{\left(\frac{L}{K \cdot \left(H+\frac{D}{2}\right)}\right)^2 + 4 \cdot N \cdot H}}{2 \cdot N} \qquad (18)$$

4.1.3. Obliczenia przelewu burzowego

Do obliczenia przelewu burzowego zastosowano wzór (19):

$$Q_{przelew} = \mu * L\sqrt{2 * g} * H^{2/3} \qquad (19)$$

Warunki brzegowe opisano równaniami (20) i (21):

$$h < ho, \;\; to\; Q = 0 \qquad (20)$$

$$h > ho;\; \mu * L\sqrt{2 * g} * H^{2/3}, \;\; to\; Q > 0 \qquad (21)$$

gdzie: H - wysokość swobodnego przepływu wody przez przelew, (m); h - wysokość warstwy przelewowej (h = h – ho), (m); ho - wysokość krawędzi przelewowej nad dnem kanału, określona głębokość, przy której zachodzi przelew (warunek brzegowy), (m); L - długość krawędzi przelewu, (m); μ - współczynnik przepływu („wydatku") przelewu, (-), dla przelewów czołowych μ =(0,6 - 0,8).

4.1.4. Algorytm działania aplikacji i funkcje zadaniowe

Działanie aplikacji Calculator_NBS przedstawiono w postaci algorytmu (Rysunek 4), który został zaimplementowany w funkcji *solveEquation* należącej do klasy *Calculate*, pełniącej rolę głównego modułu obliczeniowego aplikacji. Funkcja ta, wykorzystując dane wejściowe dostarczone przez obiekt klasy *Plot*, realizuje kompletną symulację przepływu w analizowanym układzie hydrologicznym. Zakres wykonywanych operacji obejmuje m.in. obliczenie przepływu jednostkowego, wyznaczanie wysokości zwierciadła wody, a także określenie odpływu oraz ewentualnego przelewu. Tak zintegrowane podejście umożliwia szczegółową analizę dynamiki badanego systemu w zadanych warunkach brzegowych oraz dla określonego zestawu parametrów wejściowych.

```
void Calculate::solveEquation(Plot *plot)
{
    for(int i = 0; i < plot->tMax; i++)
    {
        plot->tVals.push_back(i * plot->dt);
        plot->qlVals.push_back(functionQd(plot->tVals.at(i), plot->td, plot->m, plot->lVal, plot->alpha, plot->i0, plot->qMax, plot-
>lambda));

        if(i == 0)
        {
            double tempQ0 = 0.0;
            plot->hVals.push_back(functionH(tempQ0, plot->qlVals.at(i), plot->eVal, plot->lVal, plot->bVal, plot->dt, plot->fc));
        }

        else
            plot->hVals.push_back(functionH(plot->hVals.at(i - 1), plot->qlVals.at(i), plot->eVal, plot->lVal, plot->bVal, plot->dt,
plot->fc));

        plot->qoVals.push_back(QoEuler(plot->hVals.at(i), plot->lVal, plot->bVal, plot->fc));

        if(plot->saturatedChecked)
            plot->qoVals2.push_back(QoSaturated(plot->hVals.at(i), plot->L, plot->bVal, plot->h, plot->D, plot->K, plot->N));

        if(plot->unsaturatedChecked)
            plot->qoVals2.push_back(QoUnsaturated(plot->hVals.at(i), plot->L, plot->h, plot->D, plot->K, plot->N));

        plot->overflowVals.push_back(overflowCalc(plot->hVals.at(i), plot->h0, plot->lOverflow));
    }

    if(plot->to0Checked)
        valuesLimit(plot->hVals, plot->overflowVals, plot->qoVals, plot->qoVals2);
}
```

Rysunek 4 Widok okna algorytmu działania

Działanie funkcji rozpoczyna się od inicjalizacji danych wejściowych, podczas której tworzony jest obiekt klasy *Plot*. Obiekt ten pełni rolę kontenera parametrów wejściowych oraz pośrednika w komunikacji z graficznym interfejsem użytkownika. Następnie obiekt *Plot* przekazywany jest jako argument do funkcji *solveEquation*.

W kolejnym etapie realizowana jest symulacja przepływu w analizowanym układzie hydrologicznym. Na podstawie zdefiniowanych parametrów wejściowych, takich jak $t_{e.\ l}$, t_d, i_0, α, m, obliczane są wartości przepływu jednostkowego *qlVals*. Wartości początkowe są wyznaczane zgodnie z warunkami opisanymi przez parametry t_e, l, t_d, a następnie modyfikowane w oparciu o warunki symulacyjne oraz algorytmy zdefiniowane w metodach pomocniczych *solveVariant1* (Rysunek 5) i *solveVariant2* (Rysunek 6).

Wybór odpowiedniego wariantu obliczeniowego zależy od relacji pomiędzy t_e i t_d: dla $t_e < t_d$ wywoływana jest funkcja *solveVariant1*, natomiast dla $t_e \geq t_d$ uruchamiana jest funkcja *solveVariant2*. Podejście to umożliwia dostosowanie symulacji do różnych scenariuszy przepływu wynikających z warunków czasowych analizowanego zdarzenia opadowego.

```
void Calculate::solveVariant1(std::vector<double> &tVals, std::vector<double> &qlVals, double &te, double &l, double &td, double &i0,
double &alpha, double &m)
{
    //qDebug()<< "Wariant a: (te < td)";

    double ql =0.0;
    int i=0;

    while(ql >= 0.0)
    {
        if(i <= te)
        {
            tVals.push_back(i);
            qlVals.push_back((double)(alpha * std::pow((i0 * tVals.at(i)), m) * 100000.0)); // ql = (alpha * (i0 * t) ^ m) * 100000.0
        }

        else if(te < i && i <= td)
        {
            tVals.push_back(i);
            qlVals.push_back((double)(alpha * std::pow((i0 * te), m) * 100000.0)); // ql = (alpha * (i0 * te) ^ m) * 100000.0
        }

        else
        {
            ql = (double)(qlVals.at(i - 1) - 0.001);

            if(ql < 0.0)
                break;

            double yl = std::pow(((ql / 100000.0) / alpha), (1/m)); // yl = (ql / alpha) ^ (1 / m)
            qlVals.push_back(ql);
            tVals.push_back((double)(td + ((l / (alpha * std::pow(yl, (m-1)))) - (yl/i0)) / m)); // t = td + ((L / (alpha * yl ^ (m-1)) -
(yl / i0)) / m
        }

        i++;
    }
}
```

Rysunek 5 Widok okna funkcji solveVariant1

```
void Calculate::solveVariant2(std::vector<double> &tVals, std::vector<double> &qlVals, double &l, double &td, double &i0, double &alpha,
double &m)
{
    //qDebug()<< "Wariant b: (te > td)";

    double ql =0.0;
    int i=0;
    double tpVal = td - (td / m) + (l / (m * alpha * std::pow((i0 * td), (m-1))));

    while(ql >= 0.0)
    {
        if(i <= td)
        {
            tVals.push_back(i);
            qlVals.push_back((double)(alpha * std::pow((i0 * tVals.at(i)), m) * 100000.0)); // ql = (alpha * (i0 * t) ^ m) * 100000.0
        }

        else if(td < i && i <=  tpVal)
        {
            tVals.push_back(i);
            qlVals.push_back((double)(alpha * std::pow((i0 * td), m) * 100000.0)); // ql = (alpha * (i0 * td) ^ m) * 100000.0
        }

        else
        {
            ql = (double)(qlVals.at(i - 1) - 0.001);

            if(ql < 0.0)
                break;

            double yl = std::pow(((ql / 100000.0) / alpha), (1/m)); // yl = (ql / alpha) ^ (1 / m)
            qlVals.push_back(ql);
            tVals.push_back((double)(td + ((l / (alpha * std::pow(yl, (m-1)))) - (yl/i0)) / m)); // t = td + ((L / (alpha * yl ^ (m-1)) -
(yl / i0)) / m
        }

        i++;
    }
}
```

Rysunek 6 Widok okna funkcji solveVariant2

Interpolacja

Funkcja *interpolateValues* w klasie *Calculate* realizuje interpolację liniową wartości przepływu *qlVals* względem czasu *tVals*, w celu uzyskania jednostajnej siatki czasowej oraz odpowiadających im wartości przepływu.

Działanie rozpoczyna się od wyznaczenia minimalnej i maksymalnej wartości czasu, a następnie generowana jest nowa siatka czasowa z równym krokiem. Dla każdej nowej wartości czasu obliczana jest odpowiadająca wartość przepływu poprzez interpolację między sąsiednimi punktami z oryginalnych danych. Wyniki zapisywane są w wektorach tymczasowych, które po zakończeniu obliczeń zastępują oryginalne *tVals* i *qlVals*.

```
void Calculate::interpolateValues(std::vector<double> &tVals, std::vector<double> &qlVals)
{
    // Znajdź minimalną i maksymalną wartość czasu
    double minT = tVals.front();
    double maxT = tVals.back();

    // Oblicz nowe wartości czasu z równym odstępem
    double step = 1.0; // wartość 1.0 jako odstęp
    int numSteps = std::ceil((maxT - minT) / step);

    // Tworzenie tymczasowych wektorów
    std::vector<double> tempTVals(numSteps + 1);
    std::vector<double> tempQlVals(numSteps + 1);

    double newT = minT;
    for (int i = 0; i <= numSteps; ++i)
    {
        tempTVals[i] = newT;
        newT += step;
    }

    // Interpoluj wartości przepływu na podstawie nowych wartości czasu
    size_t j = 0;
    for (int i = 0; i <= numSteps; ++i)
    {
        double t = tempTVals[i];
        while (j < tVals.size() - 1 && t > tVals[j + 1])
            ++j;

        if (j < tVals.size() - 1)
        {
            double t1 = tVals[j];
            double t2 = tVals[j + 1];
            double ql1 = qlVals[j];
            double ql2 = qlVals[j + 1];

            double ql = ql1 + (ql2 - ql1) * (t - t1) / (t2 - t1);
            tempQlVals[i] = ql;
        }
    }

    // Skopiuj wartości z tymczasowych wektorów do oryginalnych wektorów
```

Rysunek 7 Widok okna funkcji Interpolacja

Funkcja functionQd

Funkcja *functionQd* (Rysunek 8) pełni istotną rolę w modelowaniu przepływu w systemie hydrologicznym, umożliwiając wyznaczenie chwilowej wartości przepływu Q_d w zależności od czasu t oraz zestawu parametrów modelu opisujących charakterystykę zdarzenia hydrologicznego.

```
double Calculate::functionQd(double &t, double &td, double &m, double &l, double &alpha, double &i0, double &qMax, double &lambda)
{
    double tpVal = td - (td / m) + (l / (m * alpha * std::pow((i0 * td), (m-1))));

    if(t < tpVal)
        return qMax * (t / tpVal);

    else if(t >= tpVal && t <= td)
        return qMax;

    else
    {
        double Qd = qMax * (1.0 + 1.0 / lambda - t / (lambda * td));

        if(Qd > 0.0)
            return Qd;

        else
            return 0.0;
    }
```

Rysunek 8 Widok okna funkcji functionQd

Funkcja *functionQd* uwzględnia trzy fazy: liniowy wzrost do czasu $tpVal$, stałą wartość $qMax$ do czasu t_d, oraz liniowy spadek po t_d zależny od parametru λ. Jeśli obliczony przepływ jest ujemny, funkcja zwraca wartość 0.

Funkcja QoEuler

Funkcja *QoEuler* w klasie *Calculate* realizuje obliczenia strumienia odpływu Qo w kanałach otwartych z wykorzystaniem równania Eulera, powszechnie stosowanego w analizie przepływów powierzchniowych (Rysunek 9). Funkcja bazuje na wymiarach kanału (l, b, ht) i współczynniku f_c. Wynik jest zwracany w dm^3/s. W implementacji przyjęto dodatkowe ograniczenie, zgodnie z którym wartości ujemne są redukowane do zera, co odpowiada fizycznemu warunkowi braku przepływu.

```
double Calculate::QoEuler(double &ht, double &l, double &b, double &fc)
{
    //Qo= dm^3/s
    double Qo = (double)(fc * (b * l + 2 * ht * l + 2 * b * ht) * 1000.0);

    if(Qo > 0.0)
        return Qo;

    else
        return 0.0;
}
```

Rysunek 9 Widok okna funkcji Eulera

Funkcje: QoSaturated i QoUnsaturated

Obie funkcje obliczają przepływ w warunkach nasyconych (*QoSaturated*) – rysunek 10 i nienasyconych (*QoUnsaturated*) – rysunek 11.

```
double Calculate::QoSaturated(double &ht, double &l, double &b, double &h, double D, double &K, double &N)
{
    double numerator1 = h + D;

    double denominator1 = l * b * K;
    double fraction = numerator1 / denominator1;
    double pow = std::pow(fraction, 2.0);
    double sqrt = std::sqrt(pow + 4.0 * N * ht);
    double numerator2 = -fraction + sqrt;
    double denominator2 = 2.0 * N;

    double Qo = (numerator2 / denominator2) * 1000.0;

    return Qo;
}
```

Rysunek 10 Widok okna funkcji QoSaturated

```
double Calculate::QoUnsaturated(double &ht, double &l, double &h, double &D, double &K, double &N)
{
    double numerator1 = l;
    double denominator1 = (h + (D / 2.0)) * K;
    double fraction = numerator1 / denominator1;
    double pow = std::pow(fraction, 2.0);
    double sqrt = std::sqrt(pow + 4.0 * N * ht);
    double numerator2 = -fraction + sqrt;
    double denominator2 = 2.0 * N;

    double Qo = (numerator2 / denominator2) * 1000.0;

    return Qo;
}
```

Rysunek 11 Widok okna funkcji QoUnsaturated

Funkcja przelew

Funkcja *overflowCalc* (Rysunek 12) w klasie *Calculate* służy do obliczania wartości przepływu przelewowego, który występuje w przypadku przekroczenia poziomu wysokości odniesienia *h*0.

```
double Calculate::overflowCalc(double &ht, double &h0, double &lOverflow)
{
    if(ht > h0)
    {
        double mi = 0.6;
        double g = 9.80665;
        double H = ht - h0;

        return mi * lOverflow * std::sqrt(2.0 * g) * std::pow(H, 3.0/2.0);
    }

    else
        return 0.0;
}
```

Rysunek 12 Widok okna funkcji overflowCalc

Jeśli aktualna wysokość ht jest większa niż $h0$, funkcja wyznacza wartość przelewu na podstawie różnicy wysokości $H = ht - h0$, przyjmując współczynnik przepływu $\mu = 0{,}6$ oraz przyspieszenie ziemskie $g = 9{,}80665$ m/s^2. Obliczenie bazuje na klasycznym wzorze dla swobodnego przelewu. W przeciwnym razie, gdy $ht \leq h0$, funkcja zwraca wartość 0, co oznacza brak przelewu. Funkcja ta znajduje zastosowanie w analizie pracy ogrodów deszczowych, umożliwiając identyfikację sytuacji, w których dochodzi do przepełnienia systemu retencyjnego i konieczne staje się odprowadzenie nadmiaru wody.

4.2. Model hydrodynamiczny SWMM

W badaniach wykorzystano model hydrodynamiczny SWMM (Storm Water Management Model), rozwijany od 1971 roku przez Amerykańską Agencję Ochrony Środowiska (U.S. EPA), jako narzędzie do symulacji odpływu wód opadowych oraz działania systemów kanalizacyjnych w warunkach zurbanizowanych. Program umożliwia kompleksowe modelowanie transformacji opadu w odpływ, odwzorowując procesy hydrologiczne zachodzące na powierzchni zlewni (retencja, infiltracja, spływ powierzchniowy) oraz przepływ wód w sieci kanalizacyjnej z uwzględnieniem jej geometrii, właściwości hydraulicznych i struktury topologicznej. Integracja danych

przestrzennych, opadowych i infrastrukturalnych pozwoliła na szczegółową analizę dynamiki odpływu w zmiennych warunkach zasilania i zagospodarowania terenu.

W celu uwzględnienia przestrzennego zróżnicowania warunków terenowych i użytkowych, zlewnię podzielono na jednostki obliczeniowe (subcatchments), odpowiadające obszarom o względnie jednorodnych właściwościach fizyczno-przestrzennych. Dla każdej jednostki obliczeniowej określono zestaw parametrów hydrologicznych, obejmujących: powierzchnię, długość drogi spływu, nachylenie terenu, udział powierzchni nieprzepuszczalnych, współczynniki Manninga dla powierzchni nieprzepuszczalnych i przepuszczalnych, głębokość retencji powierzchniowej oraz parametry infiltracyjne: przewodność nasyconą, ssanie kapilarne, wilgotność początkową i nasyconą. Dane pozyskano na podstawie ortofotomap i warstw GIS.

Model odpływu powierzchniowego oparty jest na bilansie wodnym - równanie (22):

$$\frac{dS}{dt} = \mathrm{P(t)} - \mathrm{I(t)} - \mathrm{E(t)} - \mathrm{Q(t)} \qquad (22)$$

gdzie: dS/dt - zmiana objętości zgromadzonej wody w czasie t (w zlewni), (m^3/s); P(t) – opad całkowity w czasie t, (m^3/s); I(t) – infiltracja w czasie t, (m^3/s), E(t) – ewapotranspiracja w czasie t, (m^3/s); a Q(t) – odpływ powierzchniowy, (m^3/s). Po wypełnieniu retencji początkowej generowany jest odpływ powierzchniowy modelowany jako efekt działania zbiornika nieliniowego, funkcja potęgowa (23):

$$\mathrm{Q} = \alpha \cdot \mathrm{h^m} \qquad (23)$$

gdzie: h – wysokość zwierciadła wody nad powierzchnią zlewni, (m); α – współczynnik odpływu (zależny od parametrów geometrycznych i szorstkości), (-); m – wykładnik nieliniowości (zwykle przyjmujący wartości od 1 do 2), (-). W przypadkach natężenia przepływu (Q) ustalonego w kanałach otwartych stosowane jest równanie Manninga (24):

$$Q = \frac{1}{n} A R^{2/3} S^{1/2} \qquad (24)$$

gdzie: A – pole powierzchni przepływu, (m^2); R – promień hydrauliczny, (m); S – nachylenie terenu, (-); n – współczynnik szorstkości hydraulicznej, ($m^{1/3} \cdot s$).

Dynamika przepływu w kanałach odwzorowana została przy użyciu nieliniowych równań Saint-Venanta dla przepływu nieustalonego. Zastosowano równanie ciągłości (25):

$$\frac{\partial A}{\partial t} + \frac{\partial Q}{\partial x} = ql \qquad (25)$$

oraz równanie pędu (26):

$$\frac{\partial Q}{\partial t} + \frac{\partial}{\partial x}\left(\frac{Q^2}{A}\right) + gA\frac{\partial h}{\partial x} = qA(S_0 - S_f) \qquad (26)$$

gdzie: ql – dopływ boczny, (m^2/s); S_0 – spadek dna kanału, (-); S_f – spadek hydrauliczny, (-); g – przyspieszenie ziemskie, (m/s^2); t – czas, (s). x – współrzędna wzdłuż kanału, (m).

Do odwzorowania przepływów w warunkach nieustalonych zastosowano moduł EXTRAN, oparty na uproszczonych równaniach Saint-Venanta, rozwiązywanych metodą różnic skończonych w schemacie explicite. Model zakłada nieściśliwość cieczy, uśrednienie parametrów w przekroju poprzecznym oraz uwzględnia straty hydrauliczne obliczane według wzorów Manninga lub Colebrooka–White'a.

Studnia kanalizacyjna modelowana jest jako węzeł, przy czym wysokość zwierciadła wody H_{node} wyznaczana jest w każdym kroku czasowym na podstawie równania bilansu masy (27):

$$\frac{dt}{dV} = \sum Q_{dop} - \sum Q_{opd} - Q_{przelew} \qquad (27)$$

Strumień wylania uwzględniany w bilansie masy węzła (27), pozwala na dynamiczne odwzorowanie przeciążeń hydraulicznych w sieci.

Wylanie następuje, gdy $H_{node} > H_{crest}$ Strumień wylania obliczany jest w zależności od geometrii wylotu:

(i) przelew swobodny- równanie (28):

$$Q_{przelew} = C_w \cdot b \cdot 2g \cdot (H_{node} - H_{crest})^{3/2} \qquad (28)$$

(ii) przelew przez otwór – równanie (29):

$$Q_{przelew} = C_d \cdot A \cdot 2g \cdot \sqrt{(H_{node} - H_{crest})} \qquad (29)$$

gdzie: V – objętość zgromadzonej wody w studni, (m^3); Q_{dop} – suma dopływów do studni, (m^3/s); Q_{odp} – suma odpływów ze studni, (m^3/s); $Q_{przelew–}$ strumień wylania przez przelew lub otwór, (m^3/s); C_w – współczynnik przelewu (dla przelewu swobodnego), (-); b– szerokość przelewu, (m); H_{node} – wysokość zwierciadła wody w studni, (m); H_{crest} – wysokość przelewu (krawędzi), (m); C_d – współczynnik wypływu (dla przelewu przez otwór), (-); A– pole powierzchni otworu odpływowego, (m^2).

Przyjęta metodyka modelowania SWMM zapewniła odwzorowanie procesów odpływu w badanej zlewni miejskiej, umożliwiając przeprowadzenie analiz diagnostycznych obciążenia sieci oraz symulację scenariuszy prognostycznych dla różnych wariantów opadów i zagospodarowania terenu.

4.3. Wykorzystywanie technik uczenia maszynowego w modelowaniu zlewni

Uczenie maszynowe zastosowano do analizy odpływu w zlewni miejskiej, umożliwiając identyfikację nieliniowych zależności niewykrywalnych w klasycznym modelowaniu. Wykorzystano algorytmy: RF (Random Forest), XGBoost (Extreme Gradient Boosting) oraz MARS (Multivariate Adaptive Regression Splines), które pozwoliły na selekcję kluczowych zmiennych oraz precyzyjną estymację odpływu na podstawie danych przestrzennych, hydrologicznych i opadowych.

RF (Random Forest)

to jedna z najpopularniejszych i najskuteczniejszych metod zespołowego uczenia maszynowego. Opiera się na budowie wielu drzew decyzyjnych i agregacji ich prognoz, co prowadzi do uzyskania stabilnych wyników. Algorytm ten, zaproponowany przez Breiman (2001), znalazł szerokie zastosowanie m.in. w hydrologii – w prognozowaniu przepływów, analizie opadów oraz ocenie ryzyka powodziowego. RF tworzy wiele drzew na podstawie losowych podzbiorów danych treningowych (bootstrap sampling) oraz losowych zestawów cech (feature bagging), co pozwala ograniczyć wariancję modelu i przeciwdziałać przeuczeniu. W przypadku regresji, prognoza dla danej obserwacji x obliczana jest jako średnia predykcji wszystkich drzew (30):

$$\hat{y} = \frac{1}{N}\sum_{i=1}^{N} T_i\,(x) \qquad (30)$$

gdzie: Ti (x) to predykcja i-tego drzewa, a N oznacza liczbę drzew w lesie.

Algorytm ten wyróżnia się odpornością na przeuczenie oraz zdolnością modelowania złożonych, nieliniowych zależności. Dodatkowo umożliwia ocenę ważności cech, co wspiera interpretację wyników i selekcję zmiennych. Liczne badania (Guo i in., 2021; Palmitessa i in., 2022) potwierdzają jego wysoką dokładność w zastosowaniach hydrologicznych. W niniejszym badaniu uczenie maszynowe zostało użyte jako rozwinięcie klasycznej regresji drzewiastej, przy czym liczba drzew została ograniczona do 300 w celu minimalizacji ryzyka nadmiernego dopasowania. Konstrukcję i walidację modelu oparto na podejściu zaproponowanym przez Fisher i in., (2019).

XGBoost (Extreme Gradient Boosting)

stanowi zaawansowaną implementację metod ensemble opartych na drzewach decyzyjnych, wykorzystującą technikę gradient boosting. W przeciwieństwie do lasów losowych (RF), w których poszczególne drzewa generowane są równolegle i niezależnie, XGBoost konstruuje model o charakterze addytywnym. Każde kolejne drzewo

wprowadzane do struktury modelu minimalizuje resztkowe błędy poprzednich estymatorów, co prowadzi do sukcesywnej poprawy jakości predykcji.
Po t iteracjach, predykcja dla obserwacji xi przyjmuje postać (31):

$$\hat{y}_i^{(t)} = \sum_{k=1}^{t} f_k(x_i) \qquad (31)$$

gdzie: $f_k(x)$ to funkcja przypisana do k-tego drzewa (32):

$$f_k(x) = w_{q(x)}, w \in R^T, q: R^d \to T \qquad (32)$$

gdzie: t - numer iteracji w procedurze uczenia, w - wektor wag przypisanych liściom drzewa, q - funkcja przypisująca obserwację do konkretnego liścia, d - liczba cech (zmiennych wejściowych), T - liczba liści w danym drzewie.
Na każdym etapie algorytmu uczenia kolejne drzewo dopasowywane jest do wartości reszt (błędów predykcji) z poprzedniego kroku, zgodnie z równaniem (33):

$$l(f) = L(f) + \Omega(f) \qquad (33)$$

gdzie L - funkcja straty, Ω - składnik regularyzujący.
W zadaniach regresyjnych najczęściej stosowaną funkcją L jest suma błędów kwadratowych (34):

$$L(f) = \sum i\ (yi - \hat{y}i)^2 \qquad (34)$$

gdzie yi to wartość obserwowana zmiennej zależnej, a ŷi to jej wartość prognozowana.

Gradient Boosting, stanowiący podstawę algorytmu XGBoost, wykorzystuje iteracyjne uczenie słabych klasyfikatorów w celu sukcesywnej redukcji błędów predykcji. Dzięki zastosowaniu mechanizmów regularyzacyjnych oraz zaawansowanej optymalizacji obliczeniowej, XGBoost charakteryzuje się wysoką dokładnością, dobrą skalowalnością i zwiększoną odpornością na przeuczenie. Metoda ta okazuje się szczególnie efektywna w analizie dużych i złożonych zbiorów danych, w których tradycyjne techniki statystyczne bywają niewystarczające (Palmitessa i in., 2022).

MARS (Multivariate Adaptive Regression Splines)

to nieliniowa metoda regresji opracowana przez Jerome'a Friedmana w 1991 roku, należąca do technik statystycznych i uczenia maszynowego. Podstawą jej działania jest wykorzystanie funkcji bazowych typu splajn, dobieranych w sposób adaptacyjny w trakcie konstruowania modelu. W przeciwieństwie do klasycznej regresji liniowej, w której stosuje się z góry ustaloną postać równania, MARS konstruuje model z wykorzystaniem funkcji przycinanych (hinge functions) tworzonych w punktach węzłowych (knots). Dzięki temu możliwe jest uchwycenie zarówno nieliniowych zależności, jak i interakcji pomiędzy

zmiennymi objaśniającymi. Metoda ta znajduje szerokie zastosowanie w różnych dziedzinach, m.in. w prognozowaniu ekonomicznym i finansowym, modelowaniu procesów środowiskowych i hydrologicznych, analizie ryzyka, inżynierii oraz w medycynie i biostatystyce. Należy podkreślić, że MARS jest narzędziem statystycznym służącym do budowy elastycznych modeli regresyjnych. W prezentowanych badaniach zastosowano ją do opisu maksymalnych przepływów w kanałach zamykających wybrane podzlewnie. Ogólna postać modelu wyrażona jest równaniem (35):

$$Q_m^* = \alpha_0 + \sum_{j=1}^{T} \cdot h(x_j^*, t_j^*) \qquad (35)$$

gdzie: α_0, α_j – empiryczne współczynniki estymowane metodą rekurencyjnego podziału przestrzeni cech (recursive partitioning of the feature space) według Friedman i Rosen (1995); T – liczba funkcji bazowych h (x_j^*, t_j^*), przy założeniu liniowej funkcje bazowe opisano równaniem (36):

$$h(x_j^*, t_j^*) = \begin{cases} \alpha_j \cdot (x_j^* - t_j) \; for \; x_j^* > t_j^* \\ 0 \; for \; x_j^* \leq t_j^* \end{cases} \qquad (36)$$

gdzie: t_j* – wartości progowe dla T; x_i*, Q_m* – odpowiednio standaryzowane zmienne niezależne (dane opadowe, charakterystyki zlewni, sieci kanalizacyjnej, wymiar fraktalny, parametry SWMM) i przepływ maksymalny (Q_m).

Współczynniki α_j interpretowano jako miary wrażliwości modelu względem zmiennych niezależnych, zgodnie z podejściem SRC (Standard Regression Coefficient). W przypadku dwóch wartości progowych t_1* < t_2*, łączny wpływ zmiennej x_j* w danym przedziale jest równy α_1+α_2. Do obliczeń liczby węzłów (T), wartości progowych (t_j*), współczynników αj zastosowano program STATISTICA 10, automatycznie identyfikując istotne zmienne.

MARS iteracyjnie buduje model w dwóch etapach: ekspansji (dodawanie par funkcji bazowych w miejscach największej poprawy dopasowania) i redukcji (wycinanie zbędnych funkcji metodą selekcji regresji wstecznej). Takie podejście pozwala na automatyczne wykrywanie istotnych zmiennych i interakcji między nimi bez konieczności wstępnego definiowania ich postaci.

5. OBIEKT BADAŃ

5.1. Zlewnia miejska w Kielcach

Zlewnia miejska zlokalizowana w południowo-wschodniej części Kielc, będących stolicą województwa świętokrzyskiego (Polska), stanowiła kluczowy obszar badań

hydrodynamicznych, które zostały wcześniej przeprowadzone i wykorzystane do walidacji tworzonych modeli uczenia maszynowego (Kiczko i in., 2018). Obszar ten, o powierzchni 63 ha, obejmuje gęsto zabudowane dzielnice mieszkalne, budynki użyteczności publicznej oraz układ dróg głównych i bocznych. Udział powierzchni nieprzepuszczalnych wynosi 40%, natomiast gęstość dróg, zgodnie z analizą GIS, osiąga 108 m·ha^{-1} (Wałek, 2019). Rzeźba terenu wykazuje niewielkie różnice wysokości – różnica pomiędzy najwyższym (271,2 m n.p.m.) a najniższym punktem (260,0 m n.p.m.) wynosi 11,2 m, co odpowiada średniemu spadkowi 0,71%. Lokalizację badanego obszaru przedstawiono na rysunku 13.

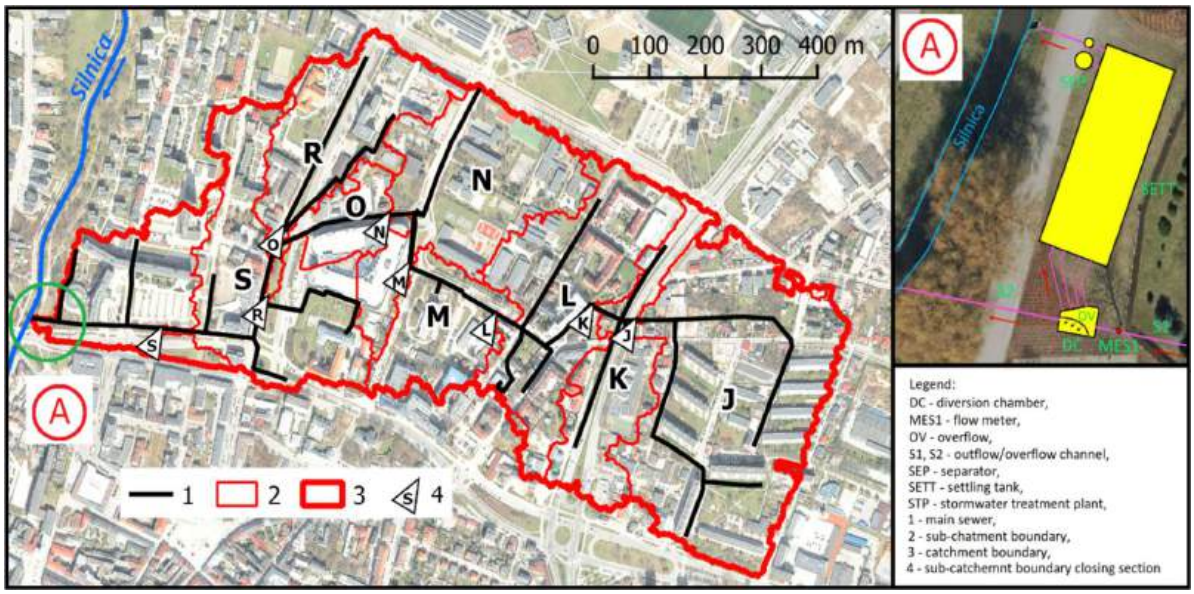

Rysunek 13 Zlewnia miejska w Kielcach (Szeląg i in., 2024)

Badana sieć kanalizacji deszczowej obejmuje 82 węzły i 72 przewody o łącznej długości 5583 m (Ø 300 – 1250 mm). Główny kolektor (1569 m, Ø 600 – 1250 mm) odprowadza wody opadowe do komory rozdzielczej (DC), skąd trafiają one do układu oczyszczania (osadnik + separator) lub – w przypadku przepełnienia (OV) – do kanału burzowego (S2) i dalej do rzeki Silnicy (Szeląg i in., 2023). Na odcinku 3,0 m przed wlotem głównego kolektora do komory DC zarejestrowany jest przepływomierz MES1, rejestrujący przepływ wody z rozdzielczością 1 minuty. Analiza danych pomiarowych z lat 2010 – 2020 wykazała obecność przepływów w zakresie 1 – 9 dm^3/s w okresach suchych, co wskazuje na infiltrację (Szeląg et al., 2022a). Dane opadowe pozyskiwano ze stacji meteorologicznej zlokalizowanej 2,5 km od granicy zlewni, prowadzącej pomiary z 1-minutową rozdzielczością od 2008 roku.

Na podstawie zgromadzonych danych opracowano i skalibrowano model hydrodynamiczny zlewni. Ocena dopasowania wykazała wysoką zgodność z pomiarami: NSE (Nash–Sutcliffe Efficiency) = 0,85 – 0,98; R^2 (Coefficient of Determination) = 0,92

– 0,96; MAE (Mean Absolute Error) = 0,021 – 0,034; RMSE (Root Mean Square Error) = 0,038 – 0,053 (Szeląg et al., 2022a).

W ramach analiz przestrzennych i modelowych zlewnię podzielono na pięć i siedem podzlewni (J, K, L, N, M, R, S), kierując się przebiegiem kolektora głównego oraz zróżnicowaniem morfologii terenu, topologii sieci kanalizacyjnej i struktury użytkowania przestrzeni, co omówiono w publikacji Szeląg i in. (2022). Podział oparto na danych przestrzennych (Fraga i in., 2016; Palmitessa i in., 2022) oraz uproszczonym podejściu modelowym wykorzystującym HEC-HMS, w którym kluczowym kryterium była struktura zagospodarowania terenu. Dla każdej z podzlewni określono zestaw charakterystyk (Tabela 2), takich jak: powierzchnia zlewni, udział powierzchni nieprzepuszczalnych, objętość kolektora, długość kolektora na jednostkę powierzchni nieprzepuszczalnej, różnica rzędnych przewodu kanalizacyjnego, objętość przewodu przed zamknięciem zlewni, różnica wysokości w zlewni, spadek dna kanału, głębokość studzienki rewizyjnej, retencja zlewni, objętość sieci kanalizacyjnej w dolnym biegu, współczynnik retencji oraz wymiar fraktalny.

Tabela 2 Charakterystyki wydzielonych podzlewni

Nr	**F**	**Imp**	**Vk**	**Gk**	**R.t.**	**Vkp**	**Jkp**	**Impd**	**Gkd**	**Vrd·Vkd^{-1}**	**FD**
	ha	-	m^3	$m \cdot ha^{-1}$	m	m^3	-	-	$m \cdot ha^{-1}$	-	-
J	12.66	0.42	157	0.0079	1.74	33.2	0.0036	0.40	0.0072	0.84	0.94
K	18.92	0.43	360.4	0.0084	1.69	28.4	0.0055	0.40	0.0063	0.79	1.01
L	27.15	0.41	557.4	0.0074	2.74	29.6	0.0058	0.42	0.0053	0.69	1.05
N	36.78	0.40	712.2	0.0081	4.49	48.7	0.0061	0.44	0.004	0.52	1.08
P	45.42	0.35	981.9	0.0082	5.64	16.1	0.0102	0.46	0.0027	0.39	1.10
R	48.31	0.42	981.9	0.0088	5.64	16.1	0.0102	0.47	0.0023	0.32	1.11
S	55.41	0.44	1240.2	0.0092	8.47	67.5	0.0078	0.55	0.0011	0.17	1.14

5.2. Dane opadowe i warunki klimatyczne dla Polski

Polska, jako obszar badań, położona jest w Europie Środkowej (49°00′ – 54°50′ N, 14°07′ – 24°09′ E) i charakteryzuje się klimatem umiarkowanym ciepłym o cechach przejściowych, wynikających z oddziaływania zarówno wpływów oceanicznych z zachodu, jak i kontynentalnych ze wschodu. Średnia roczna suma opadów w latach 1981 – 2010 wynosi około 600 mm, przy znacznym zróżnicowaniu regionalnym – od około 520 mm w centralnej części kraju do ponad 1000 mm na obszarach górskich. Największe

natężenie opadów przypada na miesiące letnie, szczególnie lipiec, natomiast przerwy bezopadowe trwają przeciętnie od 5 do 9 dni.

To zróżnicowanie przestrzenne stanowiło podstawę do analizy wpływu lokalnych warunków klimatycznych na intensywność i strukturę opadów (Kupczyk i Suligowski, 2000; Szeląg i in., 2022). Badania realizowano w dwóch komplementarnych podejściach: (1) z wykorzystaniem danych pochodzących z 32 stacji meteorologicznych IMGW, oraz (2) na podstawie danych z 29 stacji meteorologicznych IMGW.

W obu przypadkach dobór punktów pomiarowych został przeprowadzony tak, aby reprezentować sześć głównych mezoregionów fizyczno-geograficznych Polski: nadmorskie niziny, pojezierza, niziny środkowopolskie, wyżyny, kotliny podgórskie oraz obszary górskie (Rysunek 14).

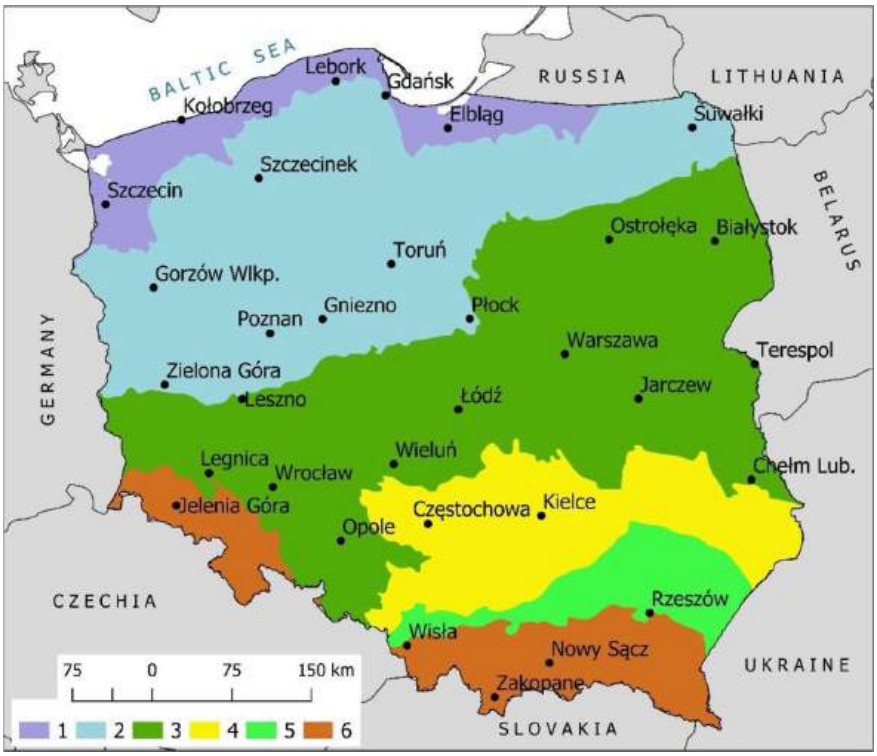

Rysunek 14 Lokalizacja stacji opadowych na tle głównych mezoregionów fizyczno- geograficznych Polski (1 – pobrzeża Bałtyku, 2 – pojezierza, 3 – niziny środkowopolskie, 4 – wyżyny, 5 – kotliny podgórskie, 6 – góry)

Podejście (1) oparto na danych z 32 stacji IMGW-PIB, koncentrując się na opadach konwekcyjnych – krótkotrwałych, intensywnych i lokalnych zjawiskach istotnych w modelowaniu odpływu w małych zlewniach miejskich. Ponad 65% takich epizodów trwało poniżej 30 minut, a ich największa częstość występowała w rejonach górskich i nadmorskich. Do ich odwzorowania opracowano krzywe $P(t_r)$ na podstawie wielomianów

drugiego stopnia, uwzględniające regionalne zróżnicowanie intensywności i czasu trwania opadów (Kupczyk i Suligowski, 2000; Szeląg i in., 2022).

Podejście (2) bazowało na danych z 29 stacji z lat 1961 – 2005, gdzie niezależne zdarzenia opadowe identyfikowano zgodnie z wytycznymi DWA-A 118 (2006), przyjmując minimalną przerwę 4 godziny i próg opadowy 5 mm (Fu i Butler, 2014). Analiza umożliwiła określenie zmienności czasowej opadów, częstości intensywnych epizodów (11 – 15 rocznie) oraz długości okresów bezdeszczowych (5 – 9 dni). Dodatkowo, na podstawie pomiarów z lat 2010 – 2019 wyodrębniono 202 zdarzenia o intensywności 2,5 – 41,2 mm, czasie trwania 15 – 150 minut i przerwach sięgających 1200 godzin (Jato-Espino i in., 2018).

Oba podejścia – oparte na różnej liczbie stacji i odmiennych procedurach analitycznych – pozwoliły na kompleksową charakterystykę warunków opadowych w Polsce w ujęciu przestrzennym (mezoregiony) i czasowym (wielolecia, okresy bezopadowe).

6. WYNIKI BADAŃ

6.1. Development of a computational tool for stormwater management in small urban catchments (A1)

W ramach przeprowadzonych analiz opracowano i przetestowano autorskie narzędzie obliczeniowe wspomagające projektowanie systemów gospodarowania wodami opadowymi w małych zlewniach miejskich. Aplikacja została wykorzystana do wymiarowania ogrodów deszczowych w zróżnicowanych warunkach geograficznych na obszarze Polski. Do głównych zalet opracowanego rozwiązania, w porównaniu z dostępnymi narzędziami, należy m.in.: ograniczona liczba wymaganych danych wejściowych, możliwość szybkiej analizy oraz projektowania obiektów zielonej infrastruktury z uwzględnieniem lokalnych uwarunkowań hydrologicznych i topograficznych, implementacja zaawansowanych modeli opartych na równaniu fali kinematycznej i bilansie wodnym, intuicyjny interfejs umożliwiający konfigurację, wizualizację oraz eksport wyników, a także możliwość przeprowadzania symulacji dla różnych scenariuszy opadowych. Narzędzie umożliwia ponadto obliczenia przelewu w przypadku przekroczenia pojemności retencyjnej oraz analizę odpływu ze złoża z uwzględnieniem możliwości jego regulacji.

W celu oceny efektywności i użyteczności opracowanego rozwiązania dokonano porównania z wybranymi, powszechnie stosowanymi modelami ogrodów deszczowych:

SWMM (Storm Water Management Model), MIKE URBAN (MIKE URBAN Water Modeling System), HYDRUS-1D (HYDRUS One-Dimensional Model) oraz MUSIC (Model for Urban Stormwater Improvement Conceptualisation). Tabela 3 przedstawia zakres zastosowań, wymagania dotyczące danych wejściowych, a także zalety i ograniczenia każdego z narzędzi. Przeprowadzona analiza wykazała, że model autorski stanowi optymalny kompromis pomiędzy prostotą obsługi a wiarygodnością wyników, co czyni go szczególnie przydatnym w warunkach ograniczonego dostępu do danych oraz konieczności szybkiej analizy projektowej.

Tabela 3 Porównanie wybranych modeli ogrodów deszczowych

Model / Narzędzie	Powierzchnia zlewni [ha]	Głębokość [m]	Kluczowe parametry	Zalety	Ograniczenia
SWMM	0.3 – 2.0	0.6 – 1.0	opady (IDF), CN, LID, przepuszczalność gruntu, czas koncentracji	integracja z siecią kanalizacyjną, wysoka dokładność	wysokie wymagania danych, złożona kalibracja
MIKE URBAN	0.5 – 2.0	0.6 – 1.2	opady, retencja, spadek, pokrycie terenu, odpływ	integracja GIS, wysoka rozdzielczość przestrzenna	wysoka złożoność, potrzeba dokładnych danych topograficznych
HYDRUS -1D	0.1 – 0.8	0.5 – 1.0	porowatość, przewodność, struktura warstw, właściwości fizykochemiczne	dokładna reprezentacja infiltracji i magazynowania	model 1D, brak reprezentacji odpływu powierzchniowego i kanalizacji
MUSIC	0.1 – 1.0	0.3 – 0.9	czas opóźnienia, odpływ, objętość retencji, typ opadu, konfiguracja warstw	intuicyjny interfejs, szybka analiza scenariuszy	uproszczony schemat infiltracji, brak dynamiki systemu
MODEL autorski	ok. 1.0	0.5 – 0.8	opad, infiltracja, wymiary geometryczne, Q_{max}, V_{max}, Q_{OR}	niewielka liczba zmiennych wejściowych, szybka analiza	uproszczona hydraulika, brak integracji z kanalizacją

W celu oceny użyteczności opracowanej aplikacji przeprowadzono obliczenia symulacyjne dla wybranej miejskiej zlewni miejskiej, charakteryzującej się zróżnicowanym zagospodarowaniem terenu oraz ograniczoną możliwością retencji

powierzchniowej. Dane opadowe wykorzystane w analizie zostały wyznaczone na podstawie parametrów intensywności opadu dla różnych czasów trwania, opracowanych na podstawie statystycznej analizy serii danych historycznych pochodzących z 32 miast w Polsce.

Zestawienie umożliwiło identyfikację charakterystycznych wzorców opadowych oraz ich przestrzennego zróżnicowania, co pozwoliło na realistyczne odwzorowanie lokalnych warunków klimatycznych w modelu. Szczególną uwagę poświęcono analizie zależności między czasem trwania opadu a pojemnością infiltracyjną – wykazano silną korelację tych parametrów (Rysunek 15).

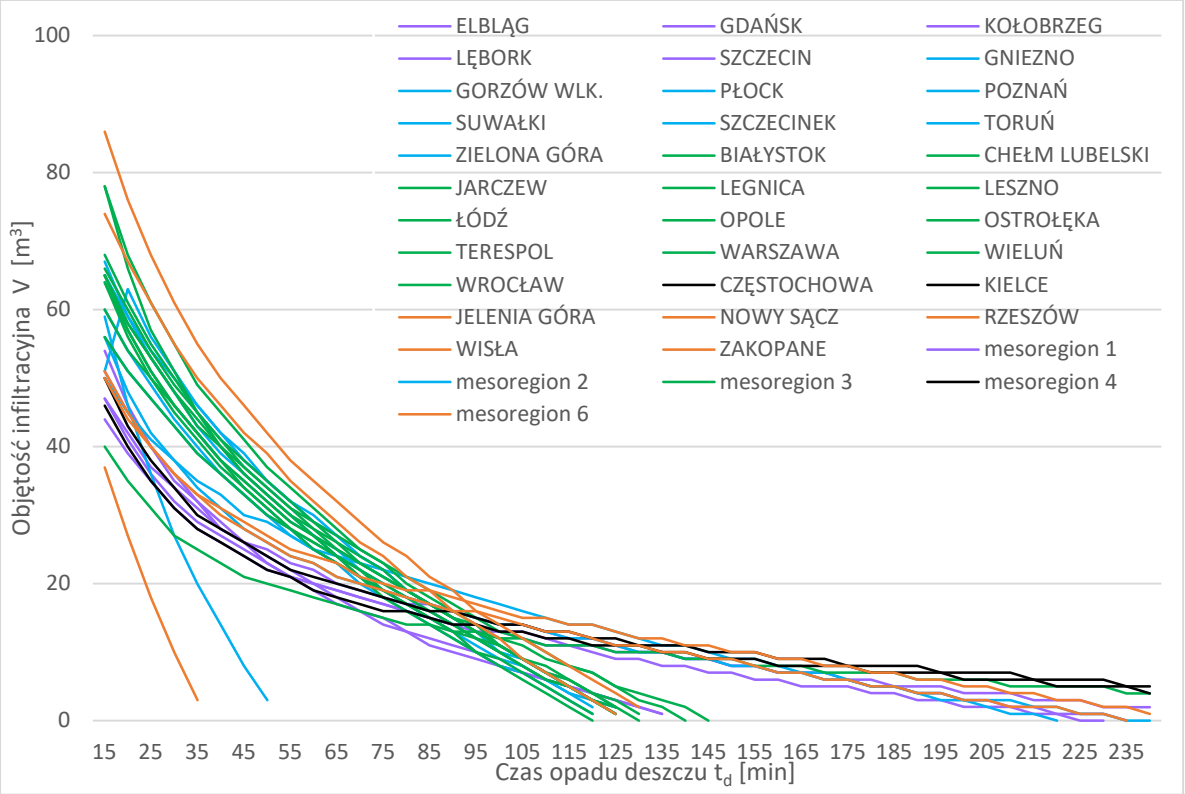

Rysunek 15 Wpływ czasu trwania opadu na zdolność infiltracyjną

Najwyższe wartości retencji (do 86 m³) zarejestrowano w Nowym Sączu podczas krótkiego, intensywnego opadu konwekcyjnego, podczas gdy dłuższe opady znacząco ograniczały zdolności infiltracyjne (np. do 2 m³ przy 130 minutach opadu). Mezoregion 6 (m.in. Nowy Sącz, Zakopane) charakteryzował się największym zróżnicowaniem wyników, potwierdzając znaczenie warunków górskich. Podobne tendencje zaobserwowano w mezoregionach 1 i 3.

Równolegle przeprowadzono analizę intensywności opadów (Rysunek 16), która wykazała istotne zróżnicowanie między miastami.

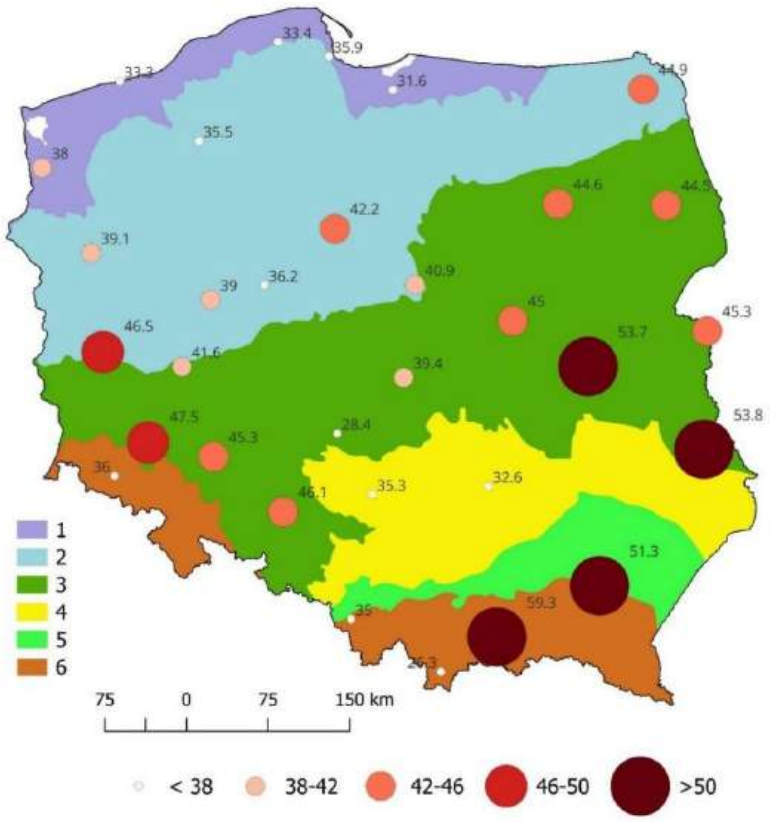

Rysunek 16 Reprezentatywna intensywność opadu

Najwyższe wartości intensywności opadu zanotowano od maksymalnych 59,3 mm/min (Nowy Sącz) po minimalne 26,3 mm/min (Zakopane). Porównanie z wynikami Szeląga i in. (2022) potwierdziło, że miasta charakteryzujące się największą intensywnością opadów wykazują również najwyższą podatność na odpływ, co znajduje odzwierciedlenie w wartościach wskaźnika wrażliwości (p_s > 0,5) i wiąże się z podwyższonym ryzykiem występowania lokalnych podtopień. Wskazuje to na konieczność regionalnego podejścia do planowania systemów odwodnienia. Zagadnienie poruszane również w literaturze zagranicznej (De Martino i in., 2010; De Paola i in., 2012).

Dodatkowa analiza funkcjonowania rowów infiltracyjnych (długość 3,0 m) ujawniła największe wartości retencji w Nowym Sączu, Chełmie Lubelskim, Jarczewie i Rzeszowie (Rysunek 17), natomiast najniższe – w Zakopanem i Kołobrzegu.

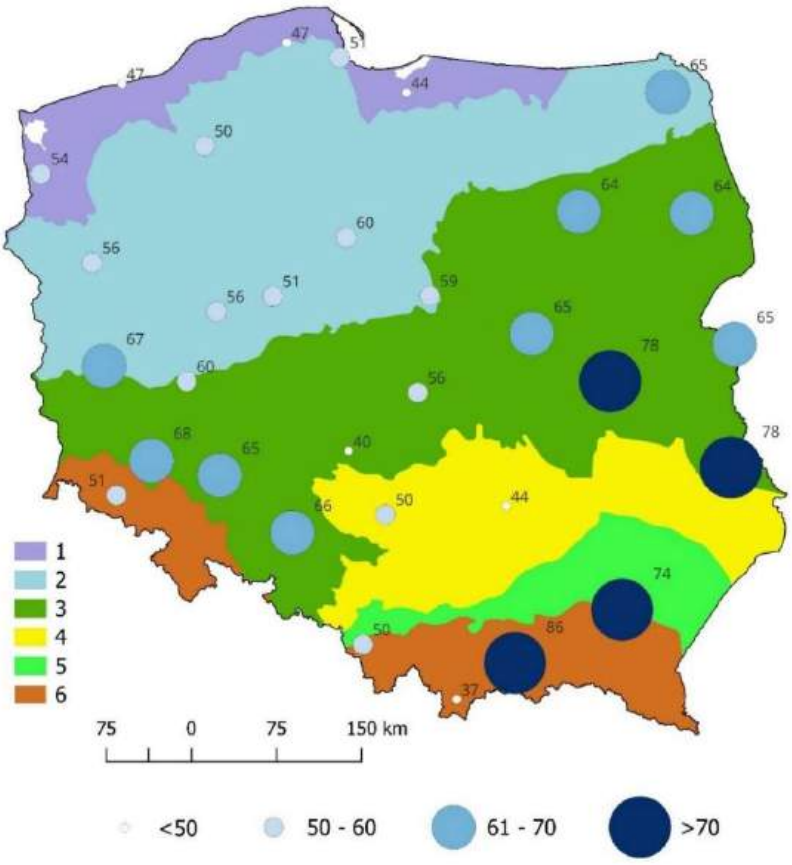

Rysunek 17 Pojemność złoża infiltracyjnego

Uzyskane wyniki podkreślają istotne znaczenie lokalnych danych opadowych i uwarunkowań fizyczno-geograficznych w projektowaniu systemów odwodnienia. Największe zdolności retencyjne odnotowano w mezoregionie 6, a najniższe – w mezoregionie 1, gdzie wysoki stopień uszczelnienia sprzyja intensyfikacji odpływu.

Zgodnie z obserwacjami Szeląg i in. (2022), wyniki te potwierdzają konieczność regionalnego podejścia do projektowania systemów odwodnienia.

6.2. The impact of physical-geographical conditions on the sizing of rain gardens: A spatial case of Poland (A2)

W projektowaniu ogrodów deszczowych oraz systemów infiltracyjnych w Polsce wciąż zbyt rzadko uwzględnia się regionalne zróżnicowanie warunków fizyczno-geograficznych, mimo że czynniki takie jak przepuszczalność podłoża, intensywność opadów, ukształtowanie terenu czy stopień uszczelnienia powierzchni znacząco wpływają na efektywność retencji i odpływu wód opadowych. Nieuwzględnianie tych uwarunkowań może prowadzić do niedoszacowania lub przeszacowania wymiarów projektowanych obiektów, co w konsekwencji obniża skuteczność funkcjonowania systemów odwodnienia.

W celu zilustrowania wpływu urbanizacji na bilans wodny zlewni, na rysunku 18 przedstawiono porównanie udziału podstawowych składowych bilansu hydrologicznego dla obszarów o zróżnicowanym stopniu uszczelnienia – od naturalnych ekosystemów po tereny silnie zurbanizowane. Zestawienie to wyraźnie ukazuje wzrost udziału odpływu powierzchniowego przy jednoczesnym spadku infiltracji i ewapotranspiracji.

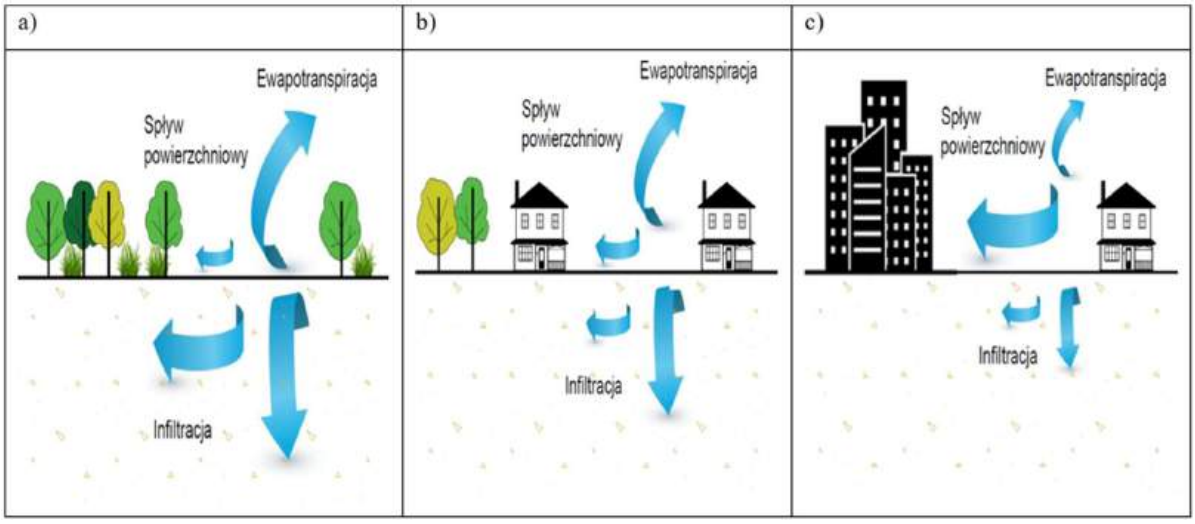

Rysunek 18 Porównanie bilansu wodnego w zlewniach: a) naturalnej, b) częściowo zurbanizowanej, c) silnie zurbanizowanej

W niniejszej pracy przyjęto podejście integrujące modelowanie hydrauliczne z analizą statystyczną i przestrzenną, pozwalające na identyfikację wpływu lokalnych uwarunkowań na projektowanie rowów infiltracyjnych. Do wymiarowania ogrodów deszczowych zastosowano omówioną w publikacji (załącznik A1), autorską aplikację obliczeniową. W ramach obliczeń uwzględniono trzy warianty uszczelnienia zlewni: niski, średni i wysoki, odzwierciedlające scenariusze urbanizacji oraz prognozowane zmiany klimatyczne, w tym wzrost intensywności opadów nawalnych. Dla każdego wariantu określono objętość złoża infiltracyjnego oraz zaprojektowano urządzenia regulujące odpływ, zapewniające minimalny poziom wody niezbędny do podtrzymania wegetacji roślinności i zapobiegające jego wysychaniu.

W kontekście poszukiwania regionalnych wytycznych do projektowania ogrodów deszczowych z uwzględnieniem danych meteorologicznych oraz fizyczno-geograficznych zastosowano analizę klastrów metodą k-średnich. Na tej podstawie wyodrębniono dwa klastry zlewni: CL1, obejmujący południowo-wschodnią Polskę, oraz CL2 – zachodnią część kraju. Klastery te różniły się m.in. rocznymi sumami opadów oraz zmiennością parametrów hydraulicznych. Dodatkowo przeprowadzona analiza korelacji wykazała

istotne związki pomiędzy położeniem geograficznym a parametrami retencji – w szczególności między długością geograficzną a objętością retencji V(40) (r = 0,524) oraz odpływem Q(40) (r = 0,599). Zaobserwowano również bardzo wysokie korelacje pomiędzy parametrami hydraulicznymi w różnych scenariuszach opadowych V(40)–V(100), (r = 0,961), co potwierdza możliwość szacowania wymiarów obiektów retencyjnych na podstawie lokalizacji oraz danych klimatycznych.

Rysunek 19 Macierz korelacji Pearsona pomiędzy parametrami geograficznymi, fizycznymi i hydraulicznymi

Analiza objętości złoża infiltracyjnego (Rysunek 20) wykazała systematyczny wzrost wymaganej pojemności rowów infiltracyjnych w miarę zwiększania się stopnia uszczelnienia we wszystkich sześciu analizowanych mezoregionach.

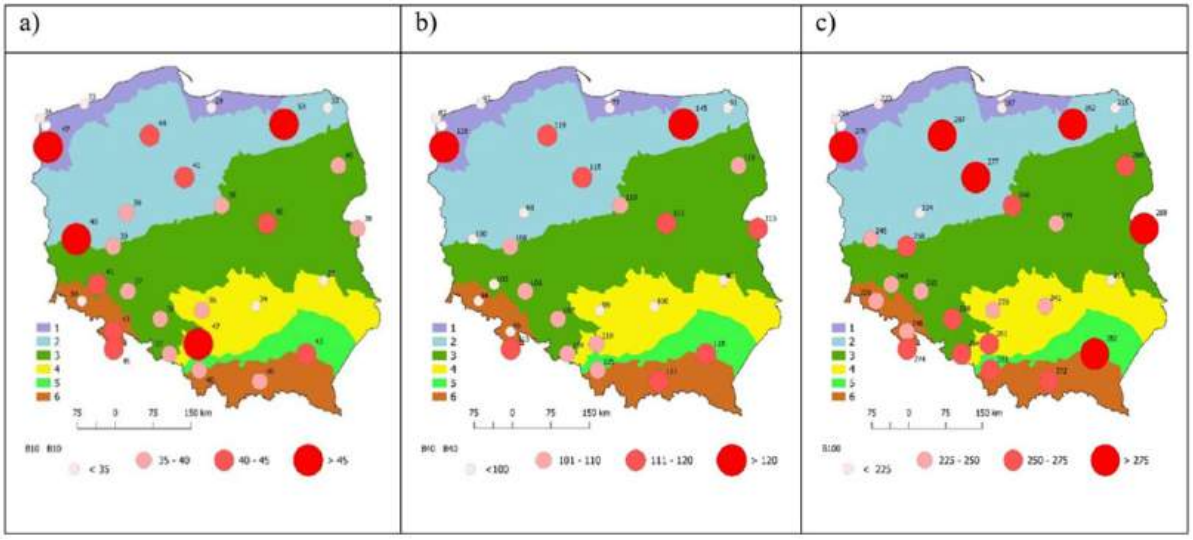

Rysunek 20 Objętość złoża infiltracyjnego z uwzględnieniem różnych stopni uszczelnienia zlewni miejskiej — (a) niski, (b) średni oraz (c) wysoki

W scenariuszu niskiego uszczelnienia wartości wynosiły 28,7 – 52,6 m³, średniego – 77,4 – 145,4 m³, a wysokiego – 187,1 – 352,8 m³. Największe objętości odnotowano w Mikołajkach (352,8 m³, mezoregion 2), a najmniejsze w Elblągu (187,1 m³, mezoregion 1). W mezoregionach 1, 2, 3 i 5 objętości przekraczały 275 m³, natomiast w 4 i 6 mieściły się w zakresie 225 – 275 m³. Największy przyrost objętości wystąpił w Terespolu (7,7%, mezoregion 3), a najmniejszy w Zielonej Górze (5,4%, mezoregion 5).

W pracy oceniono wpływ stopnia uszczelnienia powierzchni na wielkość odpływu w Polsce, uwzględniając zróżnicowane warunki fizyczno-geograficzne mezoregionów (Rysunek 21a–c).

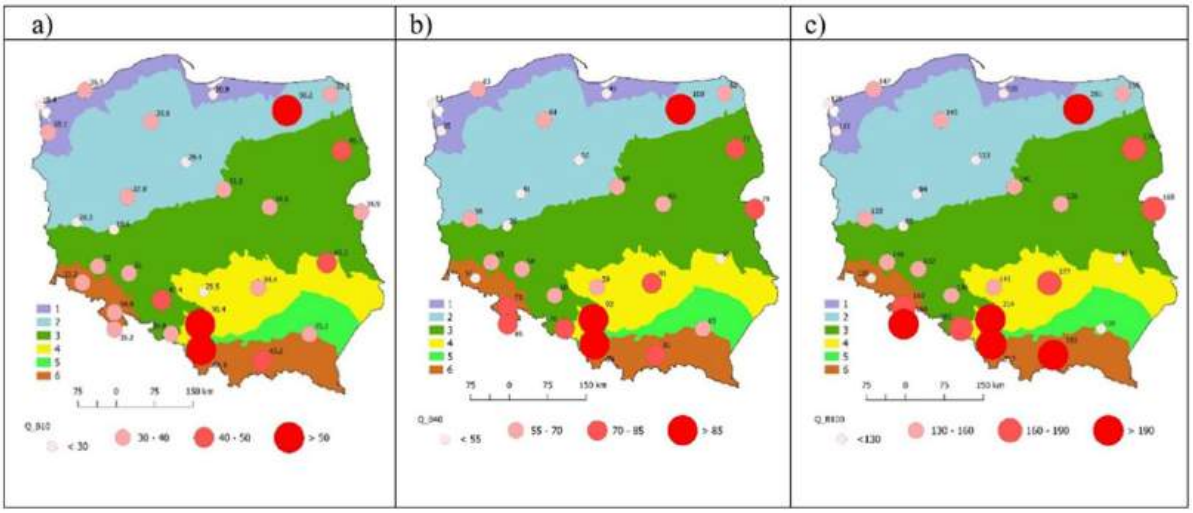

Rysunek 21 Wielkość regulowanego odpływu ze złoża infiltracyjnego z uwzględnieniem uszczelnienia zlewni miejskiej: a) małe, b) średnie, c) największe

Wyniki analizy odpływu (Rysunek 21) potwierdziły, że zwiększenie uszczelnienia powierzchni prowadzi do systematycznego wzrostu odpływu – od 30 – 40 m³/d przy uszczelnieniu niskim, przez 55 – 70 m³/d przy średnim, do 130 – 160 m³/d przy wysokim. Największe wartości odpływu stwierdzono w mezoregionach górskich (6), wyżynnych (4) i pojeziernych (2), z wyraźnym wyróżnieniem miast takich jak Bielsko-Biała, Katowice i Mikołajki. W Mikołajkach odnotowano wysokie wartości odpływu niezależnie od poziomu uszczelnienia – 56,2; 107,5; 260,8 m³/d.

Na tle powszechnie stosowanych narzędzi (SWMM, MIKE URBAN, HYDRUS-1D, MUSIC), opracowana aplikacja wyróżnia się niskimi wymaganiami wejściowymi, uniwersalnością i możliwością dostosowania do lokalnych warunków fizyczno-geograficznych. Jej główną zaletą jest możliwość symulacji różnych scenariuszy uszczelnienia i intensywności opadów, co pozwala na szybkie i trafne dopasowanie rozwiązań projektowych i modernizacyjnych do specyfiki danej zlewni miejskiej.

W skali kraju, narzędzie to może stanowić podstawę do opracowywania regionalnych wytycznych projektowych do wymiarowania ogrodów deszczowych, uwzględniających rzeczywiste uwarunkowania fizyczno-geograficzne i klimatyczne. Przyjęte podejście wpisuje się w aktualne krajowe i międzynarodowe trendy w zakresie zrównoważonego zarządzania wodami opadowymi, adaptacji infrastruktury do zmian klimatu oraz wdrażania rozwiązań opartych na przyrodzie. Dzięki wysokiej trafności prognoz i łatwej implementacji, aplikacja może znacząco zwiększyć efektywność planowania przestrzennego oraz odporność miast na ekstremalne zjawiska pogodowe.

6.3. Extended evaluation of the impact of rainfall, sewer network and land use retention on drainage system performance in a multi-criteria approach – Modeling, sensitivity analysis (A3)

W niniejszym opracowaniu przeanalizowano możliwość zastosowania regresji logistycznej (logit) jako alternatywnego, uproszczonego narzędzia predykcyjnego względem klasycznego modelu deterministycznego SWMM w analizie przeciążeń hydraulicznych systemów kanalizacji deszczowej. Wyniki przeprowadzonych analiz potwierdziły wysoką skuteczność modeli logitowych, czego dowodzą wartości wskaźnika AUC (Area Under the Curve): 0,987 dla jednostkowej objętości wylania (λ_1) oraz 0,996 dla stopnia wylania (λ_2), przy jednoczesnym utrzymaniu wysokiej czułości i swoistości (odpowiednio powyżej 94% i 93%) we wszystkich zestawach danych (uczącym, testującym i walidacyjnym). Wykazano możliwość prognozowania prawdopodobieństwa wystąpienia wylania w sieci kanalizacyjnej na podstawie wybranych charakterystyk

opadowych oraz parametrów kalibracyjnych modelu SWMM. W porównaniu z podejściem deterministycznym, proponowana metoda pozwala na znaczące ograniczenie wymagań dotyczących danych wejściowych – w szczególności danych wysokościowych, takich jak rzędne studni rewizyjnych oraz spadki kanałów – co istotnie upraszcza proces modelowania przeciążeń hydraulicznych.

W badaniu przeprowadzono ocenę wpływu zmienności czasu trwania opadów na wrażliwość modelu SWMM względem siedmiu kluczowych parametrów: α (współczynnika szerokości ścieżki spływu), β (współczynnika korekcyjnego udziału powierzchni nieprzepuszczalnych), γ (współczynnika korekcyjnego nachylenia powierzchni zlewni), D_{imp} (głębokości retencji dla powierzchni nieprzepuszczalnych), D_{per} (głębokości retencji dla powierzchni przepuszczalnych), n_{imp} (współczynnika szorstkości Manninga dla powierzchni nieprzepuszczalnych) oraz n_{sew} (współczynnika szorstkości hydraulicznej kanałów kanalizacyjnych). Analiza miała na celu określenie, które z tych parametrów w największym stopniu wpływają na prognozowanie dwóch kryteriów hydraulicznego przeciążenia systemu kanalizacyjnego: jednostkowej objętości wylania (λ_1) oraz stopnia wylania (λ_2), zdefiniowanych odpowiednio jako 13 $m^3 \cdot ha^{-1}$ i 0,32 (Sinekamp i Pinekamp, 2011).

Jako alternatywne podejście do klasycznego modelowania w środowisku SWMM, zastosowano regresję logistyczną (logit), umożliwiającą uproszczoną, lecz ilościową ocenę wpływu poszczególnych parametrów na prawdopodobieństwo wystąpienia wylania. Takie podejście pozwala na istotną redukcję zapotrzebowania na dane wejściowe w porównaniu do pełnoskalowych modeli deterministycznych, a jednocześnie dostarcza użytecznych informacji prognostycznych na potrzeby analizy przypadku (case study).

Zakres analiz obejmował epizody opadowe o czasie trwania od 15 do 135 minut, typowe dla środowisk silnie zurbanizowanych. Wyniki wykazały, że czas trwania opadu (t_r) ma istotny wpływ na wartości współczynników wrażliwości Sxi, szczególnie dla parametrów β, α, γ, n_{imp}, D_{imp} oraz n_{sew}. Wraz ze wzrostem t_r zauważono wyraźny wzrost wartości Sxi, co wskazuje na rosnącą istotność dokładnej kalibracji tych parametrów przy dłuższych opadach. Przykładowo, wartość $S\beta(\lambda 1)$ wzrosła z 0,10 przy t_r = 30 min do 2,24 przy t_r = 75 min, natomiast $S\beta(\lambda 2)$ z 0,01 do 9,71.

Na podstawie przeprowadzonej analizy można stwierdzić, że parametr β – odpowiadający za kształt krzywej odpływu – odgrywa kluczową rolę w procesie kalibracji modelu do prognozowania wystąpienia wylania, zwłaszcza przy zdarzeniach o większym czasie trwania. Wyniki przedstawiono na rysunku 22.

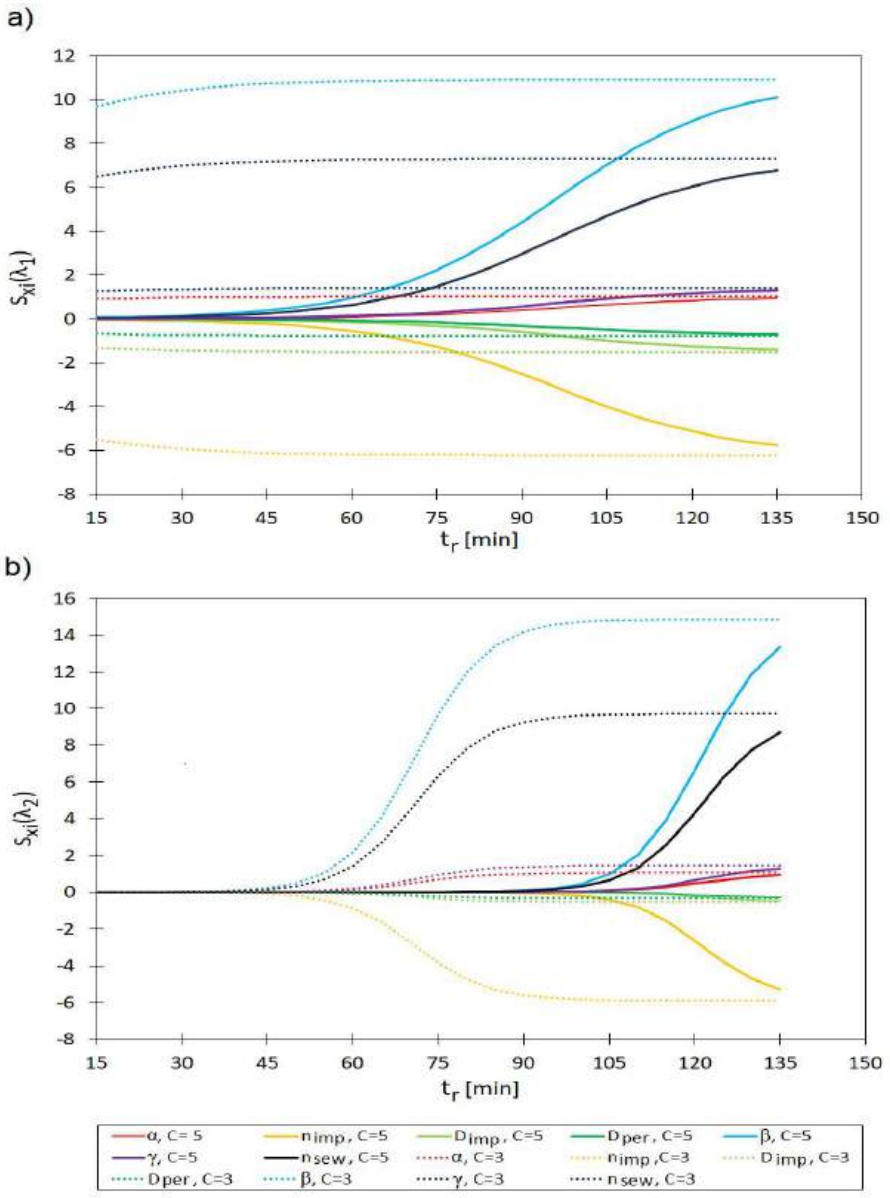

Rysunek 22 Wpływ czasu trwania opadu (t_r) i okresu (C) na współczynnik czułości. a) S(λ1)xi, b) S(λ2)xi dla wartości parametrów modelu SWMM (xi: α, β, γ, n_{imp}, D_{imp}, D_{per}, n_{sew})

Stwierdzono również, że wzrost intensywności opadu powoduje obniżenie wartości współczynników wrażliwości, co wskazuje na osłabienie wpływu parametrów modelowych na wyniki symulacji w warunkach silnych, krótkotrwałych deszczów. Wskazuje to na konieczność uwzględnienia charakterystyki opadów przy kalibracji i stosowaniu modeli predykcyjnych, szczególnie w warunkach miejskich.

W celu dalszego pogłębienia analizy zastosowano współczynnik $\kappa = t_{r2} / t_{r1}$, wyrażający stosunek czasu opadu prowadzącego do przekroczenia wartości λ_2 względem

czasu opadu prowadzącego do przekroczenia λ_1. Analizę przeprowadzono dla czterech parametrów: β, n_{sew}, n_{imp} oraz D_{imp}. Wyniki zestawiono na rysunku 23.

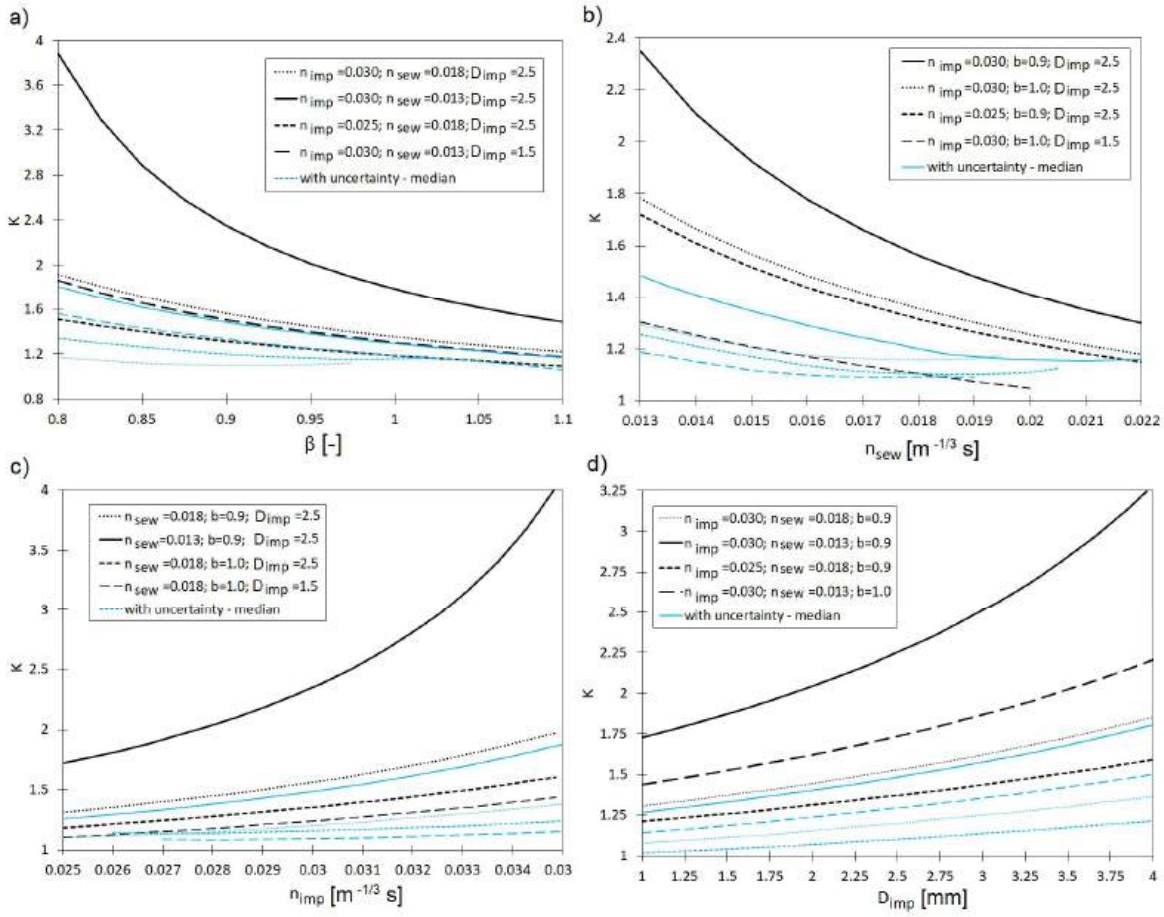

Rysunek 23 Wpływ zidentyfikowanych parametrów SWMM: a) β, b) n_{sew}, c) n_{imp} oraz d) D_{imp} na wartość κ dla C = 5

Zaobserwowano, że wzrost wartości β oraz n_{sew} prowadzi do spadku wartości κ, co oznacza, że krótszy opad jest wystarczający do przekroczenia progu λ_2. Natomiast wzrost n_{imp} i D_{imp} skutkował zwiększeniem κ, co wskazuje na wyższą odporność układu kanalizacyjnego na krótkie epizody opadowe.

Dodatkowo wykazano, że opady o większej intensywności częściej prowadzą do przekroczenia progu λ_1 niż λ_2. Sugeruje to, że system kanalizacji deszczowej jest bardziej podatny na przeciążenia objętościowe niż na pełne zalania, co należy uwzględnić w projektowaniu oraz modernizacji sieci.

Stwierdzono, że jednostkowa objętość wylania λ_1 jest skutecznym wskaźnikiem diagnostycznym dla oceny przeciążeń hydraulicznych. Właściwości retencyjne powierzchni oraz charakterystyka opadu w bezpośredni sposób determinują ryzyko wystąpienia przeciążenia. Zastosowana metoda, integrująca analizę wrażliwości z

podejściem operacyjnym, pozwala na szybką identyfikację parametrów krytycznych i lokalizacji o podwyższonym ryzyku bez konieczności wykonywania pełnych symulacji hydraulicznych.

W świetle uzyskanych wyników dalsze działania badawcze powinny być ukierunkowane na opracowanie uniwersalnego narzędzia do identyfikacji wylania ścieków w małej niehomogenicznej zlewni oraz na redukcji niepewności danych wejściowych do modelu poprzez ich optymalny dobór na etapie kalibracji.

6.4. Integrated model for the fast assessment of flood volume: Modelling – management, uncertainty and sensitivity analysis (A4)

Bazując na wynikach uzyskanych w etapie A3, opracowano uniwersalny, skalowalny model wspierający kalibrację modeli mechanistycznych oraz prognozowanie wylania ścieków. W odpowiedzi na rosnące zapotrzebowanie na narzędzia umożliwiające ocenę funkcjonowania systemów kanalizacyjnych przy ograniczonej dostępności danych oraz w warunkach narastającej złożoności przestrzennej układów sieciowych, zaproponowano model oparty na analizie logistyczno-regresyjnej. Model ten integruje informacje o strukturze przestrzennej zlewni (w tym wymiar fraktalny, FD), parametrach retencyjnych (Vrd/Vkd) oraz charakterystyce opadów (czas trwania t_r, głębokość P_t) w celu prognozowania prawdopodobieństwa przekroczenia progu objętości odpływu jednostkowego z danego epizodu opadowego ($\kappa \geq 13$ m³/ha).

Wyniki analizy wrażliwości, przedstawione na rysunku 24, wskazują, że zarówno czas trwania opadu (t_r), jak i wybrane parametry strukturalne zlewni – wymiar fraktalny (FD) oraz stosunek objętości retencyjnej do całkowitej (Vrd/Vkd) – istotnie wpływają na czułość modelu względem współczynników β i n_{imp}. Wydłużenie t_r powodowało wzrost znaczenia parametrów opisujących retencję oraz właściwości hydrauliczne powierzchni wskazując na silną zależność odpowiedzi modelu od cech epizodu opadowego (Rysunek 24c, 24d).

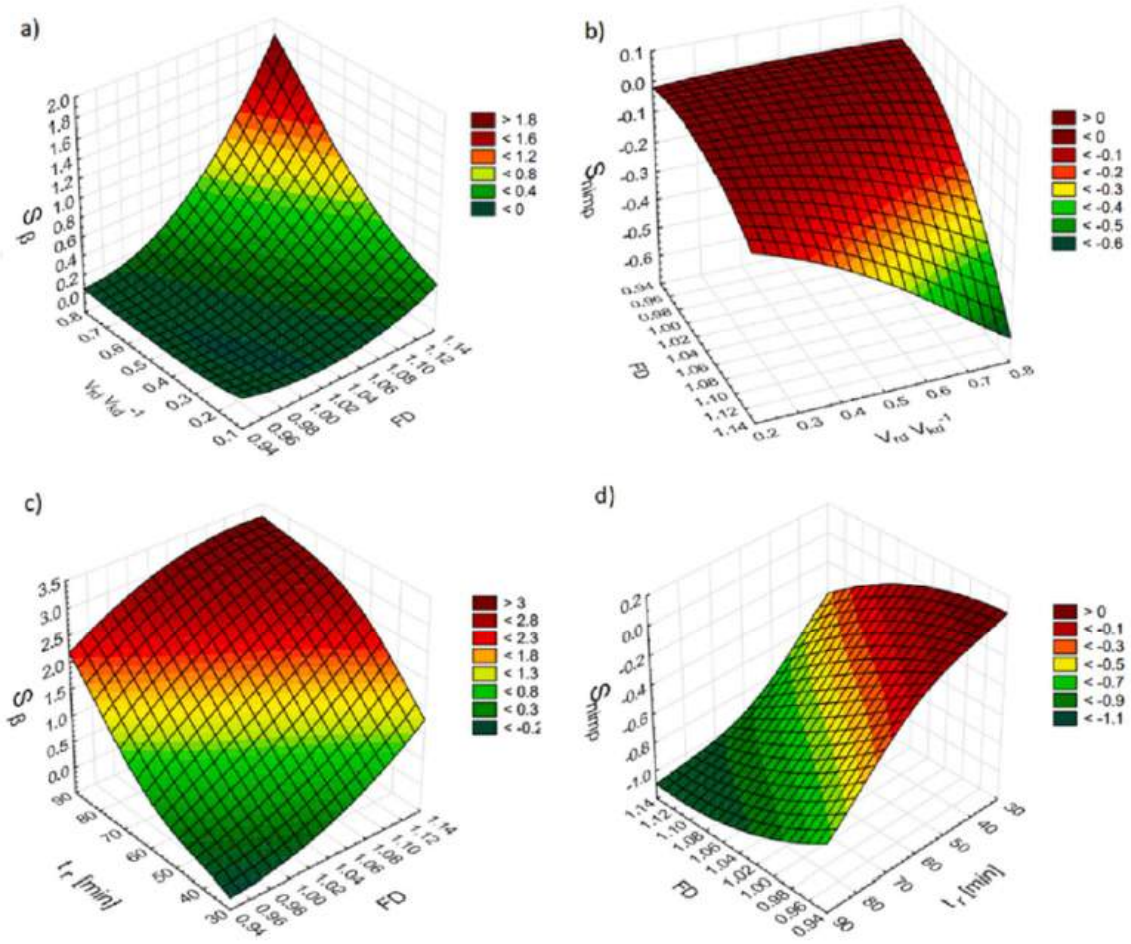

Rysunek 24 Wpływ współczynnika retencji ($Vrd \cdot Vkd^{-1}$) oraz wymiaru fraktalnego (FD) na: a) Sβ, b) Sn_{imp}. Wpływ czasu trwania opadu (t_r) oraz wymiaru fraktalnego (FD) na: c) Sβ, d) Sn_{imp}

W dalszej kolejności istotny wpływ na wyniki analizy wrażliwości GSA (Global Sensitivity Analysis) miały parametry strukturalne zlewni. Zarówno stosunek objętości retencyjnej do całkowitej (Vrd/Vkd), jak i wymiar fraktalny (FD) wywierały wyraźny wpływ na czułość modelu względem tych parametrów. Wzrost FD w zakresie od 0,94 do 1,14 powodował systematyczny wzrost wartości współczynników wrażliwości $S\beta$ i Sn_{imp}, niezależnie od długości trwania opadu (Rysunek 24a, 24b). Obserwacja ta sugeruje, że bardziej rozgałęzione i topologicznie złożone sieci kanalizacyjne są bardziej podatne na zmiany warunków powierzchniowych.

Zaobserwowane korelacje są spójne z wynikami uzyskanymi w modelu SWMM, w którym współczynniki β i n_{imp} wykazywały dominujący wpływ na maksymalne przepływy oraz objętość odpływu. Ich znaczenie rosło zarówno wraz z wydłużeniem czasu trwania opadu, jak i ze wzrostem wartości FD (Fatone i in., 2021). Powyższe wyniki jednoznacznie potwierdzają konieczność uwzględniania struktury przestrzennej sieci kanalizacyjnej – w tym topologii opisanej za pomocą FD – w procesach modelowania, kalibracji oraz

planowania modernizacji systemów odwodnienia miejskiego (Cristiano i in., 2019; Ichiba i in., 2018; Teweldebrhan i in., 2020).

Zintegrowany model umożliwia również kalibrację wybranych parametrów modelu SWMM. W tym celu zastosowano symulator Random Forest, zbudowany na podstawie danych z dwóch epizodów opadowych (24.07.2011 i 15.09.2010), które obejmowały jednoczesne pomiary przepływu (MES1) oraz opadu (stacja zlokalizowana w promieniu 2,5 km, rozdzielczość czasowa: 1 minuta). Wiarygodność symulacji oceniano na podstawie funkcji L(Q/θ), wyznaczonej metodą GLUE, przyjmując wartość referencyjną L(Q/θ) = 0,007.

W konfiguracji n_{sew} – d_{imp} – β, w której parametry n_{sew} i d_{imp} były stałe, a wartość β była obliczana, kluczowy wpływ na wartość β wykazywał parametr d_{imp}, podczas gdy wpływ n_{sew} był marginalny. Natomiast w wariancie, w którym zarówno d_{imp}, jak i β były zmienne, zaobserwowano silną interakcję pomiędzy tymi parametrami – zmiany jednego z nich przekładały się bezpośrednio na wartość n_{sew}. Wskazuje to, że w warunkach ograniczonej dostępności danych konieczne jest uwzględnianie wzajemnych zależności między parametrami retencyjnymi i hydraulicznymi.

Rysunek 25 przedstawia zależności między parametrami modelu SWMM, ukazując ich wpływ na jakość dopasowania wyników symulacji.

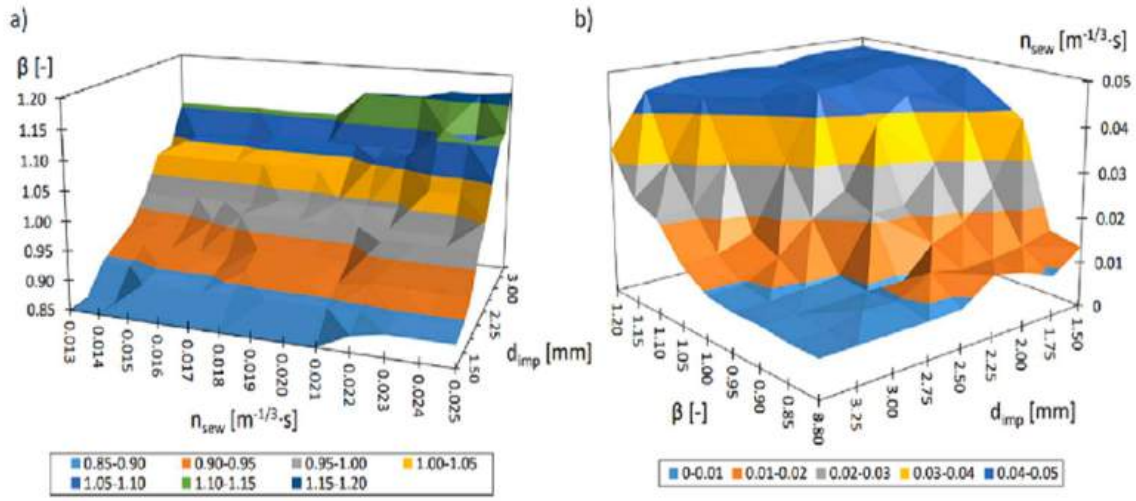

Rysunek 25 (a) Wpływ współczynnika szorstkości Manninga dla kanałów (n_{sew}) oraz głębokości retencji powierzchniowej na powierzchniach nieprzepuszczalnych (d_{imp}) na współczynnik korekcyjny dla procentu powierzchni nieprzepuszczalnych (β). (b) Wpływ głębokości retencji powierzchniowej na powierzchniach nieprzepuszczalnych (d_{imp}) oraz współczynnika korekcyjnego dla procentu powierzchni nieprzepuszczalnych na współczynnik szorstkości Manninga dla kanałów (n_{sew})

Jak pokazano na rysunku 25a, jednoczesny wzrost współczynnika korekcyjnego β (od 0,80 do 1,20) oraz współczynnika szorstkości kanałów n_{sew} (od 0,009 do 0,012 $m^{1/3} \cdot s$) wymagał zwiększenia głębokości retencji na powierzchniach nieprzepuszczalnych (d_{imp}) z 1,5 mm do 3,5 mm. Z kolei rysunek 25b przedstawia zależność odwrotną – zmiany wartości d_{imp} i β prowadzą do dostosowania parametru n_{sew}.

Spośród analizowanych zmiennych, d_{imp} wykazał najwyższą wrażliwość, wskazując na jego dominującą rolę w kalibracji modelu. Zaobserwowane interakcje potwierdzają konieczność stosowania podejścia wieloparametrycznego (Beven i Binley, 2014), ponieważ dokładność odwzorowania zjawisk hydrologicznych zależy nie tylko od wartości pojedynczych parametrów, ale również od ich wzajemnych relacji.

Podsumowując, topologia układu kanalizacyjnego, opisana przez wymiar fraktalny, stanowi kluczowy czynnik warunkujący czułość modelu względem parametrów retencyjnych i hydraulicznych. Uwzględnienie tych interakcji w modelach predykcyjnych, takich jak regresja logistyczna, nie tylko zwiększa wiarygodność prognoz powodziowych, ale także umożliwia optymalizację procesów modernizacyjnych poprzez ograniczenie kosztów kalibracji i potrzeby rozbudowanego monitoringu terenowego (Fraga i in., 2016; Martins i in., 2017).

6.5. An innovative method of predicting the maximum flow in stormwater sewage systems using soft-sensors (A5)

Problem doboru średnicy i określenia przepływu maksymalnego w małych niehomogenicznych zlewniach zlokalizowanych w zlewniach miejskich ma obecnie szeroki zasięg zarówno praktyczny, jak i badawczy (Cristiano i in., 2019; Gires i in., 2017). Obecnie zwykle uwzględnia się tylko sposób zagospodarowania terenu, a pozostałe parametry, takie jak retencja terenowa, retencja kanałowa, szorstkość hydrauliczna czy topologia sieci kanalizacyjnej (wymiar fraktalny), są często pomijane. Budzi to duże wątpliwości metodyczne, bowiem w zlewniach miejskich te parametry charakteryzują się dużą zmiennością i – w kontekście danych literaturowych oraz symulacji Monte Carlo – mają istotny wpływ na wyniki obliczeń przepływów maksymalnych oraz ocenę ryzyka przeciążenia systemu (Fraga i in., 2016; Zhang i in., 2022; Szeląg i in., 2022a).

W pracy opracowano zintegrowany model predykcyjny oparty na metodzie MARS (Friedman, 1991; Friedman i Roosen, 1995), równocześnie podejmując próbę skorelowania estymowanych współczynników w modelu empirycznym z danymi opadowymi, co ma duże znaczenie z punktu widzenia redukcji nakładów obliczeniowych

na etapie tworzenia modeli ML oraz zwiększenia efektywności kalibracji parametrów hydraulicznych w warunkach niepewności (Szeląg i in., 2024).

Przeprowadzona analiza wykazała jednoznacznie, iż rozkład czasowy intensywności opadu istotnie wpływa na wartości estymowanych parametrów w modelu regresyjnym MARS, a tym samym na kształtowanie się przepływu maksymalnego Q_m*. Wyniki przedstawione w tabeli 4, zawierającej bezwzględne wartości współczynników czułości αi, obliczonych względem pełnego zakresu zmienności zmiennych wejściowych xi, jednoznacznie wskazują na dominujący wpływ takich parametrów jak udział powierzchni nieprzepuszczalnych F_{imp}*, szorstkość kanałów n_{sew}* oraz głębokość retencji powierzchni nieprzepuszczalnych d_{imp}*. Wartości αi dla tych parametrów wykazywały znaczną zmienność pomiędzy różnymi rozkładami opadów oraz ich czasem trwania. Świadczy to o nieliniowym i interakcyjnym charakterze zależności między strukturą opadu a odpowiedzią hydrologiczną modelu.

*Tabela 4 Bezwzględne wartości współczynników w modelu MARS w zależności od rozkładu opadu * – tabela przedstawia współczynniki α_i uwzględniające maksymalny zakres zmienności x_i*

	F_{imp}*	n_{sew}*	d_{imp}*	β*	n_{imp}	α*	γ*	Gk*	FD*	Vkp*
30a_R2	0.20	0.20	0.16	0.09	0.10	0.09	0.02	0.00	0.07	0.00
30a_R3	0.20	0.08	0.20	0.11	0.07	0.11	0.02	0.03	0.17	0.00
30a_R4	0.26	0.10	0.20	0.11	0.07	0.11	0.02	0.00	0.11	0.00
30b_R2	0.43	0.26	0.10	0.10	0.11	0.10	0.02	0.09	0.00	0.01
30b_R3	0.16	0.09	0.12	0.11	0.07	0.11	0.02	0.04	0.18	0.00
30b_R4	0.19	0.18	0.14	0.14	0.07	0.14	0.02	0.03	0.18	0.00
60_R2	0.20	0.22	0.26	0.10	0.09	0.10	0.00	0.03	0.09	0.00
60_R3	0.24	0.01	0.35	0.01	0.06	0.01	0.00	0.00	0.01	0.00
60_R4	0.31	0.01	0.37	0.10	0.01	0.10	0.00	0.00	0.00	0.00

W badaniu wykorzystano trzy warianty czasowych rozkładów opadu (R2, R3, R4), przedstawione na rysunku 26, które odzwierciedlają różne scenariusze rozkładu intensywności przy zachowaniu tej samej całkowitej wysokości opadu: typ R2 cechował się wysoką intensywnością na początku epizodu, typ R3 reprezentował równomierny

rozkład w czasie, natomiast typ R4 charakteryzował się kulminacją opadu w środkowej fazie.

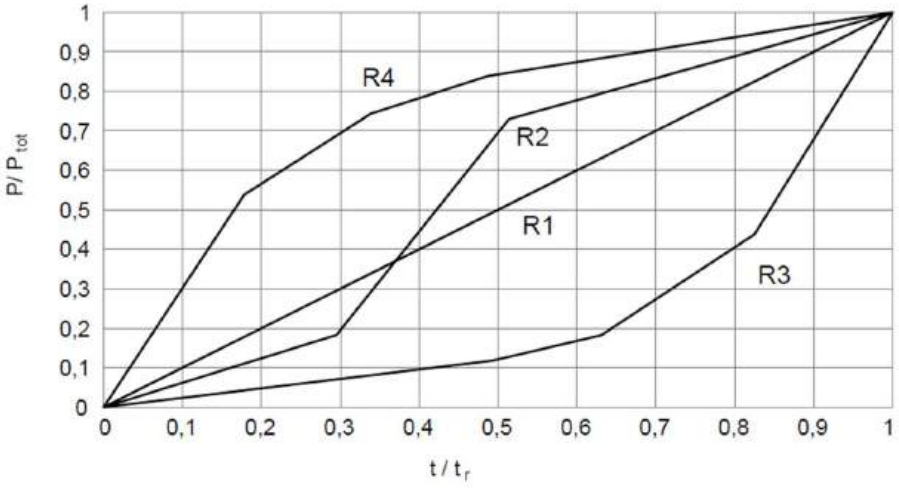

Rysunek 26 Czasowe rozkłady opadów (ξ = R1, R2, R3, R4)

Umożliwiło to zidentyfikowanie różnic w reakcji modelu na dynamikę zdarzeń opadowych oraz ocenę wrażliwości poszczególnych parametrów modelowych. Analiza wykazała, iż dla epizodów krótkotrwałych (30 min) dominujący wpływ miały n_{sew}* oraz α, natomiast w przypadku zdarzeń długotrwałych (60 min) istotne znaczenie uzyskał parametr d_{imp}* - bezpośredni związek z mechanizmami powierzchniowego retencjonowania odpływu.

Uzyskane modele oraz wyniki prognoz posłużyły jako podstawa do przeprowadzenia analizy ryzyka, w której podstawę oceny działania systemu kanalizacyjnego stanowił przepływ maksymalny, obliczany z wykorzystaniem modeli MARS. Modele te uwzględniały zarówno zmienność struktury czasowej opadów, jak i niepewność parametrów modelu SWMM. Ma to istotne znaczenie z punktu widzenia oceny niezawodności funkcjonowania systemów odwodnienia w warunkach ekstremalnych zdarzeń opadowych oraz w kontekście adaptacji infrastruktury kanalizacyjnej do prognozowanych zmian klimatycznych.

Wyniki analizy wykazały, że – jak przedstawiono w tabeli 5 – rozkład czasowy intensywności opadów istotnie wpływa na wartości estymowanych współczynników modeli MARS, często w większym stopniu niż całkowita suma opadu.

Tabela 5 Współczynnik korelacji (Rij) pomiędzy oszacowanymi współczynnikami w modelach MARS a charakterystykami opadów

	$\alpha(F_{imp})$	**α(FD)**	**α(Gk)**	**$\alpha(n_{sew})$**	**$\alpha(d_{imp})$**	**α(β)**	**$\alpha(n_{imp})$**	**α(α)**	**α(γ)**
Pt	0.37	0.48	0.88	0.42	0.00	0.05	0.42	0.63	0.16
q	0.37	0.48	0.88	0.42	0.00	0.05	0.42	0.63	0.16
$P_{t=5}$	0.45	0.59	0.91	0.38	0.08	0.10	0.17	0.63	0.20
FD_r	0.37	0.44	0.73	0.65	0.12	0.40	0.33	0.40	0.25
$P_{t=5}/P_{t=10}$	0.48	0.71	0.71	0.28	0.15	0.38	0.03	0.57	0.07
$P_{t=5}/P_{t=15}$	0.27	0.61	0.52	0.03	0.27	0.18	0.07	0.72	0.10
$P_{t=10}/P_{t=15}$	0.48	0.71	0.71	0.28	0.15	0.38	0.03	0.57	0.07
$P_{t=5}/P_t$	0.40	0.68	0.64	0.30	0.20	0.48	0.00	0.58	0.17
$P_{t=10}/P_t$	0.63	0.79	0.64	0.28	0.15	0.33	0.02	0.42	0.02
$P_{t=15}/P_t$	0.33	0.40	0.80	0.33	0.03	0.29	0.44	0.61	0.14
P_{sr}	0.45	0.71	0.60	0.15	0.08	0.55	0.18	0.52	0.20
$P_{t=5}/P_{sr}$	0.17	0.33	0.01	0.27	0.10	0.63	0.62	0.00	0.50
$P_{t=10}/P_{sr}$	0.03	0.09	0.28	0.40	0.13	0.48	0.62	0.27	0.53
$P_{t=15}/P_{sr}$	0.15	0.06	0.29	0.00	0.08	0.47	0.52	0.50	0.10
$P_{0.5tr}$	0.40	0.37	0.42	0.52	0.02	0.33	0.00	0.03	0.38
$P_{sr}/P_{0.5tr}$	0.43	0.59	0.55	0.18	0.08	0.35	0.28	0.35	0.02
$P_{t=5}/P_{0.5tr}$	0.58	0.69	0.41	0.10	0.10	0.30	0.20	0.18	0.05
$P_{t=10}/P_{0.5tr}$	0.59	0.49	0.50	0.46	0.07	0.19	0.03	0.02	0.14
$P_{t=15}/P_{0.5tr}$	0.27	0.34	0.52	0.49	0.02	0.41	0.02	0.23	0.32

Wyniki wykazały wysokie wartości współczynnika korelacji Rij, szczególnie dla: α(Gk) i Pt=5 (Rij=0,91), α(FD) i $Pt10/Pt$/Pt (Rij=0,79), a także $\alpha(\alpha)$ i $Pt5/Pt15$/Pt15 (Rij = 0,72). Oznacza to, że zmienność struktury czasowej opadu wykazuje istotną i często silniejszą korelację z estymowanymi współczynnikami modelu niż całkowita suma opadu, co podkreśla kluczowe znaczenie precyzyjnego opisu przebiegu intensywności opadu w czasie.

Wyniki symulacji probabilistycznych, przedstawione na Rysunku 27, potwierdzają złożoność analizowanych relacji.

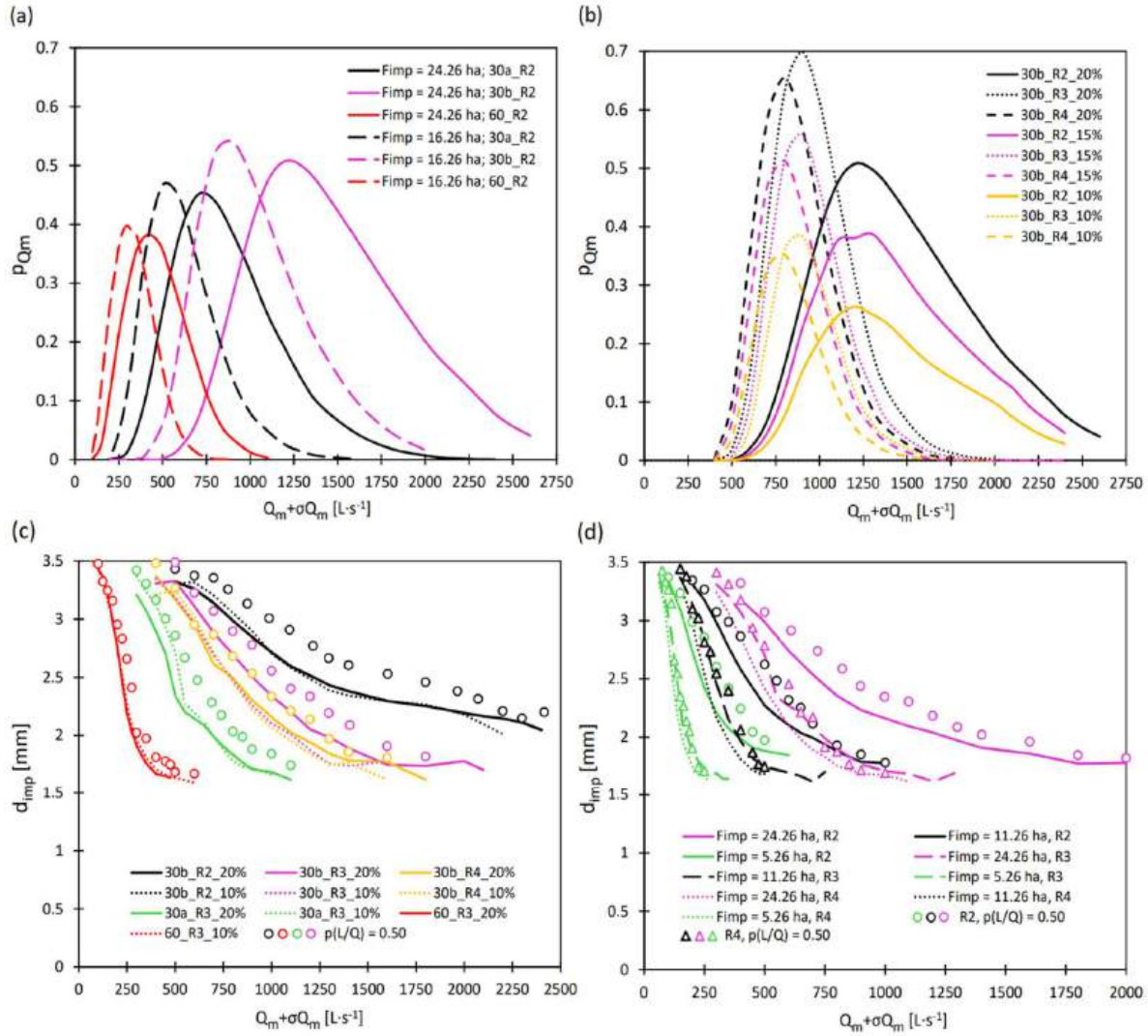

Rysunek 27 (a) Wpływ maksymalnego przepływu projektowego (Q_m), charakterystyki zlewni (F_{imp}) oraz danych opadowych na prawdopodobieństwo pQ_m; (b) Wpływ maksymalnego przepływu projektowego (Q_m), rozkładu opadu (typ R2, R3, R4) oraz dopuszczalnego progu niepewności (σ) na prawdopodobieństwo pQ_m; (c) Wpływ maksymalnego przepływu projektowego (Q_m), danych opadowych oraz dopuszczalnego progu niepewności (σ) na d_{imp}, z pominięciem i uwzględnieniem prawdopodobieństwa parametrów modelu SWMM;(d) Wpływ maksymalnego przepływu projektowego (Q_m), charakterystyki zlewni (F_{imp}) oraz czasowego rozkładu opadu na dimp, z pominięciem i uwzględnieniem wiarygodności parametrów modelu SWMM

Rysunek 27a ilustruje wpływ parametrów Q_m, F_{imp} oraz charakterystyk opadowych na prawdopodobieństwo przekroczenia wartości projektowej pQ_m, natomiast rysunek 27b uwidacznia znaczenie rozkładu czasowego opadu (R2, R3, R4) oraz niepewności modelowej σ. Zaobserwowano, że zmiana typu opadu z R3 na R2 powodowała wzrost wartości Q_m o 33%, a zwiększenie sumy opadu z 6.0 mm do 8.0 mm skutkowało wzrostem Q_m aż o 68%. Jednocześnie wzrost σ z 10% do 20% prowadził do zwiększenia zmienności

Q_m o 15–20%, co bezpośrednio wpływa na interpretację rezerwy przepustowości systemu kanalizacyjnego. Rysunek 27c i 27d przedstawiają wpływ prawdopodobieństwa parametrów modelu – uwzględniającego lub pomijającego niepewność – na estymowaną wartość głębokości retencji d_{imp}, w zależności od Q_m, F_{imp} oraz rozkładu czasowego opadu. Nieuwzględnienie niepewności parametrów modelu, wynikającej m.in. z uproszczeń w danych GIS lub zbyt wąskiego zakresu kalibracji, może prowadzić do istotnych błędów w szacowaniu objętości retencyjnej, skutkujących niedoszacowaniem wymagań projektowych.

Wyniki wskazują, że wiarygodna ocena rezerwy przepustowości wymaga uwzględnienia nie tylko zmienności opadów, lecz także niepewności kalibrowanych parametrów modelu SWMM i ich wpływu na odpowiedź modelową. Zastosowanie podejścia probabilistycznego, integrującego rozkłady opadów oraz niepewność parametrów, pozwala na realistyczną ocenę marginesu bezpieczeństwa hydraulicznego i wspiera podejmowanie trafnych decyzji modernizacyjnych w zlewniach miejskich.

Istotną rolę odgrywają przy tym parametry przestrzenne, takie jak F_{imp}* i FD*, które – jako zmienne o stabilnym wpływie na Q_m*– powinny być pozyskiwane z możliwie wysoką dokładnością przestrzenną i tematyczną. Ich jakość warunkuje poprawność kalibracji oraz interpretację wyników modelowania.

Ponadto wykazano, że rozkład czasowy opadu w znacznym stopniu kształtuje zależności między parametrami modelu a odpowiedzią systemu. Parametry hydrauliczne, takie jak n_{sew}*, α i β, wykazują nieliniowy, zmienny charakter wpływu, który silnie zależny od typu i intensywności opadu. Brak wystarczającego zróżnicowania danych opadowych utrudnia identyfikację kluczowych interakcji, ograniczając tym samym możliwości praktycznego zastosowania modeli regresyjnych.

7. PODSUMOWANIE

Opracowany w ramach rozprawy model badawczy stanowi holistyczne podejście do i projektowania systemów odwodnienia miejskiego. Uwzględnia on pełne spektrum czynników wpływających na funkcjonowanie kanalizacji deszczowej – od uwarunkowań fizycznogeograficznych i topologii zlewni, przez parametry hydrauliczne i zmienność opadów, po niepewność modelową i pomiarową. Połączenie modelowania mechanistycznego (SWMM), metod statystycznych (regresja logistyczna, MARS), technik uczenia maszynowego oraz analiz wrażliwości i ryzyka umożliwiło kompleksową ocenę

efektywności systemów kanalizacyjnych w kontekście postępującej urbanizacji i zmian klimatu.

W odpowiedzi na zidentyfikowane wyzwania opracowano zintegrowane narzędzie aplikacyjne umożliwiające spójną analizę danych opadowych, przestrzennych i infrastrukturalnych w jednym środowisku obliczeniowym. Walidacja przeprowadzona na danych z sześciu mezoregionów Polski potwierdziła jego wysoką adaptacyjność do zróżnicowanych warunków fizycznogeograficznych oraz przydatność w praktyce inżynierskiej. Rozwiązanie znajduje zastosowanie od wymiarowania elementów zielonej infrastruktury po projektowanie zbiorników retencyjnych z przelewami burzowymi, stanowiąc istotny krok w rozwoju inteligentnych systemów wspomagania decyzji w inżynierii wodno-kanalizacyjnej.

Przeprowadzone analizy wykazały silną zależność przepływów maksymalnych i objętości wylania od kombinacji parametrów modelu SWMM – takich jak współczynnik szorstkości (n_{sew}), udział powierzchni nieprzepuszczalnych (β) oraz głębokość retencji (d_{imp}) – a także od struktury czasowej opadów. Szczególne znaczenie miała sekwencja opadów, której zmiana prowadziła do wzrostu przepływów maksymalnych nawet o 30 – 70%, co wskazuje na kluczową rolę zmienności opadu w kształtowaniu dynamiki odpływu.

Zastosowane algorytmy uczenia maszynowego (RF, regresja logistyczna, MARS) osiągnęły bardzo wysoką trafność predykcyjną ($R^2 = 0,96$; RMSE = 0,038), potwierdzając ich przydatność w prognozowaniu przepływów maksymalnych oraz jednostkowej objętości wylania. Modele te nie tylko poprawiły dokładność predykcji względem podejść deterministycznych, ale również umożliwiły ograniczenie ryzyka przeciążeń hydraulicznych. Ich elastyczność pozwala na regionalizację oraz zastosowanie w różnych typach zlewni, również w warunkach ograniczonej dostępności danych. Dodatkowo wspierają one parametryzację badań terenowych i selekcję zmiennych istotnych w procesie kalibracji modeli SWMM.

Istotnym aspektem pracy była integracja analizy ryzyka i niepewności z wykorzystaniem symulacji Monte Carlo, co umożliwiło ilościową ocenę niezawodności systemów odwodnienia oraz uwzględnienie współczynników rezerwy hydraulicznej w procesie projektowym. Wzrost poziomu niepewności (σ z 10% do 20%) powodował zwiększenie zmienności przepływu maksymalnego o 15 – 20%, co pozwoliło określić marginesy bezpieczeństwa i poprawić odporność systemów na zjawiska ekstremalne. Takie podejście umożliwia skuteczne zarządzanie zlewniami w warunkach niepewności, wynikającej zarówno z niestabilności klimatycznej, jak i ograniczeń danych pomiarowych.

Cały cykl badawczy odpowiada na aktualne wyzwania związane z przeciążeniami hydraulicznymi i ryzykiem powodzi miejskich. Opracowane rozwiązania zwiększają odporność systemów odwodnienia na zjawiska ekstremalne, wspierają efektywną alokację zasobów oraz wdrażanie strategii opartych na zielonej infrastrukturze. W szerszej perspektywie mogą one stanowić podstawę do rozwoju uniwersalnych soft-sensorów odpływu, dostosowujących się do zróżnicowanych warunków klimatycznych, urbanistycznych i przestrzennych.

W świetle uzyskanych wyników, dalsze kierunki badań powinny koncentrować się na rozwoju zintegrowanych, adaptacyjnych narzędzi predykcyjnych, które będą łączyć modelowanie mechanistyczne z nowoczesnymi metodami uczenia maszynowego, takimi jak sieci głębokie (deep learning) czy algorytmy oparte na analizie szeregów czasowych (np. LSTM). Technologie te mogą znacząco zwiększyć zdolność przewidywania odpływów w warunkach wysokiej zmienności opadów oraz ograniczonej dostępności danych pomiarowych. Kluczowym obszarem dalszego rozwoju pozostaje także automatyzacja procesu kalibracji modeli oraz pełniejsze uwzględnienie zmiennych topologicznych i wysokościowych opisujących sieć kanalizacyjną. W kontekście zidentyfikowanej luki badawczej oraz postawionej hipotezy, niezbędne jest rozszerzenie analiz na inne typy zlewni miejskich, a także integracja danych klimatycznych i urbanistycznych w celu długoterminowej oceny odporności systemów odwodnienia na zjawiska ekstremalne, w tym intensywne opady krótkotrwałe i powodzie błyskawiczne.

Bibliografia

1. *Addison-Atkinson, W., Chen, A.S., Memon, F.A., Chang, T.J., 2022. Modelling urban sewer flooding and quantitative microbial risk assessment: a critical review. J. Flood Risk Mangement. 15, e12844.*
2. *Akan, A.O. (1993). Urban Stormwater hydrology – A Guide to Engineering Calculations, Technomic, Lancaster, PA.*
3. *Amiri, H., Azadi, S., Javadpour, S., Naghavi, A.A., Boczkaj, G. (2022). Selecting wells for an optimal design of groundwater monitoring network based on monitoring priority map: a Kish Island case study. Water Resour. Ind. 27, 100172 https://doi.org/10.1016/j.wri.2022.100172.*
4. *Barco, J., Wong, K.M., Stenstrom, M.K. (2008). Automatic calibration of the U.S. EPA SWMM model for a large urban catchment. J. Hydraul. Eng. 134, 466–474. https://doi.org/10.1061/(ASCE)0733-9429(2008)134:4(466)*
5. *Beven, K., Binley, A. GLUE: 20 years on. Hydrol. Process. 2014, 28, 5897–5918. https://doi.org/10.1002/hyp.10082*

6. *Boogaard, F., & Kondratenko, J. (2024). Low impact development devices DNA of cities for long term stormwater management strategies. Discover Water, 4(34). https://doi.org/10.1007/s43832-024-00090-0*
7. *Breiman, L. (2001). Random forests. Machine Learning, 45(1), 5–32. https://doi.org/10.1023/A:1010933404324*
8. *Cea, L., & Costabile, P. (2022). Flood Risk in Urban Areas: Modelling, Management and Adaptation to Climate Change. A Review. Hydrology, 9(3), 50. https://doi.org/10.3390/hydrology9030050*
9. *Chan, F.K.S., Griffiths, J.A., Higgitt, D., Xu, S., Zhu, F., Tang, Y.T. (2018). "Sponge City"in China – A breakthrough of planning and flood risk management in the urban context. Land Use Policy, 76, 772–778. https://doi.org/10.1016/j.landusepol.2018.03.005*
10. *Chen, J., Liu, L., Zhao, Y., & Li, Y. (2023). Fast prediction of urban flooding water depth based on CNN–LSTM model and hydrodynamic simulations in the central city of Zhoukou. Water, 15(7), 1397. https://doi.org/10.3390/w15071397*
11. *CIRIA (2015). The SuDS Manual: Sustainable Drainage Systems. CIRIA Report C753, London.*
12. *Cristiano, E., ten Veldhuis, M.C., Wright, D.B., Smith, J.A., van de Giesen, N. (2019). The influence of rainfall and catchment critical scales on urban hydrological response sensitivity. Water Resour. Res. 55, 3375–3390. https://doi.org/10.1029/2018WR024143*
13. *De Martino, G., De Paola, F., Fontana, N., Marini,G., & Ranucci, A. (2010). Preliminary design of combined sewer overflows and stormwater tanks in Southern Italy. Irrigation and Drainage, 60(4), 544–555. https://doi.org/10.1002/ird.591*
14. *De Paola, F., & Ranucci, A. (2012). Analysis of spatial variability for stormwater capture tanks assessment. Irrigation and Drainage, 61(6), 682–690. https://doi.org/10.1002/ird.1675*
15. *DWA-A 118E. (2006). Hydraulic Dimensioning and Verification of Drain. and Sewer Systems, DWA German Association for Water, Wastewater and Waste, Hennef, Germany.*
16. *European Commission. (2015). Towards an EU Research and Innovation policy agenda for nature-based solutions and renaturing cities. Final Report of the Horizon 2020 Expert Group on Nature-Based Solutions and Re-naturing Cities. Brussels: European Commission. https://doi.org/10.2777/479582*
17. *Fisher, A., Rudin, C. and Dominici, F. (2019). All Models are Wrong, but Many are Useful: Learning a Variable's Importance by Studying an Entire Class of Prediction Models Simultaneously. Journal of Machine Learning Research. 20: 177. 10.48550/arXiv.1801.01489.*
18. *Fletcher, T. D., Shuster, W., Hunt, W. F., Ashley, R., Butler, D., Arthur, S., ... & Viklander, M. (2015). SUDS, LID, BMPs, WSUD and more–The evolution and application of terminology surrounding urban drainage. Urban water journal, 12(7), 525-542. https://doi.org/10.1080/1573062X.2014.916314*
19. *Fraga, I., Cea, L., Puertas, J., Suárez, J., Jiménez, V., Jácome, A. (2016). Global sensitivity and GLUE-based uncertainty analysis of a 2D-1D dual urban drainage*

model. J Hydrol Eng., 2016, 21, 04016004. https://doi.org/10.1061/(ASCE)HE.1943-5584.0001335

20. *Friedman, J. H. (1991). Multivariate adaptive regression splines. The Annals of Statistics, 19(1), 1–67. https://doi.org/10.1214/aos/1176347963*
21. *Friedman, J., & Roosen, C. B. (1995). An introduction to multivariate adaptive regression splines. Statistical Methods in Medical Research, 4(3), 197–217. https://doi.org/10.1177/096228029500400303*
22. *Fu, G., Butler, D. (2014). Copula-based frequency analysis of overflow and flooding in urban drainage systems. J. Hydrol., 2014, 510, 49–58. https://doi.org/10.1016/j.jhydrol.2013.12.006*
23. *Gires, A., Tchiguirinskaia, I., Schertzer, D., Ochoa-Rodriguez, S., Willems, P., Ichiba, A., Wang, L.-P., Pina, R., Van Assel, J., Bruni, G., Murla Tuyls, D., ten Veldhuis, M.C. (2017). Fractal analysis of urban catchments and their representation in semidistributed models: imperviousness and sewer system. Hydrol. Earth Syst. Sci. 21,2361–2375. https://doi.org/10.5194/hess-21-2361-2017*
24. *Guo, K., Guan, M., Yu, D. (2021). Urban surface water flood modelling – a comprehensive review of current models and future challenges. Hydrol. Earth Syst. Sci. 25 (2843–2860), 2021. https://doi.org/10.5194/hess-25-2843-2021*
25. *Ichiba, A., Gires, A., Tchiguirinskaia, I., Schertzer, D., Bompard, P., & Ten Veldhuis, M.-C. (2018). Scale effect challenges in urban hydrology highlighted with a distributed hydrological model. Hydrology and Earth System Sciences, 22(1), 331–350. https://doi.org/10.5194/hess-22-331-2018*
26. *Jato-Espino, D., Sillanp¨a¨a, N., Andr´es-Dom´enech, I., Rodriguez-Hernandez, J. (2018). Flood risk assessment in urban catchments using multiple regression analysis. J. Water Resour. Planning Manag. 144, 04017085. https://doi.org/10.1061/(ASCE)WR.1943-5452.0000874*
27. *Jiang, Y., Zevenbergen, C., & Ma, Y. (2018). Urban pluvial flooding and stormwater management:A contemporary review of China's challenges and "sponge cities" strategy. Environmental Science & Policy, 80, 132–143. https://doi.org/10.1016/j.envsci.2017.11.016*
28. *Kiczko, A., Szeląg, B., Kozioł, A.P., Krukowski, M.,Kubrak, E., Kubrak, J., Romanowicz, R.J. (2018). Optimal capacity of a stormwater reservoir for flood peak reduction. J. Hydrol. Eng. 2018, 23, 04018008. https://doi.org/10.1061/(ASCE)HE.1943-5584.000163*
29. *Kumar, S., Vishwakarma, R. K., Tyagi, V. K., Kumar, V., Kazmi, A. A., Ghosh, N. C., Sasidharan, S., Nayak, P. C., Maurya, N. S., Hasan, R., & Joshi, H. (2024). Stormwater runoff characterization and adaptation of best management practices under urbanization and climate change scenarios. Journal of Hydrology, 635, 131231. https://doi.org/10.1016/j.jhydrol.2024.131231*
30. *Kupczyk E.; Suligowski R. Temporal and Spatial Patterns of High Intensity Rainfalls in Poland. Misc.Geogr. 2000, 9, 77–84, https://doi.org/10.2478/mgrsd-2000-090110*

31. *Kratzert, F., Klotz, D., Herrnegger, M., Sampson, A. K., Hochreiter, S. & Nearing, G. S. (2019). Towards Improved Predictions in Ungauged Basins: Exploiting the Power of Machine Learning. Water Resources Research https://doi.org/10.1029/2019WR026065*
32. *Li, X., Willems, P. (2020). A hybrid model for fast and probabilistic urban pluvial flood prediction. Water Resour. Res. 56 https://doi.org/10.1029/2019WR025128*
33. *Long, ZY., Duan, HF. (2025). Human mobility amplifies compound flood risks in coastal urban areas under climate change. Commun Earth Environ 6, 413 (2025). https://doi.org/10.1038/s43247-025-02406-x*
34. *Martins, R., Rubinato, M., Kesserwani, G., Leandro, J., Djordjevic, S., Shucksmith, J. (2017). Validation of 2D shock capturing flood models around a surcharging manhole. Urban Water J. 14, 892–899. https://doi.org/10.1080/1573062X.2017.1279193*
35. *Miller, J. D., & Hutchins, M. (2017). The impacts of urbanisation and climate change on urban flooding and urban water quality: A review of the evidence concerning the United Kingdom. *Journal of Hydrology: Regional Studies, 12*, 345–362. https://doi.org/10.1016/j.ejrh.2017.06.006*
36. *Palmitessa, R., Grum, M., Engsig-Karup, A.P. & Löwe, R. (2022). Accelerating hydrodynamic simulations of urban drainage systems with physics-guided machine learning. Water Res. 223, 118972 https://doi.org/10.1016/j.watres.2022.118972*
37. *Perdikaki, M., Makropoulos, C. & Kallioras, A. (2022). Participatory groundwater modeling for managed aquifer recharge as a tool for water resources management of a coastal aquifer in Greece. Hydrogeol J 30, 37–58. https://doi.org/10.1007/s10040-021-02427-8*
38. *Piazza, P., & Ursino, N. (2022). Modelling Infiltration Systems' Performance for Efficient, Sustainable or Circular Urban Water Drainage. Water, 14(17), 2620. https://doi.org/10.3390/w14172620*
39. *PN-EN 752:2017 Systemy kanalizacyjne poza budynkami – Zarządzanie systemami kanalizacyjnymi. Warszawa: PKN.*
40. *PN-EN 16933-1:2022 Systemy kanalizacyjne poza budynkami — Projektowanie — Część 1: Zasady rozmieszczania. Warszawa: PKN.*
41. *Pons, V., Abdalla, E. M. H., Tscheikner-Gratl, F., Alfredsen, K., Sivertsen, E., Bertrand-Krajewski, J.-L., & Muthanna, T. M. (2023). Practice makes the model: A critical review of stormwater green infrastructure modelling practice. Water Research, 236, 119958. https://doi.org/10.1016/j.watres.2023.119958*
42. *Rodríguez, M. M., Fu, G., Butler, D., Yuan, Z., & Cook, L. (2024). The effect of green infrastructure on resilience performance in combined sewer systems under climate change. Journal of Environmental Management, 353, 120229. https://doi.org/10.1016/j.jenvman.2024.120229.*
43. *Ruan, X., Sun, H., Shou, W., & Wang, J. (2024). The impact of climate change and urbanization on compound flood risks in coastal areas: A comprehensive review of methods. Applied Sciences, 14(21), 10019. https://doi.org/10.3390/app142110019*
44. *Siekmann, J., & Pinnekamp, J. (2011). Reliability analysis of sewer systems under surcharge. Water Science and Technology, 63(12), 2884–2891.*

45. *Szeląg, B., Suligowski, R., Łagód, G., Łazuka, E., Wlaź, P., Strańsky, D. (2022). Flood occurrence analysis in small urban catchments in the context of regional variability. PLOS ONE, 17(11), e0276312. https://doi.org/10.1371/journal.pone.0276312*
46. *Szeląg, B., Suligowski, R., De Paola, F., Siwicki, P., Majerek, D., Łag´od, G., 2022a. Influence of urban catchment characteristics and rainfall origins on the phenomenon of stormwater flooding: case study. Environ. Model. Softw. 150, 105335 https://doi.org/10.1016/j.envsoft.2022.105335*
47. *Szeląg, B., Kowal, P., Kiczko, A., Białek, A., Wałek, G., Majerek, D., Siwicki, P., Fatone, F., & Boczkaj, G. (2023). Integrated model for the fast assessment of flood volume: Modelling – management, uncertainty and sensitivity analysis. Journal of Hydrology, 625, 129967. https://doi.org/10.1016/j.jhydrol.2023.129967*
48. *Szeląg, B., Fatone, F., Kiczko, A., Majerek, D., Białek, A., Łagód, G., & Dąbek, L. (2024). Extended evaluation of the impact of rainfall, sewer network and land use retention on drainage system performance in a multi-criteria approach – Modelling, sensitivity analysis. Advances in Science and Technology Research Journal, 18(6), 291–303. https://doi.org/10.12913/22998624/192023*
49. *Teweldebrhan, T., Schuler, T.V., Burkhart, J.F., Hjorth-Jensen, M. (2020). Coupled machine learning and the limits of acceptability approach applied in parameter identification for a distributed hydrological model. Hydrol. Earth Syst. Sci. 24, 4641–4658. https://doi.org/10.5194/hess-24-4641-2020*
50. *U.S. Environmental Protection Agency. US EPA (2021). 2021 Climate Adaptation Action Plan.*
51. *Wałek, G. (2019). Wpływ dróg na kształtowanie spływu powierzchniowego w obszarze zurbanizowanym na przykładzie zlewni rzeki Silnicy w Kielcach. Jan Kochanowski University Press, Kielce (in Polish), 2019.*
52. *Wolfs, V. & Willems, P. (2016). Modular Conceptual Modelling Approach and Software for Sewer Hydraulic Computations. Water Resources Management, 31, 1, pp. 283–298. https://doi.org/10.1007/s11269-016-1524-2*
53. *Yang, Y. & Chui, T. F. M. (2020). Modelling and interpreting hydrological responses of sustainable urban drainage systems with explainable machine learning methods, Hydrol. And Earth Syst. Sci., 25,11, pp. 5839-5858. https://doi.org/10.5194/hess-25-5839-2021*
54. *Zhang, Z., Xu, Z., Liu, L., & Li, Y. (2022). The hydrological effect and uncertainty assessment by a Monte Carlo method based on the Storm Water Management Model (SWMM). Journal of Hydrology, 605, 127217. https://doi.org/10.1016/j.jhydrol.2022.127217*
55. *Zhao, C., Liu, C., Li, W., Tang, Y., Yang, F., Xu, Y., Quan, L., & Hu, C. (2023). Simulation of urban flood process based on a hybrid LSTM–SWMM model. Water Resources Management, 37(13), 1–17. https://doi.org/10.1007/s11269-023-03600-2*
56. *Zhou, Q. (2014). A Review of Sustainable Urban Drainage Systems Considering the Climate Change and Urbanization Impacts. Water, 6, 4, pp. 976–992. https://doi.org/10.3390/w6040976*

Wykaz rysunków

Wykaz tabel

Załączniki – teksty publikacji:

JEE Journal of Ecological Engineering

Journal of Ecological Engineering, 2025, 26(6), 410–423
https://doi.org/10.12911/22998993/202322
ISSN 2299–8993, License CC-BY 4.0

Received: 2025.01.10
Accepted: 2025.04.07
Published: 2025.04.15

Development of a computational tool for stormwater management in small urban catchments

Anita Białek[1*], Anna Musz-Pomorska[2]

[1] Faculty of Environmental Engineering, Geomatics and Renewable Energy, Kielce University of Technology, Al. Tysiąclecia Państwa Polskiego 7, 25-314 Kielce, Poland
[2] Faculty of Environmental Engineering and Energy, Lublin University of Technology, Nadbystrzycka 38D, 20-618 Lublin, Poland
* Corresponding author's e-mail: anita_bialek@interia.eu

ABSTRACT

This study presents a computational tool for designing and evaluating stormwater management devices in small urban catchments. The tool is highly versatile, supporting the testing of diverse hydrological models tailored to local conditions. It is particularly useful for designing retention tanks, sizing infiltration trench, and modernizing stormwater drainage systems. Using rainfall data from 32 cities across Poland, the study highlights the influence of regional rainfall patterns on the capacity of infiltration trenches. The highest soil capacity was observed during 15-minute convective rainfall events, with a maximum of 86 m³ in Nowy Sącz and a minimum of 37 m³ in Zakopane, influenced by the unique topographical conditions of mountainous areas. These findings underscore the need for a localized approach to stormwater system design, considering terrain and rainfall intensity. The tool facilitates sustainable stormwater management strategies, improving flood prevention and urban resilience amid dynamic climate change.

Keywords: water retention, computational tool, infiltration trench, infiltration capacity.

INTRODUCTION

Amid progressing climate change and rapid urbanization, managing stormwater in cities has become an increasingly significant challenge. Intensifying rainfall, more frequent flooding, and hydrological changes driven by rising temperatures are compromising the performance of urban water infrastructure (Gill et al., 2007; Denault et al., 2006; Taguchi et al., 2020). Urbanization exacerbates these issues by increasing impervious surfaces, such as roads and buildings, which accelerate stormwater runoff and reduce retention capacity (Chen et al., 2021; Miller et al., 2014). These phenomena underscore the urgent need to modernize urban catchments to adapt to evolving climatic conditions and the pressures of urban growth (Szeląg et al., 2022a; Musz-Pomorska and Widomski, 2022). The "sponge cities" concept, pioneered in China, offers a modern and sustainable approach to urban water management. This approach envisions cities functioning like sponges, storing rainwater and releasing it gradually (Jiang et al., 2018; Song, 2022). The goal is to mitigate flood risks while enhancing water availability during drought periods (Wang et al., 2018; Ursino, 2015). A key component of this model is the integration of green-blue infrastructure with urban hydrological systems. This includes solutions such as green roofs, parks, infiltration trenches, and retention tanks, which can reduce flood risks by 30–50% compared to traditional sewer systems (Chan et al., 2018; Zhang et al., 2019; Czerpak and Widomski, 2024).

Practical examples from Chinese cities like Shenzhen and Chongqing demonstrate that these solutions improve local water retention and positively impact water resource management (Jiang et al., 2018). Nature-Based Solutions (NBS) in urban environments are gaining prominence. These solutions – retention tanks, infiltration trenches, rain gardens, and green roofs – not only enhance

water retention but also improve urban environmental quality. For example, infiltration trenches and other natural infiltration systems enable water to seep into the soil, reducing rapid surface runoff and stabilizing the local water balance (Kabisch et al., 2017). Similarly, rain gardens act as natural filters, capturing pollutants before they enter sewer systems, thereby significantly improving urban water quality (Hatt et al., 2004).

In addition to mitigating flood risks, green-blue infrastructure improves urban microclimates, counteracting the urban heat island effect (Shariat et al., 2019). Notable examples of successful adaptation include Rotterdam, where a stormwater management system retains up to 10 million m³ of water annually, reducing runoff by 25% by Boogaard et al. (2024). In Melbourne, the "Urban Forest Strategy" expanded green space by 40%, reducing daytime urban temperatures by 1 °C to 3.8 °C through an increase in green roof coverage from 30% to 90%, effectively mitigating the urban heat island effect (Imran et al., 2018; City of Melbourne, 2012).

Modern tools for modelling catchments and retention systems, such as the Storm Water Management Model (SWMM), Model for Urban Stormwater Improvement Conceptualization (MUSIC), Modular Online Simulation Engine (MOUSE), and MIKE URBAN (a software suite developed by DHI for integrated urban water modelling, with "MIKE" referring to the Danish Hydraulics Institute), enable more effective planning and design of NBS by Hansen et al. (2014). SWMM, a widely utilized tool, provides detailed hydrological and hydraulic analyses of sewer systems, aiding in the evaluation of implemented solutions (Wu et al., 2020; Farina et al., 2023). MUSIC, particularly popular in Australia, simulates critical processes such as infiltration and sedimentation, essential for NBS. MIKE URBAN offers a comprehensive approach to urban hydrology modelling by integrating various stormwater management systems, though its technical complexity and high costs limit broader adoption (US EPA, 2015). Also diverse new approaches, algorithms and numerical methods are described as possible to apply in modelling of integrated urban water management system (Łazuka et al., 2022).

Despite these advanced tools, guidelines for designing and implementing NBS often remain incomplete and are not adapted to local climatic and infrastructural conditions, especially in Central and Eastern Europe (Kabisch et al., 2017). These gaps contribute to inadequate stormwater management, as evidenced by the 2021 floods in Western and Central Europe, which caused significant material losses (European Environment Agency, 2015).

Studies from Italy and the USA highlight the importance of modern stormwater management strategies in the context of climate change. For example, Milan's "Milan Green Plan" increased the number of green roofs and rain gardens, improving water retention and mitigating the urban heat island effect. Research (Marchioni et al., 2018; Procaccini and Monticelli, 2021; Salerno et al., 2021; Sanesi et al., 2016) shows that such solutions significantly reduce surface stormwater runoff and enhance urban water quality.

In the United States, cities like New Orleans and Houston, vulnerable to intense rainfall and hurricanes, have implemented extensive retention systems. Following Hurricane Katrina in 2005, New Orleans invested in advanced infiltration trenches and retention tanks. Regulations under Low Impact Development (LID) required developers to incorporate solutions such as green roofs and permeable surfaces, greatly improving stormwater management (Davis et al., 2012; Maimone et al., 2011).

Stormwater management remains a critical challenge in Poland and globally amidst rapid climate change and urbanization. In Poland, outdated sewer infrastructure and insufficient retention capacity emphasize the urgent need for modernization (Szeląg at al. 2022b). Adopting innovative models like China's "sponge cities" could significantly improve water retention and urban resilience to extreme weather events, including floods and droughts (Song et al., 2022; Xing et al., 2019). NBS offer a modern approach by integrating hydrological functions with urban planning, thereby enhancing cities' adaptive capacity.

This article introduces a proprietary computational application for designing, assessing, and modernizing selected NBS structures, such as detention basins, infiltration basins, infiltration trenches, and rain gardens. The developed tool integrates with existing computational software, which often provides limited support for NBS solutions, offering a distinct advantage. The application was used to evaluate the impact of regional rainfall conditions across Poland on the retention capacity of infiltration trenches. The diverse hydrological conditions in different regions underscore the need for a tailored approach to

stormwater system design to improve efficiency and resilience against extreme weather events. This tool contributes to the development of modern stormwater management strategies, strengthening urban ecosystems' resilience to climate change. Its application is vital for promoting sustainable development and ensuring hydrological safety in Poland and beyond.

METHODS AND DATA

Rainfall data and regional convection rainfall models

Rainfall data were collected from 32 meteorological stations located in various Polish cities (meteorological stations belonging to the IMGW-PIB network). Poland's climate (Central Europe), classified as temperate warm, exhibits a transitional nature between the marine characteristics of Western Europe and the continental characteristics of Eastern Europe. This results in the influx of air masses with varying thermal and humidity properties, leading to considerable variability in rainfall limit (Niedźwiedź et al., 2009; Szeląg et al., 2022b). The average annual rainfall in Poland (1981–2010) is approximately 600 mm, ranging from 520 mm in the central regions to nearly 700 mm along the Baltic coast and over 1000 mm in the mountains. The heaviest rainfall occurs from May to August, with July experiencing the highest frequency of rainfall.

The selection of rainfall stations ensured even spatial distribution across Poland, representing diverse physiogeographical conditions such as mountains, foothills, uplands, lowlands, lakes, and the coastal zone (Fig. 1).

When modelling rainfall in small urban catchments, it is essential to consider short-duration, high-intensity rainfall events, primarily associated with atmospheric convection (Kupczyk and Suligowski, 1997; Łupikasza, 2016). These events typically have a limited spatial extent (up to 10 km²) and high intensity. In Poland, such rainfall events generally last up to 90 minutes (coefficient values of $a_1 < 2.8 \cdot 10^{-3}$ and $a_2 > 0.31$ – more information in S1 Table). On the basis of the literature data reported by Szeląg et al. (2022b), convective rainfall events during the summer half-year (May – October) from 1961 to 2005 were identified using traditional pluviograph records. A four-hour gap between rainfall events was used as the defining interval (Kupczyk and Suligowski, 2000; DWA-A 118E, 2006).

The highest frequency of convective events was recorded in mountainous regions and along the Baltic coast, though their average intensity was relatively low (< 0.6 mm). Over 65% of these events lasted up to 30 minutes, with frequency decreasing as duration increased. To accurately reflect the temporal variability of rainfall

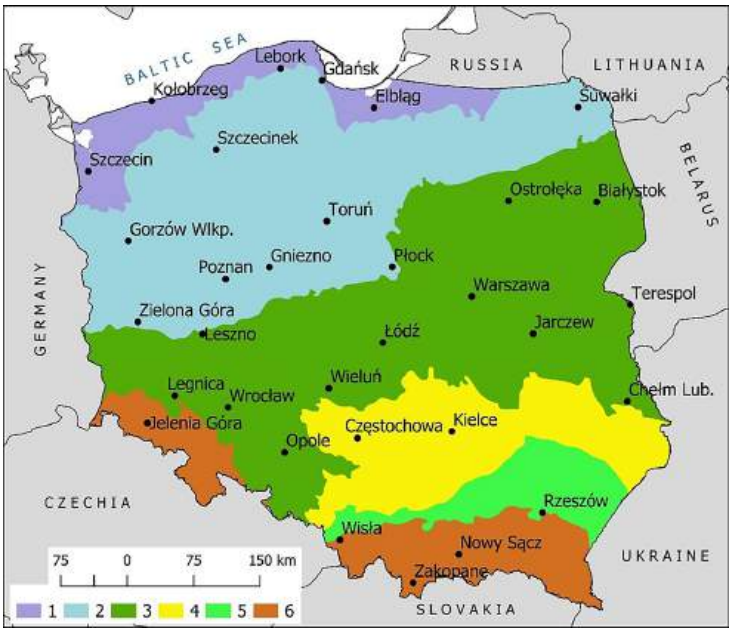

Figure 1. Location of rain gauges against the background of the main physical-geographical regions of Poland (1 – Baltic coastal lowlands, 2 – lakelands, 3 – central lowlands, 4 – uplands, 5 – sub-mountain basins, 6 – mountains)

events, 5-minute intervals were applied, ensuring that the dataset captured several episodes per year over the multi-year analysis period. For all measurement points, the 45 highest rainfall event values were selected using the peak-over-threshold method, regardless of the year of occurrence (Malihout et al., 2013).

For each rainfall station, the relationship between the rainfall depth (P) and its duration (t_r) was determined. This relationship was derived using a second-degree polynomial function to calculate the probability of stormwater flooding for the characteristics of the assumed urban catchment, based on the regional convection rainfall models determined, as described in Equation 1:

$$P_{max}(t_r) = a_1 \cdot t_r^2 + a_2 \cdot t_r + a_0 \quad (1)$$

This approach has been previously validated in hydrological studies (Kupczyk and Suligowski, 1997; Szeląg et al., 2022b).The empirical coefficients a_1, a_2, and a_0 and are provided in S1 Table. The analysis revealed that average rainfall depth for convective events increases with duration, peaking at approximately 60 minutes.

Regions with the greatest increases in average rainfall depth include central Poland (e.g., Jarczew, Leszno, Łódź, Warsaw), the lake districts (e.g., Gniezno, Poznań, Suwałki), and southeastern areas (e.g., Nowy Sącz, Rzeszów). Local topography and dynamic meteorological conditions significantly influence this distribution (Szelag et al., 2022c; Kaczmarek, 2019). Conversely, the most stable rainfall patterns with the lowest maximum intensity were observed in Kielce, Częstochowa, Wieluń, Elbląg, and Kołobrzeg. Urban heat island effects and aerosols in lowland agglomerations (e.g., Białystok, Poznań, Łódź) reduce rainfall intensity, as does the evaporation effect from the sea surface in coastal cities like Szczecin and Gdańsk.

In the applied hydrological method, unit hydrographs were employed. Rainfall data were input as pulses characterized by durations (minutes), depths (mm), and intensities (mm/min). Various scenarios for convective rainfall durations ranging from 15 to 60 minutes were applied in the analysis. Rainfall events lasting up to 60 minutes with depths exceeding 0.2 mm exhibited high variability. During the studied summer period, between 1615 and 2532 such events were recorded, averaging 36–56 events per year (Szelag et al., 2022b).

Tool to modelling of NBS (Calculator_NBS)

The developed application enables forecasting of surface runoff using the kinematic wave model (Chow et al., 1998; Singh, 1996) and its transformation through various NBS structures (Raymond et al., 2017), such as retention tanks, infiltration basins, rain gardens, and infiltration trenches (EPA, 2015). This approach facilitates the design, evaluation, and modernization of NBS solutions under urban catchment conditions and in the context of climate change. Given the limited availability of data on land use and topography, the application allows for the incorporation of custom inflow hydrograph shapes for NBS structures (European Commission, 2015). The sizing of these structures is based on identifying limiting factors such as maximum runoff and water depth in the soil, ensuring accurate capacity design. The developed tool (Calculator_NBS) was used to predict the dimensions of infiltration trenches for 32 rainfall stations in Poland for convective rainfall.

The application's sizing algorithm for green infrastructure objects is implemented in C++ programming language using the Qt Creator integrated development environment (IDE). High-resolution simulation capabilities enhance the numerical stability of the solution algorithm and minimize simulation errors.

Balance equation for green infrastructure objects (Calculator_NBS)

The balance equation has been widely applied in hydrological studies to assess the efficiency of green infrastructure in managing stormwater, as emphasized in the works of the European Commission (2015) and Beven et al. (2012). Bhaskar et al. (2016) discussed the use of the balance for green infrastructure objects in calculations, which formed the basis for analyzing water flow in stormwater sewage systems. The balance Equation 2 for green infrastructure objects can be expressed as follows:

$$dV = Q_{outS}(t)dt - Q_{out}(t)dt - \\ -Q_{inf}(t)dt - ET(t)dt \quad (2)$$

where: the input data include: $Q_{outS}(t)$ – inflow of water to the green infrastructure object at time t, (m^3/s), $Q_{out}(t)$ – runoff from the substrate at time t, including the flow to the ground, with overflow occurring if the allowable hydraulic capacity is exceeded, (m^3/s), $Q_{inf}(t)$ – volume of water

flowing to the ground per unit time t, (m^3/s), $ET(t)$ – evapotranspiration from the surface layer, (m^3/s).

The computational diagram of the infiltration system, as outlined by Piazza and Ursino (2022) and Błażejewski at al. (2018), is illustrated in Figure (Fig. 2), providing a clear visualization of water flow dynamics within the system. The presented diagram (Fig. 2) illustrates a system consisting of an impervious sub-catchment (runoff surface) that converts rainfall into runoff, and a permeable infiltration trench (surface $B \cdot L$) where infiltration occurs.

The initial form of Equation 2 for the soil, presented as Equation 3:

$$Q_{inf} = f_c \times (B \times L + h\,(B + L)) \tag{3}$$

where: Q_{inf} – stormwater infiltration flux into the soil, varying over time t, (m^3/s), f_c – infiltration rate, (mm/hr), B – width of the infiltration trench, (m), L – length of the infiltration trench, (m), h – water depth in the soil, (m).

To develop the surface runoff model $Q_{outS} = f(t)$, the kinematic wave equation (Akan, 1993) was used, defined as Equation 4:

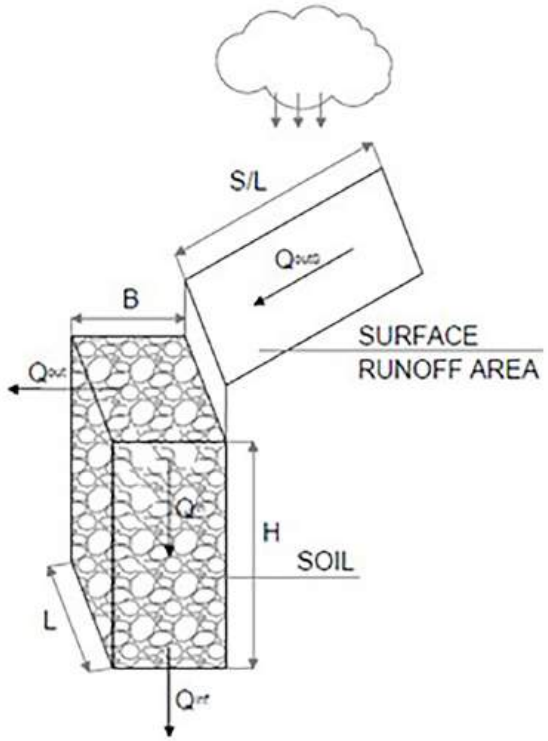

Figure 2. Schematic representation of the infiltration system

$$\frac{\partial q}{\partial x} + \frac{\partial y}{\partial t} = i - f \tag{4}$$

where: $\frac{\partial q}{\partial x}$ – flow gradient in the spatial direction, $\frac{\partial y}{\partial t}$ – change in water depth over time, i – rate of rainfall, (expressed in mm/hr), f – rate of losses from rainfall.

Taking into account the relationship $R_h = y$, where y is the thickness of the water layer (m), Equation 4 allows for modelling phenomena related to stormwater runoff over a flat surface. In a practical context, the solution of the equation allows for considering the impact of rainfall intensity and the actual infiltration rate on surface runoff processes.

According to Darcy-Weisbach's Equation 5 and 6, the friction slope S_f is calculated using the following equation:

$$S_f = \frac{f_d \cdot V^2}{8 \cdot g \cdot R_h} \tag{5}$$

for:

$$f_d = \frac{C}{Re} \tag{6}$$

where: S_f, S_0 – friction slop,(-), R_h – hydraulic radius, (m), f_d – friction factor, (-), V – average flow velocity, (m/s), C – laminar flow resistance factor, (-), Re – Reynolds number, (-), υ – kinematic viscosity of the water, (m^2/s).

The computational methodology for surface runoff is detailed in Supplementary Information – S1 Section.

At the same time, the application calculates rainwater outflow from the soil through drainage pipes, as described by Equation 7:

$$\varepsilon \cdot B \cdot L \cdot \frac{dh}{dt} = Q_{outS}(t) - Q_{out}(t) \tag{7}$$

where: ε – porosity coefficient, (-), B – width of the infiltration trench, (m), L – length of the infiltration trench, (m), dh/dt – change in water depth in the soil over time, Q_{outS} – inflow rate of stormwater to the trench, variable over time t, (m^3/s), Q_{out} – runoff rate of sewer system, variable over time t, (m^3/s).

For the saturation zone, the runoff through the drainage pipe is described by the following relationships (8) and (9):

$$Q_{out} = \frac{-\left(\frac{h + D}{L \cdot B \cdot K}\right) + \sqrt{\left(\frac{h + D}{L \cdot W \cdot K}\right)^2 + 4 \cdot N \cdot H}}{2 \cdot N} \tag{8}$$

for:

$$N = \frac{f \cdot L}{2 \cdot g \cdot A_{pipe}^2 \cdot D} + \frac{1}{2 \cdot g \cdot A_{pipe}^2} + \frac{C_L}{2 \cdot g \cdot A_{pipe}^2 \cdot \theta_{agg}^2} \quad (9)$$

where: H – thickness of the water table in the soil, (m), h – thickness of the soil above the top of the pipe, (m), D – inner diameter of the pipe, (m), L – length of the infiltration trench, (m), K – hydraulic conductivity of soil, (m/s), B – width of the infiltration trench, (m), A_{pipe} – cross-sectional area of the pipe, (m^2), Θ_{agg} – porosity of the soil, (-), C_L – coefficient of local resistances, (-), g – gravitational acceleration, (m/s^2), λ – linear resistance coefficient, (-), calculated using the formula (10):

$$\lambda = \frac{1}{\left(-2 \cdot log\left(\frac{k}{3.71 \cdot D}\right)\right)^2} \quad (10)$$

where: k – roughness of the conduit, (m), D – inner diameter of the pipe, (m).

The runoff through the drainage pipe, assuming no saturation of the soil (11):

$$Q_{out} = \frac{-\left(\frac{L}{\left(H + \frac{D}{2}\right) \cdot K}\right) + \sqrt{\left(\frac{L}{K \cdot \left(H + \frac{D}{2}\right)}\right)^2 + 4 \cdot N \cdot H}}{2 \cdot N} \quad (11)$$

One of the alternatives for runoff from the catchment area is the triangular hydrograph, which is described in detail in S2 Section.

Rainfall data for designing an infiltration trench

The analysis aimed to identify the representative rainfall duration that maximized the retention capacity of infiltration trenches, as outlined by Akan and Houghtalen (2003). Rainfall events with durations ranging from t_d = 15 to 240 minutes were analyzed at 5-minute intervals, with rainfall depth calculated using the relationship described in Equation 1.

Input data for the calculations of the infiltration trench, catchment and runoff

The study evaluated the impact of rainfall data on the design and dimensions of infiltration trenches. Specifically, it sought to determine the optimal duration of convective rainfall events for achieving maximum retention capacity. Rainfall depths were calculated for durations ranging from 15 to 240 minutes, using 5-minute increments, based on the relationship outlined in Equation 1. The following input data were used in the application, as shown in Table 1.

Calculation assumptions (representative rainfall duration time)

The computational algorithm used in this study for the design of NBS objects includes the following forecasts: Surface runoff: calculations were performed based on empirical coefficients a_1, a_2, and a_0 (S1 Table).

Capacity of the infiltration trench: a simulation of the infiltration trench was carried out based on the input parameters, such as trench length B = 3.0 m and trench width L = 20 – 400 m. Runoff was also simulated considering the input data presented in Table 1 for runoff.

RESULTS

Rainfall duration and infiltration trench capacity

The relationship between rainfall duration and infiltration capacity is shown in Figure 3, which highlights the dynamics of the infiltration process across different locations.

The analysis covered infiltration trench dimensions in 32 selected cities across Poland, focusing on how rainfall duration influences retention capacity. The study found significant similarities in infiltration capacities across various mesoregions. The highest infiltration capacity was recorded during a 15-minute convective rainfall event in Nowy Sącz (86 m³). As rainfall duration increased, infiltration capacity decreased, reaching as low as 2 m³ for a 130-minute rainfall event.

In mesoregion 6, Nowy Sącz displayed the highest infiltration capacity (86 m³), while Zakopane, also in mesoregion 6, recorded the lowest value (37 m³). The highest infiltration capacity in Nowy Sącz corresponded with the highest stormwater flooding sensitivity index (p_s), as reported by Szeląg et al. (2022b). Conversely, Elbląg showed the lowest sensitivity index (p_s = 0.20). Furthermore, the study observed that mountainous areas like Nowy Sącz, which have a high infiltration capacity and sensitivity index, are more prone to flooding during intense rainfall events. For small urban catchments with an imperviousness

Table 1. Assumed input data used for the infiltration trench, catchment, and runoff (Akan and Houghtalen, 2003)

Name	Index	Unit	Value
Infiltration trench			
Rainfall duration	t_d	min	15–240 (step 5 min)
Porosity coefficient	ε	-	0.44
Infiltration rate	fc	m/s	0.001
Width	B	m	3
Length	L	m	20–400 (step 1 m)
Catchment			
Width of flow path	B	m	10
Length of flow path	L	m	20
Manning's roughness coefficient	n	$m^{-1/3}\cdot s$	0.0015
Hydraulic gradient	S_0	-	0.001
Runoff			
Maximum water depth in the soil	h	m	1.5
Diameter of drainage pipes	D	m	0.15
Hydraulic conductivity of soil	K	m/s	0.15
Cross-sectional area of the pipe	A_{pipe}	m²	0.01766
Porosity of the soil	Θ_{agg}	-	0.3
Coefficient of local resistances	CL	-	1
Roughness of the conduit	k	m	0.001

coefficient (Imp) of 0.36, these factors underline the necessity of integrating flood risk management and land-use planning to mitigate flooding and support sustainable development.

In mesoregion 3, the infiltration capacities exhibited notable uniformity. During a 15-minute rainfall event, the average infiltration capacity ranged from 48.8 m³ (5th percentile) to 77 m³ (90th percentile). Extending the rainfall duration to 30 and 60 minutes resulted in a reduction in infiltration capacities to 46 m³ and 26 m³, respectively.

In comparison, mesoregion 1 showed lower infiltration trench capacities. For a 15-minute rainfall event, the average infiltration capacity

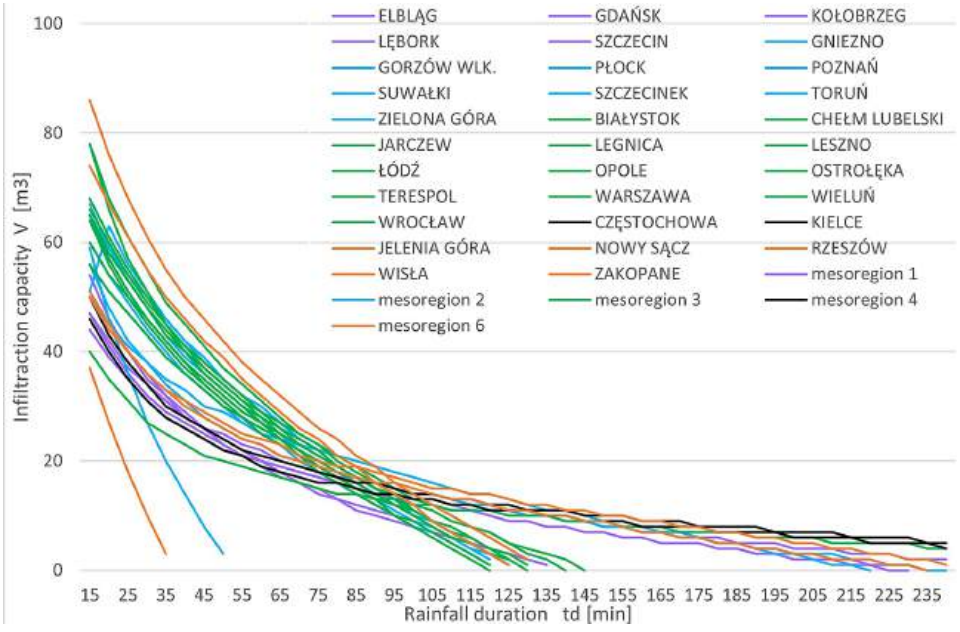

Figure 3. Effect of rainfall duration on the infiltration capacity

ranged from 44.6 m³ (5th percentile) to 52.8 m³ (90th percentile). When the rainfall duration increased to 30 and 60 minutes, the infiltration capacities declined to 34 m³ and 20 m³, respectively.

The relationship between rainfall duration and infiltration trench capacity underscores the need for improved stormwater monitoring and adaptive management, particularly in regions with lower retention capacity. The findings from Polish studies indicate that prolonged rainfall durations significantly diminish soil infiltration capacity. For instance, in mesoregion 1, the infiltration capacity for a 60-minute rainfall event is reduced to 20 m³ – less than half of the capacity observed for a shorter, 15-minute event. These results highlight the challenges cities may face in managing stormwater during extended rainfall events, necessitating tailored strategies to optimize urban drainage systems and prevent flooding.

The variations in infiltration trench capacities across cities and mesoregions are presented in Figure 4, demonstrating the spatial diversity in stormwater retention performance.

The analysis of infiltration trench capacity (V) in selected Polish cities revealed significant differences across various mesoregions. These findings are crucial for evaluating retention potential and optimizing water infrastructure planning at the national scale. Mesoregion 1 (Baltic Lakeland): Cities such as Szczecin (54 m³), Gdańsk (51 m³), and Elbląg (44 m³) exhibited lower infiltration capacities compared to other regions. Mesoregion 2: This region showed higher values, with cities like Gniezno (51 m³), Gorzów Wielkopolski (56 m³), and Płock (59 m³). Zielona Góra (67 m³) and Suwałki (65 m³) recorded the highest capacities within this region. Mesoregion 3 (Central and Eastern Poland): Higher capacities were observed, with Jarczew and Chełm Lubelski reaching 78 m³. Other cities, such as Legnica (68 m³) and Opole (66 m³), also demonstrated favorable retention capabilities, while Wieluń recorded the lowest value at 40 m³. Central cities like Częstochowa (50 m³) and Kielce (46 m³) had relatively low capacities. Mesoregion 6 (Mountainous Terrain): The highest values in Poland were recorded here, with Nowy Sącz achieving 86 m³ and Rzeszów 74 m³. However, Zakopane had the lowest capacity in the country at 37 m³, highlighting the region's variability due to its topographic conditions.

Rainfall intensity and its impact on infiltration capacity of soil in small urban catchment in Poland

Rainfall intensity analysis identified five intensity levels, highlighting areas with both heavy and moderate rainfall. The results are presented in Figure 5.

The highest recorded rainfall intensities, exceeding 50 mm/min, were observed in four cities: Chełm Lubelski (53.8 mm/min), Jarczew (53.7 mm/min), Rzeszów (51.3 mm/min), and Nowy Sącz (59.3 mm/min, the highest value, located in mesoregion 6). Rainfall intensities in the range

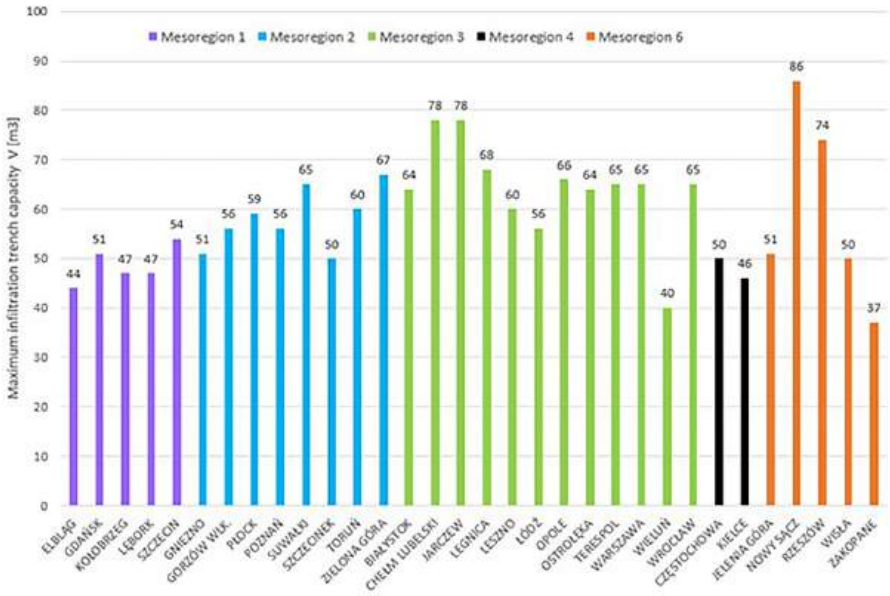

Figure 4. Maximum infiltration trench capacity V (m³) for individual cities

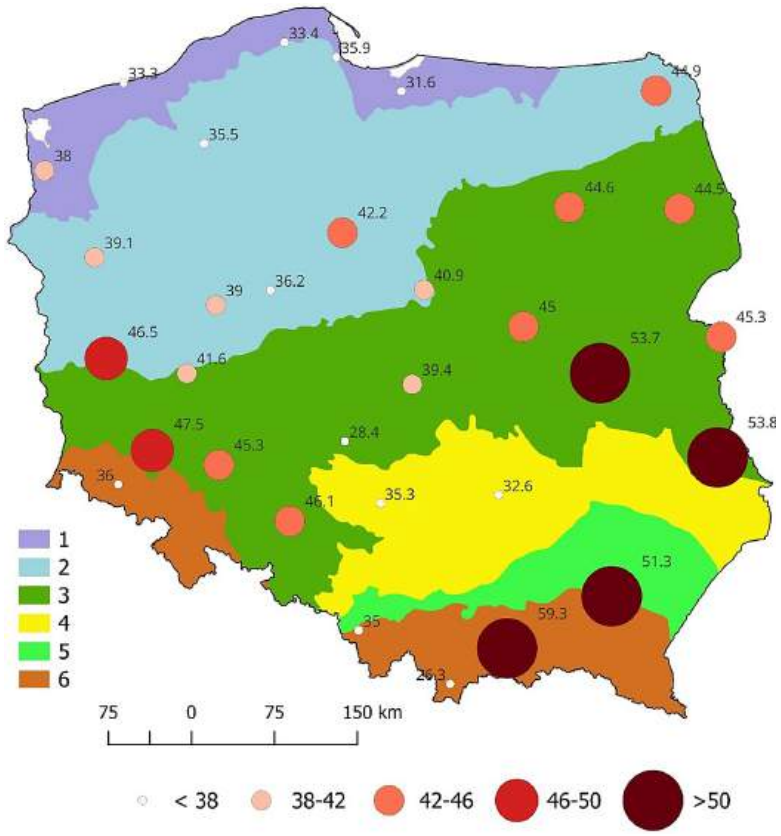

Figure 5. Representative rainfall intensity

of 46–50 mm/min were recorded in three cities: Legnica, Opole, and Zielona Góra. Seven cities: Białystok, Ostrołęka, Suwałki, Terespol, Toruń, Warsaw, and Wrocław; fell within the 42–46 mm/min range. Five cities: Gorzów Wielkopolski, Leszno, Łódź, Płock, and Poznań; reported values in the 38 – 42 mm/min range. The largest group comprised 13 cities with rainfall intensities below 38 mm/min, including Częstochowa, Elbląg, Gdańsk, Gniezno, Jelenia Góra, Kielce, Kołobrzeg, Lębork, Szczecin, Szczecinek, Wieluń, Wisła, and Zakopane, where the lowest value of 26.3 mm/min was recorded. A comparative analysis with Szeląg et al. (2022b) reveals a clear association between cities experiencing the highest rainfall intensities and areas identified as having a high vulnerability index for runoff in small catchments. Cities such as Nowy Sącz, Chełm Lubelski, Jarczew, and Rzeszów, which recorded the highest rainfall intensities, also demonstrated the highest sensitivity index values (p_s > 0.5) in Szeląg's study. This indicates that regions prone to intense, short-duration rainfall events are particularly susceptible to frequent and extensive flooding. These findings underscore the importance of incorporating local hydrological variability into flood risk management and forecasting frameworks. The impact of localized rainfall conditions is further confirmed by De Martino et al. (2010) in their study of the Campania region (Italy), which illustrates that regression models based on local rainfall data can effectively predict sewage system loads and water quality during heavy rainfall events. Similarly, De Paola et al. (2012) examined the relationships between rainfall characteristics, the geographical locations of the studied stations, and the unit capacities of the tanks analyzed in the same country. In Poland, cities such as Nowy Sącz and Rzeszów, where stormwater drainage systems are especially vulnerable to overloading, could benefit from adopting similar approaches to enhance stormwater management efficiency. Furthermore, an analysis was conducted on the performance of an infiltration trench with a maximum length of 3.0 m. The results are presented in Figure 6.

Analyzing the infiltration trench capacity for a maximum length of 3.0 meters, the results align with the spatial distribution presented in Figure 6. The highest infiltration capacities, exceeding 70 m³, were observed in Nowy Sącz (86 m³), Chełm Lubelski (78 m³), Jarczew (78 m³), and Rzeszów

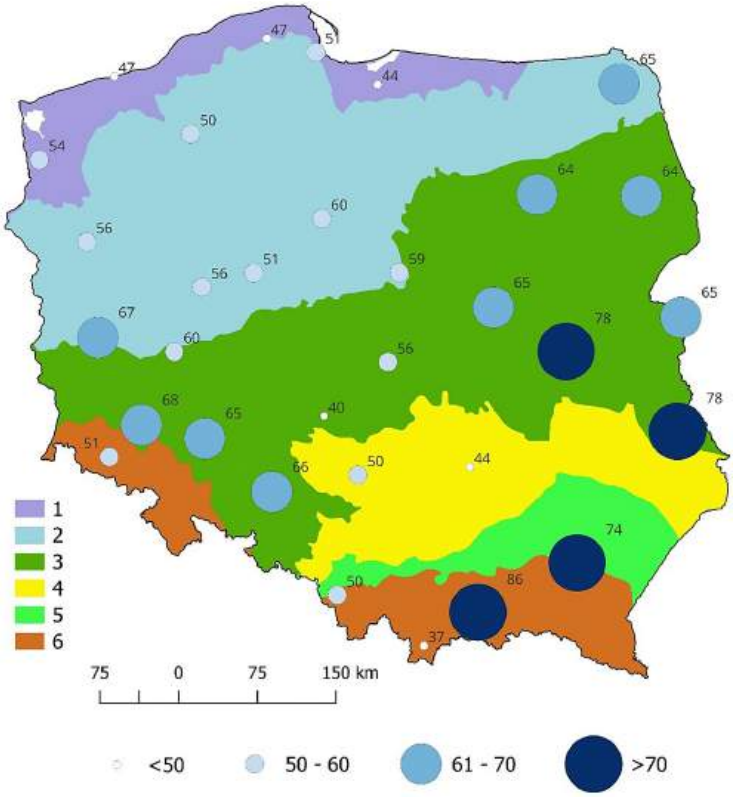

Figure 6. Infiltration trench capacity

(74 m³). These four cities, situated in mesoregions 6 and 3, exhibit the greatest retention capacities.

Infiltration capacities within the range of 61–70 m³ were recorded in six cities: Legnica, Zielona Góra, Opole, Suwałki, Terespol, and Warsaw, as well as Białystok and Ostrołęka. These cities are primarily located in central Poland, within mesoregions 3 and 2.

The largest group, comprising 13 cities, displayed infiltration capacities between 50 and 60 m³. These cities include Leszno, Toruń, Płock, Gorzów Wielkopolski, Łódź, Poznań, Szczecin, Gdańsk, Gniezno, Jelenia Góra, Częstochowa, Szczecin, and Wisła. Conversely, cities with infiltration capacities below 50 m³ included Kołobrzeg, Lębork, Kielce, Elbląg, Wieluń, and Zakopane, with Zakopane recording the lowest value of 37 m³.

In terms of mesoregional characteristics, distinct variations in rainfall and infiltration capacities are evident. Mesoregions 1 and 4 are associated with the lowest rainfall intensities (below 38 mm/min) and moderate soil capacities (44–54 m³ and 46–50 m³, respectively), promoting hydrological stability. Mesoregion 2 experiences moderately higher rainfall (35.5–46.5 mm/min) and larger soil capacities (50–67 m³), supporting improved water retention. Mesoregion 3 exhibits high variability in rainfall (28.4 – 53.8 mm/min) and soil capacity (40–78 m³). Mesoregion 6, which experiences the highest rainfall intensities (35–59.3 mm/min), also demonstrates the greatest soil capacity (50–86 m³).

These findings corroborate the results of Szeląg et al. (2022b), which emphasized that physical and geographical conditions, along with localized rainfall patterns, significantly influence the maximum permissible impermeability limit. This limit defines the threshold rainfall intensity, exceeding which triggers the occurrence of wastewater discharge in the catchment, depending on the area's impermeability. Exceeding this threshold often results in stormwater system overflows within small urban catchments. A comparison of infiltration trench capacities across Poland reveals notable differences and significant correlations between mesoregions. The greatest variability is observed in Mesoregion 1 (Baltic coast), characterized by low retention capacity but an imperviousness value (Imp_{gr}: 0.51 – 0.56), as described by Szeląg at al. (2022b). Limited water retention in this region, coupled with intense surface runoff driven by urbanization

and impermeable soils, exacerbates the challenges of water absorption. Consequently, the design and implementation of efficient stormwater management systems, such as retention tanks, infiltration trenches, and irrigation systems (NSN), are crucial in this area.

Implications of the use of green infrastructure in urban catchments

An integrated approach to stormwater management that combines GI with traditional stormwater systems and retention tanks represents a modern and effective strategy for mitigating surface runoff and improving the operational efficiency of stormwater systems. Jing et al. (2024) and Szelag et al. (2024) have substantiated that the synergistic application of both natural and engineered systems can substantially diminish flood risk and contribute to the enhancement of surface water quality.

Within the context of urban catchments, GI assumes a pivotal role in stormwater management, climate change adaptation, and water quality improvement. Research by Almaaitah (2024) demonstrated that green roofs can retain up to 63% of rainfall, while retention farms can achieve retention rates of 85–88%, which not only attenuates surface runoff but also mitigates water levels in retention tanks. Moreover, studies by Cavadini et al. (2024) in Switzerland have confirmed that bioretention infiltration zones can reduce the volume of stormwater overflows by as much as 52% in scenarios involving a 46% increase in rainfall, providing evidence that GI can effectively address the challenges associated with intensified rainfall events.

Hepcan and Canguzel (2024) evaluated GI in the context of hydrometeorological risk reduction in Izmir, highlighting that optimizing GI systems enhances water retention and fortifies urban resilience. Matías Rodríguez et al. (2024) demonstrated that green roofs and permeable pavements can augment the resilience of combined stormwater systems by 9–22%, effectively reducing stormwater overflows. Furthermore, the appropriate design of hydraulic structures has been shown to reduce peak stormwater runoff and curb soil erosion. Empirical evidence confirms that GI enhances the hydrological balance, supports biodiversity, mitigates the urban heat island effect, and reduces the burden on sewer infrastructure.

GI also exerts a positive influence on the quality of wastewater discharged into receiving water bodies. Cavadini et al. (2024) confirmed that bioretention systems can substantially decrease the concentration of pollutants, thereby improving the quality of urban waters and supporting local water resources.

Additionally, further research underscores the political and urban planning dimensions of GI. Sowby et al. (2024) emphasized the imperative to implement climate-resilient standards in water infrastructure, drawing on case studies from Copenhagen and Melbourne. Zhu et al. (2024) demonstrated that effective GI policy necessitates the integration of assessment metrics and environmental regulatory frameworks.

CONCLUSIONS

The proposed application has proven effective in addressing critical engineering and scientific challenges on a national scale, particularly in the field of stormwater management within small urban catchments. Its versatility allows for the evaluation of equations under varied assumptions and conditions, making it applicable to the design of retention tanks, the dimensioning of infiltration systems, and the modernization of stormwater infrastructure.

The analysis of data from 32 cities reveals significant disparities in rainfall intensity and the retention capacities of infiltration systems. Convective rainfall events are shown to maximize system capacity, while prolonged rainfall gradually diminishes their effectiveness. Cities such as Nowy Sącz, Chełm Lubelski, Jarczew, and Rzeszów exhibit high retention capacities, whereas cities like Elbląg, Wieluń, and Zakopane record the lowest values.

These findings emphasize the necessity of adopting localized approaches to stormwater system design, tailored to the unique geological and climatological characteristics of different mesoregions. Such strategies are essential for improving flood protection and ensuring sustainable water resource management, especially in light of increasing climate variability.

The developed tool and the insights gained from this study represent a significant advancement in enhancing urban resilience to extreme weather events. This work contributes to the sustainable development of urban ecosystems and

the promotion of hydrological safety, both in Poland and globally.

Acknowledgements

This research was funded by internal projects at Lublin University of Technology, Poland numbers FD-20/IS-6/024.

REFERENCES

1. Akan, A.O. (1993). *Urban Stormwater hydrology* – A Guide to Engineering Calculations, Technomic, Lancaster, PA.
2. Akan, A.O., & Houghtalen, R.J. (2003). *Urban Hydrology, Hydraulics, and Stormwater Quality: Engineering Applications and Computer Modelling;* John Wiley & Sons, Inc.: Hoboken, NJ, USA.
3. Almaaitah, T. (2024). Multifunctional blue-green infrastructure and low impact development for climate change adaptation. https://doi.org/10.32920/26883574.v1
4. Bhaskar, A.S., Hogan, D.M., & Archfield, S.A. (2016). Urban base flow with low impact development. *Hydrological Processes*, *30*(18), 3156–3171. https://doi.org/10.1002/hyp.10808
5. Beven, K.J. (2012). *Rainfall-runoff modelling: the primer*. John Wiley & Sons
6. Błażejewski, R., Nieć, J., Murat-Błażejewska, S., & Zawadzki, P. (2018). Comparison of infiltration models with regard to design of rectangular infiltration trenches. *Hydrological Sciences Journal, 63*(11), 1707–1716. https://doi.org/10.1080/02626667.2018.1523616
7. Boogaard, F., & Kondratenko, J. (2024). Low impact development devices DNA of cities for long term stormwater management strategies. *Discover Water*, *4*(34). https://doi.org/10.1007/s43832-024-00090-0
8. Cavadini, G. B., Rodríguez, M., Nguyen, T., & Cook, L. M. (2024). Can blue-green infrastructure counteract the effects of climate change on combined sewer overflows? study of a swiss catchment. Environmental Research Letters. https://doi.org/10.1088/1748-9326/ad6462
9. Chan, F.K.S., Griffiths, J.A., Higgitt, D., Xu, S., Zhu, F., Tang, Y.T., et al. (2018). "Sponge City" in China – A breakthrough of planning and flood risk management in the urban context. *Land Use Policy*, *76*, 772–778. https://doi.org/10.1016/j.landusepol.2018.03.005
10. Chen, V., Bonilla Brenes, J. R., Chapa, F., & Hack, J. (2021). Development and modelling of realistic retrofitted Nature-based Solution scenarios to reduce flood occurrence at the catchment scale. *Ambio*, *50*, 1462–1476. https://doi.org/10.1007/s13280-020-01493-8
11. Chow, V.T., Maidment, D.R., & Mays, L.W. (1988). Applied Hydrology; McGrawl-Hill Book Company: New York, NY, USA.
12. City of Melbourne (2012) Melbourne (Vic.). Council; Urban Forest Strategy 2012.
13. Czerpak, J., & Widomski, M.K. (2024). Numerical assessment of green infrastructure influence on hydrologic effectiveness in a suburban residential development. *Journal of Ecological Engineering*, *25*(7), 187–200. https://doi.org/10.12911/22998993/188364
14. Davis, A.P., Traver, R.G., Hunt, W.F., Lee, R., Brown, R.A., & Olszewski, J.M. (2012). Hydrologic Performance of Bioretention Storm-Water Control Measures. *Journal of Hydrologic Engineering*, *17*(5), 604–614. https://doi.org/10.1061/(ASCE)HE.1943-5584.0000467
15. De Martino, G., De Paola, F., Fontana, N., Marini, G., & Ranucci, A. (2010). Preliminary design of combined sewer overflows and stormwater tanks in Southern Italy. *Irrigation and Drainage*, *60*(4), 544–555. https://doi.org/10.1016/j.proenv.2013.06.013
16. Denault, C., Millar, R.G., & Lence, B.J. (2006). Assessment of Possible Impacts of Climate Change in an Urban Catchment. *Journal of the American Water Resources Association*, *42*(3), 685–697. https://doi.org/10.1111/j.1752-1688.2006.tb04485.x
17. De Paola, F., Ranucci, A. (2012). Analysis of spatial variability for stormwater capture tank assessment. *Irrigation and Drainage*, *61*, 682–690. https://doi.org/10.1002/ird.1675
18. DWA-A 118E. (2006) Hydraulic Dimensioning and Verification of Drain. and Sewer Systems, DWA German Association for Water, Wastewater and Waste, Hennef, Germany
19. European Commission. (2015). Towards an EU Research and Innovation policy agenda for nature-based solutions and renaturing cities. Final Report of the Horizon 2020 Expert Group on Nature-Based Solutions and Re-naturing Cities. Brussels: European Commission. https://doi.org/10.2777/479582
20. Farina, A., Di Nardo, A., Gargano, R., van der Werf, J.A., & Greco, R. (2023). A simplified approach for the hydrological simulation of urban drainage systems with SWMM. *Journal of Hydrology*, *623*, 129757. https://doi.org/10.1016/j.jhydrol.2023.129757
21. Gill, S., Handley, J., Ennos, A., & Pauleit, S. (2007). Adapting cities for climate change: The role of the green infrastructure. *Built Environment*, *33*(1), 115–133. https://doi.org/10.2148/benv.33.1.115
22. Hansen, L., Borup, M., Møller, A., & Mikkelsen, P. (2014). Flow forecasting using deterministic updating of water levels in distributed hydrodynamic

urban drainage models. *Water*, *6*(8), 2195–2211. https://doi.org/10.3390/w6082195

23. Hatt, B., Fletcher, T., Walsh, C.J. & Taylor, S.L. (2004). The influence of urban density and drainage infrastructure on the concentrations and loads of pollutants in small streams. *Environmental Management*, *34*, 112–124. https://doi.org/10.1007/s00267-004-0221-8
24. Hepcan, Ç., & Canguzel, A. (2024). The impact of blue-green infrastructure on climate resilience for hydrometerological hazards: The case of Bayraklı, İzmir. *Deleted Journal*. https://doi.org/10.58816/duzceod.1413255
25. Imran, H.M., Kala, J., Ng, A.W.M., & Muthukumaran, S. (2018). Effectiveness of green and cool roofs in mitigating urban heat island effects during a heatwave event in the city of Melbourne in southeast Australia. *Journal of Cleaner Production*, *197*(1), 393–405. https://doi.org/10.1016/j.jclepro.2018.06.179
26. Jiang, Y., Zevenbergen, C., & Ma, Y. (2018). Urban pluvial flooding and stormwater management: A contemporary review of China's challenges and "sponge cities" strategy. *Environmental Science & Policy*, *80*, 132–143. https://doi.org/10.1016/j.envsci.2017.11.016
27. Jing, J., Hou, J., Pan, Z. et al. (2024). Simulation and Evaluation of Collapsible Risk of Low Impact Development Rainwater System in Collapsible Loess Area. *Water Resour Manage 38*, 5485–5505. https://doi.org/10.1007/s11269-024-03896-8
28. Kabisch, N., Korn, H., Stadler, J., & Bonn, A. (2017). *Nature-Based Solutions to Climate Change Adaptation in Urban Areas—Linkages Between Science, Policy and Practice*. In: Kabisch, N., Korn, H., Stadler, J., Bonn, A. (eds) Nature-Based Solutions to Climate Change Adaptation in Urban Areas. Theory and Practice of Urban Sustainability Transitions. Springer, Cham. https://doi.org/10.1007/978-3-319-56091-5_1
29. Kaczmarek, Z., & Kaczmarek, A. (2019). Spatial distribution of precipitation in Poland. *Geographical Journal*, *31*(2), 125–139.
30. Kupczyk E. & Suligowski R. (1997). *Statistical description of the rainfall structure as the input to hydrological models*. In Prediction of the design storms and floods; Soczyńska U. (Ed.), University of Warsaw Publisher: Warsaw, 191–212
31. Kupczyk E. & Suligowski R. (2000). Temporal and spatial patterns of high intensity rainfalls in Poland. *Miscellanea Geographica*, *9*, 77–84. https://doi.org/10.2478/mgrsd-2000-090110
32. Łazuka, E., Futa, A., Jastrzębska, M., Łagód, G., Szeląg, B., & Fatone, F. (2022). The applications of graph algorithms to modeling of integrated urban water management system. *Advances in Science and Technology Research Journal*, *16*(5), 277–89. https://doi.org/10.12913/22998624/155037
33. Łupikasza E. (2016). *The climatology of air-mass and frontal extreme precipitation*. Study of meteorological data in Europe. Springer International Publishing AG Switzerland.
34. Maimone, M., O'Rourke, D.E., Knighton, J.O., & Thomas, C.P. (2011). Potential Impacts of Extensive Stormwater Infiltration in Philadelphia. *Environmental Engineer and Scientist*: *Applied Research and Practice*, *14*, 29–39.
35. Mailhot, A., Lachance-Cloutier, S., Talbot, G., & Favre, A.C. (2013). Regional estimates of intense rainfall based on the Peak-Over-Threshold (POT) approach. *Journal of Hydrology*, *476*, 188–199. https://doi.org/10.1016/j.jhydrol.2012.10.036
36. Marchioni, M., & Becciu, G. (2018). Infiltration-exfiltration system for stormwater runoff volume and peak attenuation. *International Journal of Safety and Security Engineering*, *8*(4). https://doi.org/10.2495/SAFE-V8-N4-473-483
37. Miller, J.D., Kim, H., Kjeldsen, T.R., Packman, J., Grebby, S., & Dearden, R. (2014). Assessing the impact of urbanization on storm runoff in a peri-urban catchment using historical change in impervious cover. *Journal of Hydrology*, *515*, 59–70. https://doi.org/10.1016/j.jhydrol.2014.04.011
38. Musz-Pomorska, A., & Widomski, M.K. (2022). Analysis of the impact of the degree of catchment sealing on the operation of drainage system. *Applied Water Science*, *12*(11), 1–9. https://doi.org/10.1007/s13201-022-01774-5
39. Niedźwiedź, T., Twardosz, R., Walanus, A. (2009). Long-term variability of precipitation series in east central Europe in relation to circulation patterns. *Theoretical and Applied Climatology*, *98*, 337–350. https://doi.org/10.1007/s00704-009-0122-0
40. Piazza, P.; & Ursino, N. (2022). Modelling infiltration systems' performance for efficient, sustainable or circular urban water drainage. *Water*, *14*, 2620. https://doi.org/10.3390/w14172620
41. Procaccini, G., & Monticelli, C. (2021). A green roof case study in the urban context of milan: integrating the residential and cultivation functions for sustainable development. *Water*, *13*(2), 137. https://doi.org/10.3390/w13020137
42. Raymond, C.M., Frantzeskaki, N., Kabisch, N., Berry, P., Breil, M., Nita, M. R., & et al. (2017). A framework for assessing and implementing the co-benefits of nature-based solutions in urban areas. *Environmental Science & Policy*, *77*, 15–24. https://doi.org/10.1016/j.envsci.2017.07.008
43. Rodríguez, M. M., Fu, G., Butler, D., Yuan, Z., & Cook, L. (2024). The effect of green infrastructure on resilience performance in combined sewer

systems under climate change. *Journal of Environmental Management, 353*, 120229. https://doi.org/10.1016/j.jenvman.2024.120229

44. Salerno, F., Valsecchi, L., Minoia, R., Copetti, D., Tartari, G., Guyennon, N., Colombo, N., Pirola, N., Barozzi, B., Bellazzi, A., & Marziali, L. (2021). Factors Controlling the Hydraulic Efficiency of Green Roofs in the Metropolitan Area of Milan (Italy). *Sustainability*, *13*(24), 13638. https://doi.org/10.3390/su132413638
45. Sanesi, G., Colangelo, G., Lafortezza, R., Calvo, E., & Davies, C. (2016). Urban green infrastructure and urban forests: a case study of the Metropolitan Area of Milan. *Landscape Research*, *42*(2), 164–175. https://doi.org/10.1080/01426397.2016.1173658
46. Shariat, R., Roozbahani, A., & Ebrahimian, A. (2019). Risk analysis of urban stormwater infrastructure systems using fuzzy spatial multi-criteria decision making. *Science of The Total Environment*, *647*, 1468–1477. https://doi.org/10.1016/j.scitotenv.2018.08.074
47. Singh, V. P. (1996). *Kinematic Wave Modeling in Water Resources*: Surface Water Hydrology. John Wiley & Sons
48. Song, C. (2022). Application of nature-based measures in China's sponge city initiative: Current trends and perspectives. *Nature-Based Solutions*, *2*, 100010. https://doi.org/10.1016/j.nbsj.2022.100010
49. Sowby, R. B., Jones, D., & George, G. (2024). Policy options to support climate-conscious urban water planning. *Earth, 5*(4), 896–903. https://doi.org/10.3390/earth5040045
50. Szeląg, B., Łagód, G., Musz-Pomorska, A., Widomski, M.K., Stránský, D., Sokáč, M., Pokrývková, J., & Babko, R. (2022a). Development of rainfall-runoff models for sustainable stormwater management in urbanized catchments. *Water*, *14*(13), 1997. https://doi.org/10.3390/w14131997
51. Szeląg, B., Suligowski, R., Łagód, G., Łazuka, E., Wlaź, P., Strańsky,´ D., & et al. (2022b). Flood occurrence analysis in small urban catchments in the context of regional variability. *PLOS ONE*, *17*(11), e0276312. https://doi.org/10.1371/journal.pone.0276312
52. Szeląg, B., Suligowski, R., De Paola, F., Siwicki, P., Majerek, D., & Łagoód, G. (2022c). Influence of urban catchment characteristics and rainfall origins on the phenomenon of stormwater flooding: Case study. *Environmental Modelling & Software, 150*, 105335. https://doi.org/10.1016/j.envsoft.2022.105335
53. Szeląg, B., Fatone, F., Kiczko, A., Majerek, D., Białek, A., Łagód, G., Piotrowicz, A., Dąbek, L. (2024). Extended evaluation of the impact of rainfall, sewer network and land use retention on drainage system performance in a multi-criteria approach – modeling, sensitivity analysis. *Advances in Science and Technology Research Journal. 18*(6), 291–303. https://doi.org/10.12913/22998624/192023
54. Taguchi, V.J., Weiss, P.T., Gulliver, J.S., Klein, M.R., Hozalski, R.M., Baker, L.A & et al. (2020). It is not easy being green: recognizing unintended consequences of green stormwater infrastructure. *Water*, *12*(2), 522. https://doi.org/10.3390/w12020522
55. Ursino, N. (2015). Risk analysis of sustainable urban drainage and irrigation. *Advances in Water Resources*, *83*, 277–284. https://doi.org/10.1016/j.advwatres.2015.06.011
56. US EPA. (2015). Storm Water Management Model (SWMM)
57. Wang, S., & Wang, H. (2018). Extending the Rational Method for assessing and developing sustainable urban drainage systems. *Water Research*, *144*, 112–125. https://doi.org/10.1016/j.watres.2018.07.022
58. Wu, T., Song, H., Wang, J., & Friedler, E. (2020). Framework, Procedure, and Tools for Comprehensive Evaluation of Sustainable Stormwater Management: A Review. *Water*, *12*(5), 1231. https://doi.org/10.3390/w12051231
59. Xing, Y., Ni, G., Yang, L., Yang, Y., Xing, P., & Sun, T. (2019). Modeling the impacts of urbanization and open water surface on heavy convective rainfall: A case study over the emerging Xiong'an City, China. *ournal of Geophysical Research: Atmospheres, 124*, 9078–9098. https://doi.org/10.1029/2019JD030359
60. Zhang, C., He, M., & Zhang, Y. (2019). Urban sustainable development based on the framework of Sponge City: 71 case studies in China. *Sustainability*, *11*(6), 1544. https://doi.org/10.3390/su11061544
61. Zhu, X., Zhang, Y., Zhu, H., & Zhao, W. (2024). Systematic review and research frontier analysis of urban green infrastructure policy tools. *Fengjing Yuanlin, 31*(11), 86–93. https://doi.org/10.3724/j.fjyl.202402020082

JEE Journal of Ecological Engineering

Journal of Ecological Engineering, 2025, 26(10), 460–476
https://doi.org/10.12911/22998993/207167
ISSN 2299–8993, License CC-BY 4.0

Received: 2025.05.04
Accepted: 2025.07.15
Published: 2025.07.25

The impact of physical-geographical conditions on the sizing of rain gardens: A spatial case of Poland

Anita Białek[1*], Grzegorz Łagód[2]

[1] Faculty of Environmental Engineering, Geomatics and Renewable Energy, Kielce University of Technology, 25-314 Kielce, Poland
[2] Faculty of Environmental Engineering and Energy, Lublin University of Technology, 20-618 Lublin, Poland
* Corresponding author's e-mail: anita_bialek@interia.eu

ABSTRACT

Rain gardens are playing an increasingly significant role in the adaptation of urban areas to climate change, particularly in light of the growing frequency and intensity of rainfall events. The objective of this study was to assess the influence of physical and geographical conditions on the design, sizing, and effectiveness of rain gardens in Poland, with a particular focus on runoff control and regulation in the context of climate change adaptation. A computational tool was developed, integrating the kinematic wave equation with dynamic flow control algorithms, to support the modelling and optimization of infiltration systems. Analysis of meteorological data from 29 stations (covering 37 to 44 years of observations), along with soil infiltration characteristics, revealed a strong correlation between catchment imperviousness and the required infiltration trench capacity as well as the volume of controlled runoff. The highest storage capacity requirements were observed in Mikołajki (52.6–352.8 m³), while the lowest were observed in Elbląg (28.7–187.1 m³). The maximum controlled runoff volumes occurred in Katowice (91.4–213.7 m³) and Mikołajki (56.2–260.8 m³), while the lowest were recorded in Świnoujście (18.4–126.2 m³), Leszno (19.6–87.9 m³), and Poznań (32.7–84.9 m³). The developed tool offers substantial support for enhancing the resilience of urban retention systems, highlights the importance of implementing advanced stormwater management strategies under changing climatic conditions.

Keywords: water retention, urban catchments, computational tool, rain gardens, runoff control.

INTRODUCTION

Ongoing urbanization of catchments and climate change are leading to increased rainfall intensity, resulting in greater runoff volumes, more frequent overflow events, and elevated flood risks. These changes directly impact urban quality of life in urban areas by increasing the likelihood of flooding and overloading existing sewer infrastructure (Shuster et al., 2022; Sakib et al., 2023; Bibi et al., 2023).

Literature data (Li and Babcock, 2020; Zhang et al., 2018) indicate that Nature-Based Solutions (NBS), such as retention basins, infiltration trenches, and rain gardens, effectively reduce and delay stormwater runoff, thereby improving the urban water balance (Bowler et al., 2010; Ferreira et al., 2021). The implementation of these technologies reduces flood risk in urban areas (Rogger et al., 2017), enhances stormwater quality, and supports infiltration processes by removing pollutants such as heavy metals, organic compounds, and suspended solids (Sharma and Malaviya, 2021; Ferreira et al., 2021). Cities like Singapore and Lisbon demonstrate the effectiveness of integrating NBS with traditional water infrastructure (Ramísio et al., 2022; Hasan et al., 2024).

Research shows that infiltration trenches with regulated runoff can reduce peak flow rates by up to 40% in urbanized areas and help limit erosion (Zhang et al., 2018; Dai et al., 2023), while green roofs can retain 50–80% of annual rainfall, depending on climate and system design (Li and Babcock, 2020).

For NBS facilities to effectively reduce pollution and delay stormwater runoff, appropriate modelling is essential. The storm water management model (SWMM) is one of the most commonly used tools for analyzing the hydrological performance of such solutions. However, its implementation requires detailed input data, which in practice can result in data gaps or inaccuracies, potentially affecting the quality of design. In response to these challenges, simplified models have been developed, based on available data, enabling quick estimations of solution effectiveness. Studies (Pons et al., 2023) show that simplified models are particularly effective for smaller catchments.

Rain gardens, as an example of NBS, are gaining increasing recognition in cities worldwide due to their efficiency in stormwater management and their support for sustainable development and climate change adaptation (Li and Babcock, 2020; Shuster et al., 2022). A key aspect of designing such solutions is calculating water runoff to ensure adequate soil moisture for plant growth and effective water retention (Meerow et al., 2017; Zhang et al., 2018). The performance of NBS installations depends on the appropriate selection of vegetation capable of withstanding variable hydrological conditions, particularly during heavy rainfall and prolonged droughts (Palermo et al., 2023; Zhao et al., 2024).

In Poland, despite the growing popularity of rain gardens, there is a lack of systematic analyses incorporating long-term rainfall data and climate change projections. Examples from cities such as Gdańsk, Poznań, Warsaw, and Łódź highlight increasing investments in sustainable infrastructure, yet integration with long-term runoff modelling is often missing (Kucharczyk & Piłat, 2019; Szulczewska et al., 2016). Gdańsk has implemented the SWMM model for flow analysis but did not consider comprehensive long-term rainfall analysis, which could improve project effectiveness over time (Kasprzyk et al., 2022). In Warsaw and Kraków, studies that account for long-term rainfall variability and climate change are still lacking (Jakubowska, 2020; Wolski et al., 2021).

To provide a clearer overview of the advantages and limitations of GI (Green Infrastructure) and modelling tools, particularly in the context of runoff management, a summary of their benefits and challenges is presented in Table 1.

In Poland, there is still a lack of advanced tools for modelling and designing GI systems that would account for long-term rainfall data and regional variability in climatic conditions. Previous studies on the design of retention systems, such as rain gardens or infiltration trenches, often overlook the integration of hydrological and climatic variables, which limits the effectiveness of these solutions. Sustainable stormwater management requires a synergy between NBS technologies and dynamic hydrological models, tailored to the specific environmental conditions of a given area.

In response to this issue, the aim of this study was to analyze the impact of rainfall conditions and physical characteristics of urban catchments on the hydraulic parameters of rain gardens, including both the volume of the infiltration trench and the dynamics of runoff during inter-event periods across Poland. The study was based on meteorological data from 29 rainfall stations, covering a period of 37 to 44 years. The analysis included 26 939 rainfall events, which served as the basis for calculations related to the effectiveness of infiltration systems, enabling a comprehensive assessment of the impact of meteorological variables on the functioning of rain gardens across the country in the context of specific urban catchment characteristics.

METHODOLOGY

Urban development simulations were conducted (Figure 1 a-c), covering the impact of increased impervious surface area on the effectiveness of rain gardens in stormwater retention and infiltration, as well as providing guidelines for optimizing their design and implementation in urban catchments across Poland.

The analysis was conducted using a custom computational application, which enabled: (a) modelling runoff from the catchment based on rainfall data using the kinematic wave equation, (b) calculating the runoff hydrograph, (c) designing the volume of the infiltration trench for the rain garden, and (d) forecasting the required runoff control between rainfall events to maintain the minimum water level in the trench essential for plant growth. Figure 2 presents the dialog window displaying the available functions of the tool.

The tool was developed in C^{++} and implemented in the Qt Creator environment. The application allows for the modelling of retention tanks, infiltration trenches, and infiltration basins, with runoff directed either to the ground

Table 1. Advantages and disadvantages of GI elements and modelling tools in stormwater management

Aspect	Advantages	Disadvantages	Studies
Green infrastructure elements	– Increased retention and infiltration of stormwater. – Support for biodiversity (e.g., green corridors, pollinator habitats). – Reduced flood risk and less load on drainage systems. – Mitigation of urban heat island effect and improved urban aesthetics.	– Require large areas, which can be limiting in densely built-up zones. – High initial construction and maintenance costs. – Dependence on local conditions, which may require adjustments. – Requires major investments in urban spaces, often in existing infrastructure.	Li & Babcock (2014) showed that green roofs can retain 50–80% of annual rainfall depending on climate and design. Example from London and Copenhagen (Van Mechelen et al., 2015) – green roofs supporting bee and butterfly populations. Zhang et al. (2018) – controlled-runoff infiltration trenches reduce peak flow intensity by 40%. Bowler et al. (2010) showed that urban greenery lowers air temperature by 1–3 °C, improving thermal comfort.
Modelling tools	– Accurate analysis of retention, runoff, and water quality (e.g., SWMM, HEC-RAS, InfoWorks ICM). – Optimizes design and forecasts GI system performance under changing conditions.	– Limited data availability; require precise local input data. – Requires complex model calibration, which may be time-consuming.	SWMM model (EPA, 2015) – used for analyzing stormwater drainage systems, including GI. HEC-RAS (Brunner, 2010) – used for flow analysis in sewers and ditches, including GI context.
Need for modeling	– Accurate prediction of GI performance during extreme rainfall events. – Supports investment decisions and local adaptation of systems.	– Expensive implementation; requires access to detailed datasets. – Requires specialist knowledge and modelling expertise.	Hydrus (Šimůnek et al., 2005) – tool for analyzing water and pollutant transport in soils within GI systems. InfoWorks ICM – used to model complex urban water systems.
Runoff control approach	– Better runoff control, flood prevention, and climate change adaptation. – Reduces peak runoff, improving system performance.	– Requires complex flow regulation; expensive and time-intensive to implement. – Risk of malfunction in case of system failure or poor regulation.	Zhang et al. (2018) – controlled-runoff trenches reduce peak flow by 40%. Li & Babcock (2014) – regulated runoff in green roof systems enhances stormwater management.
Inter-event water retention	– Enhances long-term water retention, especially during dry periods. – Increases absorption capacity for later events.	– Excess water retention may cause drainage issues during future events. – Requires continuous monitoring and adaptation to changing hydrological conditions.	Yang et al. (2016) – residual water in infiltration systems improves water availability during dry periods. Caparrós-Martínez et al. (2020) – studied residual water in GI systems and its impact on retention under varying conditions.
Regionalized analyses	– Allows for inclusion of local hydrological and climatic differences. – Supports the development of locally adapted standards.	– Requires extensive data and model calibration; time-consuming and costly. – Difficulties in obtaining accurate regional data may limit result precision.	Zhang et al. (2018) – regional analysis of GI impact on flow in various climates and hydrological conditions. Li & Babcock (2014) – use of regional meteorological data in modelling green roof performance.

or directly to the sewer system. Additionally, a runoff regulation function was incorporated, which is crucial for designing infiltration trenches integrated with vegetation and supporting sustainable stormwater management. The tool facilitated the simulation of long-term rainfall sequences, allowing water systems to adapt to changing climatic conditions and varying rainfall intensities. The algorithm's implementation in the software enabled rapid and accurate hydrological analyses.

Various hydrological modelling tools are widely used to evaluate the performance of rain gardens and green infrastructure in urban environments. Among the most frequently cited are SWMM, MIKE URBAN, HYDRUS-1D, and MUSIC (Shen et al., 2021; Li et al., 2020; Zhang et al., 2022; Šimůnek et al., 2005; Wang et al.,

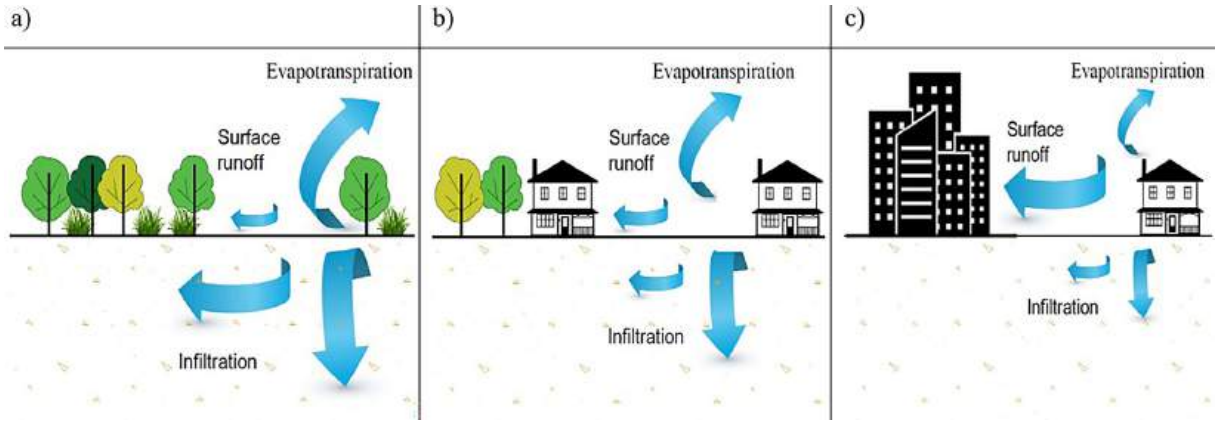

Figure 1. Catchment urbanization scenarios considering three levels of imperviousness: (a) low, (b) medium, and (c) high

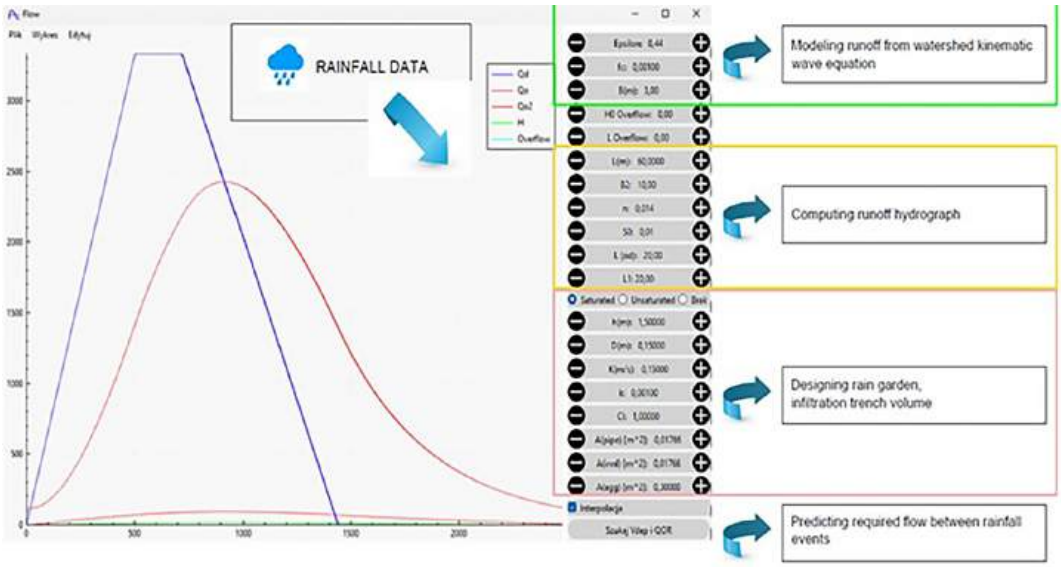

Figure 2. The dialog window displaying the available functions of the tool

2018). These models typically address catchment areas ranging from 0.1 to 2.0 hectares and incorporate parameters such as rainfall intensity, soil permeability, and retention depth. Their complexity spans from advanced simulations integrated with sewer networks and GIS systems (e.g., SWMM) to simplified frameworks designed for conceptual and spatial analysis (e.g., MUSIC). While advanced models demand extensive data inputs and calibration, simplified tools enable quicker assessments with lower data requirements, making them particularly valuable during early planning stages. A summary of the key features of these models is presented in Table 2, providing guidance for practitioners and researchers in selecting the most suitable tool for specific urban hydrology applications.

Rainfall data

The rainfall analysis was based on data from 29 IMGW-PIB stations (Institute of Meteorology and Water Management – National Research Institute) located in various parts of Poland, ensuring their spatial representativeness. The distribution of the stations is shown in Figure 3.

Poland, located in the zone of a temperate warm climate, is characterized by high rainfall variability due to the influence of both maritime and continental climates (Niedźwiedź et al., 2009; Szeląg et al., 2022). The average annual rainfall totals around 600 mm, but these values vary regionally – from 520 mm in the central part of the country to over 1000 mm in the mountains (Szeląg et al. 2024; Bogdanowicz and Stachý,

Table 2. Comparison of selected rain garden models

Model / Tool	Catchment area [ha]	Depth [m]	Key parameters	Advantages	Limitations
SWMM	0.3–2.0	0.6–1.0	Rainfall (IDF), CN, LID, soil permeability, time of concentration	Integration with sewer network, high accuracy	High data requirements, complex calibration
MIKE URBAN	0.5–2.0	0.6–1.2	Rainfall, retention, slope, land use, runoff	GIS integration, high spatial resolution	High complexity, topographic data required
HYDRUS-1D	0.1–0.8	0.5–1.0	Porosity, conductivity, layer structure, physicochemical properties	Accurate representation of infiltration and storage	1D model, no surface runoff or sewer representation
MUSIC	0.1–1.0	0.3–0.9	Delay time, runoff, retention volume, rainfall type, layer configuration	Intuitive GUI, fast scenario analysis	Simplified infiltration scheme, no system dynamics
Proprietary model	approx. 1.0	0.5–0.8	Rainfall, infiltration, geometric dimensions, Q_{max}, V_{max}, Q_{OR}	Few input variables, fast analysis	Simplified hydraulics, no sewer network simulation

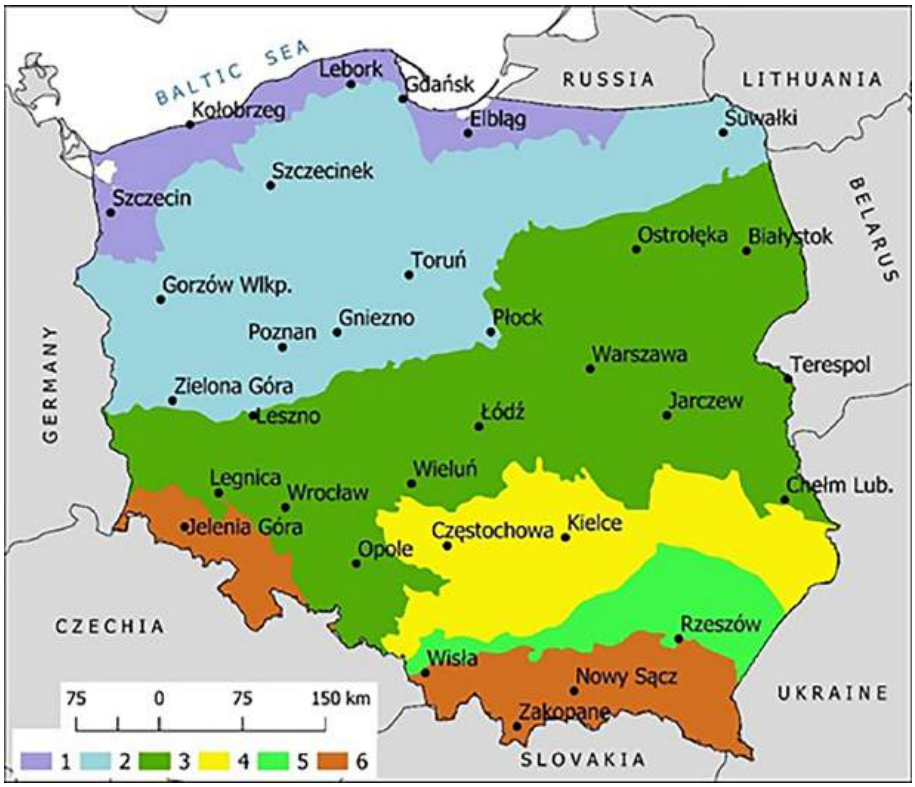

Figure 3. Location of rain gauges against the background of the main physical-geographical regions of Poland (1 – Baltic coastal lowlands, 2 – lakelands, 3 – central lowlands, 4 – uplands, 5 – sub-mountain basins, 6 – mountains); Source: Białek and Musz-Pomorska (2025)

1998). In cities with high urbanization, rainfall is more frequent and intense, mainly due to atmospheric convection, which increases flood risk and requires appropriate drainage system design (Kupczyk and Suligowski, 1997; Łupikasza, 2016). Particularly in mountainous and coastal areas, the highest intensity rainfall is recorded (Szeląg et al., 2022).

The identification of independent rainfall events was carried out according to the DWA – A 118 methodology, based on the analysis of three basic criteria: minimum inter-event time (MIT), minimum rainfall volume, and minimum intensity. According to this method, rainfall events with intensities below 0.5 mm were excluded from the analysis, allowing for more accurate results in the context of hydrological process modelling and runoff assessment in urban catchments. The study included rainfall data from 1961–2005, providing a long-term picture

of rainfall variability. The detailed methodology is discussed by Szeląg et al. (2023a). It is also worth noting that, on average, dry periods in Poland last from 5 to 9 days, which is an important factor in assessing rainfall variability in different cities. Furthermore, the average annual rainfall exceeding 5 mm in intensity ranges from 11 to 15 mm, depending on the region, which also affects the hydrological characteristics of individual cities. Detailed results and rainfall data sets used in the calculations are presented in Table S1 (supplementary materials).

Sizing of rain gardens

The application for modelling runoff in infiltration systems supports the design of rain gardens by combining mathematical calculations with hydrological processes (Białek and Musz-Pomorska, 2025). Using Darcy's equation, it analyzes water infiltration into the soil, taking into account soil permeability and moisture content, while surface runoff is modeled using the kinematic wave equation, considering rainfall intensity and terrain shape. The tool allows for the design of rain gardens that effectively manage stormwater in various atmospheric conditions, including during intense rainfall or prolonged droughts.

Modelling runoff using the kinematic wave equation method

The kinematic wave equation, used in modelling surface runoff in infiltration systems, analyzes water flow by accounting for changes in water levels, soil infiltration capacity, and the impact of dry periods on runoff, thereby supporting the assessment of water retention efficiency by vegetation and soil. The kinematic wave Equation 1 can be expressed as follows:

$$\frac{\partial q}{\partial x} + \frac{\partial y}{\partial t} = i - f \tag{1}$$

where: $\frac{\partial \mathrm{q}}{\partial \mathrm{x}}$ – flow gradient in the spatial direction, $\frac{\partial y}{\partial t}$ – change in water depth over time, i – rate of rainfall, (expressed in mm/hr), f – rate of losses from rainfall.

The surface runoff model for flat-bottom systems is based on the kinematic wave equation, the Darcy–Weisbach equation, and Manning's formula.

A simplified water balance for rain gardens is commonly used to evaluate the performance of green infrastructure (European Commission, 2015; Beven et al., 2012). Bhaskar et al. (2016) also applied this approach in green infrastructure flow analysis to support stormwater system modelling. The water balance equation (2) is expressed as:

$$dV = Q_{outS}(t)dt - Q_{out}(t)dt - \\ - Q_{inf}(t)dt - ET(t)dt \tag{2}$$

where: the input data include: $Q_{outS}(t)$ – inflow of water to the green infrastructure object at time t, (m^3/s), $Q_{out}(t)$ – runoff from the substrate at time t, including the flow to the ground, with overflow occurring if the allowable hydraulic capacity is exceeded, (m^3/s), $Q_{inf}(t)$ – volume of water flowing to the ground per unit time t, (m^3/s), $ET(t)$ – evapotranspiration from the surface layer, (m^3/s).

The computational scheme of the infiltration system is shown in the figure (Figure 4).

The initial form of Equation 2 for the soil, presented as Equation 3:

$$Q_{inf} = f_c \times \left(B \times L + h\,(B + L)\right) \tag{3}$$

$$Q_{outS}(t) - Q_{out}(t) = \varepsilon \cdot B \cdot L \cdot \frac{dh}{dt} \tag{4}$$

The solution of the balance equation for green infrastructure facilities (2) was used for the calculations of the infiltration trench, with appropriate transformations of relationships (5) and (6):

$$Qdmax \times \frac{t}{tp} - f_c \times \left(B \times L + h(B + L)\right) \\ = \varepsilon \times B \times L \times \frac{dh}{dt} \tag{5}$$

$$Qdmax \left(1 + \frac{1}{\lambda} - \frac{t}{\lambda \times tp}\right) - \\ - f_c \times (B \times L + h(B + L)) = \varepsilon \times B \times L \times \frac{dh}{dt} \tag{6}$$

where: Q_{inf} – stormwater infiltration flux into the soil, varying over time t, (m^3/s), f_c – infiltration rate, (mm/hr), B – width of the infiltration trench, (m), L – length of the infiltration trench, (m), h – water depth in the soil, (m), Q_{outS} – inflow rate of stormwater to the trench, variable over time t, (m^3/s), Q_{out} – runoff rate of sewer system, variable over time t, (m^3/s), Q_{dmax} – rainwater

infiltration flow into the ground, variable over time t, (m³/s), ε – porosity coefficient, (-), t – duration of rainfall, (min); t_p – time to reach maximum flow, (min), λ – linear resistance coefficient, (-), dh/dt – change in water depth in the soil over time.

For the saturation zone, the runoff through the drainage pipe is described by the following relationships (7) and (8):

$$Q_{out} = \frac{-\left(\frac{h + D}{L \cdot B \cdot K}\right) + \sqrt{\left(\frac{h + D}{L \cdot W \cdot K}\right)^2 + 4 \cdot N \cdot H}}{2 \cdot N} \quad (7)$$

for:

$$N = \frac{f \cdot L}{2 \cdot g \cdot A_{pipe}^2 \cdot D} + \frac{1}{2 \cdot g \cdot A_{pipe}^2} + \frac{C_L}{2 \cdot g \cdot A_{pipe}^2 \cdot \theta_{agg}^2} \quad (8)$$

where: H – thickness of the water table in the soil, (m), h – thickness of the soil above the top of the pipe, (m), D – inner diameter of the pipe, (m), L – length of the infiltration trench, (m), K – hydraulic conductivity of soil, (m/s), B – width of the infiltration trench, (m), A_{pipe} – cross-sectional area of the pipe, (m²), Θ_{agg} – porosity of the soil, (-), C_L – coefficient of local resistances, (-), g – gravitational acceleration, (m/s²), λ – linear resistance coefficient, (-), calculated using the formula (9):

$$\lambda = \frac{1}{\left(-2 \cdot log\left(\frac{k}{3.71 \cdot D}\right)\right)^2} \quad (9)$$

where: k – roughness of the conduit, (m), D – inner diameter of the pipe, (m).

Rain garden sizing assumptions

This study utilised independent rainfall events and delineated dry periods to determine:

- Infiltration trench volume (V),
- Runoff from the infiltration trench (Q_{OR}).

The optimal ratio of infiltration trench volume to catchment area is crucial for effective water retention, and its regulation through runoff control plays a key role in this process. An insufficient volume can result in excessive runoff, as noted by Fletcher and Shuster (2013). The analysis also took into account dry periods, which can affect the

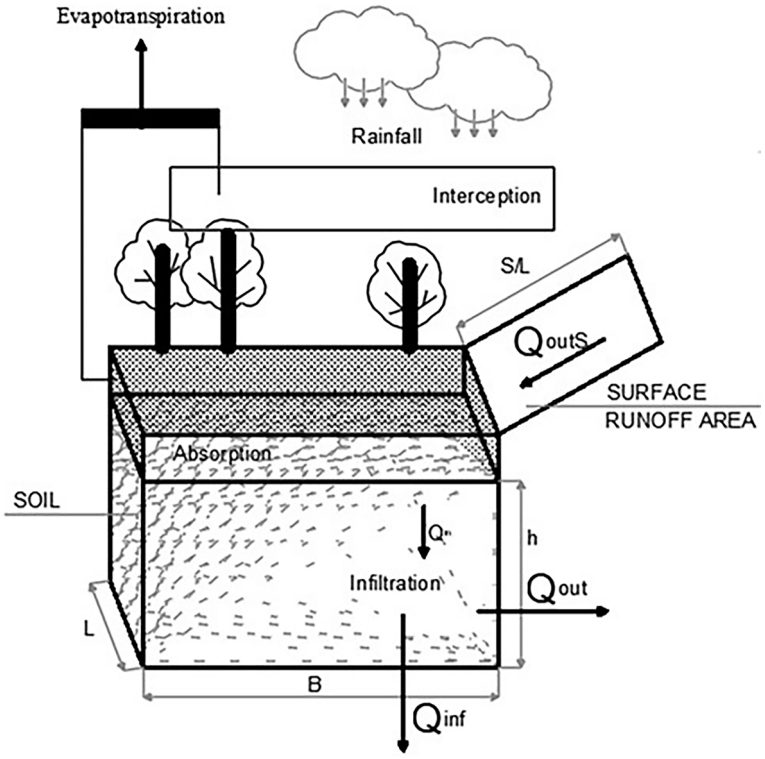

Figure 4. Schematic representation of the infiltration system

efficiency of infiltration systems. Prolonged dry periods may reduce soil infiltration capacity, impacting the ability to maintain adequate moisture levels in rain gardens, especially in the context of changing climatic conditions (Liu and Tan, 2014).

A system depth of 1.5 m and a minimum water level of 0.30 m in the infiltration trench were assumed to ensure constant retention and protect plants from desiccation (Li and Davis, 2009). Calculations encompassed three scenarios with increasing impervious surface areas in the catchment, reflecting urbanisation processes.

Designated rainfall events (Table S1- supplementary materials) were analysed, and the infiltration trench volume was calculated using Equation 11:

$$V = \varepsilon \cdot B \cdot L \cdot h_{max} \quad (10)$$

The application employs a proprietary method that models not only individual values for infiltration trenches concerning independent rainfall events but also accounts for dry periods. Regulated runoff, dependent on the dry period, can be modeled using Equation 12:

$$Q_{OR} = \varepsilon \cdot B \cdot L \cdot h_{max} \cdot t_{bd} \quad (11)$$

where: V – volume of the infiltration trench, (m³); ε – porosity coefficient, (-); B – width of the trench, (m), assumed B = 3 m; L – length of the trench, (m); h_{max} – maximum depth of the trench, (m), assumed h_{max} = 1.5 m; Q_{OR} – runoff from the infiltration trench, (m³/s); t_{bd} – dry period (s), derived from IMGW rainfall data for the period 1961–2005 for various Polish cities (Table S1 – supplementary materials).

Assumptions for calculations

The following input data were used in the application, as shown in Table 3.

RESULTS

Infiltration trenches are increasingly recognized as vital components in modern stormwater management strategies, facilitating the retention and gradual percolation of rainwater into the soil. Their effectiveness is influenced by factors such as soil permeability, rainfall intensity, and the available infiltration area. Proper design of infiltration systems, like rain gardens, is essential for mitigating flood risks and enhancing the hydrological balance in urbanized areas.

Table 3. Assumed input data used for the infiltration trench, catchment, and runoff (Akan and Houghtalen, 2003)

Name	Index	Unit	Value
Infiltration trench			
Rainfall duration	t_d	min	step 5 min
Porosity coefficient	ε	-	0.44
Infiltration rate	*fc*	m/s	0.001
Width	*B*	m	3
Length	*L*	m	to 200
Catchment			
Width of flow path	*B*	m	10, 40, 100
Length of flow path	*L*	m	20
Manning's roughness coefficient	*n*	$m^{-1/3} \cdot s$	0.0015
Hydraulic gradient	S_0	-	0.001
Runoff			
Maximum water depth in the soil	*h*	m	1.5
Diameter of drainage pipes	*D*	m	0.15
Hydraulic conductivity of soil	*K*	m/s	0.15
Cross-sectional area of the pipe	A_{pipe}	m²	0.01766
Porosity of the soil	Θ_{agg}	-	0.3
Coefficient of local resistances	*CL*	-	1
Roughness of the conduit	*k*	m	0.001

To investigate potential spatial differentiation in infiltration efficiency, the data were analyzed using k-means clustering – a widely used unsupervised machine learning method that partitions observations into k distinct clusters based on their similarity. The algorithm minimizes variance within clusters while maximizing differences between them, ensuring that data points within a cluster are more similar to each other than to those in other clusters.

In this analysis, the number of clusters (k) was set to two, based on a preliminary spatial assessment. The aim was to distinguish general areas with differing geographic and climatic characteristics that may affect the performance of nature-based stormwater management solutions.

As a result of the analysis, two distinct clusters – CL1 and CL2 – were identified, reflecting key spatial and rainfall-related differences within the study area. Table 4 presents the average values of key variables (latitude, longitude, and annual rainfall) for each cluster, along with variability indicators such as variances and quantiles at three thresholds (10, 40, and 100), illustrating the internal diversity of each group.

The analysis revealed that Cluster CL1, located in the southeastern region (Lat = 51.92; Long = 20.29), experiences higher mean annual rainfall (592.09 mm) compared to Cluster CL2 (Lat = 52.14; Long = 17.08; Rainfall = 585.00 mm). Furthermore, CL1 consistently shows higher values of both variances and quantiles, suggesting greater internal variability within this group. In contrast, CL2 exhibits lower variability and a more homogeneous distribution of parameters.

This pattern of regional differentiation aligns with the approach described by Szeląg et al. (2023b), which underscores the value of identifying spatial and statistical variability as a foundation for further modelling and classification. Although the inter-cluster differences are moderate, they are systematic and substantiate the presence of meaningful regionalization. To further validate the segmentation, advanced cluster quality assessments such as silhouette analysis or ANOVA (Analysis of Variance) are recommended, in line with established practices in environmental data analysis and spatial hydrological modelling.

Complementing the clustering results, a correlation analysis was conducted to assess the relationships between geographic variables and hydraulic performance metrics. The outcomes, summarized in Figure 5, confirm statistically significant correlations – particularly between longitude and key hydraulic indicators.

For example, longitude demonstrated a strong positive correlation with retention volume V(40) (r = 0.524) and outflow Q(40) (r = 0.599). Very high correlations were also observed between retention volumes under different rainfall scenarios, such as V(40) and V(100) (r = 0.961), as well as between Q(40) and Q(100) (r = 0.928). These findings underscore the potential to estimate infiltration trench dimensions using geographic location and rainfall data, without the need for complex hydraulic modelling.

The use of a standardized 1-hectare catchment area – selected based on the literature (De Paola and De Martino, 2013; De Paola and Ranucci, 2012; Aldrees and Dan'azumi, 2023) as representative of urban micro-catchments in Poland – strengthens the practical relevance of the results for planning green infrastructure in urban environments.

Analysis of infiltration trench volume

The conducted analysis of infiltration trench volumes under various urban catchment sealing scenarios (Figures 6a–c) provides valuable insights into the potential of infiltration systems, including rain gardens, for stormwater management in urbanized areas of Poland.

The results indicate a significant increase in the required volume of infiltration trenches across all six mesoregions, which is a key element in assessing the changing structure of rainfall infiltration on a national scale, considering the ongoing urbanization of urban catchments and the resulting increase in land sealing. In the first sealing scenario (Figure 6a), the volumes of the infiltration trench predominantly ranged from below 36 m³ to

Table 4. Mean parameter values in clusters CL1 and CL2

Parameter	Lat	Long	Rainfall	V(10)	V(40)	V(100)	Q(10)	Q(40)	Q(100)
CL1	51.92121	20.28939	592.0909	10.92833	19.08945	44.46508	2.209315	3.387168	7.621287
CL2	52.13519	17.07593	585.0000	10.34620	17.80728	41.39799	1.876057	2.979982	6.666438

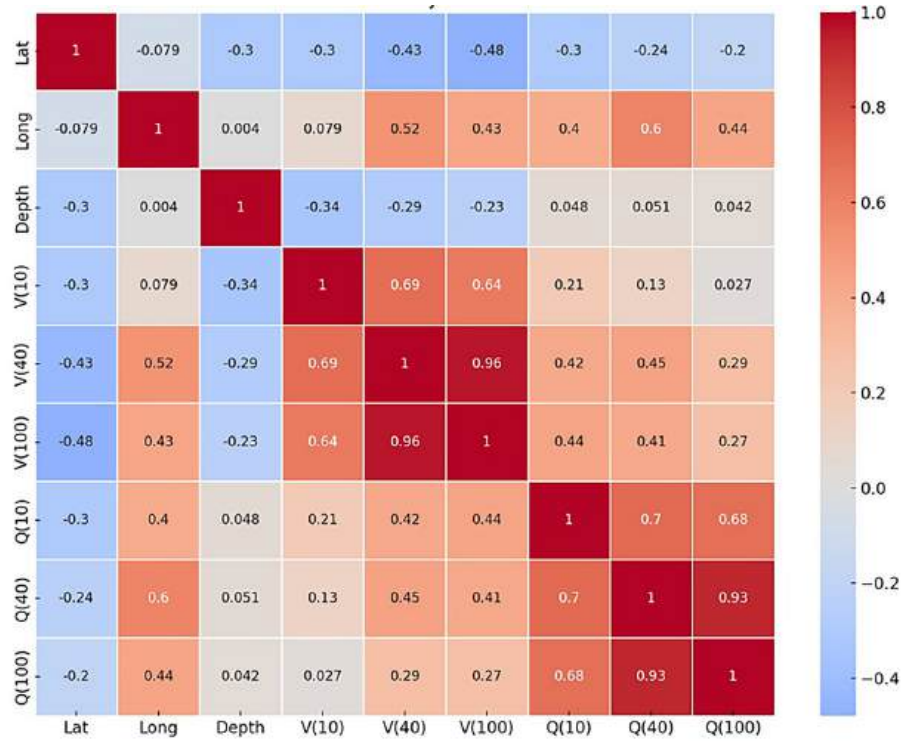

Figure 5. Pearson correlation matrix between geographical, physical, and hydraulic parameters

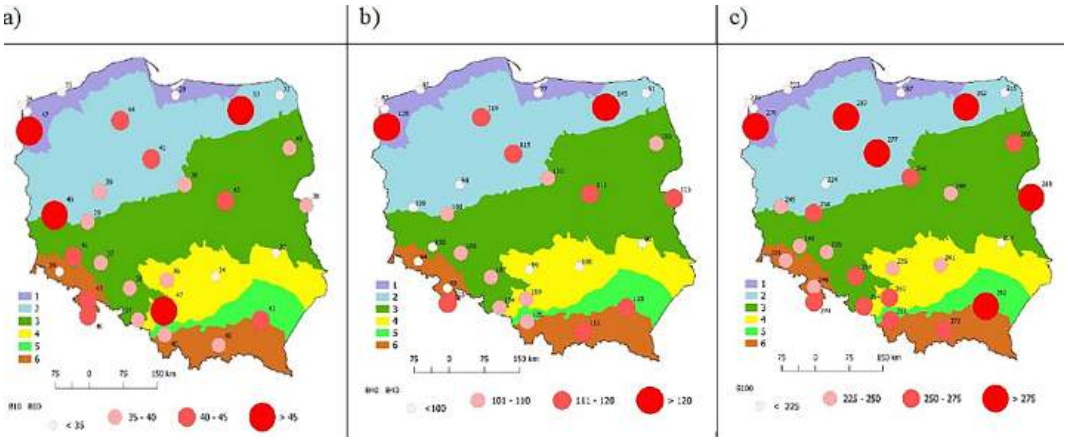

Figure 6. The volume of the infiltration trench, considering varying degrees of urban catchment sealing: (a) low, (b) medium, and (c) high

about 40 m³; in the second scenario (Figure 6b), they oscillated between 101 and 110 m³, while in the third scenario (Figure 6c), the volumes ranged from 250 m³ to approximately 275 m³. The largest trench volumes, regardless of the sealing degree, were recorded in Mikołajki (Mesoregion 2), where the values were 52.6 m³, 145.4 m³, and 352.8 m³, while the smallest volumes occurred in Elbląg (Mesoregion 1), with values of 28.7 m³, 77.4 m³, and 187.1 m³. In the first sealing scenario (Figure 6a), the highest trench volumes were recorded in lowland, lakeland, and upland areas: Mikołajki (52.6 m³), Szczecin (47.2 m³), Katowice (46.9 m³), and Zielona Góra (45.1 m³), while values below 35 m³ were observed in lowland, lakeland, upland, and mountain basin areas – in Elbląg (28.7 m³), Kołobrzeg (33.3 m³), Suwałki (32.0 m³), Lublin (32.3 m³), Kielce (34.3 m³), and Jelenia Góra (33.9 m³).

The analysis of the percentage increase in trench volume in relation to urbanization changes revealed that the highest increase was recorded in Terespol (7.7%), while the lowest was in Zielona Góra (5.4%). In cities with the highest

trench volume values, the increases were as follows: Mikołajki (6.7%), Szczecin (5.9%), Katowice (5.6%), and Zielona Góra (5.4%). In cities with lower trench volumes, similar growth rates were observed: Elbląg (6.5%), Kołobrzeg (6.6%), Suwałki (6.7%), Lublin (6.5%), Kielce (7.0%), and Jelenia Góra (6.7%).

The research conducted in the six mesoregions of Poland revealed significant variation in infiltration trench volumes depending on the degree of surface sealing. The largest trench volumes were recorded in Mikołajki (Mesoregion 2), where the values in the three sealing scenarios were 52.6 m³, 145.4 m³, and 352.8 m³, which is consistent with the characteristics of lakeland regions where the presence of numerous water bodies and highly permeable soils promotes infiltration. The smallest volumes occurred in Elbląg (Mesoregion 1) – 28.7 m³, 77.4 m³, and 187.1 m³ – which is related to denser development and poorer conditions for infiltration. In lowland and upland mesoregions such as Szczecin, Katowice, and Zielona Góra, trench volumes were varied and dependent on local topographical conditions and soil types.

In the highest sealing scenario (Figure 6c), trench volumes were characterized by a wider range, with volumes exceeding 275 m³ in Mesoregions 1, 2, 3, and 5, while in other mesoregions, they oscillated between 225 m³ and 275 m³. The division into mesoregions enables a more accurate assessment of the infiltration capacity of individual areas and their demand for infiltration trenches. The results of the analyses suggest that cities with a high degree of sealing require larger trench volumes, while lakeland regions benefit from better natural water retention conditions.

The obtained results confirmed the need to adjust stormwater management strategies in different mesoregions to increase their resilience to extreme weather events in the face of climate change. Similar challenges related to surface sealing are occurring worldwide. For example, in Singapore, as part of the "ABC Waters Programme" (Lim et al., 2016; Yau et al., 2017), green spaces were increased and rain gardens were implemented, enabling effective stormwater management. In New York, the "Green Infrastructure Plan" successfully reduced surface runoff by 1.2 million m³ per year (Rosenzweig and Fekete, 2018).

The analysis of infiltration trench volumes in different mesoregions of Poland revealed distinct differences in the structure of rainfall infiltration, closely linked to the degree of watershed sealing. In cities with a higher degree of sealing, such as Szczecin, the highest retention capacities were observed, with trench volumes exceeding 45 m³, 120 m³, and 275 m³ in three different sealing scenarios. Climate change may affect the water retention capacity in different mesoregions, with lowland and lakeland areas potentially experiencing periodic flooding due to increased rainfall intensity, while upland and mountain regions may face sudden surface runoff leading to erosion.

Analysis of runoff volume from the infiltration trench in an urban catchment

Changes in land use structure, particularly in urbanized areas, have a key impact on the water balance. Surface sealing, such as covering it with concrete, asphalt, or building roofs, limits the infiltration of rainfall, leading to an increase in surface runoff (Arnold and Gibbons, 1996; Fletcher et al., 2013). This phenomenon is commonly observed worldwide, especially in cities with a high degree of urbanization, such as New York, Tokyo, or Paris.

This study analyzes the impact of surface sealing on surface runoff in Poland, taking into account the diverse physical and geographical conditions of individual mesoregions (Figure 7a-c). The analysis considers three surface sealing scenarios: low, medium, and high.

The results of the analysis indicate significant variability in the size of runoff depending on the degree of sealing and specific geographic conditions. In the first scenario (Figure 7a), characterized by a low degree of sealing, cities with runoff values in the range of 30–40 m³/d dominate. In the second scenario (Figure 7b), with medium sealing, runoff ranges from 55 to 70 m³/d, while in the third scenario (Figure 7c), with the highest sealing, runoff values increase to the range of 130–160 m³/d. Observations show that as the surface sealing increases, the number of cities with higher surface runoff also increases.

The highest runoff values are found in mountainous (Mesoregion 6), upland (Mesoregion 4), and lake regions (Mesoregion 2), where terrain morphology and lithological properties promote intensification of surface runoff. In the analysis of the impact of urban catchment sealing on runoff, cities with the highest runoff values (> 50 m³/d) at a low degree of sealing (Figure 7a) include

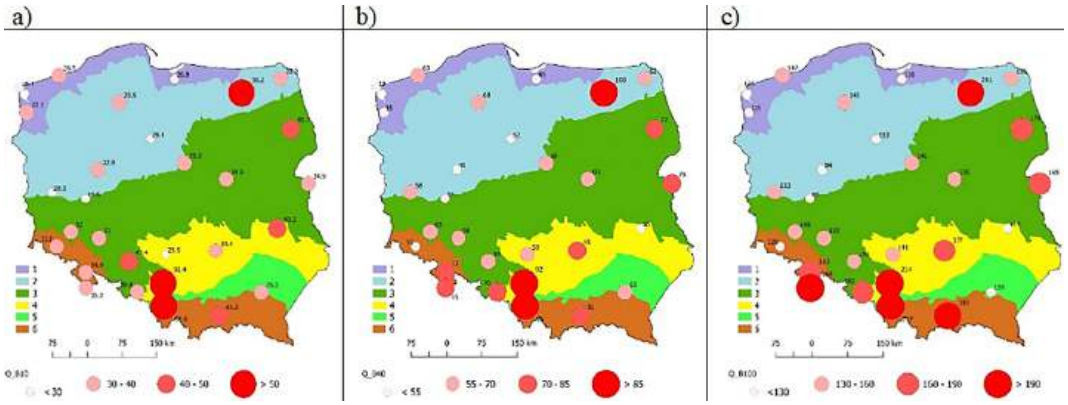

Figure 7. The size of the regulated runoff from the infiltration trench considering the sealing of the urban catchment: a) small, b) medium, c) high

Katowice (Mesoregion 4), Mikołajki (Mesoregion 2), and Bielsko-Biała (Mesoregion 6). In conditions of increased sealing (> 100 m³/d, Figure 7c), this trend remains particularly noticeable in mountainous areas, especially in Bielsko-Biała and Nowy Sącz (Mesoregion 6).

A specific case is Mikołajki (Mesoregion 2), where runoff values remained high regardless of the degree of catchment sealing (Figure 7a – 56.2 m³/d; Figure 7b – 107.5 m³/d; Figure 7c – 260.8 m³/d).

The results of the analysis confirmed the significant variability of runoff depending on the degree of sealing and specific geographic conditions, which is supported by numerous studies conducted worldwide. Research by Booth et al. (2002) in the United States indicates that in cities like New York, Los Angeles, and Chicago, intense surface sealing leads to a significant increase in runoff, resulting in overloaded sewer systems and increased flood risk. In Chicago, the rapid discharge of water into the sewer system limits infiltration, leading to soil moisture deficits and affecting the microclimate (Shuster et al., 2005). In Europe, studies conducted by Salvadore et al. (2015) in London and Paris showed that surface sealing in these cities led to a more than 70% increase in surface runoff compared to natural areas (Zhou et al., 2017; Fletcher et al., 2013). Similar observations were made in Asian cities such as Beijing and Tokyo. As studies by Li et al. (2020) and Endo et al. (2021) indicated, the increase in sealed surfaces in these metropolises leads to a reduction in the concentration time of runoff and an increase in its peak values, which burdens drainage systems and increases the risk of local flooding.

In Poland, particularly in cities such as Warsaw and Kraków, hydrological studies conducted by Szulc and Zelewski (2021) and Banasik et al. (2014) indicate a significant increase in surface runoff, which now exceeds 60% compared to earlier years, mainly due to intensive urbanization and infrastructure development. These changes lead to overloaded sewer systems and an increased flood risk, particularly in areas with higher levels of sealing.

At the international level, solutions based on green infrastructure, such as rain gardens, infiltration systems, and green roofs, show positive effects in reducing surface runoff. Research by van de Meene et al. (2011) in the Netherlands shows that the implementation of such solutions allowed a 30% reduction in runoff, effectively reducing flood risk in cities with high levels of urbanization.

Dependence between catchment sealing, infiltration trench volume, and runoff from the infiltration trench

To investigate the relationship between the degree of catchment sealing and the volume of the infiltration trench (Figure 8a) as well as runoff from the infiltration trench (Fig. 8b) in cities in Poland, the data presented in Figure 8 were analyzed.

The data presented in Figure 8a show clear differences in the impact of surface sealing on the volume of the infiltration trench across various mesoregions of Poland. Particularly in the mesoregion 3 (Terespol) and the mesoregion 4 (Kielce), where sealing has the greatest effect, noticeable changes in the water balance are observed, and an increase in sealing leads to a reduction in the land's ability to infiltrate rainfall.

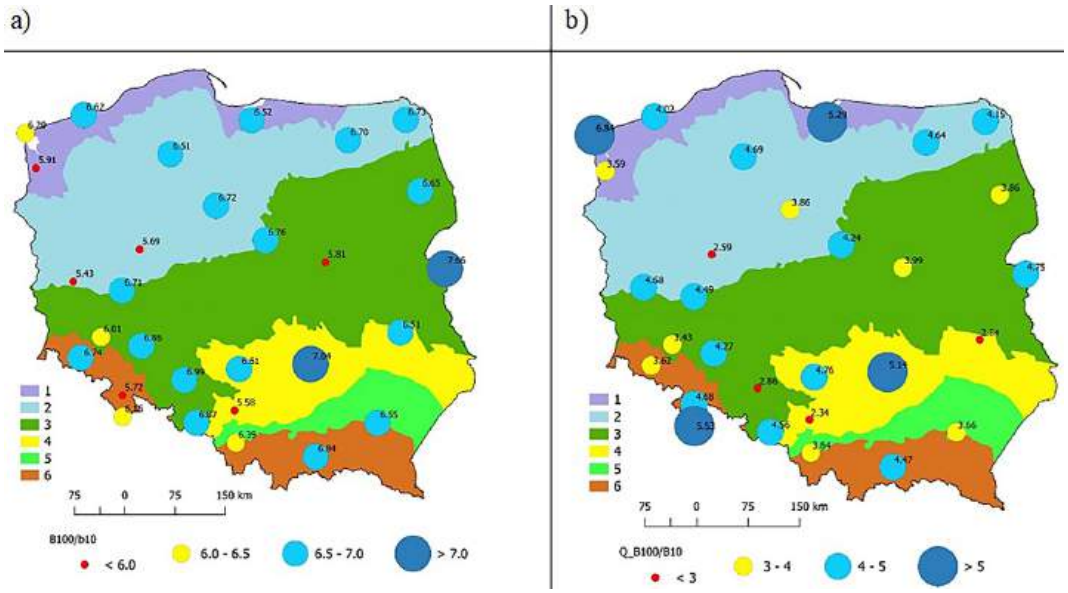

Figure 8. The relationship between catchment sealing and: a) the volume of the infiltration trench; b) runoff from the infiltration trench in cities in Poland

On the other hand, in Poznań (Mesoregion 2) and Katowice (Mesoregion 4), where the impact of sealing on the volume of the infiltration trench is smaller, this may be due to other geographical or hydrological factors, such as soil type, terrain structure, or the presence of retention infrastructure.

The data in Figure 8b show a clear variation in the relationship between catchment sealing and runoff from the infiltration trench in Poland. The greatest impact of sealing on runoff was recorded in the 1st mesoregion, with values of 6.84 in Świnoujście and 5.29 in Elbląg. In lowland regions, sealing significantly contributes to an increase in runoff, due to smaller terrain slopes and more intensive development. In contrast, in Katowice (Mesoregion 4) and Poznań (Mesoregion 2), where runoff relationships are smaller (2.34 and 2.59, respectively), the impact of sealing on surface runoff is less pronounced.

According to global studies, the relationship between catchment sealing and runoff depends on local geographical conditions. In lowland regions, such as Sydney (Australia) or Świnoujście and Elbląg (Poland), surface sealing leads to a significant increase in runoff due to limited infiltration. Increased urbanization in lowland areas leads to a significant rise in stormwater runoff, which is consistent with research in the Netherlands (de Lange et al., 2019), where runoff increased by over 70% due to intensive urbanization. In these regions, other factors, such as terrain structure, the presence of green infrastructure (e.g., rain gardens), or natural water retention, can reduce the impact of sealing on runoff, as confirmed by the findings of Barton et al. (2021) regarding ecological solutions in water management. Studies by Jafari et al. (2020) indicate that in lowland regions of Australia, such as around Sydney, surface sealing leads to a significant increase in runoff, while in more mountainous regions, such as the United States (Leopold et al., 2018), sealing has a lesser impact on runoff due to favorable terrain morphology and natural water retention.

In mountainous areas, such as Nowy Sącz or Bielsko-Biała (Mesoregion 6), the ratio of sealing to the volume of the infiltration trench remains high, exceeding a value of 6 (Figure 8a). In this region, due to the varied terrain morphology, water tends to naturally infiltrate, which means that despite high levels of sealing, runoff does not increase as drastically as in lowland areas. For example, in Bielsko-Biała, the runoff ratio with medium sealing is 3.84, and in Nowy Sącz, it is 4.47 (Figure 8b). Furthermore, the presence of green infrastructure, such as stormwater retention systems, may also contribute to limiting the intensity of runoff in these areas.

These results highlight the importance of considering specific geographical, urban, and climatic conditions in hydrological analyses and stormwater management in different regions.

CONCLUSIONS

This study investigated the impact of changing rainfall patterns and the characteristics of urban catchments on the effectiveness of rain gardens in six mesoregions of Poland. The analysis was based on meteorological data from 29 stations covering a period of 37 to 44 years, as well as a custom-built simulation tool that accounted for three levels of land sealing. The research showed an increase in the required volume of the infiltration trench across all regions in response to increased sealing. In the first scenario, the volumes of the trench ranged from 28.7 m³ (Elbląg) to 52.6 m³ (Mikołajki), in the second scenario from 77.4 m³ to 145.4 m³, and in the third scenario from 187.1 m³ to 352.8 m³. The largest infiltration capacities were recorded in Mikołajki, Szczecin, and Katowice, while the smallest were in Elbląg, Kołobrzeg, and Suwałki. The highest relative increase in trench volume occurred in Terespol (7.7%), while the lowest was in Zielona Góra (5.4%). In lake regions such as Mikołajki, natural soil conditions favored more efficient infiltration.

Surface runoff analysis revealed higher runoff volumes in cities with a high degree of sealing, particularly in mountainous, upland, and lake regions. In the case of high sealing, runoff reached values from 130 m³/d to 160 m³/d, while with low sealing, it was limited to 30–40 m³/d. The highest runoff was observed in Katowice and Mikołajki, despite differences in the level of urbanization. The correlation between catchment sealing and increases in the volume of the infiltration trench and runoff was particularly pronounced in lowland regions, while in mountainous regions (e.g., Bielsko-Biała, Nowy Sącz), the increase in runoff was moderate.

The developed application enables the design of infiltration systems tailored to changing urban and climatic conditions. The results underscore the importance to consider local physical-geographical variability in the process of planning sustainable stormwater management. Strategies based on the development of rain gardens can significantly enhance the resilience of cities to the impacts of climate change, while simultaneously improving the quality of life for residents and the quality of the urban environment.

REFERENCES

1. Akan, A.O. (1993). Urban Stormwater hydrology – A Guide to Engineering Calculations, Technomic, Lancaster, PA.
2. Aldrees, A. M., Dan'azumi, S. (2023). Application of analytical probabilistic models in urban runoff control systems' planning and design: A review. *Water Practice and Technology, 18*(2), 414–428. https://doi.org/10.2166/wpt.2023.019
3. Arnold, C. L., Gibbons, C. J. (1996). Impervious surface coverage: The emergence of a key environmental indicator. *Journal of the American Planning Association, 62*(2), 243–258.
4. Banasik, K., Krajewski, A., Sikorska-Senoner, A. E., Hejduk, L. (2014). Curve number estimation for a small urban catchment from recorded rainfall-runoff events. *Archives of Environmental Protection, 40*(3), 21–30. https://doi.org/10.2478/aep-2014-0032
5. Beven, K.J. (2012). *Rainfall-runoff modelling: the primer*. John Wiley & Sons
6. Bhaskar, A.S., Hogan, D.M., Archfield, S.A. (2016). Urban base flow with low impact development. *Hydrological Processes, 30*(18), 3156–3171. https://doi.org/10.1002/hyp.10808
7. Białek, A., Musz-Pomorska, A. (2025). Development of a computational tool for stormwater management in small urban catchments. *Journal of Ecological Engineering, 26*(6), 410–423. https://doi.org/10.12911/22998993/202322
8. Bibi, T. S., Kara, K. G. (2023). Evaluation of climate change, urbanization, and low-impact development practices on urban flooding. *Heliyon, 9*(1), e12955. https://doi.org/10.1016/j.heliyon.2023.e12955
9. Bogdanowicz, E., Stachý, J. (1998). *Maksymalne opady deszczu w Polsce. Charakterystyki projektowe*. Instytut Meteorologii i Gospodarki Wodnej, Warszawa.
10. Booth, D. B., Hartley, D., Jackson, R. (2002). Forest cover, impervious-surface area, and the mitigation of stormwater impacts. *Journal of the American Water Resources Association, 38*(3), 835–845.
11. Bowler, D. E., et al. (2010). Urban green spaces and health: A review of evidence. *Landscape and Urban Planning, 97*(3), 147–157.
12. Brunner, G. W. (2010). *HEC-RAS River Analysis System: Hydraulic Modeling and Applications (2nd ed.)*. U.S. Army Corps of Engineers, Hydrologic Engineering Center.
13. Caparrós-Martínez, J. L., Milán-García, J., Rueda-López, N., de Pablo-Valenciano, J. (2020). Green infrastructure and water: An analysis of global research. *Water, 12*(6), 1760. https://doi.org/10.3390/w12061760

14. Dai, J., Xu, J., Wu, X., Wu, S., Zhang, Y., Wang, F. (2023). Urban rainwater utilization: A review of management modes and harvesting systems. *Frontiers in Environmental Science, 11*, 1025665. https://doi.org/10.3389/fenvs.2023.1025665
15. De Paola, F., Ranucci, A. (2012). Analysis of spatial variability for stormwater capture tanks assessment. *Irrigation and Drainage, 61*(6), 682–690. https://doi.org/10.1002/ird.1673
16. De Paola, F., De Martino, F. (2013). Stormwater tank performance: Design and management criteria for capture tanks using a continuous simulation and a semi-probabilistic analytical approach. *Water, 5*(4), 1699–1711. https://doi.org/10.3390/w5041699
17. DWA-A 118E. (2006). *Hydraulic Dimensioning and Verification of Drain. and Sewer Systems.* DWA German Association for Water, Wastewater and Waste, Hennef, Germany.
18. Endo, T., Taniguchi, T., Kazama, S. (2021). Impact of urban surface conditions on peak runoff and time of concentration under changing climate in Tokyo. *Hydrology Research Letters, 15*, 58–65. https://doi.org/10.3178/hrl.15.58
19. European Commission. (2015). *Towards an EU Research and Innovation policy agenda for nature-based solutions and renaturing cities.* Final Report of the Horizon 2020 Expert Group on Nature-Based Solutions and Re-naturing Cities. Brussels: European Commission. https://doi.org/10.2777/479582
20. Ferreira, L., et al. (2021). Natural systems for stormwater management: Case studies and solutions. *Environmental Management Journal, 45*(2), 123–138.
21. Fletcher, T. D., Shuster, W. D. (2013). The role of urban infiltration systems in managing stormwater runoff. *Hydrological Processes, 27*(6), 913–926. https://doi.org/10.1002/hyp.9224
22. Fletcher, T. D., Andrieu, H., Hamel, P. (2013). Understanding, management and modelling of urban hydrology and its consequences for receiving waters. *Advances in Water Resources, 51*, 261–279. https://doi.org/10.1016/j.advwatres.2012.09.001
23. Gao, X., Liu, X., Zhang, L., Wang, Z. (2016). Effects of water retention in green infrastructure systems on hydrological performance under different conditions. *Environmental Science & Technology, 50*(4), 2190–2198. https://doi.org/10.1021/acs.est.5b03979
24. Hasan, F., Medley, P., Drake, J., Chen, G. (2024). Advancing hydrology through machine learning: insights, challenges, and future directions using the CAMELS, caravan, GRDC, CHIRPS, PERSIANN, NLDAS, GLDAS, and GRACE datasets. *Water, 16*(13), 1904. https://doi.org/10.3390/w16131904
25. Jakubowska, M. (2020). Zielona infrastruktura w Warszawie: Ogrody deszczowe jako element zarządzania wodami opadowymi. *Urban Studies, 52*(5), 1237–1250.
26. Kasprzyk, M., Szpakowski, W., Poznańska, E. (2022). Technical solutions and benefits of *introducing rain gardens–Gdańsk case study. Science of The Total Environment, 838, 156460.* https://doi.org/10.1016/j.scitotenv.2022.156460
27. Kucharczyk, M., Piłat, D. (2019). Wdrażanie ogrodów deszczowych w polskich miastach: Przykład Gdańska. *Infrastruktura i Ekologia Terenów Wiejskich, 4*(1), 45–56.
28. Kupczyk, E., Suligowski, R. (1997). *Statistical description of the rainfall structure as the input to hydrological models*. In U. Soczyńska (Ed.), Prediction of the design storms and floods 191–212. University of Warsaw Publisher.
29. Kupczyk, E., Suligowski, R. (2000). Temporal and spatial patterns of high intensity rainfalls in Poland. *Miscellanea Geographica, 9*, 77–84. https://doi.org/10.2478/mgrsd-2000-090110
30. Li, H., Babcock, R. (2014). Green roofs for stormwater management and urban sustainability. *Environmental Science & Technology, 48*(2), 121–130.
31. Li, X., Babcock, R. W. (2020). Stormwater management through green infrastructure: The role of rain gardens and permeable pavements in urban areas. *Environmental Management, 65*(5), 863–875.
32. Li, J., Zhao, R., Li, Y., Li, H. (2020). Simulation and optimization of layered bioretention facilities by HYDRUS-1D model and response surface methodology. *Journal of Hydrology, 586*, 124813. https://doi.org/10.1016/j.jhydrol.2020.124813
33. Lim, H. S., Lu, X. X. (2016). Sustainable urban stormwater management in the tropics: An evaluation of Singapore's ABC Waters Program. *Journal of Hydrology, 538*, 842–862. https://doi.org/10.1016/j.jhydrol.2016.04.063
34. Liu, X., Tan, S. K. (2014). Effects of dry periods and soil type on the performance of stormwater infiltration systems. *Journal of Hydrology, 519*, 3015–3024. https://doi.org/10.1016/j.jhydrol.2014.08.026
35. Łupikasza, E. (2016). *The climatology of air-mass and frontal extreme precipitation. Study of meteorological data in Europe.* Springer International Publishing AG Switzerland.
36. Meerow, S., Newell, J. P. (2017). Spatial planning for multifunctional green infrastructure: Growing resilience in Detroit. *Landscape and Urban Planning, 159*, 62–75. doi:10.1016/j.landurbplan.2016.10.005
37. Niedźwiedź, T., Twardosz, R., Walanus, A. (2009). Long-term variability of precipitation series in east central Europe in relation to circulation patterns. *Theoretical and Applied Climatology, 98*, 337–350. https://doi.org/10.1007/s00704-009-0122-0
38. Palermo, S. A., Turco, M., Pirouz, B., Presta, L.,

Falco, S., De Stefano, A., Frega, F., Piro, P. (2023). Nature-based solutions for urban stormwater management: An overview. *IOP Conference Series: Earth and Environmental Science, 1196*(1), 012027. https://doi.org/10.1088/1755-1315/1196/1/012027

39. Pons, V., Abdalla, E. M. H., Tscheikner-Gratl, F., Alfredsen, K., Sivertsen, E., Bertrand-Krajewski, J.-L., Muthanna, T. M. (2023). Practice makes the model: A critical review of stormwater green infrastructure modelling practice. *Water Research, 236*, 119958. https://doi.org/10.1016/j.watres.2023.119958
40. Ramísio, P. J., Brito, R. S., Beceiro, P. (2022). Accessing synergies and opportunities between nature-based solutions and urban drainage systems. *Sustainability, 14*(24), 16906.
41. Rogger, M., Agnoletti, M., Alaoui, A., Bathurst, J. C., Bodner, G., Borga, M., … Blöschl, G. (2017). Land use change impacts on floods at the catchment scale: Challenges and opportunities for future research. *Water Resources Research, 53*(7), 5209–5219. doi:10.1002/2017wr020723
42. Rosenzweig, B., Fekete, B. (2018). *Green Infrastructure Plan: Opportunities for Innovation in Climate-Change Resilience. In A. Corrêa d'Almeida* (Ed.), Smarter New York City: How City Agencies Innovate (pp. 150–180). Columbia University Press. https://doi.org/10.7312/dalm18374-010
43. Sakib, M. S., Alam, S., Shampa, Murshed, S. B., Kirtunia, R., Mondal, M. S., Chowdhury, A. I. A. (2023). Impact of urbanization on pluvial flooding: Insights from a fast growing megacity, Dhaka. *Water, 15*(21), 3834. https://doi.org/10.3390/w15213834
44. Scholes, L., Huelin, P. (2008). The role of green infrastructure in managing urban stormwater. *Water and Environment Journal, 22*(1), 1–9.
45. Sharma, R., Malaviya, P. (2021). Management of stormwater pollution using green infrastructure: The role of rain gardens. *WIREs Water, 8*(2). https://doi.org/10.1002/wat2.1507
46. Shen, C., Xia, H., Fu, X., Wang, X., Wang, W. (2021). Developing green infrastructure strategies based on the analysis of sewer system critical components. *Water 13*, 2694.
47. Shuster, W. D., Bonta, J., Thurston, H., Warnemuende, E., Smith, D. R. (2005). Impacts of impervious surface on watershed hydrology: A review. *Urban Water Journal, 2*(4), 263–275. https://doi.org/10.1080/15730620500386529
48. Shuster, W. D., Rhea, L. K., Bonta, J., Thurston, H., Warnemuende, E., Smith, D. R. (2022). Managing urban stormwater with green infrastructure: A review of the effectiveness and challenges. *Urban Water Journal, 19*(1), 1–11. https://doi.org/10.1080/15730620500386529
49. Šimůnek, J., Šejna, M., Saito, H., Van Genuchten, M. T., Leij, F. J. (2005). *The HYDRUS-1D software package for simulating the movement of water, heat, and multiple solutes in variably saturated media (Version 3.0).* University of California, Riverside.
50. Szulczewska, B., Giedych, R., Maksymiuk, G. (2016). Can we face the challenge: how to implement a theoretical concept of green infrastructure into planning practice? Warsaw case study. *Landscape Research, 42*(2), 176–194. https://doi.org/10.1080/01426397.2016.1240764
51. Szeląg, B., Suligowski, R., Łagód, G., Łazuka, E., Wlaź, P., Strańsky, D. (2022). Flood occurrence analysis in small urban catchments in the context of regional variability. *PLOS ONE, 17*(11), e0276312. https://doi.org/10.1371/journal.pone.0276312
52. Szeląg, B., Kowal, P., Kiczko, A., Białek, A., Wałek, G., Majerek, D., Siwicki, P., Fatone, F., Boczkaj, G. (2023a). Integrated model for the fast assessment of flood volume: Modelling – management, uncertainty and sensitivity analysis. *Journal of Hydrology, 625*, 129967. https://doi.org/10.1016/j.jhydrol.2023.129967
53. Szeląg, B., Zaborowska, E., Mąkinia, J. (2023b). An algorithm for selecting a machine learning method for predicting nitrous oxide emissions in municipal wastewater treatment plants. *Journal of Water Process Engineering, 54*, 103939. https://doi.org/10.1016/j.jwpe.2023.103939
54. Szeląg, B., Fatone, F., Kiczko, A., Majerek, D., Białek, A., Łagód, G., Piotrowicz, A., Dąbek, L. (2024). Extended evaluation of the impact of rainfall, sewer network, and land use retention on drainage system performance in a multi-criteria approach – Modeling, sensitivity analysis. *Advances in Science and Technology Research Journal, 18*(6), 291-303. https://doi.org/10.12913/22998624/192023
55. Szulc, M., Zelewski, Ł. (2021). Analysis of urban runoff changes in Polish metropolitan areas. *Water, 13*(9), 1234.
56. Van Mechelen C. (2015). Urban green roofs as a tool for ecological improvement and stormwater management. *Landscape and Urban Planning, 143*, 10–18.
57. Wang, M., Zhang, D. Q., Su, J., Dong, J. W., Tan, S. K. (2018). Assessing hydrological effects and performance of low impact development practices based on future scenarios modeling. *Journal of Cleaner Production, 179*, 12–23. https://doi.org/10.1016/j.jclepro.2018.01.096
58. Wolski, M., Pięta, W., Jarzyna, T. (2021). Pilotażowe wdrażanie ogrodów deszczowych w Krakowie: Zrównoważone zarządzanie wodami opadowymi. *Acta Scientiarum Polonorum, 20*(3), 45–56.
59. Yang, Y., Chui, T.F.M., (2016). Optimal design of green and grey stormwater infrastructure for small urban catchment based on life-cycle cost-effectiveness analysis. *AGU Fall Meeting, San Francisco,*

CA, United States (H13M-1598)

60. Yau, W. K., Radhakrishnan, M., Liong, S.-Y., Zevenbergen, C., Pathirana, A. (2017). Effectiveness of ABC waters design features for runoff quantity control in urban Singapore. *Water, 9*(8), 577. https://doi.org/10.3390/w9080577
61. Zhang, K., Chui, T. F. M. (2018). A comprehensive review of spatial allocation of LID-BMP-GI practices: Strategies and optimization tools. *Science of The Total Environment, 621*, 915–929. doi:10.1016/j.scitotenv.2017.11.281
62. Zhang, D., Ding, X., Liu, J., Mei, C. (2022). Review on mechanism and technical measures of urban rainwater harvesting. In *IOP Conference Series: Earth and Environmental Science 983*, 012106. IOP Publishing. https://doi.org/10.1088/1755-1315/983/1/012106
63. Zhao, S., Yue, B. (2023).Nature-based solutions: Establishing a comprehensive framework for addressing urban waterlogging management. *Integrated Environmental Assessment and Management, 19*(6), 1414–1421. https://doi.org/10.1002/ieam.4786
64. Zhou, Q., Mikkelsen, P. S., Halsnæs, K., Arnbjerg-Nielsen, K. (2017). Framework for economic pluvial flood risk assessment considering climate change effects and adaptation benefits. *Journal of Hydrology, 549*, 692–704. https://doi.org/10.1016/j.jhydrol.2017.03.066

Advances in Science and Technology Research Journal

Advances in Science and Technology Research Journal, 18(6), 291–303
https://doi.org/10.12913/22998624/192023
ISSN 2299-8624, License CC-BY 4.0

Received: 2024.07.18
Accepted: 2024.08.15
Published: 2024.09.08

Extended Evaluation of the Impact of Rainfall, Sewer Network and Land Use Retention on Drainage System Performance in a Multi-Criteria Approach – Modeling, Sensitivity Analysis

Bartosz Szeląg[1*], Francesco Fatone[2], Adam Kiczko[1], Dariusz Majerek[3], Anita Białek[4], Grzegorz Łagód[5], Adam Piotrowicz[6], Lidia Dąbek[4]

[1] Department of Hydraulic and Sanitary Engineering, Warsaw University of Life Sciences, ul. Nowoursynowska 166, 02-787, Warsaw, Poland

[2] Department of Science and Engineering of Materials, Polytechnic University of Marche Ancona, Ancona 60121, Italy

[3] Department of Applied Mathematics, Lublin University of Technology, ul. Nadbystrzycka 38, 20-618 Lublin, Poland

[4] Faculty of Environmental Engineering, Geomatics and Renewable Energy, Kielce University of Technology, al. Tysiąclecia Państwa Polskiego 7, 25-314, Kielce, Poland

[5] Department of Water Supply and Wastewater Disposal, Lublin University of Technology, ul. Nadbystrzycka 40B, 20-618 Lublin, Poland

[6] Department of Environmental Protection Engineering, Lublin University of Technology, ul. Nadbystrzycka 40B, 20-618 Lublin, Poland

* Corresponding author's e-mail: bszelag@tu.kielce.pl

ABSTRACT

An extensive methodology for analyzing the impact of catchment and sewer network retention on drainage system operating conditions during hydraulic overloading is presented. To evaluate the performance of the sewer system and identify the need for repair actions, logistic regression models were developed to predict the unit flooding volume and manhole overflowing. An advanced sensitivity analysis was performed to determine the key parameters (retention and roughness of impervious and pervious areas as well as sewer channel retention) conditioning the reduction of uncertainty in the simulation results and ensuring the assumed hydraulic effect. A coefficient expressing the quotient of the duration of rainfall conditioning the exceedance of the limits of the unit flooding volume (13 $m^3 \cdot ha^{-1}$) as well as the degree of overflowed manholes (0.32) was determined, allowing the determination of the key performance criterion of the sewer network to take corrective action depending on field and channel retention. It was shown that the catchment area retention had the key influence on the conditions of sewer operation and the probability of remedial work. Increasing the rainfall duration led to a decrease in sensitivity coefficients with respect to the identified parameters of the SWMM model, which is important when selecting rainfall events for the calibration and validation sets. The usefulness of the developed methodology was demonstrated at the stage of building mechanistic models, which is of significance when planning field studies.

Keywords: stormwater system, environmental impact, multi-criteria approach, modelling, SWMM, GLUE, sensitivity analysis.

INTRODUCTION

Climate change, ongoing urbanization, and reduced pipe throughput contribute to the deterioration of receiving waters, resulting in an increased frequency and volume of stormwater flooding events in urban catchments [1, 2, 3]. To mitigate these impacts on the environment and living standards, decision-makers need to modernize stormwater networks through the implementation of green infrastructure or pipe retention systems [4, 5]. Ensuring optimal solutions,

including hydraulic effects, requires adherence to stormwater network operation standards defined by the European Standard EN 752 [6]. This standard determines the total number of stormwater flooding events within the assumed period [7, 8, 9]. Additionally, quantitative criteria, expressing the depth of stormwater [10], i.e. determining the unit flooding volume per paved area of catchment (referred to as specific flood volume) and specifying the degree of overflowed manholes in the stormwater network (referred to as degree of flooding) were introduced [11].

Depending on the available criteria, modeling can be performed using different computational tools [12, 13, 14, 15]. Mechanistic models (MCM) are usually applied for this purpose, enabling the modeling of hydraulic conditions in a stormwater network, as well as the depth and area of flooding [16, 17]. This usually requires integrating the hydraulic model with the digital terrain model (DTM) [18, 19]. If data are unavailable, simplified solutions can be used, modeling the volume of stormwater flooding for individual manholes. One of the most commonly used simplified approaches is SWMM (Storm Water Management Model) [18, 20]. The prediction of flooding is a complex issue resulting from the interaction of land use, surface runoff, channel flow, and hydraulic characteristics of manholes [21, 22, 23]. To account for the above factors, a number of coefficients are included in the mechanistic models, which require calibration [24, 25]. This leads to over-parameterization of MCM models, resulting in problems with the identification of calibrated parameters [26, 27]. The strong interaction between parameters, the limited number of inputs to developed MCM models, the simplified de-parameterization of land use, as well as the layout of the sewer network lead to problems with model calibration and influence the uncertainty of predictions [25, 28].

Sensitivity analysis constitutes an approach to reduce the number of calibrated parameters [29, 30, 31], especially integrated with uncertainty analysis. This approach is often used during the implementation of optimization methods for the parameter identification. A literature review [32, 33] indicates that sensitivity analysis is also carried out by global and local methods, which do not take into account any influence of local rainfall conditions and the variability of identified parameters on the simulation results.

MCM models enable prediction of continuous values (flood volume, number of flooded manholes), but prevent prediction of the need to undertake repair action [25]. This limitation can result in problems with planning field studies during the development step of MCM models to be used for catchment management. Currently, there is a lack of guidelines for selecting rainfall events for the calibration and validation set [27], which has a major impact on the fitting of predictions to measurements and the reliability of the resulting predictions as a basis for making decisions on corrective actions [34].

This study presents the possibility of implementing the given computational methodology with respect to proposed parameters, such as specific flood volume and the degree of flooding, as the operating criteria for stormwater networks. A logistic regression model already applied for simulating stormwater network operation was used for this purpose [35]; however, its use in the applied approach constitutes a novel application. Moreover, in terms of specific flood volume and degree of flooding, an innovative analysis has been proposed that involves the development of a sensitivity coefficient of the hydrodynamic model. This enables the effect of (i) the influence of rainfall intensity, (ii) the frequency of its occurrence, and (iii) the parameters to be identified. So far, this aspect has not been considered in the proposed catchment model and calibration procedures to determine operational parameters.

STUDY AREA

The investigated urban catchment is located in the city of Kielce, Poland (Eastern Europe). Kielce is found in the Świętokrzyskie Region with an average population density of about 107 persons·km^{-2} [25]. The studied catchment is positioned in the southeastern part of the city and is occupied with housing estates, public utility buildings, and the main streets. The impervious areas in the catchment constitute 40%, whereas the remaining part is pervious. It was determined that the retention of the impervious areas amounts to 2.5 mm, whereas that of pervious areas is equal to 6.0 mm [9]. The road network density in the analyzed area amounts to 108 m·ha^{-1}. The elevation of the highest point of the catchment is 271.20 m a.s.l., whereas that of the lowest one is 260.0 m a.s.l. In the considered catchment, the total length of the stormwater network amounts

to 5584 m, including the main pipe, which has a length of 1569 m. The diameter of the main pipe ranges from 600 to 1250 mm, whereas the diameters of the side pipes range from 300 to 1000 mm. The slopes of the pipes are within the range of 0.04 to 3.90% [25].

The catchment area under study is depicted in Figure 1. The map shows the catchment boundaries, as well as the main sewer and side channels. The stormwater from the catchment flows into a diversion chamber (DC); up to a depth of 0.42 m, the entire volume of stormwater is directed to a stormwater treatment plant (STP). The treated stormwater is discharged to the Silnica River. If, due to intense rainfall, the level of stormwater in the DC exceeds 0.42 m, it is discharged through an overflow structure (OV) into the Silnica River. A MES-1 flow meter was installed ca. 3 m from the diversion chamber inlet to measure and record the flow every minute during intense rainfall events. Location of devices is shown in Figure 1.

Based on data spanning 2010–2020, it was observed that MES-1 flow meter recorded flows ranging from 1 to 9 $dm^3 \cdot s^{-1}$ during dry periods, suggesting infiltration. The flow meter's probe gauges water level (via water level pressure measurement) and average flow rate of stormwater (utilizing the Doppler effect). These measurements, combined with the specific shape and dimensions of the canal, enable the built-in microprocessor to calculate the volumetric flow rate of stormwater. A rainfall station, conducting continuous rainfall measurements since 2008 at a 1 – minute resolution, is located 2.5 km away from the catchment border.

RESEARCH METHODOLOGY

In this section the innovative and multicriteria methodology is presented, mainly based on the operational evaluation of stormwater networks (Figure 2). It considers two criteria, including:

- specific flood volume, determining the unit flooding volume per 1 ha of the catchment:

$$\lambda_1 = \frac{\sum_{i=1}^{K} V_{t(i)}}{A_{imp}} \quad (1)$$

where: V_t is the volume of stormwater flooding from the i-th manhole, K is the number of manholes in the stormwater network, and A_{imp} is the impervious area,

- degree of flooding, i.e. the degree of overflowed manholes in the stormwater network:

$$\lambda_2 = \frac{\sum_{i=1}^{K} N_{K,f}}{K} \quad (2)$$

where: $\Sigma N_{K,f}$ – the number of overflowed manholes in the stormwater network.

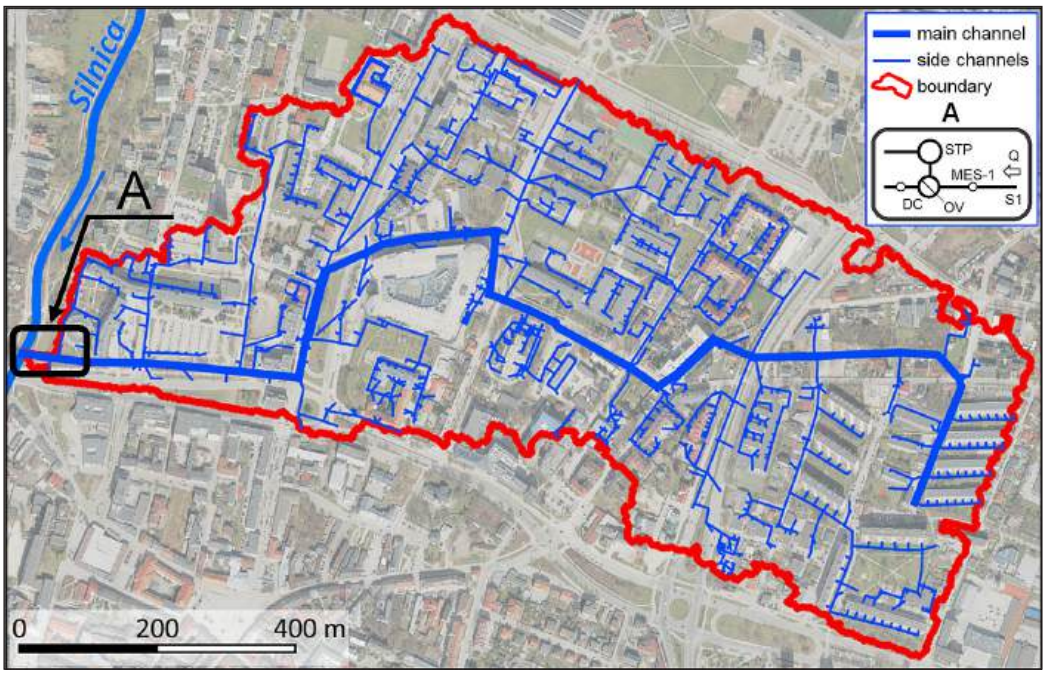

Figure 1. Investigated catchment in Kielce, Poland. MES-1 – flow meter, OV – overflow structure, DC – diversion chamber, STP – stormwater treatment plant

According to Siekmann and Pinnekamp [11], a stormwater network requires urgent modernization for the values of $\lambda_1 > 13$ m^3·ha^{-1} and values of $\lambda_2 > 0.32$. The maximum values of λ_1 and λ_2 presented above constituted the basis for developing the logistic regression models. Such parameters are the most important in decision making regarding the repair action of existing systems. The proposed computation algorithm consists of 6 modules (Figure 2). The development of algorithm includes four steps:

- Modules 1, 2 – collecting the data and developing of mechanistic model,
- Module 3 – uncertainty analysis with GLUE method,
- Modules 4, 5 – development of a logistic regression model to assess the relationship between specific flood volume and degree of flooding with sensitivity analysis,
- Module 6 – analysis of the dependence of the duration of rainfall that results in exceeding the thresholds of specific flood volume and degree of flooding.

Separation of independent rainfall events (DWA-A118)

In the analysis the independent rainfall events (with uniformed distribution) for modeling of stormwater network operation were separated, based on continuous rainfall time series (2010–2019). On the basis of the performed analysis of the rainfall data, it was observed that the number of rainfall events in any year ranged from 12 to 30 (202 rainfall events), in which the rainfall depths were in the range of P_t = 5.2–80.2 mm, the maximum 30 – minute rainfall depths in a rainfall event in any year were equal to $P_{t=30}$ = 2.5–41.2 mm, the rainfall durations were t_r = 15–150 min and the dry period was t_{rd} = 6–336 h. Since the uncertainty of the SWMM parameters is included in the calculations, the selection of rainfall events for modeling of operation of the stormwater network is not a simple task. The detailed methodology is discussed by Szeląg et al. [25].

Rainfall frequency was established by considering rainfall characteristics such as depth and duration, utilizing the regional model for Poland introduced by Bogdanowicz and Stachy [36].

Mechanistic model of the catchment (SWMM)

Modeling of the investigated catchment was performed using a calibrated mechanistic model developed in SWMM. The analyses were based on a mechanistic model with an area of 62 ha, comprising 92 subcatchments with areas ranging from 0.12 ha to 2.10 ha (as shown in Figure 1), whereas the imperviousness equaled 5–90%. The considered model consists of 72 pipes and 82 manholes. During calibration, it was determined that the retention depth of the impervious areas D_{imp} = 2.50 mm, pervious areas D_{per} = 6.0 mm, Manning roughness coefficients of impervious and pervious areas were n_{imp} = 0.025 m$^{-1/3}$·s and n_{per} = 0.10 m$^{-1/3}$·s. The width of the run-off path was determined based on the dependence $W = \omega \cdot A^{0.50}$, where ω = 1.35. The considered catchment model constituted the basis for the analyses related to the quantity and quality of stormwater, tank dimensioning, and operation of the stormwater overflow structure [9, 25].

In the applied approach, the stormwater operational parameters (specific flood volume, degree of flooding) were predicted using the "Flooding"

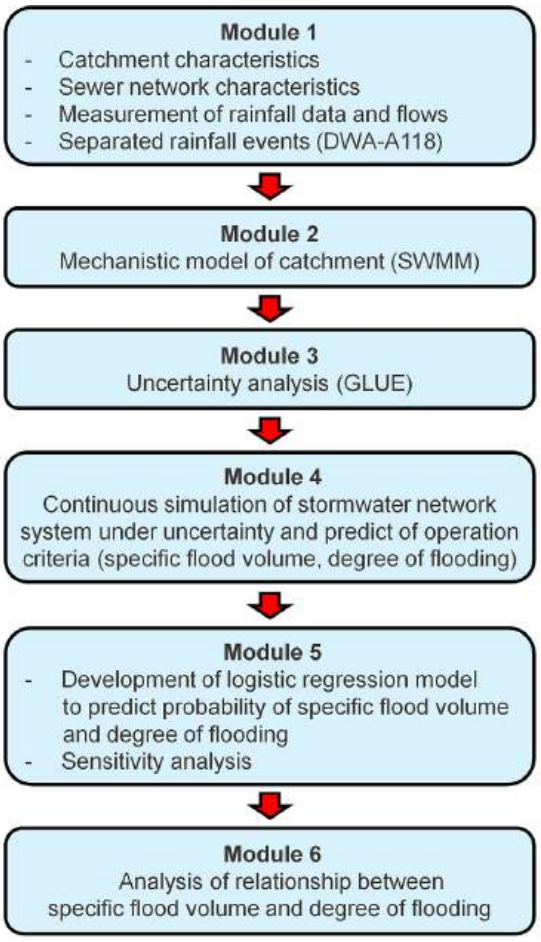

Figure 2. Calculation algorithm of the methodology for analyzing the operation of a stormwater network in the context of the specific flood volume and the degree of flooding

option for a single junction, which enables a reduction in the quantity of measurement data required [9].

Uncertainty analysis (GLUE) methodology

In this paper, the generalized likelihood uncertainty estimation (GLUE) method was used for uncertainty analysis. The theoretical basis of the method is discussed in detail in the studies by Beven and Binley [37] and Romanowicz and Beven [38]. In the GLUE method, the basis for the identification of parameter distributions was Bayesian estimation, in which for the assumed a priori parameter distributions the so called a posteriori distributions were determined by the likelihood function. The following parameters (uniform distribution) were included in the SWMM model: coefficient for flow path width (α), retention depth of impervious areas (D_{imp}), retention depth of pervious areas (D_{per}), Manning's roughness coefficient for impervious areas (n_{imp}), Manning's roughness coefficient for pervious areas (n_{per}), Manning's roughness coefficient of sewer channels (n_{sew}), correction coefficient for subcatchments slope (γ) and correction coefficient for percentage of impervious areas (β). Details on the parameters used are provided by Kiczko et al. [39] and Szeląg et al. [40].

Measures of goodness of fit of the results and a posteriori distributions were calculated based on simulations performed for the observed hyetograms and hydrograms. For both events utilized in parameter identification (15 September 2010 – P_t = 9.2 mm, t_r = 286 min, and 8 July 2011 – P_t = 8.2 mm, t_r = 60 min), 96% of observed points were encompassed by the confidence bands. In the validation sets 89% of observed points fell within the bands for the May 30, 2010 event (P_t = 12.5 mm, t_r = 107 min), and 60% for the July 30, 2010 event (P_t = 16.5 mm, t_r = 270 min).

Continuous simulation of stormwater systems

Based on the separated (M = 200) rainfall events for the catchment area, the operation of the stormwater drainage network was simulated by determining the volume of flooding for each i-th manhole and the number of overflowed manholes. There were 5000 simulations of SWMM parameters combinations – a priori distribution (Section: Uncertainty analysis (GLUE) methodology) of independent rainfall events, for which λ_1 and λ_2 were determined. The data obtained was used to develop a logit model, with 80% of the data used for training, 10% for testing, and the other 10% for validation. To simulate the stormwater network operation, regarding the logistic regression models, rainfall events for which the rainfall depth P_t > 5.0 mm were selected. It resulted in the rainfall duration in the range 10–135 minutes.

Logistic regression model to predict the probability of the operation criteria

The logit model describes the following general dependence:

$$p = \frac{\exp(\alpha_0 + \alpha_1 \cdot x_1 + \alpha_2 \cdot x_2 + \alpha_3 \cdot x_3 + \cdots + \alpha_i \cdot x_i)}{1 + \exp(\alpha_0 + \alpha_1 \cdot x_1 + \alpha_2 \cdot x_2 + \alpha_3 \cdot x_3 + \cdots + \alpha_i \cdot x_i)} = \frac{exp(X)}{1 + exp(X)} \quad (3)$$

where: p – probability of exceeding the maximum value of the specific flood volume (λ_1) and the degree of flooding (λ_2); α_0 – absolute term; α_1, α_2, α_3, α_i – values of coefficients estimated with the maximum likelihood method, X – vector describing the linear combination of the independent variables; x_i – independent variables describing rainfall characteristics, e.g., rainfall depth, its duration, and the parameters calibrated in the SWMM. Identification of independent variables was performed using a stepwise algorithm that also eliminates correlated independent variables [41].

In the performed analyses, identification of the data obtained from the SWMM simulation to the binary form was based on the following criteria:

a) when $\lambda_1 \geq 13$ m^3·ha^{-1}, then 1, in the remaining cases 0,
b) when $\lambda_2 \geq 0.32$, then 1, in the remaining cases 0.

Following literature findings [11], values $\lambda_1 \geq 13$ m^3·ha^{-1} and $\lambda_2 \geq 0.32$ correspond to $p \geq 0.5$. Specificity (SPEC), sensitivity (SENS) and accuracy (ACC) were used to assess the goodness of fit between predictions and measurements.

Sensitivity analysis

In the performed investigations, the analysis of model sensitivity was carried out using local sensitivity analysis [24, 42, 43]. In the proposed solution the sensitivity coefficient was defined, described by the following Equation:

$$S_{x_j} = \frac{\partial p}{\partial x_i} \cdot \frac{x_i}{p} = \frac{p(x_{i,g} + \Delta x_i) - p(x_{i,g};\, \lambda)}{(x_{i,g} + \Delta x_i) - x_{g,i}} \cdot \frac{x_i}{p(x_{i,g};\, \lambda)} = \\ = \alpha_i \cdot x_i \cdot \left(1 - p(x_{i,g};\, \lambda)\right) \quad (4)$$

where: x_i – values of independent variables, λ – values of λ_1 and λ_2 parameters which constitute the basis for assessing the operation of the stormwater network, $p(x_{i,g} + \Delta x_i)$ – probability of exceeding $\lambda_1(\lambda_2)$ for the value $(x_{i,g} + \Delta x_i)$, $p(x_{i,g}, \lambda)$ – probability of exceeding the value $\lambda_1(\lambda_2)$ for the set of independent variables involving rainfall characteristics and calibrated SWMM parameters. The individual steps for calculating the sensitivity coefficients according to Equation 4 are given in Szeląg et al. [40]. On the basis of Equation 4, sensitivity coefficients were calculated for the calibrated SWMM parameters using the models to predict the probability of specific flood volume and degree of flooding in the stormwater network. These calculations were done for t_r = 15–135 min and C = 3, 5 assuming the SWMM parameters were determined from calibration [39].

Relationship between the specific flood volume and degree of flooding

Based on literature review [9, 11], it can be concluded that the probability of a specific flood volume (λ_1) and a degree of flooding (λ_2) depends on the rainfall data (rainfall depth and duration) and the parameters calibrated, used in SWMM (D_{imp}, D_{per}, n_{imp}, n_{per}, n_{sew}, α, β, γ, etc.). It was assumed, following Siekmann and Pinnekamp [11], that when the value of λ_1 = 13 m^3·ha^{-1} or λ_2 = 0.32, then the stormwater network requires repair action and the calculated values of the probability of a specific flood volume and the probability of a degree of flooding are equal to 0.5. For p = 0.50, by appropriately transforming Equation 3, it can be written that X = 0 (where X – linear combination of independent variables included in logistic regression models). For the above assumptions, the ratio of rainfall durations for which λ_1 = 13 m^3·ha^{-1} and λ_2 = 0.32 can be written with an Equation of the form:

where: κ – coefficient in the form of $t_{r2}(\lambda_2) \cdot t_{r1}(\lambda_1)^{-1}$, which describes the relative difference between the duration of rainfall for which λ_1 = 13 m^3·ha^{-1} or λ_2 = 0.32; α_0^1, α_1^1, α_2^1, α_3^1, α_4^1, α_5^1, α_6^1, α_7^1, α_8^1, α_9^1, α_{10}^1 – coefficients estimated by the method of maximum likelihood in the logit model for predicting specific flood volume; α_0^2, α_1^2, α_2^2, α_3^2, α_4^2, α_5^2, α_6^2, α_7^2, α_8^2, α_9^2, α_{10}^2 – coefficients estimated by the method of maximum likelihood in the logit model for predicting degree of flooding.

RESULTS AND DISCUSSION

Uncertainty analysis (GLUE)

Calculations of the stormwater network operation in the considered catchment accounting for uncertainty showed that the median values of the specific flood volume (λ_1) in the range t_r = 30–135 min for return period C = 2, 3 and 5 were 19–24 m^3·ha^{-1}, 36–44 m^3·ha^{-1} and 53–70 m^3·ha^{-1}. The λ_1 values for t_r = 30 min and for C values of 2, 3, and 5 within the 95% confidence interval varied within the ranges 8–42 m^3·ha^{-1}, 21–67 m^3·ha^{-1} and 40–90 m^3·ha^{-1} [9]. The median values of the degree of flooding (λ_2) for t_r = 30–135 min and for C values of 2, 3, and 5 were 0.10–0.65, 0.64–0.87 and 0.87–0.93. The situation is shown in Figure 3.

Determination of the logistic regression model to predict the probability of the specific flood volume and the degree of flooding

The ROC AUC scores obtained for λ_1 and λ_2 were 0.987 and 0.996, respectively. The coefficients (α_i) determined in the models (using forward stepwise algorithm), testing probability (p_{test}), standard deviation (S.dev) and measures of fit (SENS and SPEC) for the training, testing, and validation sets are presented in Table 1. Based on the data in Table 1, it can be determined that among the independent variables including rainfall characteristics and parameters calibrated in the SWMM (β, n_{sew}, D_{imp}, n_{imp}, α), only n_{per} has no

$$\kappa = \frac{\alpha_0^1 - \alpha_0^2 + (\alpha_1^1 - \alpha_1^2) \cdot C + \alpha_2^1 \cdot t_r + (\alpha_3^1 - \alpha_3^2) \cdot D_{imp} + (\alpha_4^1 - \alpha_4^2) \cdot D_{per} + (\alpha_5^1 - \alpha_5^2) \cdot n_{imp}}{\alpha_2^2 \cdot t_r} + \\ + \frac{(\alpha_6^1 - \alpha_6^2) \cdot n_{per} + (\alpha_7^1 - \alpha_7^2) \cdot n_{sew} + (\alpha_8^1 - \alpha_8^2) \cdot \alpha + (\alpha_9^1 - \alpha_9^2) \cdot \beta + (\alpha_{10}^1 - \alpha_{10}^2) \cdot \gamma}{\alpha_2^2 \cdot t_r} \quad (5)$$

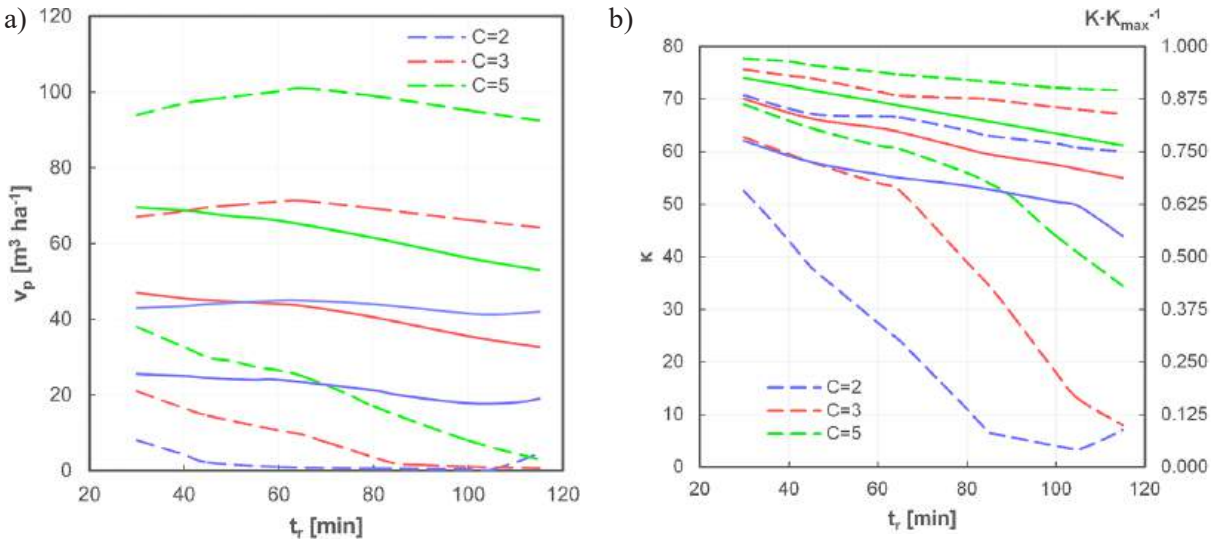

Figure 3. The rainfall duration (t_r) and its frequency (C) effect on sewer performance measures: (a) λ_1, (b) λ_2 accounting for the model uncertainty

Table 1. Values of the coefficients in the developed logit model and measures of fit between the results of calculations and measurements

Variables	$\lambda_1 \geq 13$ m³·ha⁻¹			$\lambda_2 \geq 0.32$		
	Value	S. dev	p_{test}	Value	S. dev	p_{test}
Intercept	**-24.150**	0.420	< 0.001	**-21.222**	0.44	< 0.001
C	**3.743**	0.043	< 0.001	**4.33**	0.089	< 0.001
t_r	**-0.061**	0.001	< 0.001	**-0.152**	0.003	< 0.001
α	**0.860**	0.033	< 0.001	**0.841**	0.056	< 0.001
n_{imp}	**-247.016**	3.960	< 0.001	**-225.47**	6.591	< 0.001
n_{per}	-1.242	1.531	< 0.424	1.023	2.672	< 0.702
D_{imp}	**-0.546**	0.016	< 0.001	**-0.206**	0.027	< 0.001
D_{per}	**-0.129**	0.011	< 0.001	**-0.054**	0.018	0.003
β	**12.241**	0.160	< 0.001	**16.729**	0.338	< 0.001
γ	**1.430**	0.105	< 0.001	**1.458**	0.179	< 0.001
n_{sew}	**408.920**	4.366	< 0.001	**568.55**	10.568	< 0.001
Train	SENS = 96.56%; SPEC = 97.86% Acc = 95.92%			SENS = 94.48%; SPEC = 99.51% Acc = 98.76%		
Test	SENS = 95.15%; SPEC = 93.10% Acc = 92.15%			SENS = 95.48%; SPEC = 93.51% Acc = 94.06%		
Validation	SENS = 95.23%; SPEC = 93.34% Acc = 94.36%			SENS = 95.30%; SPEC = 91.20% Acc = 92.12%		

Note: variables in bold are statistically significant.

statistically significant influence (for the assumed significance level of 0.05) on the calculation results of the probability of specific flood volume and probability of degree of flooding. Simultaneously, while analyzing the data in Table 1, it was noted that the developed logit models were characterized by high prediction. This is confirmed by sufficiently high values of SENS > 94%, SPEC > 93% and Acc > 92% for the training, testing, and validation sets, respectively.

Sensitivity analysis

The influence of the return period (assumed as C = 3, and 5), rainfall duration (t_r = 15–135 min) and the parameters calibrated in the SWMM on the sensitivity of the model for $p_{\lambda 1}$ and $p_{\lambda 2}$ prediction was determined. The sensitivity coefficients for the calibrated SWMM parameters (α, β, γ, D_{imp}, D_{per}, n_{imp}, n_{sew}) with respect to the models for the $p_{\lambda 1}$ and $p_{\lambda 2}$ calculations are shown

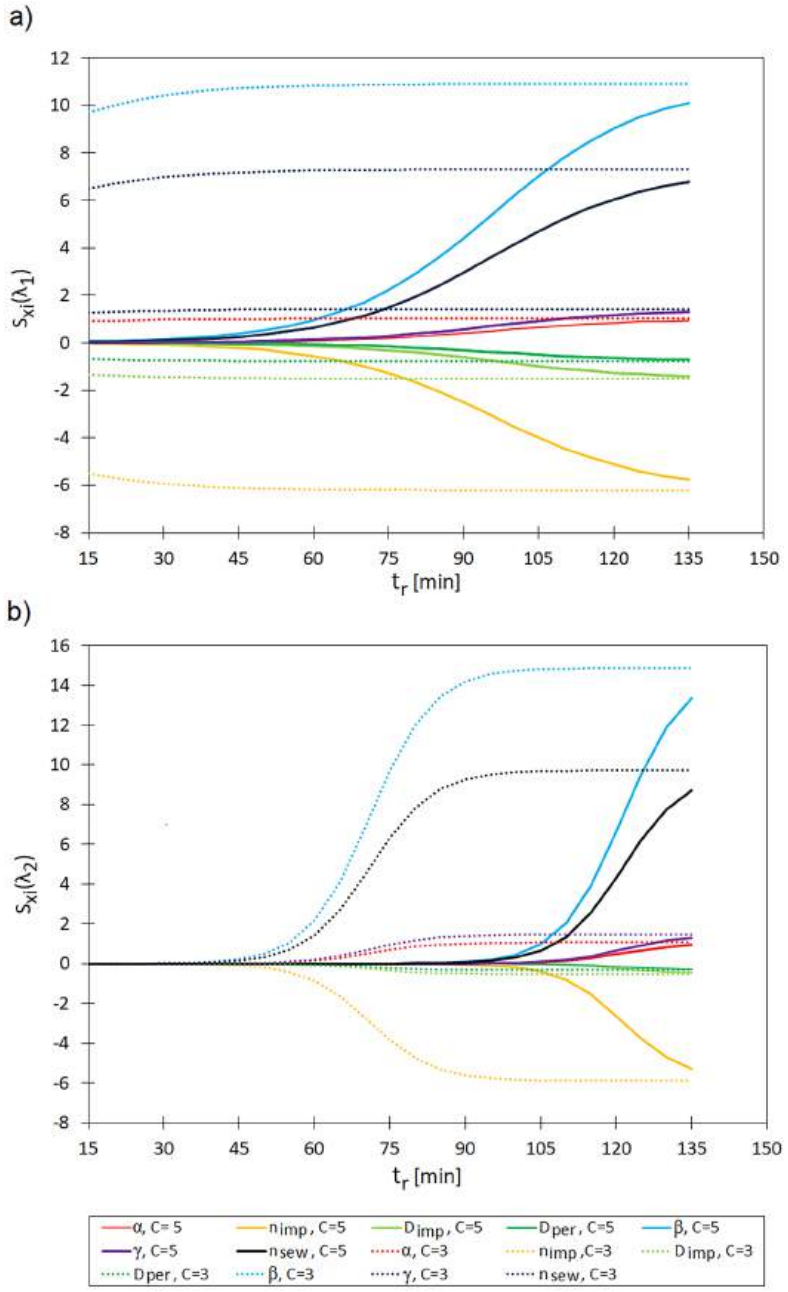

Figure 4. Influence of the rainfall duration (t_r) and return period (C) on the sensitivity coefficient: a) $S(\lambda_1)x_i$, b) $S(\lambda_2)x_i$ for the values of SWMM parameters (x_i: α, β, γ, n_{imp}, D_{imp}, D_{per}, n_{sew})

in Figure 4a and 4b. It was demonstrated that for t_r = 15–135 min and C = 3–5, the correction coefficient for the percentage of impervious areas, Manning's roughness coefficient for impervious areas and the Manning's roughness coefficient of sewer had a key influence on the specific flood volume and the degree of flooding (Figure 4). The curves obtained and the range of variation in the sensitivity coefficients indicate that the other parameters of the SWMM model describing catchment retention (retention depth of impervious and pervious areas, width of the runoff path, average longitudinal slope of the catchment) are less important. It was shown that increasing the duration of rainfall for C = 3, and 5 led to an increase in the sensitivity coefficients with respect to the calibrated SWMM parameters, and thus the models simulating the specific flood volume (λ_1) and the degree of flooding (λ_2). While analyzing the course of the obtained curves (Figure 4a and 4b) for C = 3, and 5, it was found that the maximum values of the sensitivity coefficients (S_β, S_α, S_γ, S_{nimp}, S_{dimp}, S_{nsew}) were obtained for t_r = 105 min. For example, for t_r = 30 min and C = 5, the

sensitivity coefficient $S_\beta(\lambda_1) = 0.10$, while for t_r = 75 min, $S_\beta(\lambda_1) = 2.24$ was obtained. For t_r = 30 min and C = 5, the sensitivity coefficient $S_\beta(\lambda_2) = 0.01$, and for t_r = 75 min, $S_\beta(\lambda_2) = 9.71$. It was found that increasing the return period (C) and average rainfall intensity led to a decrease in the sensitivity coefficient $S_{xi,}$ showing the influence of calibrated SWMM parameters on the $p_{\lambda 1}$ and $p_{\lambda 2}$ values. For C = 3, the influence of rainfall duration for t_r = 15–45 min on the calculation of S_{xi} with respect to the value of $p_{\lambda 1}$ is shown in Figure 4a. The results of the calculations performed for the probability of the degree of flooding and C = 3 showed a negligible influence of the rainfall duration on the sensitivity coefficients for t_r > 105 min with respect to the identified SWMM parameters (Figure 4b).

Determination of the relation between the degree of flooding depending on SWMM parameters

Based on Equation 5, the quotients of the rainfall duration (C = 5) determining the probability of the specific flood volume and the degree of flooding equal to $p_{\lambda 1} = p_{\lambda 2} = 0.50$, which is equivalent to λ_1 = 13 m³·ha^{-1} and λ_2 = 0.32, were determined. Calculations were done for the values β = 0.8–1.0, D_{imp} = 1.0–4.0 mm, n_{imp} = 0.013–0.030 m$^{-1/3}$·s and n_{sew} = 0.013–0.025 m$^{-1/3}$·s. The results of the analyses are presented in Figure 5.

It was found that the values of the degree of flooding in the stormwater network (λ_2 = 0.32) were obtained for longer rainfall durations than those conditioning the specific flood volume at λ_1 = 13 m³·ha^{-1}. This was confirmed by the calculated values of $\kappa = t_{r2} \cdot t_{r1}^{-1}$ (Figure 5), which are greater than one. It was proven that rainfall with a higher mean rainfall intensity led to λ_1 exceeding 13 m³·ha^{-1} rather than λ_2 exceeding 0.32 and indicates the need for stormwater network modernization. The κ value is strongly influenced by the calibrated SWMM parameters describing retention catchment (Figure 5 a, b, c, d). It was found that increases in β and n_{sew} led to a decrease in the κ value (Figure 5a and 5b). This means that the relative difference between the rainfall duration indicating the need for modernization in the context of λ_1 = 13 m³·ha^{-1} and λ_2 = 0.32 decreased. An increase in n_{imp} and D_{imp} led to an increase in κ, as indicated by an increase in the rainfall duration t_{r2} relative to t_{r1} conditioning λ_2 = 0.32 and λ_1 = 13 m³·ha^{-1} (Figure 5c and 5d).

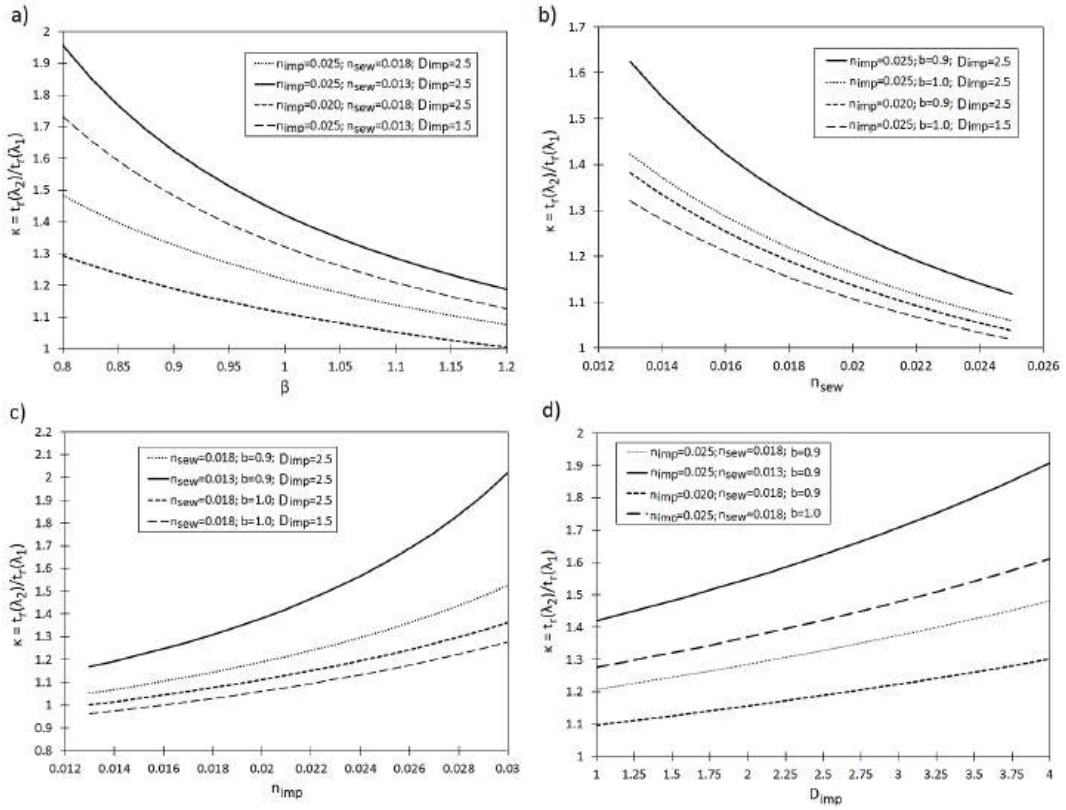

Figure 5. Influence of the identified SWMM parameters. (a) β, (b) n_{sew}, (c) n_{imp} and (d) D_{imp} on the value of κ for C = 5

Discussion

Extensive sensitivity analysis

Based on the proposed sensitivity coefficients for the logistic regression model, calculations of their values with respect to the identified SWMM parameters were performed. The conducted calculations showed that the correction coefficient for the percentage of impervious areas (β), Manning's roughness coefficient of sewer channels (n_{sew}) and Manning's roughness coefficient for impervious areas (n_{imp}) have key influences on the specific flood volume and degree of flooding. The calculation results obtained in this paper are consistent with those of Fu et al. [44], who performed simulations for an urban catchment (200 ha) in the UK and showed the significant influence of the runoff coefficient on the volume flooding from each manhole. This was consistent with the calculations of Brown et al. [45] that were conducted for a large catchment in southern England. Using the results of hydrograph measurements as the basis of the GLUE + GSA simulations, they showed that the retention depth of impervious areas and Manning's roughness coefficient of sewer channels have a strong influence on the results of catchment runoff calculations. The abovementioned calculation results were also consistent with those of Thorndahl [46], who, while performing a continuous simulation of the stormwater network operation in the Freylev catchment, developed a statistical model using the FORM method to calculate stormwater flooding from each manhole. The calculation results obtained in the present study, compared to the study of other authors [45, 47], showed a large influence of the rainfall duration and the return period on the sensitivity coefficients. The consideration of rainfall intensity, which is usually omitted at this stage of sensitivity analysis, is of great importance from the point of view of selecting rainfall-runoff events for the identification of SWMM parameters and validation of the hydrodynamic catchment model [48]. The results obtained indicate that omitting rainfall intensity at the sensitivity analysis stage can lead to problems in determining which SWMM parameters can be omitted at the calibration step. This problem was signaled by Fraga et al. [30], who performed sensitivity calculations for each rainfall event using the GSA method, obtaining different values of sensitivity coefficients.

The criteria for the functioning of the rainwater drainage network analysis

The consideration of two criteria of stormwater network operation (i.e., specific flood volume and degree of flooding) enabled the evaluation of the operation of the drainage system in the context of making decisions concerning its modernization, i.e., taking corrective measures including sewer channels cleaning or reducing their roughness coefficient. The applied solution allowed the assessment of the performance of the stormwater system at the spatial scale in the qualitative aspect (degree of flooding) and in the quantitative aspect (specific flood volume). Current methods tend to focus on a local approach in which a hydrodynamic model of the catchment is developed using landscape and manhole design data, which are important for determining the depth and area of flooding [16, 49]. These models are complex to implement and require data that are not always easy to obtain, which can lead to problems with their calibration. The solution applied in the present study, compared to the currently used methods [17] in which a criterion for the operation of the sewage network is imposed, allows its optimal selection on the basis of κ values considering the variability of calibrated SWMM parameters.

CONCLUSIONS

Currently, the analysis of stormwater network operation under hydraulic overload conditions is a frequently addressed issue because the simulation tools are the basis for decision making on the modernization of the drainage system. For these tools to be useful for making such decisions, it is necessary to calibrate the models. In the present study a multicriteria methodology for simulation of specific flood volume and the degree of flooding was provided, using the logistic regression method. The developed simulators enable the need for repair actions to be indicated and allow the determination of the key parameters of the SWMM model that need to be identified, which is important from the point of view of planning field tests prior to its calibration. The approach adopted in the study allows reducing the uncertainty of the simulation results and improving the reliability of the obtained predictions, which is reflected in the achievement of the assumed effect of decrease in hydraulic load.

Based on the sensitivity coefficients determined, the influence of calibrated SWMM parameters on the calculations results of the specific flood volume and degree of flooding was identified. The results of the calculations showed that the correction coefficients for the percentage of impervious areas, impervious area retention and Manning's roughness coefficient of sewer channels had a key influence on the specific flood volume, and the degree of flooding. Moreover, given that the values of sensitivity coefficients depended on rainfall intensity, conducting the assessment to appropriately select rainfall-runoff events for identifying and validating SWMM parameters seems to be advisable.

Considering the usefulness of the obtained calculation results, further analysis is advisable to establish the minimum period of continuous rainfall measurements for the development of logit models, then verify the obtained models for the calculation of specific flood volume and the degree of flooding for urban catchments with other characteristics and determine the range of their applicability. It is also advisable to consider extending the models with the characteristics of other urban catchments (area, catchment imperviousness, slope, land use, etc.) and stormwater networks (channel retention, diameters including slope, length of pipes, etc.) and finally their spatial arrangement.

REFERENCES

1. Rathnayake, U., Faisal Anwar, A.H.M. Dynamic control of urban sewer systems to reduce combined sewer overflows and their adverse impacts. J. Hydrol. 2019, 579, 124150. https://doi.org/10.1016/j.jhydrol.2019.124150
2. Müller, A., Österlund, H., Marsalek, J., Viklander, M. The pollution conveyed by urban runoff: A review of sources. Sci. Total Environ 2020, 709, 136125. https://doi.org/10.1016/j.scitotenv.2019.136125
3. Chang, H., Pallathadka, A., Sauer, J., Grimm, N.B., Zimmerman, R., Cheng, C., Iwaniec, D.M., Kim, Y., Lloyd, R., McPhearson, T., Rosenzweig, B., Troxler, T., Welty, C., Brenner, R., Herreros-Cantis, P. Assessment of urban flood vulnerability using the social-ecological-technological systems framework in six US cities. Sustain. Cities Soc 2021, 68, 102786. https://doi.org/10.1016/j.scs.2021.102786
4. McGarity, A.E. Watershed systems analysis for urban storm-water management to achieve water quality goals. J. Water Resour. Plan. Manag. 2013, 139, 464–477. https://doi.org/10.1061/(asce)wr.1943-5452.0000280
5. Eshtawi, T., Evers, M., Tischbein, B., Diekkrüger, B. Integrated hydrologic modeling as a key for sustainable urban water resources planning. Water Res. 2016, 101, 411–428. https://doi.org/10.1016/j.watres.2016.05.061
6. EN 752. Drain and sewer systems outside buildings – Sewer system management, 2017.
7. Baek, S.S., Ligaray, M., Pyo, J., Park, J.P., Pachepsky, Y., Chun, J.A., Cho, K.H. A novel water quality module of the SWMM model for assessing low impact development (LID) in urban watersheds. J. Hydrol., 2020, 586, 124886. https://doi.org/10.1016/j.jhydrol.2020.124886
8. Kordana, S., Słyś, D. An analysis of important issues impacting the development of stormwater management systems in Poland. Sci. Total Environ., 2020, 727, 138711. https://doi.org/10.1016/j.scitotenv.2020.138711
9. Szeląg, B., Kiczko, A., Łagód, G., De Paola, F. Relationship between rainfall duration and sewer system performance measures within the context of uncertainty. Water Res Manage., 2021, 35, 5073–5087. https://doi.org/10.1007/s11269-021-02998-x
10. Environment Agency. Thames Catchment Flood Management Plan - Chapter 3: Current flood risks and management. Environment Agency, Bristol, UK. 2009. Document available online: http://www.jubileeriver.co.uk/CFMP%202008%2008%20Chapter%203.pdf
11. Siekmann, M., Pinnekamp, J. Indicator Based Strategy to Adapt Urban Drainage Systems in Regard to the Consequences Caused by Climate Change, in: 12th International Conference on Urban Drainage. 2011, 11–16.
12. Jayasooriya, V.M., Ng, A.W.M. Tools for modeling of stormwater management and economics of green infrastructure practices: A review. Water Air Soil Pollut., 2014, 225, 1–20. https://doi.org/10.1007/s11270-014-2055-1
13. Hung, F., Harman, C.J., Hobbs, B.S., Sivapalan, M. Assessment of climate, sizing, and location controls on green infrastructure efficacy: A timescale framework. Water Resour. Res. 2020, 56. e2019WR026141. https://doi.org/10.1029/2019WR026141
14. Platz, M., Simon, M., Tryby, M. Testing of the storm water management model low impact development modules. J Am Water Resour Assoc., 2020, 15, 283–296. https://doi.org/10.1111/1752-1688.12832
15. Shojaeizadeh, A., Geza, M., Hogue, S.T. GIP-SWMM: A new green infrastructure placement tool coupled with SWMM. J. Environ. Manage., 2021, 277, 111409. https://doi.org/10.1016/j.jenvman.2020.111409
16. Martins, R., Leandro, J., Djordjević, S. Influence

of sewer network models on urban flood damage assessment based on coupled 1D/2D models. J. Flood Risk Manag., 2018, 11, S717–S728. https://doi.org/10.1111/jfr3.12244

17. Mignot, E., Li, X., Dewals, B. Experimental modelling of urban flooding: A review. J. Hydrol., 568, 2019, 334–342. https://doi.org/10.1016/j.jhydrol.2018.11.001
18. Leandro, J., Martins, R. A methodology for linking 2D overland flow models with the sewer network model SWMM 5.1 based on dynamic link libraries. Water Sci. Technol., 2016, 73, 3017–3026. https://doi.org/10.2166/wst.2016.171
19. Teng, J., Jakeman, A.J., Vaze, J., Croke, B.F.W., Dutta, D., Kim, S. Flood inundation modelling: A review of methods, recent advances and uncertainty analysis. Environ. Model. Softw. 2017, 90, 201–216. https://doi.org/10.1016/j.envsoft.2017.01.006
20. Bisht, D.S., Chatterjee, C., Kalakoti, S., Upadhyay, P., Sahoo, M., Panda, A. Modeling urban floods and drainage using SWMM and MIKE URBAN: A case study. Nat. Hazards, 2016, 84, 749–776. https://doi.org/10.1007/s11069-016-2455-1
21. Ochoa-Rodriguez, S., Wang, L., Gires, A., Pina, R., Reinoso-Rondinel, R., Bruni, G., Ichiba, A., Gaitan, S., Cristiano, E., Asssel, J., Kroll, S., Murlà-Tuyls, D., Tisserand, B., Schertzer, D., Tchiguirinskaia, I., Onof, C., Willems, P., ten Veldhuis, A.E.J. Impact of spatial and temporal resolution of rainfall inputs on urban hydrodynamic modelling outputs: A multi- catchment investigation. J. Hydrol., 2015, 531, 389–407.
22. Peleg, N., Blumensaat, F., Molnar, P., Fatichi, S., and Burlando, P. Partitioning the impacts of spatial and climatological rainfall variability in urban drainage modeling. Hydrol. Earth Syst. Sci., 2017, 21, 1559–1572. https://doi.org/10.5194/hess-21-1559-2017
23. Cristiano, E., ten Veldhuis, M.C., van de Giesen, N. Spatial and temporal variability of rainfall and their effects on hydrological response in urban areas – a review. Hydrol. Earth Syst. Sci., 2017, 21, 3859–3878. https://doi.org/10.5194/hess-21-3859-2017
24. Bárdossy, A. Calibration of hydrological model parameters for ungauged catchments. Hydrol. Earth Syst. Sci., 2007, 11, 703–710. https://doi.org/10.5194/hess-11-703-2007
25. Szeląg, B., Kowal, P., Kiczko, A., Białek, A., Wałek, G., Majerek, D., Siwicki, P., Fatone, F., Boczkaj, G. Integrated model for the fast assessment of flood volume: Modelling – management, uncertainty and sensitivity analysis. Journal of Hydrology, 2023, 625, part A, 129967. https://doi.org/10.1016/j.jhydrol.2023.129967
26. Szeląg, B., Gawdzik, J. Assessment of the effect of wastewater quantity and quality, and sludge parameters on predictive abilities of non-linear models for activated sludge settleability predictions. Pol. J. Environ. Stud., 2017, 26(1), 315–322. https://doi.org/10.15244/pjoes/64810
27. Szeląg, B., Majerek, D., Eusebi, A.L., Kiczko, A., de Paola, F., McGarity, A., Wałek, G., Fatone, F. Tool for fast assessment of stormwater flood volumes for urban catchment: A machine learning approach. Journal of Environmental Management, 2024, 355, 120214, https://doi.org/10.1016/j.jenvman.2024.120214
28. Bartkiewicz, L., Szeląg, B., Studziński, J. Impact assessment of input variables and ANN model structure on forecasting wastewater inflow into sewage treatment plants. Ochrona Środowiska, 2016, 38, 29–36. (in Polish)
29. Beven, K., Binley, A. The future of distributed models: model calibration and uncertainty prediction. Hydrol. Process. 1992, 6, 279–298. https://doi.org/10.1002/hyp.3360060305
30. Fraga, I., Cea, L., Puertas, J., Suárez, J., Jiménez, V., Jácome, A. Global sensitivity and GLUE-based uncertainty analysis of a 2D-1D dual urban drainage model. J Hydrol Eng., 2016, 21, 04016004. https://doi.org/10.1061/(ASCE)HE.1943-5584.0001335
31. Mannina, G., Cosenza, A., Viviani, G. Micropollutants throughout an integrated urban drainage model: Sensitivity and uncertainty analysis. J. Hydrol., 2017, 554, 397–405. https://doi.org/10.1016/j.jhydrol.2017.09.026
32. Morio, J. Global and local sensitivity analysis methods for a physical system. Eur. J. Phys., 2011, 32, 1577–1583. https://doi.org/10.1088/0143-0807/32/6/011
33. Razavi, S., Gupta, H.V. What do we mean by sensitivity analysis? The need for comprehensive characterization of "global" sensitivity in Earth and Environmental systems models, Water Resour. Res., 2015, 5, 3070–3092. https://doi.org/10.1002/2014WR016527
34. Bąk, Ł., Szeląg, B., Sałata, A., Studziński, J. Modeling of heavy metal (Ni, Mn, Co, Zn, Cu, Pb, and Fe) and PAH content in stormwater sediments based on weather and physico-geographical characteristics of the catchment-data-mining approach. Water, 2019, 11, 626. https://doi.org/10.3390/w11030626
35. Szeląg, B., Suligowski, R., De Paola, F., Siwicki, P., Majerek, D., Łagód, G. Influence of urban catchment characteristics and rainfall origins on the phenomenon of stormwater flooding: Case study. Environmental Modelling & Software, 2022, 150, 105335. https://doi.org/10.1016/j.envsoft.2022.105335
36. Bogdanowicz, E., Stachỳ, J. Maximum rainfall in Poland. Design Characteristics. Research Materials, s: Hydrology and Oceanology, 23. IMGW, Warszawa 1998.
37. Beven, K., Binley, A. GLUE: 20 years on. Hydrol. Process. 2014, 28, 5897–5918. https://doi.org/10.1002/hyp.10082
38. Romanowicz, R.J., Beven, K.J. Comments on generalised likelihood uncertainty estimation. Reliab.

Eng. Syst. Saf. 2006, 91, 1315–1321. https://doi.org/10.1016/j.ress.2005.11.030

39. Kiczko, A., Szeląg, B., Kozioł, A.P., Krukowski, M., Kubrak, E., Kubrak, J., Romanowicz, R.J. Optimal capacity of a stormwater reservoir for flood peak reduction. J. Hydrol. Eng. 2018, 23, 04018008. https://doi.org/10.1061/(asce)he.1943-5584.0001636
40. Szelag, B., Suligowski, R., Studziński, J., De Paola, F. Application of logistic regression to simulate the influence of rainfall genesis on storm overflow operations: A probabilistic approach. Hydrology and Earth System Sciences. 2020, 24, 595–614, https://doi.org/10.5194/hess-24-595-2020.
41. Harrell, F.E. Regression Modeling Strategies: With Applications to Linear Models, Logistic Regression, and Survival Analysis. Springer Series in Statistics, New York. 2001.
42. Petersen, B., Gernaey, K., Henze, M., Vanrolleghem, P.A. Evaluation of an ASM1 model calibration procedure on a municipal – industrial wastewater treatment plant. J. Hydroinform, 2002, 4, 15–38. https://doi.org/10.2166/hydro.2002.0003
43. Barco, J., Wong, K.M., Stenstrom, M.K. Automatic Calibration of the U.S. EPA SWMM Model for a Large Urban Catchment. J. Hydraul. Eng. 2008, 134, 466–474. https://doi.org/10.1061/(ASCE)0733-9429(2008)134:4(466)
44. Fu, G., Butler, D., Khu, S-T., Sun, S. Imprecise probabilistic evaluation of sewer flooding in urban drainage systems using random set theory. Water Resour Res, 2011, 47. https://doi.org/10.1029/2009WR008944
45. Brown, J.D, Spencer, T, Moeller, I. Modeling storm surge flooding of an urban area with particular reference to modeling uncertainties: A case study of Canvey Island, United Kingdom. Water Resour Res, 2007, 43. https://doi.org/10.1029/2005WR004597
46. Thorndahl, S. Stochastic long term modelling of a drainage system with estimation of return period uncertainty. Water Sci Technol, 2009, 59, 2331–2339. https://doi.org/10.2166/wst.2009.305
47. Fu, G., Butler, D. Copula-based frequency analysis of overflow and flooding in urban drainage systems. J. Hydrol., 2014, 510, 49–58. https://doi.org/10.1016/j.jhydrol.2013.12.006
48. Fatone, F., Szeląg, B., Kiczko, A., Majerek, D., Majewska, M., Drewnowski, J., Łagód, G. Advanced sensitivity analysis of the impact of the temporal distribution and intensity of rainfall on hydrograph parameters in urban catchments. Hydrol. Earth Syst. Sci., 2021, 25, 5493–5516, https://doi.org/10.5194/hess-25-5493-2021
49. Chen, A.S., Leandro, J., Djordjevi´c, S. Modelling sewer discharge via displacement of manhole covers during flood events using 1D/2D SIPSON/P-DWave dual drainage simulations. Urban Water J., 2016, 13, 830–840. https://doi.org/10.1080/1573062X.2015.1041991

Journal of Hydrology 625 (2023) 129967

Contents lists available at ScienceDirect

Journal of Hydrology

journal homepage: www.elsevier.com/locate/jhydrol

Research papers

Integrated model for the fast assessment of flood volume: Modelling – management, uncertainty and sensitivity analysis

Bartosz Szeląg [a,*], Przemysław Kowal [b], Adam Kiczko [a], Anita Białek [c], Grzegorz Wałek [d], Dariusz Majerek [e], Piotr Siwicki [a], Francesco Fatone [f], Grzegorz Boczkaj [b,g,*]

[a] Institute of Environmental Engineering, Warsaw University of Life Sciences-SGGW, 02-797 Warsaw, Poland
[b] Department of Sanitary Engineering, Faculty of Civil and Environmental Engineering, Gdansk University of Technology, 80-233, Gdansk, Poland
[c] Faculty of Environmental, Geomatic and Energy Engineering, Kielce University of Technology, 25-314 Kielce, Poland
[d] Department of Environmental Sciences and Geo-Information, Jan Kochanowski University in Kielce, Poland
[e] Department of Applied Mathematics, Lublin University of Technology, Lublin, Poland
[f] Department of Science and Engineering of Materials, Environment and Urban Planning-SIMAU, Polytechnic University of Marche Ancona, 60121 Ancona, Italy
[g] EKOTECH Center, Gdansk University of Technology, 80-233, Gdansk, Poland

ARTICLE INFO

Keywords:
SWMM
Fractal dimension
Random forest
Logistic regression
Water management

ABSTRACT

The specific flood volume is an important criterion for assessing the performance of sewage networks. It has been shown that its value is greatly influenced by the layout of the sewers in the catchment area, which is usually expressed by a fractal dimension. Currently, only mechanistic models (such as SWMM) enable the determination of the impact of the layout of the sewers on flooding volume, but they require additional and robust calculations. In the presented study an integrated tool has been proposed that includes: a flooding volume simulator based on rainfall data, catchment and sewage network characteristics, sewers layout expressed by fractal dimension. A logistic model can be applied for fast flooding volume estimation as an alternative approach to SWMM, design and upgrade sewer layout even with limited access to data (spatial planning, architectural concepts, etc.). Using the random forest (RF) method, a likelihood function simulator was developed, which enabled the analysis of interactions and optimal selection of combinations of SWMM model parameters for calibration. It has been shown that the higher the fractal dimension and retention coefficient (the ratio of surface to sewer retention), the greater the influence of SWMM parameters on the specific flood volume.

1. Introduction

The specific flood volume is one important criterion for evaluating the performance of sewer networks that forms the basis for taking corrective actions (De Paola and Ranucci, 2012; Lu et al., 2017; Barros et al., 2021). This parameter was proposed by Siekmann and Pinnekamp (2011) and describes the volume of stormwater flooding per unit of paved area. Determining the sewer flood volume in urban catchments requires expensive measurement methods, hence the need for simulation models (Dill et al., 2022; Efstratiadis et al., 2022).

In order to reduce the number of operations required and investment costs, mechanistic models (MCMs) (describing surface runoff, flow rate, and flood volume during hydraulic overload) are currently recommended (Seis et al., 2018; Addison-Atkinson et al., 2022, Amiri et al., 2022). In particular, one of the most commonly used models is the SWMM (Stormwater Management Model) developed by the EPA (Guo et al., 2021; Ma et al., 2022). These models take into account the characteristics of the catchment area and the sewer network, as well as their layout (Ogden et al., 2011; Tsoukalas et al., 2020), but it is not possible to consolidate the given factors into a single parameter as fractal dimension or bifurcation ratio (Diao et al., 2022; Nikolopoulos et al., 2022). In addition, the models are over-parameterized hence there are problems with the optimal selection of calibrated parameters, as previously pointed out in numerous studies (Fu et al., 2011, Fraga et al., 2016). The disadvantages of MCMs include their high specificity, as a single catchment model can only be applied to one case.

Taking into account the limitations of MCMs, machine learning methods (MLMs) were implemented to simulate sewer flooding (Mehedi et al., 2022). Compared to MCMs, MLMs are a more versatile approach, their application is not restricted to a specific site, so they can be applied

* Corresponding authors.
E-mail addresses: bszelag@tu.kielce.pl (B. Szeląg), grzegorz.boczkaj@pg.edu.pl (G. Boczkaj).

https://doi.org/10.1016/j.jhydrol.2023.129967
Received 26 May 2023; Received in revised form 26 June 2023; Accepted 14 July 2023
Available online 20 July 2023

to catchments with different characteristics. Despite applications in the water and stormwater industry (Perdikaki et al., 2022; Morán-Valencia et al., 2023), MLMs have not been applied in a specific flood volume simulator, taking into account characteristics of catchments and sewer networks, their layouts, catchment retention and sewer capacity. Therefore, MLMs constitute an alternative to mechanistic models. MLMs have been also developed to identify manhole flooding (Jato-Espino et al., 2018, Li and Willems, 2020) based on catchment and sewer network characteristics. Due to the local nature of the tools, they were further extended and a model was developed to simulate a specific flood volume in a catchment (Szeląg et al., 2022b).

Simplifying the layout of sewer network (reduction of sewer volumes) affects the results of flow and flood simulations (Barros et al., 2021; Guo et al., 2021). Calculations for several sewer networks with MCM models showed that one of the parameters influencing the hydrogram, sewer depth in also sewer flooding was the layout of the sewers in the catchment area (Ogden et al., 2011; Mediero et al., 2022). Due to the complex geometry of sewer networks, an attempt was made to evaluate their quantification to a single parameter (La Barbera and Rosso, 1989; Diao et al., 2022). This parameter was aimed to allow comparison of sewer networks and support decision-making on the direction of sewer layout development in the catchment area (Ichiba et al., 2018; Barros et al., 2021; Schackow et al., 2020). It was shown that the parameter for identifying the layout of the sewers and development in the catchment area was the fractal dimension (Ghosh et al., 2006). Gires et al. (2017) demonstrated the relationship between fractal dimension and land use by plotting the characteristics of a sewer network. Ichiba et al. (2018) developed an integrated tool for fractal dimension identification and sewer modeling using MCM. By performing calculations for sample catchments, they showed the influence of fractal dimension on the hydrogram.

Currently, the layout of the sewer network in the catchment expressed by fractal dimension has not been considered in MLMs. Despite numerous modelling approaches, no integrated system has been developed that includes the simulation of a specific flood volume and the analysis of interactions between calibrated parameters in the context of their selection. Moreover, no attempt has been made to subdivide urban catchments in terms of the influence of calibrated parameters on a specified flood volume.

The aim of this paper was to develop an integrated system for analysing the operation and management of a sewer network. The proposed system included: (a) simulator of the specific flood volume obtained on the basis of logistic regression (an alternative to the mechanistic SWMM model), (b) model for analysing the interaction of calibrated parameters of the SWMM model using the random forest method, (c) tool for optimising the operation of the sewer network. In comparison to the previously developed MLMs, the main feature of the new simulator is the consideration of the layout of the sewer network expressed by fractal dimensions, which enables the simulator to be applied to catchments with different characteristics. Another research task was to validate whether the developed random forest model allows the selection of SWMM parameters to optimize MCM calibration and to analyse the interaction between calibrated parameters, taking into account the matching of computational results with measurements.

Furthermore, the model was validated to facilitate the design and planning of modernisations by considering the sewer network layout and catchment area characteristics. This validation process helped identify alternative options that could minimize investment costs.

2. Study object

The analyzed catchment is located in Kielce (Poland) in the Świętokrzystkie voivodeship (Fig. 1). It lies in the south-eastern part of the city (center) and covers residential neighborhoods, public buildings, as well as main and side streets. The catchment spreads over an area of 63 ha, including 40% impervious and 60% pervious areas.

It was indicated that the depth of depression storage on impervious areas equal to 2.5 mm, whereas those of pervious areas were equal to 6.0 mm (Szeląg, 2013). The density of roads in the analyzed area equal 108 m·ha^{-1} (Wałek, 2019). The difference in the highest (271.20 m.a.s.l.) and lowest (260 m.a.s.l.) coordinates is merely 11.20 m, which gives an average slope of surface equal to 0.71%. It was determined that the length of the main sewer is 1569 m, with a diameter of 600 – 1250 mm. The diameter for the side sewers was between 300 and 1000 mm, with the slope of the sewers equal to 0.04 – 3.90%.

The analyzed stormwater sewers are separated from the municipal sewage system, and stormwater flows through a main sewer into the diversion chamber (DC). When filled below 0.42 m, stormwater makes its way into the stormwater treatment plant consisting of a longitudinal settling tank (SETT) and separator (SEP), and after treatment, into the Silnica River. During intense rainfalls, where the fill exceeds the overflow edge (OV), the stormwater is discharged into the overflow sewer

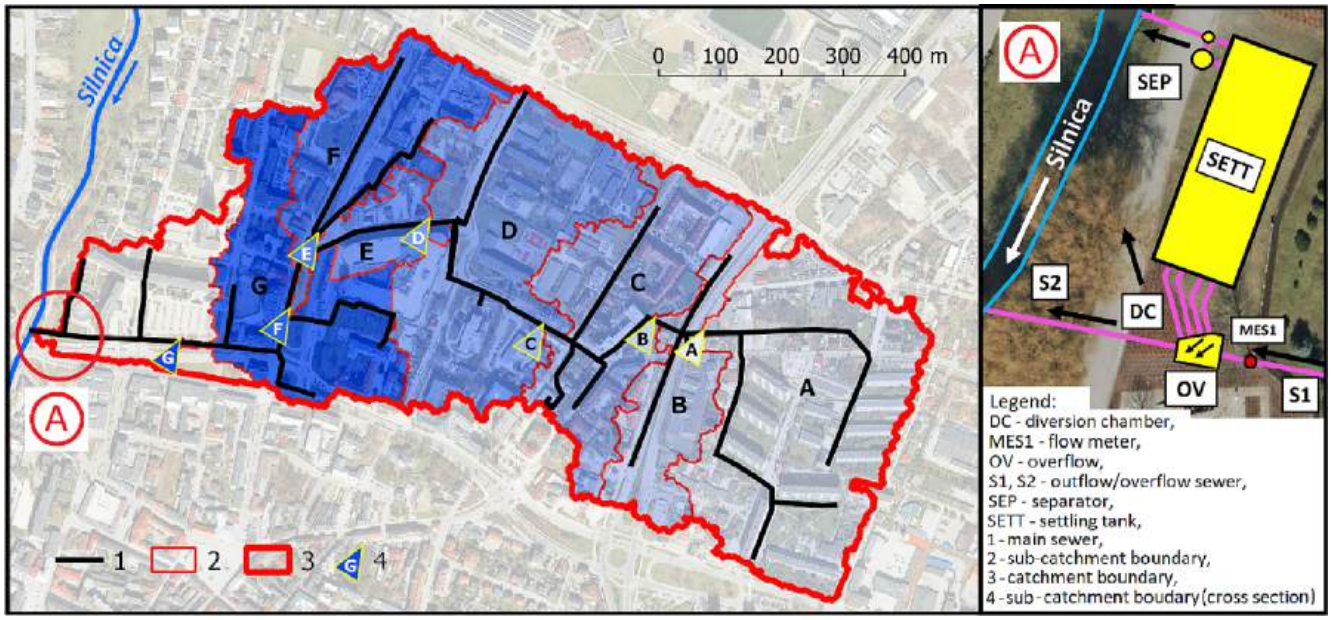

Fig. 1. Diagram of analyzed urban catchment in Kielce.

(S2). At a distance of 3.0 m from the inflow of the main sewer (S1) to the DC, a MES1 flow meter with a resolution of 1 min of flow value during intense rainfalls was installed. The probe of the flow meter measures the level (by measuring the water level pressure) and average flow rate of stormwater (via the Doppler effect), which, with the specific shape and dimensions of the canal, allow the calculation (by means of a built-in microprocessor) of the volumetric flow rate of the stormwater.

The analysis of data in the period 2010 – 2020 showed that, during the dry period, flows of 1 – 9 $dm^3 \cdot s^{-1}$ were noted by a MES 1 flow meter, which indicated the occurrence of infiltration. The carried out observations of the operation of the network in the period 2008 – 2019 showed that, in the analyzed catchment, floodings occurred as a result of intense rainfalls (Szeląg et al., 2022a). Measurements of rainfalls have been constantly carried out since 2008 at 1 min. intervals for rainfall events by the station located within 2.5 km from the catchment boundary.

2.1. Division of sub-catchments

For the present analyses, 7 sub-catchments were separated along the length of the collector. The adopted division into sub-catchments was conditioned by the variation of catchment characteristics, stormwater network, and changes in the geometry of the sewer system along the main sewer (in the context of fractal dimension calculations), as previously discussed in detail by Szeląg (2013) and Wałek (2019), using GIS (Geographic Information System) techniques. The integration of GIS data analysis with a mechanistic model enabled generation of more input data (combination of rainfall data, catchment characteristics, sewer network, SWMM parameters, specific flood volume) to developed simulator proposed in this study.

Table 1 gives the range of variation in catchment characteristics, sewer network and fractal dimensions for the 7 sub-catchments identified.

where: F – area of the catchment; Imp(u) – impervious of the catchment; Vk – volume of the main sewer; Gk – length of the main sewer on the impervious surface in the catchment; R.t. – difference in the coordinates of the sewer; Vkp – downstream volume of the sewer; dH –maximum difference in terrain elevation in the catchment area; Jkp – downstream slope of the sewer bottom; Hst – manhole depth downstream of the catchment area; Gkd – downstream length of a sewer per impervious area; Vrd – catchment retention calculated as $Vrd = F \cdot (Imp(u) \cdot d_{imp} + (1\text{-}Imp(u)) \cdot d_{per})$, (where: d_{imp} – depth of depression storage on impervious areas; d_{per} - depth of depression storage on pervious areas); Vkd – the volume of the sewer network in the downstream; $Vrd \cdot Vkd^{-1}$ – indicates of the coefficient retention; FD – the fractal dimension (calculated according to section 3.2).

3. Calculation methodology

An integrated computational algorithm, including a simulator, fractal dimension of sewers network, sensitivity and uncertainty analyses, for analysing the sewer flooding was presented (Fig. 2). The basis for sewer performance evaluation was the specific flood volume calculated from the formula:

$$k = \frac{\sum_{i=1}^{M} V_{t(i)}}{A_{paved}} \quad (1)$$

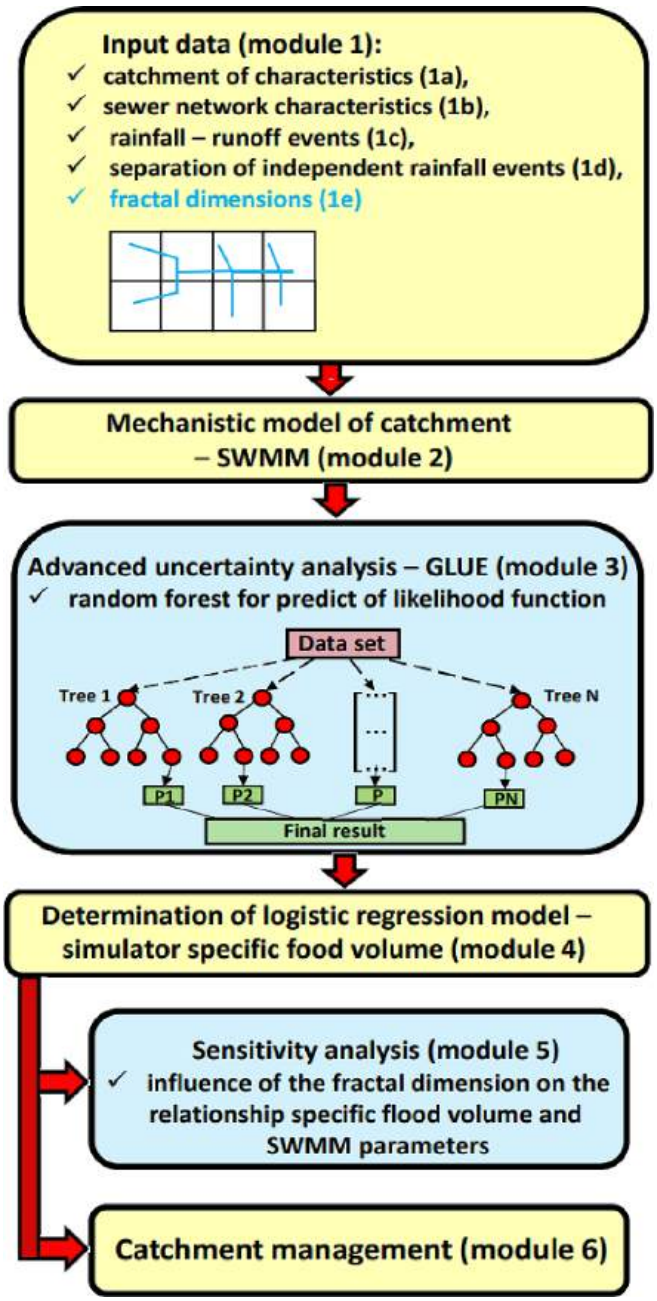

Fig. 2. Diagram of the integrated calculation algorithm for modeling sewer flooding. The new features implemented in this study, compared to the previously proposed algorithm by Szeląg et al, (2022b), are highlighted in blue. (For interpretation of the references to colour in this figure legend, the reader is referred to the web version of this article.)

where: V_t – volume of sewer flooding from i^{th} manhole of the sewer network, M – number of manholes, A_{paved} – paved area.

For urban catchments (Poland, Germany), it has been demonstrated that sewer networks with $\kappa \geq 13$ $m^3 \cdot ha^{-1}$ require modernization

Table 1
Range of variation in catchment characteristics, sewer network and fractal dimensions for the 7 sub-catchments.

No.	F	Imp(u)	Vk	Gk	R.t.	Vkp	dH	Lk	Jkp	Impd	Hst	dH	Gkd	Vrd/Vkd	FD
	ha	–	m^3	m/ha	m	m^3	m	m	m/m	–	m	m	m/ha	–	
min	12.66	0.34	157	0.0071	1.69	16.1	0.21	20.5	0.0036	0.40	1.42	0.25	0.0011	0.17	0.94
mean	35.08	0.37	725.3	0.0081	4.47	33.8	0.33	53.7	0.0073	0.45	2.22	1.22	0.0042	0.53	1.06
max	55.41	0.39	1240.2	0.0092	8.47	67.5	0.67	96.5	0.0102	0.55	2.36	1.80	0.0072	0.84	1.16

(Siekmann and Pinnekamp, 2011; Szeląg, 2013).

The main concept of the computation algorithm of the specific flood volume, applied in this study, has been developed by Szeląg et al. (2022b). In this study, the previous algorithm was extended in order to incorporate the layout of the sewer network by defining a fractal dimension. Furthermore, in the developed model and new approaches for the SWMM parameters calibration and identifying interactions between them, were performed by the random forest method, in the context of reducing the uncertainty of simulation results. The analyses in Modules 1, 2 and 4 comprise successive steps, the aim of which is to develop a model to identify the specific flood volume for urban catchments of arbitrary characteristics. The use of the proposed model in most cases will be limited to Modules 5, 6. The approach was dedicated to fast assess the performance of the sewer network under data-limited conditions (at the stage of catchment extension, spatial planning), or to help in planning the development of the MCM model in the context of data collection with adequate accuracy. In the applied model, only an extended uncertainty analysis requires the collection of rainfall - runoff data (Module 3) to perform the calculations.

3.1. Calibrating data collection (modules 1a-1c)

Calibrating data have been briefly presented in the chapter 2.

3.2. Identifying independent rainfall events (module 1d)

For the identification of independent rainfall events, the DWA-A 118E (2006) guidelines and simulation results of sewer network operation (specific flood volume, degree flooding) with uncertainty were used, as discussed in detail in Szeląg et al. (2022b). Convective rainfall ($P_t \geq 5$ mm, $t_r \leq 150$ min) was assumed for the simulation calculations. The analyses for the period (2010 – 2018) showed the number of convectional rainfall events in each year ranged from 12 to 30, which gave a total number of 200 rainfall events. In the selected rainfall events, the rainfall depth was $P_t = 5.2 – 45$ mm, with the maximum of 30-minute rainfall depth equal to $P_{t=30} = 2.5 – 30.0$ mm, and the duration of rainfall being $t_r = 15$——150 min.

3.3. Calculations of the fractal dimension (module 1e)

In the analyses found below, the box method was used to determine the fractal measure, in which the image was placed on a regular grid, consisting of squares with side measurements equal to τ, next determining the number of boxes covering the image (sectioned subcatchments). The number which is indicated N(τ) (the number of boxes) depends on the size of the elements of the grid and, in subsequent iterations, the size of τ is gradually decreased. Determining the body measurement relies on establishing in what manner N(τ) changes depending on τ. For complex sewer networks, the number of elements in subsequent iterations is not constant. Therefore, the box size is determined as a limiting value, where the length of the box (τ) in the grid strives to achieve zero. For the assumed number of boxes N(τ), with a length of side τ covering the image (sewerage network in the sectioned subcatchment), the box measurement is determined as:

$$FD = lim_{\tau \to 0} \frac{log(N(\tau))}{log\left(\frac{1}{\tau}\right)} \quad (2)$$

The box dimension involves determining the $\log(N(\tau) = f(\log(\tau^{-1}))$ relationship and approximating the relationship using the linear function. Figure S1 was used to calculate the fractal dimensions of the sewer networks in the separated sub-catchments. For each sub-catchment, between N = 4 and 1024 boxes (Ichiba et al., 2018) were used for FD calculations. It was shown that the lowest value of FD = 0.94 was obtained for sub-catchment A and the highest for sub-catchment G (FD = 1.16), as discussed in detail in Szeląg (2013) and Wałek (2019). The "box count" function in MATLAB was used to calculate the FD. Gires et al. (2018) during an analysis of the operation of ten sewer networks, showed that FD = 0.97——1.77, confirming that the sewer layouts separated in sub-catchments are among the typical ones.

3.4. Mechanistic model of the catchment - SWMM (module 2)

The mechanistic model of the catchment in Kielce was used to simulate the volume of flooding in the sub-catchments under uncertainty. Model input data, methods for identifying catchment and sewer network characteristics, and model calibration methodology are given in the study Szeląg et al. (2022b). The model was constructed from 82 nodes and 72 sewers. Calibration of the catchment model showed that for the 6 measured rainfall – runoff events, a high fitting of the modelled volumes of hydrograms was obtained, resulting in the Nash – Sutcliff coefficient of 0.85 and 0.98, and a coefficient of determination equal to 0.85 – 0.99. Hydrograph volumes and maximum flows did not exceed 5% compared to measurements.

Using the developed SWMM model, calculations of volume flooding (without sub-catchment division) were performed according to the methodology described in Szeląg et al. (2022b). In the present study, calculations of volume flooding in sub-catchments (A, B, C, D, E, F, G) were performed for separated rainfall events ($P_t \geq 5.0$ mm and $t_r \leq 150$ min) taking into account the uncertainty results simulation (*a posteriori distribution* of SWMM parameters). Based on the results of the simulated volume flooding and the characteristics of each sub-catchment, the specific flood volume was determined, which provided the basis for the development of the logistic regression model.

3.5. Advanced uncertainty analysis – GLUE (module 3)

3.5.1. GLUE

In this paper, the Generalized Likelihood Uncertainty Estimation (GLUE) method was used for uncertainty analysis. The theoretical basis of the method is discussed in detail in the studies by Beven and Binley (2014), Romanowicz and Beven (2006). In the GLUE method, the basis for the identification of parameter distributions was Bayesian estimation, in which for the assumed *a priori parameter distributions* the so-called *a posteriori* distributions were determined by the likelihood function. The uniform distributions of the SWMM parameters (correction coefficient of percentage area - β, coefficient for flow path width - α, depth of depression storage on impervious areas – d_{imp}, depth of depression storage on pervious areas – d_{per}, Manning roughness coefficient for of impervious areas – n_{imp}, Manning roughness coefficient for of pervious areas – n_{per}, Manning roughness coefficient of sewer channels – n_{sew}, correction coefficient for subcatchments slope - γ) were assumed in this study (Table S2). Measurement data for 24 July 2011 and 15 September 2010 were used to calculate 95% confidence intervals, credibility functions, and *a posteriori* distribution of SWMM parameters. Data for the 30 May 2010 event and for 30 July 2010 were used for validation. A detailed description of the subsequent computational steps is discussed in Szeląg et al. (2022b) and in Supplementary Materials – section S1.

3.5.2. Calculations of likelihood functions using random forest

The random forest (RF) method, a modification of the regression tree (RT) method, developed by Breiman (2001) was used in the study. A single tree was replaced by a forest of trees connected in parallel. The simulation results from the model were the arithmetic mean of all the involved forest. In the RF model, the identification of the model structure consisted of determining the number of trees in the forest. To ensure that the model does not exhibit over-fitting, the tree structure of the forest including leaves and nodes was optimized in accordance to Louppe (2015). The model was developed so that the number of trees did not exceed 300. The algorithm for building the RF model and determining validity was discussed in detail by Fisher et al. (2019). The

coefficient of determination (R^2), mean absolute error (MAE), root mean squared error (RMSE) were used to assess the fit of the simulation results of the likelihood function with the RF model to the empirical data obtained in the GLUE analyses; the S2 (Support Information) section provides the relationships for calculating the fit measures listed above.

Based on the results of calculations in the GLUE method and SWMM model parameters (Table S2), a model for simulating the likelihood function $L(Q/\theta)$ was developed applying the model of random forests. The data for developing the model are discussed in detail in Szeląg et al. (2022b). In the model, the input was the SWMM parameters (α, β, γ, n_{imp}, d_{imp}, d_{imp}, n_{sew}) and the output was the likelihood function. The data for developing the model are discussed in detail in Szeląg et al. (2022b). The entire dataset of 5000 cases was randomly divided into a train and a test sample, in the proportions of 70% and 30%, respectively. One hyper parameter was calibrated based on 10-fold cross-validation.

3.5.3. Analysis of interaction between SWMM parameters

Basing off of this model, the methodology of the analysis of interactions between SWMM model parameters has been given for the assumed level of compliance of results with the measurements – the values of the likelihood functions $L(Q/\theta)_s$. Parameters which have a strong influence on the calculations of hydrograph and describing the surface and sewer retention, i.e. β, n_{sew}, d_{imp} (Kiczko et al. 2018). For the assumed values of $L(Q/\theta)_s$ and SWMM parameters using the random forest model, problems of the form were solved:

$$d_{imp} = F^{-1}\left(\beta^*, n^*_{sew}, \varphi, L(Q/\theta)_s\right) for \beta^* = 0.8 - 1.2; n^*_{sew} = 0.013 - 0.025 \quad (3)$$

$$n_{sew} = F^{-1}\left(\beta^*, d^*_{imp}, \varphi, L(Q/\theta)_s\right) for \beta^* = 0.8 - 1.2; d^*_{imp} = 1.5 - 3.5 \quad (4)$$

$$\varphi = f(\alpha^c, \gamma^c, {n_{per}}^c, {d_{per}}^c) \quad (5)$$

where: $F^{-1}(\hat{A}\cdot)$ – inverse function allowing the RF model to determine the values of selected SWMM parameters; φ – constant value calculated with RF model for SWMM parameters (α^c, γ^c, n^c_{per}, d^c_{per}) determined according to hydrodynamic model calibration (Szeląg et al., 2022b); n_{sew}* - value of Manning roughness coefficient of sewer assume to solved Eq. (3); d_{imp}* - retention depth of impervious areas assume to solved Eq. (4); $L(Q/\theta)_s$– value of likelihood function assume to calculation of Eq. (3), (4); in the study, the maximum value was used for the calculation. Based on the computational results, curves β = f(d_{imp}, n_{sew}) and n_{sew} = f(d_{imp}, β) were drawn to determine the character of the interactions between the selected SWMM parameters.

3.6. Determination of logistic regression model – Simulator specific flood volume (module 4)

Logistic regression model is a tool used for classification (supervised learning) and according to the literature (Jato-Espino et al., 2018; Ukkonen and Mäkelä, 2019) represents one of many methods of ML. The logit model in the general form, for calculations of exceeding the specific flood volume, is was described by a formula:

$$p_m = \frac{\exp(\alpha_0 + \alpha_1\hat{A}\cdot x_1 + \alpha_2\hat{A}\cdot x_2 + \alpha_3\hat{A}\cdot x_3 + \cdots + \alpha_i\hat{A}\cdot x_i)}{1 + \exp(\alpha_0 + \alpha_1\hat{A}\cdot x_1 + \alpha_2\hat{A}\cdot x_2 + \alpha_3\hat{A}\cdot x_3 + \cdots + \alpha_i\hat{A}\cdot x_i)} = \frac{\exp(X)}{1+\exp(X)} = \frac{\exp(X = X_{SWMM} + X_{RAIN} + X_{CTCH})}{1+\exp(X = X_{SWMM} + X_{RAIN} + X_{CTCH})} \quad (6)$$

where p_m – is the probability of specific flood volume being exceeds, which in this case also implies the probability of the need for modernization; α_0 – absolute term; α_1, α_2, α_3, α_i – values of coefficients estimated with the maximum likelihood method, X – vector describing the linear combination of the independent variables; X_{SWMM} – linear combination of SWMM model parameters (Table S2); X_{RAIN} – linear combination of rainfall characteristics (the duration of the rainfall event, depth of the rainfall, maximum 30-minute rainfall depth in a rainfall event) assumed for the calculations based on studies by Zhou et al. (2019), Li and Willems (2020); Szeląg et al. (2022a); X_{CTCH} – the combination of the linear characteristics of the subcatchments divisions (Table 1) used to develop Eq. (6) based on literatury (Jato-Espino et al., 2018; Thorndahl and Willems, 2008). The methodology of the estimation of coefficient, model acuraccy and estimation of the otpimized p_m value was briebly describe in the SI (section S3). The coefficients (α_i) were determined by 10-fold cross-validation.

Based on the simulation results of the SWMM model (Section 3.3), the dependent variables were determined for the development of the logit model. When the value obtained from the calculation $\lambda \geq 13$ $m^3 \cdot ha^{-1}$ then the dependent variable was taken equal to 1, otherwise 0. This pointed to, on one hand, problems with the performance of the stormwater sewer network in the context of limiting values given by Siekmann and Pinnekamp (2011) and the need to carry out the modernization of the sewer network.

3.7. Sensitivity analysis (module 5)

In the framework of the present analyses, the method of local sensitivity analysis was applied. The analytical equation of the form (Fatone et al., 2021) was used to calculate the sensitivity coefficient in the logistic regression method:

$$S_{xi} = \varepsilon_i\hat{A}\cdot x_i\hat{A}\cdot(1 - p_m) \quad (7)$$

where: p_m – the probability of specific flood volume for the assumed constant value of the rainfall data, catchment characteristics and SWMM model parameters (a detailed description of the calculation of the sensitivity coefficients is given in section S4 – Support Information); x_i – independent variables; ε_i – coefficients estimated in a logistic regression model. A detailed discussion of Eq. (7), and the assumptions made for its derivation are discussed in Fatone et al. (2021).

A rainfall duration in the range of $t_r = 30 - 90$ min a for $P_t = 12.5$ mm was assumed (maximum mean intensity equal of the 70 $l\cdot(s\cdot ha)^{-1}$). For the assumed rainfall data, the SWMM calibrated parameters (Szeląg et al., 2022b) and the assumed catchment characteristics, the relationship $S_{xi} = f(t_r, X_{CTCH})$ was determined. The influence of the variability of SWMM model parameters (β, n_{sew}) on the sensitivity coefficients (S_{xi}) for the catchment caused by the convectional rainfall with a duration time of $t_r = 30$ min was also analyzed. The depth of convective rainfall was determined using the Suligowski model - section S5 in Support Information.

3.8. Catchment management (module 6)

In this study, the decision to modernize the catchment was based on an assessment of the existing condition. Calculations regarding the operation of the sewer network under conditions of a convectional rainfall $t_r = 30$ min were carried out. On their basis, the value of the probability of exceeding the specific flood volume in the specific subcatchments (A-G).

In an effort to introduce systems of equations which form the basis for the improve of sewer network performance, two variants, i.e., prior to modernization and post-modernization (Fig. S2a), were considered. The following relationships describing surface retention of catchment before and after the modernisation were formulated for the pre-modernisation option:

$$V_u = F_u\hat{A}\cdot d_u \quad (8)$$

$$d_u = d_{imp} \bullet Imp(u) + d_{per} \bullet (1 - Imp(u)) \quad (9)$$

Where the following formula was obtained after making appropriate substitutions:

$$\frac{V_{rd}}{V_{kd}} = \frac{F_u \hat{A}\cdot\left[Imp(u)\hat{A}\cdot\left(d_{imp} - d_{per}\right) + d_{per}\right]}{V_t} \tag{10}$$

For the post-modernization variant (Fig. S2b), we can formulate the following relationships:

$$Imp(u)^* = Imp(u)\hat{A}\cdot(1 - x_{red}) \tag{11}$$

$$d_u^* = d_{imp}\hat{A}\cdot Imp(u)^* + d_{per}\hat{A}\cdot(1 - Imp(u)^*) \tag{12}$$

$$d_u^* = Imp(u)\hat{A}\cdot\left(d_{imp} - d_{per}\right)\hat{A}\cdot(1 - x_{red}) + d_{per} \tag{13}$$

Which, after appropriate substitutions, gives us:

$$\frac{V_{rd}^*}{V_{kd}} = \frac{F_u \hat{A}\cdot\left[Imp(u)\hat{A}\cdot(d_{imp} - d_{per})\hat{A}\cdot(1 - x_{red}) + d_{per}\right]}{V_t} \tag{14}$$

where: V_u - volume of average surface retention depth of catchment; d_u, d_u* - average surface retention depth of catchment before and after modernisation; Imp(u), Imp(u)* - catchment impervious before and after modernisation; x_{red} - rate of reduction in catchment impervious, values in the range 0—1 were assumed; V_t = Vkd - sewer network capacity.

Assuming that the probability of specific flood volume depends on z - characteristics of the catchment and t - parameters of the SWMM model, it can be written that improving the conditions of the sewer network when $p_m > p_{m,cr}$ requires an adjustment of the independent variables satisfying the relationships:

$$\begin{cases} p_m \le p_{m,cr} \\ 4.8 \ge d_{imp} \ge 0.8 \\ 6.8 \ge d_{per} \ge 0.8 \\ \left(\frac{V_{rd}}{V_{kd}}\right)_{max} \ge \frac{V_{rd}}{V_{kd}} \ge \left(\frac{V_{rd}}{V_{kd}}\right)_{min} \\ Imp(u)_{max} \ge Imp(u) \ge Imp(u)_{min} \\ \cdots \\ w = 1, 2, 3, \cdots, z \end{cases} \tag{15}$$

where: p_m – the probability of the specific flood volume; $p_{m,cr}$ – the threshold probability of the specific flood volume, exceeding of which indicates $\lambda \ge 13$ $m^3 \cdot ha^{-1}$; $Imp(u)_{min,\ max}$ – minimum and maximum values for catchment impervious – Table S1; w – number of limiting conditions.

In order to solve the system of Equations (15), the need arises to implement an optimization method, keeping in mind the limitations arising from the scope in which the developed model logistic regression model can be applied.

4. Results

4.1. Random forest for predict likelihood function (module 3)

The optimal number of variables used in each decision tree was 8, based on minimal RMSE value 0.008 on test set, which shows very good performance of the model. Comparison of fitted and observed values also indicated that the model describes the dependent variable well (Figure S3). The importance values were determined for each SWMM parameter as presented in Table S3. It was confirmed that the greatest influence on the likelihood function was exerted by the following parameters, respectively: retention depth of impervious areas, correction coefficient for percentage of impervious areas, Manning's roughness coefficient of sewers, as confirmed by the importance of 0.078, 0.076 and 0.022. Manning's roughness coefficient of impervious areas, coefficient for flow path width, Manning's roughness coefficient of pervious areas and depth of depression storage on pervious areas had a much smaller influence, which was confirmed by the obtained values of importance 0.018, 0.010 and 0.004. The influence of correction coefficient for subcatchment slope was negligible, as confirmed by the importance values equal to 0 (Table S3).

4.1.1. Interaction between SWMM parameter models

For the assumptions discussed in detail in Section 3.4.3 using the determined RF model and SWMM parameters ($\alpha^c = 1.35$, $\gamma^c = 1.10$, $n^c_{imp} = 0.025$ $m^{-1/3}\cdot s$, $n^c_{per} = 0.120$ $m^{-1/3}\cdot s$, $d^c_{per} = 6.0$ mm, $L(Q/\theta)_s = 0.007$) the curves were determined $\beta = f(n_{sew}, d_{imp})$ i $n_{sew} = f(\beta, d_{imp})$ – (Fig. 3a, 3b). It was found that in order to obtain a high fitting (hydrograph) of the calculation results with the measurements, an increase in correction coefficient of percentage area (β) and Manning roughness coefficient of sewers (n_{sew}) determines the need for an increase in retention depth of impervious area – d_{imp} (Fig. 3), and the relationship $d_{imp} = f(\beta, n_{sew})$ was close to linear.

The relationship $\beta = f(d_{imp}, n_{sew})$ showed that a pattern of d_{imp} requires an increase in β in order to maintain high fitting (hydrograph) between measurements and simulations, while n_{sew} has a negligible influence on the simulation results (Fig. 3a). For $d_{imp} = 1.5$—3.5 mm, $\beta = 0.8$—1.2, in order for the likelihood function to be approximately $L(Q/\theta)_s = 0.007$ (the maximum value obtained in this study) the n_{sew} determined at the calibration step should be 0.009—0.012 $m^{-1/3}\cdot s$ (Fig. 3b). With increasing d_{imp}, the value of β has an increasing influence on n_{sew}. For $d_{imp} = 1.5$ mm, an increase in β from 0.80 to 0.90 requires an increase in n_{sew} from 0.012 to 0.038 $m^{1/3}\cdot s^{-1}$; for $d_{imp} = 2.5$ mm, an increase in nsew from 0.008 $m^{1/3}\cdot s^{-1}$ to 0.013 $m^{1/3}\cdot s^{-1}$ is required.

4.2. Determination of logistic regression

4.2.1. Mechanistic model of catchment (simulation of the performance of the sewer network under uncertainty)

Based on SWMM model simulations results of rainfall events while accounting for the uncertainty of SWMM parameters (Table 1), the specific flood volume was determined for the selected catchments (median and corresponding percentiles – 5, 25, 50, 75, 95); the results of calculations have been presented in Figure S4. The greatest median value of the specific flood volume was found for catchment A (15.8 $m^3\cdot ha^{-1}$) located furthest from the outlet to the Silnica, for which the smallest fractal dimension FD = 0.94 and F = 12.66 ha was shown. The smallest specific flood volume was found for catchment G (8.2 $m^3\cdot ha^{-1}$), whose FD = 1.14 and F = 55.41 ha. The uncertainty of SWMM parameters has a strong influence on the results of specific flood volume calculations, as confirmed by the variability of values 5% and 95% percentile for the analyzed subcatchments. Analysis of values of the 95% percentile revealed that the maximum specific flood volume (13 $m^3\cdot ha^{-1}$) was exceeded in each subcatchment, which indicated the need the modernization of the sewer network.

4.2.2. Determination of logistic regression

Using specific flood volume results, a logistic regression model was determined for the separated catchments. Training data (80%) were used to develop the model, followed by validation (20%). The model for calculating the probability of specific flood volume was described by the linear combination:

$$X = 1.51\hat{A}\cdot P_t - 0.10\hat{A}\cdot t_r + 0.12\hat{A}\cdot\alpha - 41.86\hat{A}\cdot n_{imp} - 0.04\hat{A}\cdot d_{imp} + 3.66\hat{A}\cdot\beta + 0.22\hat{A}\cdot\gamma + \\ + 143.72\hat{A}\cdot n_{sew} - 24.03\hat{A}\cdot FD - 3.98\hat{A}\cdot\frac{Vrd}{Vkd} \tag{16}$$

The depth of depression storage on impervious, the Manning roughness coefficient of impervious areas, the correction factor for percentage of impervious area (β), the Manning roughness coefficient of sewers and correction coefficient to slope were found to influence the

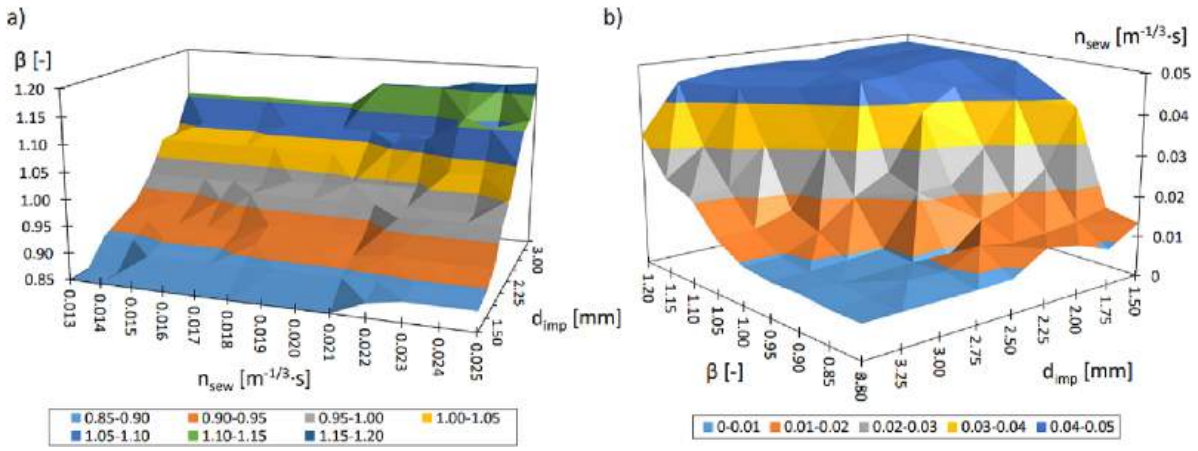

Fig. 3. (a) Influence of Manning's roughness coefficient of sewers (n_{sew}) and the depth of depression storage on impervious (d_{imp}) on the correction coefficient for the percentage of impervious areas (β). (b) Influence of depth of depression storage on impervious (d_{imp}) and correction coefficient for percentage of impervious areas on Manning's roughness coefficient of sewers (n_{sew}).

probability of specific flood volume. For the remaining parameters, the tested probability values were shown to be higher than 0.05, hence they were not included in further calculations. The Manning roughness coefficient of impervious areas, the fractal dimension and the retention coefficient were shown to lead to a reduction in p_m. The results of the standard deviation, test probability (p - test) calculations for the resulting logit model are given in Table S4. The results of calculations regarding standard deviation, test probability (p – test) for the obtained logit model have been given in Table S4.

By subsequently substituting the values of $p_m = 0.05 – 0.99$, it was

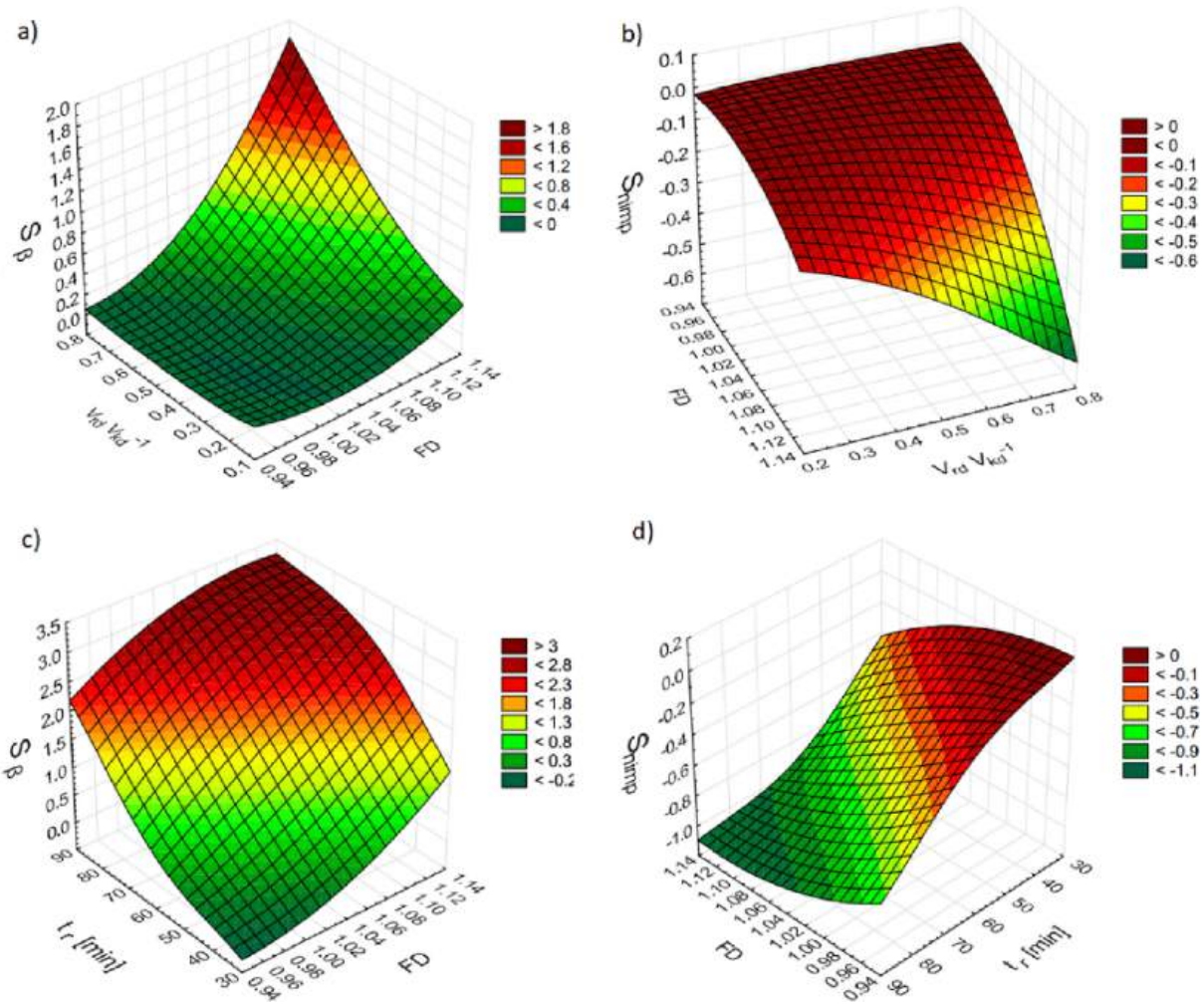

Fig. 4. Influence of retention ratio ($Vrd \cdot Vkd^{-1}$), fractal dimension (FD) on: a) $S_β$, (b) S_{nimp}. Influence of rainfall duration (tr) and fractal dimension (FD) on: c) $S_β$, (d) S_{nimp}.

confirmed that the greatest predictive abilities were obtained for $p_m = p_{cr} = 0.58$, while the specificity (SPEC) and sensitivity (SENS) values for the training set are 80.18%, 89.49% respectively, and Accuracy (Acc) was 86.25%.

4.3. Sensitivity analysis (module 5)

Based on Eq. (7) the estimated sensitivity coefficents S_β and S_{nimp} were recognized as a influential SWMM parameters (describing surface retention of catchment) significantly affecting the specific flood volume. For $t_r = 30$ min and $P_t = 9.62$ mm, based on SWMM parameters calibration data from Kiczko et al. (2018), estimated senisivity was FD = 0.94 – 1.14 and $Vrd \cdot Vkd^{-1} = 0.1 – 0.8$ (Fig. 4a, 4b). In addition, assesements of S_β, S_{nimp} as a function of rainfall duration ($t_r = 30 – 90$ min, $P_t = 12.5$ mm) for FD = 0.94 – 1.14 (Fig. 4c, 4d). The calculation results for the other SWMM parameters (α, d_{imp}, n_{sew}, γ) are included in Figures S5 – S8 in the Supplementary Information.

It was determined that increasing the duration of rainfall (t_r) leads to an increase in the values of S_β, S_{nimp}. This indicates that the influence of β, n_{imp} on the specific flood volume is the highest for $t_r = 90$ min and the lowest for $t_r = 30$ min (Fig. 4a, 4b).

It was shown that as the fractal dimension increases, the influence of β, n_{imp} on the values of specific flood volume increases. It was confirmed that, apart from the fractal dimension, the influence of $Vrd \cdot Vkd^{-1}$ on the specific flood volume was significant (Fig. 4c, 4d). It was found that with increasing FD and $Vrd \cdot Vkd^{-1}$ the influence of β and n_{imp} on κ increases, which is confirmed by the calculated values of S_β and S_{nimp}. The maximum values of the sensitivity coefficients were obtained for FD = 0.94 and $Vrd \cdot Vkd^{-1} = 0.80$, which are $S_\beta = 1.86$ and $S_{nimp} = -0.60$, respectively.

4.4. Catchment management (module 6)

Calculations of the performance of the sewer network for the existing condition showed that for the sub-catchment (A - G) the values obtained were $p_m \geq 0.58$, indicating the need for a corrective action approach (Fig. 5). Further analyses were performed for sub-catchment S as representative of the area under consideration.

Based on the Equations (15) for the assumed values of α, β, γ, n_{sew} (Kiczko et al. 2018), the influence of $n_{imp} = 0.020 – 0.025$ $m^{-1/3} \cdot s$, $d_{imp} = 2.3$—2.6 mm on the values of Imp(u) conditioning to obtain the limiting value of $p_m = 0.58$ was determined. In the second variant, the limiting conditions were taken into account (range of applicability of the logistic regression model) and for obtaining $p_m = 0.58$ depending on n_{imp} the values of Imp(u), d_{imp}, d_{per} were optimised. The results of calculations are presented in Fig. 5, and the calculated values of depth of depression storage on impervious (d_{imp}), pervious area (d_{per}) for variant II are summarised in Table S5.

Based on the curves in Fig. 5, it can be concluded that in sub-catchment G it is possible to improve the operating conditions of the sewer network and reduce the specific flood volume by appropriately selecting the values of n_{imp} and d_{imp}. It is shown that in order to keep $\kappa = 13$ $m^3 \cdot ha^{-1}$ constant despite an increase in Imp(u), n_{imp} and d_{imp} should be increased. The curves obtained (Fig. 5) and the values of Imp(u) confirm that the neglect of the boundary conditions in variant I leads to results outside the range of applicability of the determined logit model. Therefore, the limitations were taken into account and calculations were performed again. Based on the results (Fig. 5, Table S5), it was found that the inclusion of boundary conditions leads to improved simulation results and the SWMM parameters and Imp(u) is within the applicability range of the developed logit model.

The increase in Imp(u) compared to $Imp(u)_{min} = 0.35$ for the variant when the constraints were neglected was compensated by an increase in d_{imp} and d_{per}. In contrast, the decrease of Imp(u) to $Imp(u)_{max} = 0.44$ was obtained by decreasing d_{imp}, d_{per}.

5. Discussion

Modeling the process of flooding in urban catchments is one of the current research topics (Guo et al., 2021). This is due to the complex nature of the phenomenon, the course of which depends on the layout of sewers, hydraulic conditions in the sewer network (pipes, manholes), landscape (Martins et al., 2017). Mechanistic models requiring calibration of many parameters were usually used for flooding analysis (Li et al., 2022, Ma et al., 2022). Due to the strong interaction between them and the problems and their determination for existing sewer networks, it has become a major challenge to obtain high agreement between measurements and simulations. Therefore, an attempt was made to

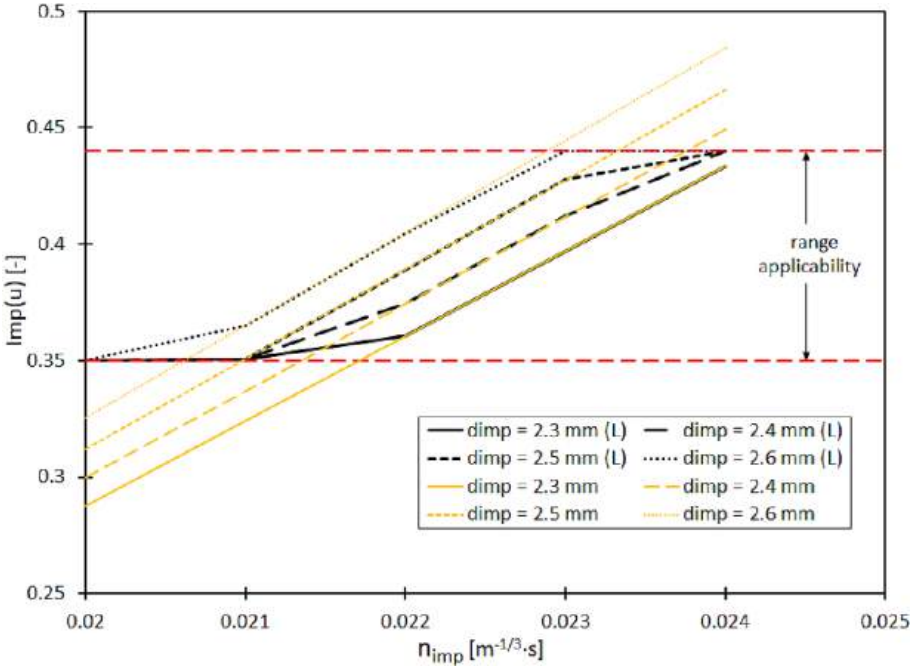

Fig. 5. Influence of Manning roughness coefficient (n_{imp}) and depth of depression storage on impervious (d_{imp}) on Imp(u) on the example of sub-catchment G.

implement machine learning methods for simulating flooding as an alternative to MCM models (Mehedi et al., 2022).

The methodology proposed in this study enabled: a) the estimation of the specific flood volume for a catchment with arbitrary characteristics using logistic regression taking into account the layout of sewers, b) the determination of the influence of the parameters included in the mechanistic models (SWMM) and the interaction between them on the simulation results by means of sensitivity analysis and extended uncertainty analysis. To date, such a wide range of analyses have been performed for mechanistic models (Luo et al., 2022), but due to the specificity of urban catchments (spatial data layout of land use and the sewer network) the modules mentioned above have been applied independently (Table S6). For instance, Szeląg et al. (2022a) developed an integrated tool to simulate the identification of flooding in a catchment (rainfall data, catchment characteristics, sewer network density) and optimise management, but excluding its layout of sewers. Szeląg et al. (2022b) further developed this approach by designing a tool for assessing the need for sewer network modernisations that includes an extended uncertainty and sensitivity analysis (Table S6). However, the model focused on the impact of surface retention of catchment and capacity on system operating conditions, ignoring catchment and sewer network characteristics as well as layout of sewers. In the present study, the integration of modules allowed the range of computational tools used to be extended (Table S6) and, in addition to simulating and assessing the performance of sewer networks with hydrodynamic models, it was also possible to perform calculations with a limited range of input data, which potentially will reduce the cost of field surveys at the planning step of developing MCM models.

5.1. Model to determine specific flood volume

Based on the literature (Mehedi et al., 2022) that flooding is a complex process influenced by land use, surface retention of catchment and the characteristics of the sewer network, including its layout. Capturing the aforementioned factors is possible mainly in mechanistic models (Guo et al., 2021). Using MCM models, it is not possible to directly determine the impact of the layout of the sewer on the magnitude of the flooding (Cao et al., 2020); this requires the determination of additional parameters, such as the fractal dimension.

Calculations with the MCM for the Dead Run catchment (Baltimore, USA) for heavy rainfall showed that increasing the density of the sewer network from 0.4 to 3.9 km/km^{-2} led to an increase in maximum flow from 28.9 m^3/s^{-1} to 40.7 m^3/s^{-1} and outflow volume from 0.468·10^6 m^3 to 0.605·10^6 m^3. These calculations were made on the assumption that the layout of the sewer network was omitted, despite the fact that it differed significantly for the options considered, as shown by Ogden et al. (2011). To address these limitations, Ichiba et al. (2018) developed an integrated system including an MCM model and a tool for calculating the fractal dimension of a sewer network based on DTMi data. The effect of increasing the resolution of the spatial data was shown to increase the fractal dimension and reduce the maximum flow. However, the calculations they performed were not designed to look for general relationships between hydraulic conditions and the spatial layout of the sewer network and land use.

The ML models developed to date have not considered the layout of the sewers and have included a limited range of input data; determined by the task for which they were to be used (Table S6). Yan et al. (2018) and Ke et al. (2022) included rainfall data in their ML models, but omitted catchment and sewer network characteristics, making them applicable to real - time - control (RTC) systems for single catchments. Thorndahl and Willems (2008) predicted manhole flooding based on surface retention of catchment and sewer capacity; although the algorithm was universal, the computational efforts were large and the feasibility of applying the tool to other catchments was limited (Table S6). The aforementioned approach was extended by Jato-Espino et al. (2018) taking into account catchment impervious, slope and sewer capacity. Li and Willems (2020) additionally included spatial variation in land use and sewer network in a simplified manner. Szeląg et al. (2022a), Chapi et al. (2017) extended the applicability of the models by including rainfall data, catchment and the sewer network characteristics, but omitted the capacity of the sewers and their layout.

It can be concluded that previously developed ML models allowed analysis of sewer capacity but excluded evaluation of the impact of layout of sewer network in the catchment on flooding. The above ML limitations were eliminated in the proposed model, which took into account the factors included in the MCM models, i.e. rainfall data, land use, surface retention of catchment, characterstics of sewer network, as well as layout of sewers. The advantages of the proposed model include the possibility of estimating the specific flood volume even with a limited range of input data, which is the case at the stage of spatial planning of urban areas, architectural concepts in which the impact layout of the sewer network on operating conditions can be designed or modernized.

5.2. Sensitivity analysis (rainfall data)

In the present study, it was shown that an increase in rainfall duration leads to an increase in the effect of SWMM model parameters on flood volume. These findings were confirmed by Fraga et al. (2016), who performed GSA computations for rainfall events t_r = 10—140 min, P_t = 4.6 – 20.6 mm showing differences in Sobol indices for independent rainfall events. However, they made no attempt to explain these differences. The influence of rainfall on sensitivity results was also presented by Freni and Oliveri (2005), who, for the Montagena catchment (Italy), showed that an increase in return period leads to a decrease in sensitivity coefficients. The above relationships were also demonstrated by Szeląg et al. (2022), who developed a model to identify modernization of sewer network based on the degree of flooding and specific flood volume.

Rainfall duration was found to influence the sensitivity coefficients for SWMM parameters, which was also confirmed in the studies of Fatone et al. (2021). They demonstrated that increasing the rainfall intensity leads to lower sensitivity coefficients for the maximum flow. The highest sensitivity coefficients were obtained for the temporal distribution of R3 rainfall (cumulative rainfall for 0.5·t_r equal 0.15), and the lowest values for R1 rainfall (constant rainfall intensity).

5.3. Sensitivity analysis (retention coefficient, fractal dimension)

It was found that increasing the value of the fractal dimension and retention coefficient leads to an increase in the sensitivity coefficients. The relationship between the retention coefficient (Vrd·Vkd^{-1}), the fractal dimension (FD) and the flood volume made it possible to subdivide urban catchments in the criteria for the influence of SWMM parameters on specific flood volume. Using the obtained relationship between specific flood volume and FD and Vrd·Vkd^{-1}, it is possible to support the location of measuring devices in the catchment (reduce their number) and reduce the scope of input data collection for the development of MCM models, thus reducing the cost of performing field surveys. The implementation of the proposed model for optimising the location of flow meters (guided by the variability of the values of the sensitivity coefficients) is simpler than the currently used methods, which require the use of advanced computational algorithms (Guo et al., 2021).

In this study, the influence of catchment characteristics, the topology of the sewage system, on the sensitivity coefficients for SWMM parameters was also demonstrated. Similar relationships were confirmed by the analyses of Cristiano et al. (2019), who performed sensitivity calculations for 5 independent urban catchments in the USA. However, they applied simplified procedure without direct analyses of the impact of catchment and sewer network characteristics on the sensitivity coefficients. Therefore, it has not been possible to identify which factor determines the greatest differences in results of rainfall data.

5.4. Advanced uncertainty analysis

In addition, in our model, we included a function simulator based on a random forest (RF) depending on SWMM parameters. An alternative solution was given by Teweldebrhan et al. (2020), who used RF - random forest, k-NN - k nearest neighbor, MLP - multilayer perceptron to calculate the confidence interval. Proposed approach enhanced compatibility between measurement results with the simulations and at the same time reduces their uncertainty. The proposed methodology, compared to those commonly applied (Shrestha et al., 2009), enabled the analysis of the interactions between the identified SWMM parameters and the optimal selection of their combination for calibration. Determining the parameters to be identified plays an important role from the point of view of selecting the methods for their determination under field conditions, which directly affects the cost of performing the measurements. The likelihood function simulator developed using the random forest method allowed optimal selection of SWMM parameters and a reduction in simulation uncertainty of the specific flood volume. The literature (Yu et al., 2015; Zhang and Li, 2015) shows that a reduction in simulation uncertainty was also obtained using simulators (BT, MLP) for 95% confidence interval calculations.

6. Conclusions

Developing computational tools, under data-limited conditions, for rapid estimation of sewer network operating conditions is crucial for intense rainfall events. This study presents an integrated tool that simulates specific flood volume and improved operating conditions for catchments with different characteristics and analyses the impact of MCM model parameters on sewer flooding using sensitivity and uncertainty analysis. The study validated the logistic regression model as an alternative approach to the SWMM model and the random forest model for interaction analysis and parameter calibration of MCM models. The developed tool can estimate specific flood volume under limited data access and analyze sewer network performance at the step of spatial planning and sewer network layout planning to reduce sewer flooding. The tool can also determine the impact of simplifications of the sewer network layout on specific flood volume simulations and input data to mechanistic models, reducing the cost of measurements and conducting field surveys. The study shows that increasing the fractal dimension and retention coefficient leads to an increase in sensitivity coefficients, which can be taken into account when developing mechanistic models of catchments, calibrating them, and determining the number and location of measuring instruments. The model inclusion of fractal dimension, land use and retention of the sewer network interactions helps optimize and design the sewer layout in urban catchments.

CRediT authorship contribution statement

Bartosz Szeląg: Conceptualization, Methodology, Project administration, Supervision, Visualization, Writing – original draft, Writing – review & editing. **Przemysław Kowal:** Project administration, Supervision, Writing – original draft, Writing – review & editing, Visualization. **Adam Kiczko:** Writing – original draft, Writing – review & editing. **Anita Białek:** Writing – original draft, Writing – review & editing. **Grzegorz Wałek:** Visualization, Writing – original draft. **Dariusz Majerek:** Methodology, Writing – original draft. **Piotr Siwicki:** Writing – review & editing. **Francesco Fatone:** Writing – review & editing. **Grzegorz Boczkaj:** Project administration, Supervision, Writing – original draft, Writing – review & editing.

Declaration of Competing Interest

The authors declare that they have no known competing financial interests or personal relationships that could have appeared to influence the work reported in this paper.

Data availability

No data was used for the research described in the article.

Appendix A. Supplementary data

Supplementary data to this article can be found online at https://doi.org/10.1016/j.jhydrol.2023.129967.

References

Addison-Atkinson, W., Chen, A.S., Memon, F.A., Chang, T.J., 2022. Modelling urban sewer flooding and quantitative microbial risk assessment: a critical review. J. Flood Risk Mangement. 15, e12844.

Amiri, H., Azadi, S., Javadpour, S., Naghavi, A.A., Boczkaj, G., 2022. Selecting wells for an optimal design of groundwater monitoring network based on monitoring priority map: a Kish Island case study. Water Resour. Ind. 27, 100172 https://doi.org/10.1016/j.wri.2022.100172.

Barros, V.G., John Rapaglia, J., Richter, M.B., Andrighi, J.F., 2021. Design process in the urban context - mobility and health in special flood hazard area. Int. J. Disaster Risk Reduct. 59, 102170 https://doi.org/10.1016/j.ijdrr.2021.102170.

Beven, K., Binley, A., 2014. GLUE: 20 years on. Hydrol. Process. 28, 5897–5918. https://doi.org/10.1002/hyp.10082.

Breiman, L., 2001. Mach. Learn. 45, 5–32. https://doi.org/10.1023/A:1010933404324.

Cao, X.J., Lyu, H., Ni, G., Tian, F., Ma, Y., Grimmond, C.S.B., 2020. Spatial scale effect of surface routing and its parameter upscaling for urban flood simulation using a grid-based model. Water Resour. Res. 56 (1–22), 440. https://doi.org/10.1029/2019wr025468.

Chapi, K., Singh, V.P., Shirzadi, A., Shahabi, H., Bui, D.T., Pham, B.T., Khosravi, K., 2017. A novel hybrid artificial intelligence approach for flood susceptibility assessment. Environ. Model. Softw. 95, 229–245. https://doi.org/10.1016/j.envsoft.2017.06.012.

Cristiano, E., ten Veldhuis, M.C., Wright, D.B., Smith, J.A., van de Giesen, N., 2019. The influence of rainfall and catchment critical scales on urban hydrological response sensitivity. Water Resour. Res. 55, 3375–3390. https://doi.org/10.1029/2018WR024143.

De Paola, F., Ranucci, A., 2012. Analysis of spatial variability for stormwater capture tank assessment. Irrig. Drain. 61, 682–690. https://doi.org/10.1002/ird.

, K., Berardi, L., B. Laucelli, D.B., Ulanicki, B. Giustolisi, O. (2022). Topological and hydraulic metrics-based search space reduction for optimal re-sizing of water distribution networks. Journal of Hydroinformatics 24, 610–621. .

Dill, J., Dagios, R.N., Barros, V.G., 2022. Public policies on water resource management and its impacts on the context of climatic changes and alterations in land use and land cover in small and protected rainforest river basins. Environ. Sci. Policy 137, 191–204. https://doi.org/10.1016/j.envsci.2022.08.021.

DWA-A 118E, 2006. Hydraulic Dimensioning and Verification of Drain and Sewer Systems. DWA German Association for Water, Wastewater and Waste, Hennef, Germany.

Efstratiadis, A., Dimas, P., Pouliasis, G., Tsoukalas, I., Kossieris, P., Bellos, V., Sakki, G.K., Makropoulos, C., Michas, S., 2022. Revisiting flood hazard assessment practices under a hybrid stochastic simulation framework. Water 14, 457. https://doi.org/10.3390/w14030457.

Fatone, F., Szeląg, B., Kiczko, A., Majerek, D., Majewska, M., Drewnowski, J., Łagód, G., 2021. Advanced sensitivity analysis of the impact of the temporal distribution and intensity of rainfall on hydrograph parameters in urban catchments. Hydrol. Earth Syst. Sci. 25, 5493–5516. https://doi.org/10.5194/hess-25-5493-2021.

Fisher, A., Rudin, C. and Dominici, F. (2019). All Models are Wrong, but Many are Useful: Learning a Variable's Importance by Studying an Entire Class of Prediction Models Simultaneously. Journal of Machine Learning Research. 20: 177. 10.48550/arXiv.1801.01489.

Fraga, I., Cea, L., Puertas, J., Suárez, J., Jiménez, V., Jácome, A., 2016. Global sensitivity and GLUE-based uncertainty analysis of a 2D–1D dual urban drainage model. J. Hydrol. Eng. 21, 04016004. https://doi.org/10.1061/(ASCE)HE.1943-5584.0001335.

Freni, G., Oliveri, O., 2005. Mitigation of urban flooding: a simplified approach for distributed stormwater management practices selection and planning. Urban Water J. 2, 215–226. https://doi.org/10.1080/15730620500386461.

Fu, G., Butler, D., Khu, S.T. Sun, S. (2011). Imprecise probabilistic evaluation of sewer flooding in urban drainage systems using random set theory, Water Resources Research. 47: 1–13. 10.1029/2009WR008944, 2011.

Ghosh, I.; Hellweger, F.L.; Fritch, T.G. Fractal Generation of Artificial Sewer Networks for Hydrologic Simulation. In Proceedings of the ESRI International User Conference, San Diego, CA, USA, 7–11 August 2006.

Gires, A., Tchiguirinskaia, I., Schertzer, D., Ochoa-Rodriguez, S., Willems, P., Ichiba, A., Wang, L.-P., Pina, R., Van Assel, J., Bruni, G., Murla Tuyls, D., ten Veldhuis, M.C., 2017. Fractal analysis of urban catchments and their representation in semi-distributed models: imperviousness and sewer system. Hydrol. Earth Syst. Sci. 21, 2361–2375. https://doi.org/10.5194/hess-21-2361-2017.

Guo, K., Guan, M., Yu, D., 2021. Urban surface water flood modelling – a comprehensive review of current models and future challenges. Hydrol. Earth Syst. Sci. 25 (2843–2860), 2021. https://doi.org/10.5194/hess-25-2843-2021.

Ichiba, A., Gires, A., Tchiguirinskaia, I., Schertzer, D., Bompard, P., Ten Veldhuis, M.C., 2018. Scale effect challenges in urban hydrology highlighted with a distributed

hydrological model. Hydrol. Earth Syst. Sci. 22, 331–350. https://doi.org/10.5194/hess-22-331-2018.
Jato-Espino, D., Sillanpää, N., Andrés-Doménech, I., Rodriguez-Hernandez, J., 2018. Flood risk assessment in urban catchments using multiple regression analysis. J. Water Resour. Planning Manag. 144, 04017085. https://doi.org/10.1061/(ASCE)WR.1943-5452.0000874.
Ke, Q., Tian, X., Bricker, J., Tian, Z., Guan, G., Cai, H., Huang, X., Yang, H., Liu, J., 2022. Urban pluvial flooding prediction by machine learning approaches – a case study of Shenzhen city, China. Adv. Water Resour. 145, 103719 https://doi.org/10.1016/j.advwatres.2020.103719.
La Barbera, P., Rosso, R., 1989. On the fractal dimension of stream networks. Water Resour. Res. 25, 735–741. https://doi.org/10.1029/WR025i004p00735.
Li, X., Willems, P., 2020. A hybrid model for fast and probabilistic urban pluvial flood prediction. Water Resour. Res. 56 https://doi.org/10.1029/2019WR025128.
Li, X., Erpicum, S., Mignot, E., Archambeau, P., Pirotton, M., Dewals, B., 2022. Laboratory modelling of urban flooding. Sci. Data 9 (1). https://doi.org/10.1038/s41597-022-01282-w.
Louppe, G. (2015). Understanding Random Forests: From Theory to Practice (arXiv: 1407.7502). arXiv. 10.48550/arXiv.1407.7502.
Lu, Y., Xu, H., Wang, Y., Yang, Y., 2017. Evaluation of water environmental carrying capacity of city in Huaihe River Basin based on the AHP method: A case in Huai'an City. Water Resour. Ind. 18, 71–77. https://doi.org/10.1016/j.wri.2017.10.001.
Luo, P., Luo, M., Li, F., Qi, X., Huo, A., Wang, Z., He, B., Takara, K., Nover, D., Wang, Y., 2022. Urban flood numerical simulation: Research, methods and future perspectives. Environ. Model. Softw. 156, 105478 https://doi.org/10.1016/j.envsoft.2022.105478.
Ma, B., Wu, Z., Hu, C., Wang, H., Xu, H., Yan, D., Soomro, S., 2022. Process-oriented SWMM real-time correction and urban flood dynamic simulation. J. Hydrol. 605, 127269 https://doi.org/10.1016/j.jhydrol.2021.127269.
Martins, R., Rubinato, M., Kesserwani, G., Leandro, J., Djordjevic, S., Shucksmith, J., 2017. Validation of 2D shock capturing flood models around a surcharging manhole. Urban Water J. 14, 892–899. https://doi.org/10.1080/1573062X.2017.1279193.
Mediero, L., Soriano, E., Oria, P., Bagli, S., Castellarin, A., Garrote, L., Mazzoli, P., Mysiak, J., Pasetti, S., Persiano, S., Santillán, D., Schröter, K., 2022. Pluvial flooding: High-resolution stochastic hazard mapping in urban areas by using fast-processing DEM-based algorithms. J. Hydrol. 608, 12764. https://doi.org/10.1016/j.jhydrol.2022.127649.
Mehedi, A., Virginia Smith, V., Hossein Hosseiny, H., Jiao, X., 2022. Unraveling the complexities of urban fuvial food hydraulics through AI. Sci. Rep. 12, 18738. https://doi.org/10.1038/s41598-022-23214-9.
Morán-Valencia, M., Flegl, M., Güemes-Castorena, D., 2023. A state-level analysis of the water system management efficiency in Mexico: two-stage DEA approach. Water Resour. Ind. 29, 100200 https://doi.org/10.1016/j.wri.2022.100200.
Nikolopoulos, D., Kossieris, P., Tsoukalas, I., Makropoulos, C., 2022. Stress-testing framework for urban water systems: a source to tap approach for stochastic resilience assessment. Water 14, 154. https://doi.org/10.3390/w14020154.
Ogden, F.L., Pradhan, N.R., Downer, C.W., Zahner, J.A., 2011. Relative importance of impervious area, drainage density, width function, and subsurface storm drainage on flood runoff from an urbanized catchment. Water Resour. Res. 47, W12503. https://doi.org/10.1029/2011WR010550.
Perdikaki, M., Makropoulos, C., Kallioras, A., 2022. Participatory groundwater modeling for managed aquifer recharge as a tool for water resources management of a coastal aquifer in Greece. Hydrgeol. J. 30 (1), 37–58.
Romanowicz, R.J., Beven, K.J., 2006. Comments on generalised likelihood uncertainty estimation. Reliab. Eng. Syst. Saf. 91, 1315–1321. https://doi.org/10.1016/j.ress.2005.11.030.
Schackow, A., Effting, C., Barros, V.G., Gomes, I.R., da Costa Neto, V.S., Delandréa, M.S., 2020. Permeable concrete plates with wastes from the paper industry: reduction of surface flow and possible applications. Constr. Build. Mater. 250, 118896.
Seis, W., Zamzow, M., Caradot, N., Rouault, P., 2018. On the implementation of reliable early warning systems at European bathing waters using multivariate Bayesian regression modeling. Water Res. 143, 301–312. https://doi.org/10.1016/j.watres.2018.06.057.
Shrestha, L., Kayastha, N., Solomatine, D.P., 2009. A novel approach to parameter uncertainty analysis of hydrological models using neural networks. Hydrol. Earth Syst. Sci. 13, 1235–1248. https://doi.org/10.5194/hessd-6-1677-2009.
Siekmann, M., Pinnekamp, J. (2011). Indicator based strategy to adapt urban drainage systems in regard to the consequences caused by climate change. In: 12th International Conference on Urban Drainage. 11–16, 2011.
Szeląg, B., 2013. Influence of the Hydrogramme Shape on the Capacity and Selection of Drains of a Small Retention Reservoir. University of Technology, Kielce. PhD thesis.
Szeląg, B., Majerek, D., Kiczko, A., Łagód, G., Fatone, F., McGarity, A. (2022b). Analysis of sewer network performance in context of modernization: modeling, sensitivity, uncertainty analysis. Journal of Water Resources Planning and Management. 148: 1 – 12. http.//doi.org/10.1061/(ASCE)WR.1943 – 5452.0001610.
Szeląg, B., Suligowski, R., De Paola, F., Siwicki, P., Majerek, D., Łagód, G., 2022a. Influence of urban catchment characteristics and rainfall origins on the phenomenon of stormwater flooding: case study. Environ. Model. Softw. 150, 105335 https://doi.org/10.1016/j.envsoft.2022.105335.
Teweldebrhan, T., Schuler, T.V., Burkhart, J.F., Hjorth-Jensen, M., 2020. Coupled machine learning and the limits of acceptability approach applied in parameter identification for a distributed hydrological model. Hydrol. Earth Syst. Sci. 24, 4641–4658. https://doi.org/10.5194/hess-24-4641-2020.
Thorndahl, S., Willems, P., 2008. Probabilistic modelling of overflow, surcharge and flooding in urban drainage using the first-order reliability method and parameterization of local rain series. Water Res. 42, 455–466. https://doi.org/10.1016/j.watres.2007.07.038.
Tsoukalas, I., Kossieris, P., Makropoulos, C., 2020. Simulation of non-gaussian correlated random variables, stochastic processes and random fields: introducing the anySim R-package for environmental applications and beyond. Water 12, 1645. https://doi.org/10.3390/w12061645.
Ukkonen, P., Mäkelä, A., 2019. Evaluation of machine learning classifiers for predicting deep convection. J. Adv. Model. Earth Syst. 11, 1784–1802. https://doi.org/10.1029/2018MS001561.
Wałek, G. (2019). Wpływ dróg na kształtowanie spływu powierzchniowego w obszarze zurbanizowanym na przykładzie zlewni rzeki Silnicy w Kielcach. Jan Kochanowski University Press, Kielce (in Polish), 2019.
Yan, J., Jin, J., Chen, F., Yu, G., Yin, H., Wang, W., 2018. Urban flash flood forecast using support vector machine and numerical simulation. J. Hydroinf. 20, 221–231. https://doi.org/10.2166/hydro.2017.175.
Yu, J.J., Qin, X.S., Larsen, O., O., 2015. Applying ANN emulators in uncertainty assessment of flood inundation modelling: a comparison of two surrogate schemes. Hydrol. Sci. J. 60, 2117–2131. https://doi.org/10.1080/02626667.2014.943232.
Zhang, W., Li, T., 2015. The influence of objective function and acceptability threshold on uncertainty assessment of an urban drainage hydraulic model with generalized likelihood uncertainty estimation methodology. Water Resour. Manag. 29, 2059–2072. https://doi.org/10.1007/s11269-015-0928-8.
Zhou, Y., Shen, D., Huang, N., Guo, Y., Zhang, T., Zhang, Y., 2019. Urban flood risk assessment using storm characteristic parameters sensitive to catchment-specific drainage system. Sci. Total Environ. 659, 1362–1369. https://doi.org/10.1016/j.scitotenv.2019.01.004.

Archives of Environmental Protection
Vol. 51 no. 3 pp. 54–73

PL ISSN 2083-4772
DOI:10.24425/aep.2025.156009

An innovative method of predicting the maximum flow in stormwater sewage systems using soft-sensors

Krzysztof Barbusiński[1], Bartosz Szeląg[2], Anita Białek[2]*, Marek Kalenik[3], Tomáš Bakalár[4]

[1]Department of Water and Wastewater Engineering, Silesian University of Technology, Gliwice, Poland
[2]Faculty of Environmental Engineering, Geomatics and Renewable Energy, Kielce University of Technology, Poland
[3]Institute of Environmental Engineering, Warsaw University of Life Sciences-SGGW, Poland
[4]Institute of Earth Resources, Faculty of Mining, Ecology, Process Control and Geotechnologies, Technical University of Košice, Slovak Republic

*Corresponding author's e-mail: anita_bialek@interia.eu

Keywords: Model uncertainty, soft sensors, maximum flow prediction, machine learning - ML, energy consumption optimization, MARS model

Abstract: Developing universal hydrological models for modeling urban catchments remains one of the major challenges in contemporary hydrology. This study aimed to create a model that integrates catchment characteristics, sewer network topology, sewer storage capacity, and rainfall data, along with a sensitivity analysis of input parameters. The goal was to evaluate the potential of advanced analytical methods, specifically, Multivariate Adaptive Regression Splines (MARS) and soft-sensor technology, to improve peak flow (Q_m) forecasting in stormwater systems. The results showed that combining MARS models with soft sensors yields high forecasting accuracy (R^2 = 0.96, RMSE = 0.038), even under variable rainfall conditions. However, the development of universally applicable model relationships proved challenging due to difficulties in parameterizing the model under changing rainfall scenarios. Additionally, the inclusion of a risk analysis method also enabled consideration of sewer network capacity and introduced a safety margin coefficient to assess system flexibility under future climate conditions. While the proposed approach does not lead to the creation of universal tools, it offers valuable insights for further research on adapting sewer systems to evolving hydrological conditions. The findings suggest promising directions for the development of cost-free, zero-emission soft sensors and models adaptable across diverse urban catchments.

Introduction

Peak flow (Q_m) is an important criterion used as the basis for selecting pipe diameters. To determine Q_m, Monte Carlo Method (MCM) models were commonly used. However, these models make it difficult to identify the factors such as catchment characteristics, topology, network layout, and storage on maximum flow in non-homogeneous catchments. This knowledge is crucial for decision-making regarding the modernization and reconstruction of sewer networks, especially in the context of climate change, urbanization, and sediment deposition in pipes.

Developing an MCM model is a complex task that requires collecting detailed data on land use, sewer network geometry (pipes, manholes), topology, and rainfall - runoff measurements. This involves the installation of stations to monitor flow rates and rainfall (Cristiano et al. 2019). The data collected enables calibration of MCM models (Guo et al. 2021, Fraga et al. 2016). However, these models tend to be over-parameterized, which complicates the identification of coefficients related to depression storage, sewer storage, and similar parameters. In urban catchments, it is particularly important to select an appropriate flow measurement method, choose suitable locations of the measurement point and define the measurement period. These factors influence the operational costs of measurement equipment, in particular, energy consumption, which affects measurement efficiency and accuracy.

Literature data (Bach et al. 2020, De Paola and Ranucci 2012) show that selecting an appropriate flow measurement method and optimizing sensor placement are key to effective stormwater system management (Tabuchi et al. 2020, Zhang et al. 2021). Techniques used to determine flow variation in sewer networks include pressure, acoustic, ultrasonic, electromagnetic, and optical methods (Shi et al. 2021, Luiso et al. 2017, Wong and Kerez 2016). These methods offer high measurement accuracy, provided that device placement complies with manufacturer requirements (Kumar et al. 2021, Wu et al. 2023, Moon et al. 2023). The choice of measurement technique should be based on a detailed analysis

Table 1. Advantages and disadvantages of flow measurement methods in stormwater sewage systems

Measurement Method	Advantages	Disadvantages	Flow Rate	Flow Velocity (v)	Location	Cost and Energy Reduction	Impact of Specific Conditions
Ultrasonic Sensors	- High accuracy (±1-2%) - Non-contact method, minimal interference - Real-time monitoring	- Sensitive to temperature changes and contamination - High purchase and installation costs	Effective across a wide range (0.1 to 10 m^3/s)	Velocities from 0.1 to 5 m/s	Small catchment areas	High initial costs, but long-term savings; low energy consumption	Sensitive to contamination, which may affect accuracy and maintenance costs
Electromagnetic Sensors	- Can measure over a wide range of flows - No moving parts, minimizing breakdowns - Rapid response to flow changes	- Requires calibration - Installation and maintenance costs	High accuracy at high flow rates (up to 25 m^3/s)	Velocities from 0.5 to 10 m/s	Small and large catchment areas	High initial costs, but long-term savings due to low maintenance	Requires adaptation to environmental conditions and sediment, which may affect efficiency
Hydraulic Measurements	- Simple installation, low cost - Low failure rate, easy to maintain - Effective in mountainous areas	- Low accuracy in low flow conditions - Sensitive to water level changes	Suitable for low and medium flows (up to 5 m^3/s)	Velocities from 0.1 to 3 m/s	Good for monitoring small catchments	Low cost, but limited energy-saving potential due to passive measurements	Sensitive to water level changes and sediment, which may affect accuracy and efficiency
Monitoring Cameras	- Allows analysis of water quality and flow - Can detect blockages and irregularities - Provides visual data	- High purchase and maintenance costs - Image quality affected by weather conditions	Effective in various flow conditions	Flow velocity estimation based on video analysis	Small catchment areas	Operational costs can be high, but provide valuable analytical data	Dependent on lighting conditions and contamination, which may limit effectiveness
Pressure Sensors	- Low purchase and installation costs - Enables measurement at various locations - Simple calibration	- Sensitive to contamination and sediment - Limited accuracy in low flow rates	Works well in low flow conditions	Velocities depend on the model and may be hard to determine	Small catchment areas	Low costs, but frequent maintenance and cleaning needed to avoid measurement errors	Frequent maintenance due to sediment can impact long-term costs
Doppler Sensors	- High accuracy in velocity measurements - Suitable for challenging conditions, including polluted waters - Real-time monitoring	- High purchase cost - Requires calibration and adaptation to specific local conditions	High accuracy across various flow rates	Velocities from 0.1 to 6 m/s	Small catchment areas	High initial costs, but can bring long-term savings	Requires adaptation to local conditions, which may increase installation and maintenance costs
Optical Sensors	- Ability to detect contamination and water properties - Rapid response to water state changes - Non-contact measurement method	- Sensitive to light changes and contamination - Purchase and maintenance costs may be high	Effective in diverse flow conditions	Velocities from 0.1 to 4 m/s	For small, polluted catchment areas	Initial costs may be moderate, but maintenance is needed to maintain accuracy	Variable lighting conditions may impact measurements; contamination may limit effectiveness
Acoustic Measurement	- Can measure in challenging conditions, e.g., polluted waters - Low system interference - Can detect blockages	- Highly sensitive to ambient noise - Requires calibration and regular maintenance	Effective for low and medium flows	Velocities from 0.1 to 5 m/s	Small and medium catchments	Low operational costs after initial investment	Impact on accuracy due to contamination and ambient noise

of the catchment's specific conditions, such as its size, land use variability, sewer network topology, and the directions of rainfall movement (Guo et.al. 2021, Rosenzweig et al. 2021). This analysis should be supplemented by an economic evaluation that includes installation and operational costs (Addison-Atkinson et al. 2022, Amiri et al. 2022). Ultrasonic, electromagnetic, and Doppler sensors generally have high initial operating costs. However, this is compensated for by the high measurement accuracy and the potential reduction in operating costs over time. Conversely, optical sensors and cameras may incur higher operating costs but provide valuable data for forecasting wastewater quality, which can ultimately reduce the costs associated with the installation and operation of measurement systems (Gong et al. 2022).

A detailed discussion of the advantages and disadvantages of the currently used flow measurement techniques, considering factors such as catchment size, wastewater quality, site specific conditions, cost, and energy efficiency, is given in Table 1.

Due to the challenges associated with developing mechanistic models and the high costs of direct flow measurements, machine learning (ML) approaches have gained increasing attention (Perdikaki et al., 2022, Morán-Valencia et al., 2023). ML techniques enable the prediction of peak flows based on input–output relationships (Szeląg et al., 2022b), however, many models lack mechanisms to quantify the influence of input variables. Applications to date include sewer flooding prediction (Szeląg et al., 2022a) and hydrograph forecasting (Yang and Chui, 2020, Palmitessa et al., 2022), typically using rainfall and land use characteristics as predictors (Duan et al., 2020). Analytical ML models, particularly those based on modified multivariate regression (e.g., incorporating threshold or smoothing functions), offer a means to evaluate input significance without requiring additional computations (Bhaskar et al., 2018), although their application to peak flow prediction remains limited (Li et al., 2022).

Risk analysis has become integral to assessing sewer system performance under uncertainties associated with climate change and catchment dynamics (Yao et al., 2023). Commonly evaluated metrics include maximum flow rates, flooding volumes, and manhole surcharge occurrences (Mondal et al., 2023). While recent studies have addressed the impacts of rainfall variability over extended periods (Beven, 2020, Napiorkowski et al., 2023), model calibration uncertainties are often overlooked. Accounting for increased runoff resulting from changes in climate and land use is critical for ensuring system resilience (Guan et al., 2015). To address these challenges, Willems et al. (2013) employed conceptual models such as CGM, SGT, and MCM to simulate rainfall impacts and inform system upgrade strategies, while Hauger et al. (2006) proposed a safety-factor-based risk approach to simplify catchment interactions. Adjustments to intensity–duration–frequency (IDF) curves have also been advocated to account for evolving rainfall extremes (Birgani et al., 2013).

Nevertheless, ML models for sewer flow prediction frequently remain oversimplified, often neglecting storm variability, storage processes, and network topology. In risk-based designs (Addison-Atkinson et al., 2022, Amiri et al., 2022), the omission of calibration uncertainties, such as storage capacity variations and roughness coefficients, can lead to underestimation of system vulnerabilities.

A methodology is presented for developing a model to forecast maximum flow based on rainfall data, land use, catchment storage, sewer network topology, and their spatial arrangement within the catchment using machine learning techniques. For this purpose, the MARS (Multivariate Adaptive Regression Spline) model was used. This model provides an analytical relationship that simplifies the identification interactions among the above-mentioned factors and enables straightforward evaluation of input-output relationships without the need for additional calculations. The resulting ML model

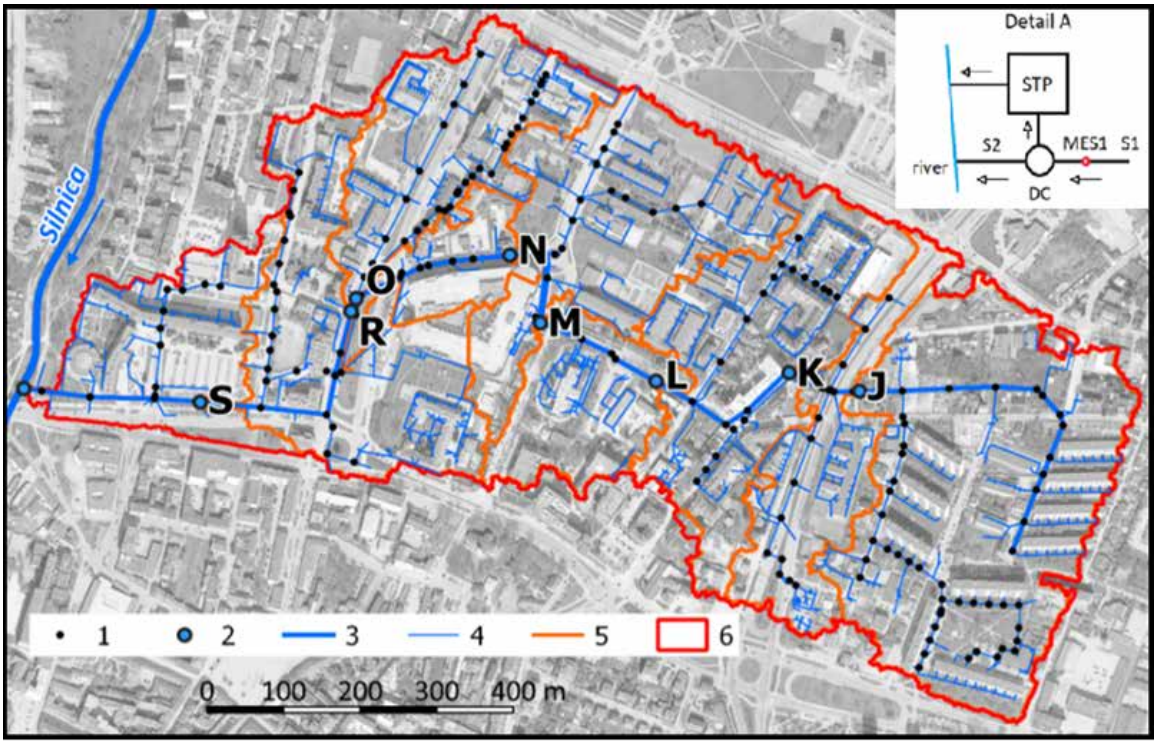

Figure 1. Diagram of analyzed urban catchment in Kielce

can serve as a cost-free soft sensor for predicting maximum flow in stormwater drainage networks. Additionally, a risk analysis was conducted, addressing the issue of catchment modernization in the context of maximum flow reduction under conditions of uncertainty in field and sewer storage.

Methods and data

Study area

The urban catchment area under consideration is located in Kielce, Poland - the capital of the Świętokrzyskie region. It is located in the southeastern part of the city (city center) and includes residential neighborhoods, public buildings, main and secondary streets (Fig.1).

The catchment area covers 63 ha, 40% of which is impervious. Spatial analyses per-formed using GIS tools showed that road density in the area is 108 m·ha-1 (Kiczko et al. 2018). The elevation difference between the highest (271.2 m above sea level) and lowest (260.0 m above sea level) points in the catchment is 11.2 m. The main sewer is 1,569 m long, with diameters ranging from 600 to 1,250 mm. Side sewer diameters range from 300 -to 1,000 mm, and sewer slopes vary from 0.04% to 3.90 %. The sewer system is a separation system. Stormwater from the catchment area flows through a collector to a diversion chamber (DC), from which, at a depth of less than 0.42 m, it flows to the stormwater treatment plant (STP) and then discharges into the Silnica River. During heavy rainfall, when the depth of the separation chamber (DC) exceeds the ordinate of the overflow threshold (OV), excess rainwater is discharged into the discharge canal (S2), which also drains into the Silnica River.

At the outflow from the catchment, an MES1 flow meter was installed 3.0 meters from the inlet of the collector (S1) to the diversion chamber (DC). This device records flow values at 1-minute intervals during heavy rainfall events. Analysis of the MES1 data collected between 2010 and 2020 showed that, during dry period, flows ranging from 1 to 9 $dm^3 \cdot s^{-1}$ were recorded, indicating the presence of infiltration. A rainfall station is located 2.5 km from the catchment boundary, where continuous rainfall measurements have been carried out since 2008, also with a resolution of 1 minute.

Delineation of sub-catchments and characteristics

In the analyzed catchment, 7 sub-catchments (J, K, L, N, M, R, and S) were separated (Fig. 1). This division was based, on one hand, on the alignment of the main collector and, on the other hand, on the need to account for variations in catchment characteristics, the sewer network, and its layout for the purpose of developing a maximum flow simulation model. The boundaries of the sub-catchments were established using spatial data, including land use analyses and sewer network layout (Szeląg et al.2013). These analyses were confirmed by Walek (2019), who separated sewer sub-basins, including side-sewer sub-basins, within the Silnica River catchment. He also estimated the variability of peak flows and their durations using a simplified approach based on the HEC - HMS model, which considered only land use. Based on these considerations, the study catchment was subdivided along the main sewer (Figure 1). The selection of model input characteristics was supported by a literature review (Szeląg et al., 2016), which examined the characteristics of the catchment and the sewer network parameters commonly used in models simulating stormwater system performance (e.g., maximum flow, flooding volume, manhole overflow). Table 2 presents detailed characteristics of land development and the sewer network for each of the separated sub-catchments.

Methodology

An algorithm was developed to created models for analyzing the influence of spatial catchment characteristics, sewer network topology and its layout (using the fractal dimension), and runoff-related parameters on peak flow in response to rainfall (Figure 2). The parameters considered include storage depth, the Manning roughness coefficient for impervious areas, a correction factor for mean slope and impervious area, runoff path width, and the Manning roughness coefficient for sewers.

Machine learning, specifically, the MARS model, was used to calculate the peak flow as an alternative to mechanistic models such as SWMM (Storm Water Management Model). The analytical form of the MARS model allows for the analysis

Table 2. Characteristics of the delineated sub-catchments

No.	F	Imp	Vk	Gk	R.t.	Vkp	Jkp	Impd	Gkd	Vrd·Vkd^{-1}	FD
	ha	-	m^3	$m \cdot ha^{-1}$	m	m^3	-	-	$m \cdot ha^{-1}$	-	-
min	12.66	0.35	157	0.0079	1.74	16.1	0.0036	0.40	0.0011	0.17	0.94
max	55.41	0.44	1240	0.0092	8.47	67.5	0.0102	0.55	0.0063	0.84	1.14

where: F - area of the catchment area; Imp - impervious of the catchment area; Vk - volume of the collector; Gk - length of the collector per impervious area in the catchment area; R.t. - difference in ordinates of thesewer; Vkp - volume of the sewer preceding the catchment closure section; dHp - difference in ordinates to the catchment closure section; Jkp - slope of the bottom of the sewer preceding the catchment closure section; Hst - depth of the manhole in the closure section; Imp - impervious of the catchment area below the closure section; Gkd - length of the collector per impervious area below the closing cross-section; Vrd - storage of the catchment area above the closing cross-section defined as Vrd = F - (Imp - d_{imp} + (1 - Imp) - d_{per}), Vkd - volume of the sewer network in the lower stream, FD - fractal dimension (calculations according to Section - Calculation of fractal dimensions).

of the influence and interaction between selected variables within their range of variability. The proposed model also supports risk analysis (Butler et al. 2014, Ursino et al. 2015), enabling the evaluation of sewer system performance under uncertainty (storage of catchment, sewerage network, rainfall due to climate change). This approach facilitates improvements in system operation by incorporating the probabilistic nature of SWMM model parameters.

Calculation of fractal dimensions

To estimate the fractal dimension, the box method was used. In this approach, the image (in this study, the route of the sewer network – Fig. A1), was placed on a grid of square boxes, each with side lengths of τ. The number of boxes $N(\tau)$ covering the image (i.e., the canal network) was then counted. This number depends on the size of the grid elements and decreases as τ is reduced in subsequent iterations. The box dimension was calculated by analyzing how $N(\tau)$ varies with τ. For complex sewer grids, the number of elements in successive iterations is not constant and the box dimension was defined as the boundary value where the length of the side of the box (τ) in the grid tends to zero. For the assumed number of boxes $N(\tau)$ with side length τ covering the image (the sewer network in the separated sub-catchment), the box dimension was calculated from the formula:

$$FD = lim_{\tau \to 0} \frac{log(N(\tau))}{log\left(\frac{1}{\tau}\right)} \quad (1)$$

Practically, the box dimension is determined by analyzing the relationship $\log(N(\tau) = f(\log(\tau\text{-}1))$, which is then approximated using a linear function. Based on the sewer network (Fig. A1) and the time distributions of rainfall events (Fig. A2), the fractal dimensions were calculated.

Mechanistic model

The mechanistic model of the catchment includes 92 sub-catchments, with areas ranging from 0.12 to 2.10 ha and imperviousness varying between 5 and 95%. The model includes 82 manholes and 72 pipes. The storage depths for impervious (D_{imp}) and pervious (D_{per}) areas were set to 2.50 mm and 6.00 mm, respectively. Manning's roughness coefficients were $n_{imp} = 0.025\ m^{-1/3} \cdot s$ for impervious areas and $n_{per} = 0.10\ m^{-1/3} \cdot s$ for pervious (n_{per}) areas, as determined during the model calibration step (Szeląg et al. 2016). The width of the runoff path (W) was calculated as $W = \theta \cdot A^{0.50}$, where θ is the flow path correction coefficient and A is the catchment area. The highest agreement between calculation and measurements was obtained for $\theta = 1.35$. Model calibration using 6 rainfall-runoff events resulted in a Nash - Sutcliff efficiency coefficient ranging from 0.85 to 0.98, and a coefficient of determination between 0.85 and 0.99. The differences in hydrograph volumes and peak flows did not exceed 5% compared to measurements, confirming a high level of agreement between calculated and measured values (Szeląg et al. 2016).

Calculation of uncertainty by GLUE method (Generalized Likelihood Uncertainty Estimation)

In the present analyses, for the assumed uniform distributions of SWMM parameters (correction coefficient of impervious area, correction coefficient of flow path, Manning co-efficient of impervious and pervious area, Manning coefficient of sewer storage, storage depth of impervious and pervious area) (Tab. A1) and measured rainfall - runoff events (calibration: 24th July 2011 and 15th September; validation: 30th May 2010 and 30th July 2010), a posteriori distributions of SWMM parameters, 95% confidence interval, and likelihood function values were calculated. For the calibration data (30th May

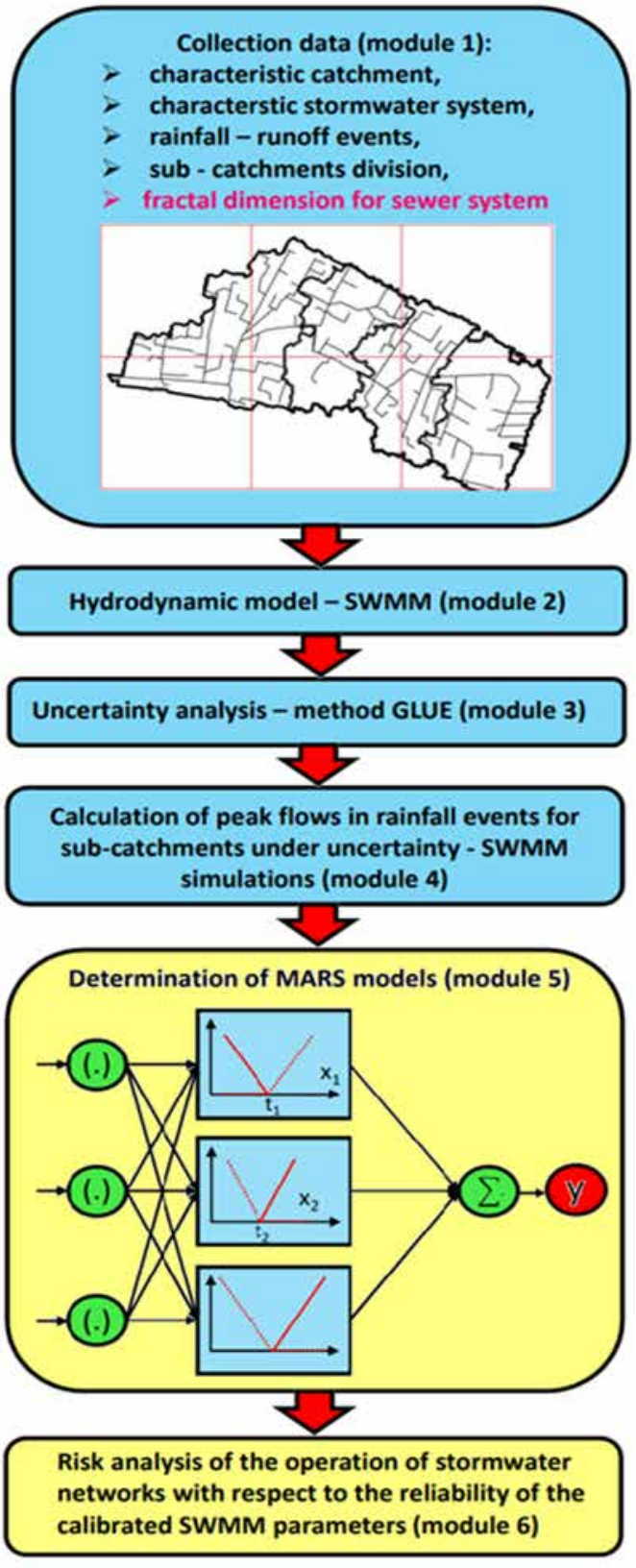

Figure 2. Scheme for the development of model to calculate peak flows in a sewer network and risk analysis

2010 and 8th July 2011), up to 96% of the measurement data were found to be within the calculated confidence intervals. For the validation set (15th September 2010), 90% of the observations were within the confidence interval, while for the event on 30th of July 2010, 70% of the observations covered the determined 95% confidence interval. A detailed discussion of the computational methodology used in the uncertainty analysis is provided in Szeląg et al. (2022 a).

Simulations of sewer network operation

Using the developed hydrodynamic model of the catchment, peak flow calculations were performed at the cross-sections closing sub-catchments J, L, N, R, and S under uncertainty associated with the calibrated SWMM parameters (the correction coefficient percentage area, storage depth of impervious and pervious areas, Manning coefficient for impervious and pervious areas, the correction coefficient for slope, and the Manning coefficient for sewer storage). Using the posteriori distributions of the SWMM parameters, peak flow simulations were performed for assumed rainfall data at the sub-catchment closure cross sections. The following rainfall events were assumed for the analyses: t_r = 30 min (P_t = 6.0 mm and 8.0 mm) and tr = 60 min (P_t = 6.0 mm) for temporal rainfall distribution types R2, R3, R4 (according to DWA A – 118, 2006). These data describe different rainfall loads on the sewer network (potential consequences of climate change) for the catchment in Kielce, and help to explain runoff variability and the occurrence of various flow conditions in the sewers (Szeląg et al. 2016). Rainfall with t_r = 60 min generates gravity flow conditions throughout the sewer network. In contrast, for tr = 30 min and Pt = 6.0 mm, storm overflow (OV) discharge occurs, and for P_t = 8.0 mm, pressure flows and hydraulic backflows are observed in the sewer system (Szeląg et al. 2016).

Development of MARS model

In the present analyses, the MARS method was used to describe the peak flow in the sewers closing the separated sub-catchments. The model can be expressed in general form as:

$$\boldsymbol{Q_m^* = \alpha_0 + \sum_{j=1}^{T} \cdot h(x_j^*, t_j^*)} \tag{2}$$

where: α_0, α_j are empirical coefficients estimated by recursive partitioning of the feature space (Friedman and Roosen 1995); T is the number of basis functions h(x_j*, t_j*), assuming that a linear basis function is described by the equation:

$$\boldsymbol{h(x_j^*, t_j^*) = \begin{cases} \alpha_j \cdot (x_j^* - t_j) \; for \; x_j^* > t_j^* \\ 0 \; for \; x_j^* \le t_j^* \end{cases}} \tag{3}$$

where: t_j* are threshold values for the T basis functions (Fig. A3); x_i*, Q*$_m$ denote the standardized independent variables (e.g., rainfall data, catchment characteristics, sewer network, fractal dimension, SWMM parameters) and the standardized maximum flow (Q_m).

In equation (3), the basis function takes the form of a linear relationship that incorporates threshold values (t_j). In this context, and drawing on the principles of linear regression and the Standard Regression Coefficient (SRC) sensitivity analysis method, the obtained values of α_j for individual independent variables, in their variation intervals, are interpreted as indicators of model sensitivity (Wang et al., 2019). For two threshold values ($t_1^* < t_2^*$) determined with respect to a single independent variable (x_j^*), the MARS function takes the form $Q^*_m = \alpha_j \text{-} x_j^* + ... + \alpha_0 \; (x_j^* > t_1^*)$ i $y = \alpha_2 \text{-} x_{j^*} + ... + \alpha_0 \; (x_j^* > t_2^*)$. In this case, the combined effect of α in the interval (t_1^*; t_2^*) is equal to $\alpha_1+\alpha_2$. To determine the number of nodes (T), threshold values (t_j^*), and coefficients α_j, the STATISTICA 10 software was used. This program automatically identifies statistically significant independent variables.

Risk analysis including reliability of SWMM parameters

To analyze the performance of the sewer network, the design peak flow was used, taking into account the allowable error in its identification (σ), which is described by the following equation (4):

$$\begin{aligned} \boldsymbol{Q_m^p} &= \boldsymbol{Q_m \cdot (1 \pm \sigma)} \\ \boldsymbol{Q_{m(L)}^p} &= \boldsymbol{Q_m \cdot (1 - \sigma)} \\ \boldsymbol{Q_{m(U)}^p} &= \boldsymbol{Q_m \cdot (1 + \sigma)} \\ \boldsymbol{Q_m^p} &= \boldsymbol{< Q_{m(L)}^p ; Q_{m(U)}^p >} \end{aligned} \tag{4}$$

where: σ represents the allowable uncertainty threshold of the maximum flow Q_m. Values of σ = 0.10, 0.15, and 0.20 were considered in the calculations, and can be interpreted as safety factors that influence the reserve capacity of the designed sewer system, e.g. due to climatic changes in rainfall.

The performance of the drainage system under uncertainty (e.g., variability in temporal rainfall distribution and SWMM model parameters) was assessed based on the probability of occurrence of the peak design flow:

$$\boldsymbol{hp_{Qm}} = \frac{\sum_{i=1}^{k} Z_k}{N} \tag{5}$$

where: Z_k represents the function describing the exceeding of the maximum flow Q^p_m:

$$\boldsymbol{Z_k = \begin{cases} Z_k = 1 \rightarrow Q_{m(U)}^p \ge Q_m(X_R, X_{CTCH}, x_1, x_2, \dots, x_p) \ge Q_{m(L)}^p \\ Z_k = 0 \rightarrow Q_m(X_R, X_{CTCH}, x_1, x_2, \dots, x_{p=P}) \ge Q_{m(U)}^p \\ Z_k = 0 \rightarrow Q_m(X_R, X_{CTCH}, x_1, x_2, \dots, x_{p=P}) \le Q_{m(L)}^p \end{cases}} \tag{6}$$

where: N – number of Monte Carlo (MC) samples; Q_m $(x_1, x_2, x_3, \dots, x_j)$ – value of the peak flow for the sub-catchment for the assumed characteristics of the catchment, the sewer network, and SWMM model parameters; X_R – vector of rainfall data combinations (e.g., rainfall depth, duration, and temporal distribution of the event), X_{CTCH} – vector of combinations of catchment and sewer network characteristics, p = 1, 2, 3, …, P.

The risk analysis proposed in the present study included the following computational steps:

- identification of a posteriori (GLUE) distributions of SWMM parameters (N = 5000 samples),
- simulation of the maximum flow in separated sub-catchments for rainfall events, taking into account uncertainties (Section A1),
- calculation of the probability of maximum design flow (pQm) from equation (5) in rainfall events with σ = 0.10, 0.15, and 0.20,

- determination of SWMM parameters - n_{imp}, d_{imp}, β, n_{sew} (neglecting the likelihood function) based on the a posteriori distributions:

$$\boldsymbol{f(x_p) = \{x_{p,1}, x_{p,2}, \dots, x_{p,s}\} \rightarrow x_{p,s} = }$$
$$\boldsymbol{= F^{-1}\left(< Q^p_{m(L)}; Q^p_{m(U)} >, X_R, X_{CTCH}, x^*_{p-1}, \dots, x^*_P\right)}$$
$$\boldsymbol{for\ p = 1, 2, 3, .., P}$$
$$\boldsymbol{s = 1, 2, 3 \dots, N < 5000} \quad (7)$$

where: $\boldsymbol{F^{-1}\left(< Q^p_{m(L)}; Q^p_{m(U)} >, X_R, X_{CTCH}, x^*_{p-1}, \dots, x^*_P\right)}$ inverse function $Q_m \pm \sigma \cdot Q_m$ to identify SWMM parameter distributions based on p_{Qm}; s - number of p-values of these SWMM parameters; f() – empirical distributions of p = 1, 2, 3, ..., P - SWMM parameters; x_p,s - s - p-values of this SWMM parameter assuming $Q^p_{m(U)} \geq Q^p_m \geq Q^p_{m(L)}$; x^*_{p-1}, …., x^*_p- p - 1, ..., P values of SWMM parameters obtained from uncertainty calculations (a posteriori distribution). The final result obtained was the vectors [x_p, ..., x^*_{p-1}, x^*_p].

Determination of 0.50 percentiles of SWMM parameters and preparation of the curves: $n_{imp} = f(Q_m \pm \sigma \cdot Q_m)$, $d_{imp} = f(Q_m \pm \sigma \cdot Q_m)$, $\beta = f(Q_m \pm \sigma \cdot Q_m)$, $n_{sew} = f(Q_m \pm \sigma \cdot Q_m)$ for σ = 0.10, 0.15, 0.20

In this study, the distributions of SWMM parameters (n_{imp}, d_{imp}, β, n_{sew}) were determined for two variants. In the first, the likelihood function was neglected, while in the second variant, it was included. For the determined SWMM parameters (x_p) that satisfy the condition described by relation (Section A1, equation 2A), the corresponding value of L(Q/θ) was obtained. On this basis, the 0.50 percentiles of the likelihood function were identified, and the corresponding vectors of SWMM parameters were determined, as follows: [n_{imp}, …., x_P^*], [d_{imp}, …., x_P^*], [β, …, x_P^*] i [n_{sew} …., x_P^*].

Results

Influence of uncertainty on the results of peak flow calculations

Based on the results of runoff simulations in the separated sub-catchments (J, L, N, R, S), considering the uncertainty in SWMM parameters for the assumed rainfall events (t_r = 30, 60 min), the variability of peak flow was assessed using percentiles (25%, 50%, 75%) (Fig. A5). Example simulation results of Q_m for the considered sub-catchments, with t_r = 30 min and P_t = 6.0 mm (rainfall type R2), are presented in Fig. 4. The highest value of Q_m = 0.75 $m^3 \cdot s^{-1}$ (percentile 0.50) was obtained for sub-catchment S, while the lowest was observed in the sub-catchment J, with Q_m = 0. 25 $m^3 \cdot s^{-1}$. The uncertainty in the SWMM parameters was found to have a significant impact on the variability of the peak flow (Q_m), as confirmed by the percentile values (25%, 50%, 75%) for the sub-catchments (Fig. 3).

For the sub-catchment S, the Q_m value varies between 0.48 and 1.82 $m^3 \cdot s^{-1}$, and for the sub-catchment J, it is in the range of 0.09 - 0.49 $m^3 \cdot s^{-1}$.

Development of MARS models for peak flow calculations

Fig. 4 shows the relationship between R, RMSE, and MAPE values for the obtained MARS models; Table A2 gives the results for the learning set (80%) and test set (20%).

The best fit between calculations and analysis was obtained for t_r = 30 min, P_t = 8.0 mm (type R3) obtaining R^2 = 0.96, MAE = 0.021, RMSE = 0.038, while the largest simulation errors Q_m^* occurred for rainfall type R2 (R^2 = 0.92, MAE = 0.034, RMSE = 0.058). Models developed for t_r = 60 min (rainfall types R2, R3, R4) exhibited worse predictive performance (R^2 = 0.90 - 0.92, MAE = 0.027 - 0.031, RMSE = 0. 050 - 0.059) compared to models determined for t_r = 30 min and P_t = 6.0 mm, P_t = 8.0 mm (type R2, R3, R4), which achieved R^2 = 0.92 - 0.96, MAE = 0.021 - 0.034, and RMSE = 0.038 - 0.053.

Identification of the impact of independent variables on maximum flow based on rainfall data

MARS model

Using the results of SWMM calculations in the sub-catchments (J, K, L, N, P, R) including associated uncertainties, MARS models were developed based on the assumed rainfall data (rainfall depth, duration, and temporal distribution of

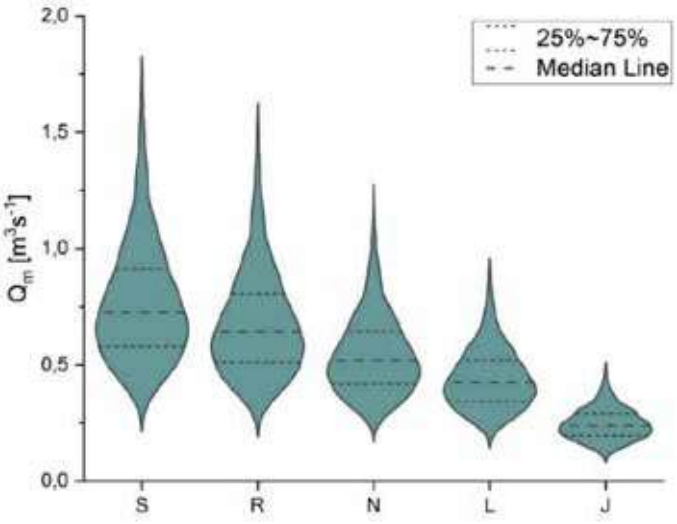

Figure 3. Influence of SWMM parameter uncertainty on peak flow (Qm) in sub-catchments (J, L, N, R, S) for rainfall type R2 and tr = 30 mm and Pt = 6.00 mm

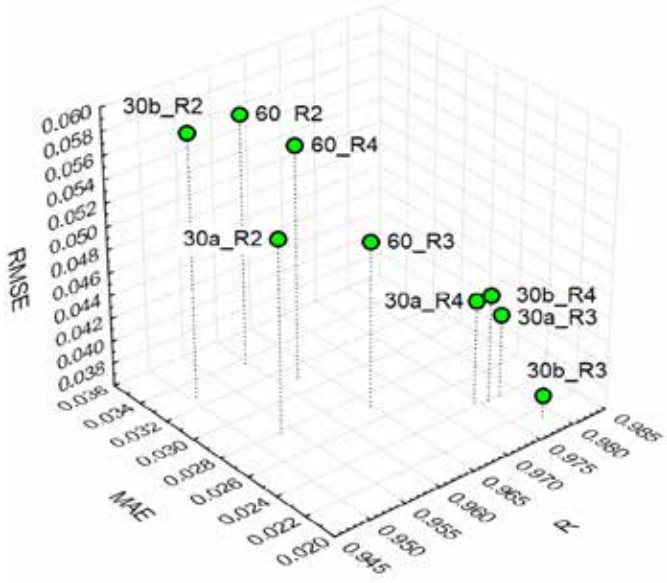

Figure 4. Relationship between RMSE, MAE, R for determined MARS models in relation to assumed rainfall data

rainfall in the event). The calculated threshold values (t) and empirical coefficients (αi) for MARS models are presented in Tables A3, A4 and A5 in Appendix A. An example model for rainfall 30a_R (t_r = 30 min, P_t = 8.0 mm, rainfall type R2) is described by the following equation:

$$Q_m^* = 0.146 + 0.198*\max(0; F_{imp}^*-0.00) - 0.196*\max(0; n_{sew}^*-0.451) + 0.276*\max(0; 0.451-n_{sew}^*) - 0.160*\max(0; d_{imp}^*-0.154) - 0.167*\max(0; 0.154-d_{imp}^*) - 0.01*\max(0; n_{imp}^*-0.329) + 0.173*\max(0; 0.329-n_{imp}^*) + 0.095*\max(0; \alpha-0.38) - 0.151*\max(0; 0.380-\alpha) + 0.07*\max(0; \beta-0.722) - 0.082*\max(0; 0.722-\beta) + 0.07*\max(0; FD-0.00) - 0.024*\max(0; 0.75-\gamma) + 0.071*\max(0; n_{sew}^*-0.225) + 0.068*\max(0; n_{imp}^*-0.863)$$

Across the full range of variation in F_{imp}* and FD* values, a uniform influence of these independent variables on Q_m* is observed. In contrast, for n_{sew}*, n_{imp}*, β*, α*, γ* within the range x_i^* = <0; 1>, their influence on Q_m* varies, as confirmed by the α_i coefficients values (Figure A5). For $n_{sew}^* \leq 0.225$, an increase in n_{sew}* led to an increase in Q_m* of 0.0276 per $0.1 \cdot n_{sew}^*$. For $0.451 > n_{sew}^* > 0.225$, an increase in Q_m* of 0.035 per $0.1 \cdot n_{sew}^*$ takes place. However, when $n_{sew} > 0.451$, a decrease in Q_m* of 0.0196 per $0.1 \cdot n_{sew}$ is observed. Table 3 presents the αi coefficients in the MARS models for the assumed rainfall conditions (type R2, R3, and R4 for scenarios 30a, 30b, 60).

Influence of rainfall data on sensitivity (catchment characteristics, drainage network)

F_{imp}* had the highest influence on Q_m* under the P_t = 6.0 mm, type R3 temporal rainfall distribution, and also for P_t = 8.0 mm type R2 rainfall. In contrast, Vkp exhibited the lowest influence (Table 3). An increase in from P_t = 6.0 mm to P_t = 8.0 mm for type R2 rainfall (e.g., the influence of climate change) led to a greater influence of F_{imp} on Q_m* (Fig. 5a). For rainfall types R3 and R4, the opposite trend was observed. For the same types (R3 and R4), an increase in P_t led to greater sensitivity of Q_m* to changes in FD (Fig. 5b). The highest influence of FD* on Q_m* was observed under type R3 rainfall conditions, while the lowest influence occurred under type R2, regardless of whether P_t was 6.0 mm or 8.0 mm.

Influence of rainfall data on sensitivity (SWMM parameters)

For rainfall types R2, R3, and R4, an increase in P_t from 6.0 mm to 8.0 mm resulted in an increase in the sensitivity of Q_m* by 2.0 - 27.7% for α, β, n_{imp} and by 12.5 - 80.0% for n_{sew}. In contrast, an opposite trend was observed for d_{imp}. Under t_r = 30 min and P_t = 6.0 mm (types R3 and R4), d_{imp} had the greatest influence on Q_m*, while n_{imp} had the least. For t_r = 30 min and P_t = 8.0 mm (types R2 and R4) n_{sew} showed the highest sensitivity of maximum flow to changes, with α_i values ranging from 0.18 to 0.26; under rainfall type R3, d_{imp} remained the dominant influencing factor. For t_r = 60 min and rainfall types R2, R3, and R4, d_{imp} had the highest sensitivity in the Q_m* model.

The impact of precipitation characteristics on estimated coefficients in the MARS model

Table 4 presents the results of correlation coefficient (R_{ij}) calculations between the MARS model coefficients and rainfall characteristics. Very high correlations (R_{ij} = 0.7- 0.9) were shown for Gk and P_t = 5 (R_{ij} = 0.91), α(FD) and $P_{t=10/Pt}$ (R_{ij} = 0.79) and α(α) and $P_{t=5}/P_{t=15}$ (R_{ij} = 0.72). High correlations (R_{ij} = 0.5 - 0.7) was found between $\alpha(F_{imp})$ and $P_{t=5,10}/P_{0.5tr}$, with the highest R value observed for $P_{t=10}/Pt$ (Table 4). Similarly, high correlations were obtained for α(β) and $P_{t=5}/P_{sr}$ (R_{ij} = 0.63), as well as for $\alpha(n_{imp})$ with both $P_{t=5}/P_{sr}$, and $P_{t=10}/P_{sr}$. Based on the above results, the empirical relationships were derived: α(FD) = $f(P_{t=10}/P_t)$ and α(Gk) = $f(P_{t=5})$. Both models yielded R^2 = 0.50, suggesting a nonlinear relationship between the variables (Fig A4).

Probability of maximum design flow – rainfall characteristics – catchment characteristics – SWMM model parameters

Based on sub-catchment flow simulations, the probability of exceeding the maximum design flow (p_{Qm}) was determined for the assumed rainfall data. The simulated maximum flows (Q_m) ranged from 25 to 2000 $L \cdot s^{-1}$, depending on catchment characteristics such as F_{imp} and FD (Figures 5a, 5b). On this basis, empirical cumulative distribution functions (CDFs)

Table 3. The absolute values of the coefficients in the MARS model depending on the distribution of rainfall (* - the table shows the coefficients α_i including the maximum range of variation x_i).

	F_{imp}*	n_{sew}*	d_{imp}*	β*	n_{imp}	α*	γ*	Gk*	FD*	Vkp*
30a_R2	0.20	0.20	0.16	0.09	0.10	0.09	0.02	0.00	0.07	0.00
30a_R3	0.20	0.08	0.20	0.11	0.07	0.11	0.02	0.03	0.17	0.00
30a_R4	0.26	0.10	0.20	0.11	0.07	0.11	0.02	0.00	0.11	0.00
30b_R2	0.43	0.26	0.10	0.10	0.11	0.10	0.02	0.09	0.00	0.01
30b_R3	0.16	0.09	0.12	0.11	0.07	0.11	0.02	0.04	0.18	0.00
30b_R4	0.19	0.18	0.14	0.14	0.07	0.14	0.02	0.03	0.18	0.00
60_R2	0.20	0.22	0.26	0.10	0.09	0.10	0.00	0.03	0.09	0.00
60_R3	0.24	0.01	0.35	0.01	0.06	0.01	0.00	0.00	0.01	0.00
60_R4	0.31	0.01	0.37	0.10	0.01	0.10	0.00	0.00	0.00	0.00

Table 4. Correlation coefficient (Rij) between estimated coefficients in MARS models and rainfall characteristics

	$\alpha(F_{imp})$	α(FD)	α(Gk)	$\alpha(n_{sew})$	$\alpha(d_{imp})$	α(β)	$\alpha(n_{imp})$	α(α)	α(γ)
Pt	0.37	0.48	0.88	0.42	0.00	0.05	0.42	0.63	0.16
q	0.37	0.48	0.88	0.42	0.00	0.05	0.42	0.63	0.16
$P_{t=5}$	0.45	0.59	0.91	0.38	0.08	0.10	0.17	0.63	0.20
FD_r	0.37	0.44	0.73	0.65	0.12	0.40	0.33	0.40	0.25
$P_{t=5}/P_{t=10}$	0.48	0.71	0.71	0.28	0.15	0.38	0.03	0.57	0.07
$P_{t=5}/P_{t=15}$	0.27	0.61	0.52	0.03	0.27	0.18	0.07	0.72	0.10
$P_{t=10}/P_{t=15}$	0.48	0.71	0.71	0.28	0.15	0.38	0.03	0.57	0.07
$P_{t=5}/P_t$	0.40	0.68	0.64	0.30	0.20	0.48	0.00	0.58	0.17
$P_{t=10}/P_t$	0.63	0.79	0.64	0.28	0.15	0.33	0.02	0.42	0.02
$P_{t=15}/P_t$	0.33	0.40	0.80	0.33	0.03	0.29	0.44	0.61	0.14
P_{sr}	0.45	0.71	0.60	0.15	0.08	0.55	0.18	0.52	0.20
$P_{t=5}/P_{sr}$	0.17	0.33	0.01	0.27	0.10	0.63	0.62	0.00	0.50
$P_{t=10}/P_{sr}$	0.03	0.09	0.28	0.40	0.13	0.48	0.62	0.27	0.53
$P_{t=15}/P_{sr}$	0.15	0.06	0.29	0.00	0.08	0.47	0.52	0.50	0.10
$P_{0.5tr}$	0.40	0.37	0.42	0.52	0.02	0.33	0.00	0.03	0.38
$P_{sr}/P_{0.5tr}$	0.43	0.59	0.55	0.18	0.08	0.35	0.28	0.35	0.02
$P_{t=5}/P_{0.5tr}$	0.58	0.69	0.41	0.10	0.10	0.30	0.20	0.18	0.05
$P_{t=10}/P_{0.5tr}$	0.59	0.49	0.50	0.46	0.07	0.19	0.03	0.02	0.14
$P_{t=15}/P_{0.5tr}$	0.27	0.34	0.52	0.49	0.02	0.41	0.02	0.23	0.32

where: FD_r - fractal dimension of the temporal distribution of rainfall in the event; $P_{t=5}$, $P_{t=10}$, $P_{t=15}$ - maximum 5-, 10-, 15-minute rainfall depth in the episode; P_t - rainfall depth in the episode; P_{sr} - average 5-minute rainfall depth in the episode, $P_{0.5\cdot tr}$ - rainfall depth for $t = 0.5 \cdot t_r$.

of SWMM parameters (n_{imp}, β, d_{imp}, n_{sew}), which condition the non-exceedance of Q_m values, were developed. The 50th percentile values were extracted from the CDFs, and curves of $d_{imp} = f(Q_m, F_{imp}, FD)$ were prepared for rainfall scenarios 30a, 30b, 60 of types R2, R3, and R4. Example curves for dimp, identified as the SWMM parameter with the greater influence on Q_m*, are shown in Figures 5c and 5d. The computed values of other SWMM parameters (n_{imp}, β and n_{sew}) are provided in Table A3.

A non-linear relationship between Q_m and the probability of exceeding the design flow (p_{Qm}) was observed (Figs 5a and 5 b). As Q_m increases, the value of p_{Qm} initially rises to a peak and then decreases. A decrease in rainfall depth (P_t) leads to a decrease in p_{Qm}, while an inverse relationship was found for F_{imp}. The highest p_{Qm} values (σ=20%) were obtained for rainfall type R3 ($p_{Qm} = 0.70$), and the lowest for R2 ($p_{Qm} = 0.51$) (Figure 5b). Additionally, increasing the allowable uncertainty threshold in Q_m leads to a reduction of p_{Qm}. For rainfall types R3 and R4, the value of σ has a negligible influence on the maximum flow. However, for rainfall type R2, it leads to a decrease in $Q_m = f(\max\{p_{Qm}\})$ by 4% (from 1270 $L \cdot s^{-1}$ to 1220 $L \cdot s^{-1}$).

The figures (Fig. 5a and Fig. 5b) confirmed the strong interaction between catchment characteristics (F_{imp}, FD), rainfall data, and the acceptable uncertainty threshold (σ). A change in rainfall distribution, from R3 to R2 (F_{imp} = 24.26 ha), in the context of calculations for verifying sewer capacity, performance evaluation, or climate-smart sewer design, leads to a 33.3% increase in Q_m (Figure 5b). Meanwhile, an increase in P_t = 6.0 mm to P_t = 8.0 mm (under R2 temporal rainfall distribution) results in a 68% increase in Q_m (Figure 5a). The calculation results for the remaining variants are presented in Figure A8 in Appendix A.

An increase in catchment imperviousness (from F_{imp} = 16.26 ha to F_{imp} = 24.26 ha), for rainfall duration t_r = 30 min

and P_t = 6.0 mm (type R2), led to a 42% increase in Q_m. It was found that as σ increases, the range of variability of Q_m also increases for the assumed values of p_{Qm} = const, across rainfall types R2, R3, and R4 (Figure 5b). In practice, an increase in σ indicates a greater reserve of sewer capacity at the design stage and an increase in the reliability of system operation during heavy rainfall.

In addition to catchment characteristics, the significant influence of SWMM model parameters on Q_m simulation results was confirmed (Figures 5c and 5d). It was found that a reduction in the Manning roughness coefficient of impervious areas (n_{imp}) and the sewer roughness coefficient (n_{sew}) leads to an increase in Q_m (0.5th percentile), while the impervious area correction factor (β) shows an inverse relationship. For a rainfall duration of t_r = 30 min and P_t = 8.0 mm, it was shown that despite an increase from F_{imp} = 11.17 ha (FD = 1.08) to F_{imp} = 15.26 ha (FD=1.14), as a result of catchment urbanization, it is possible to maintain a constant flow of Q_m = 1000 $L \cdot s^{-1}$ by increasing the Manning roughness coefficient from n_{imp} = 0.0157 $m^{-1/3} \cdot s$ to 0.018 $m^{-1/3} \cdot s$ (Figure 5d).

The inclusion of the likelihood function was shown to have a significant impact on the calculated values of d_{imp}, n_{imp}, n_{sew}, and β, as confirmed by the resulting curves (Fig. 5c, d). The introduction of the likelihood function during the identification of SWMM parameters influencing Q_m, under a defined uncertainty threshold (σ), leads to an increase in their values by approximately 2 – 15% compared to the variant where the likelihood function is omitted.

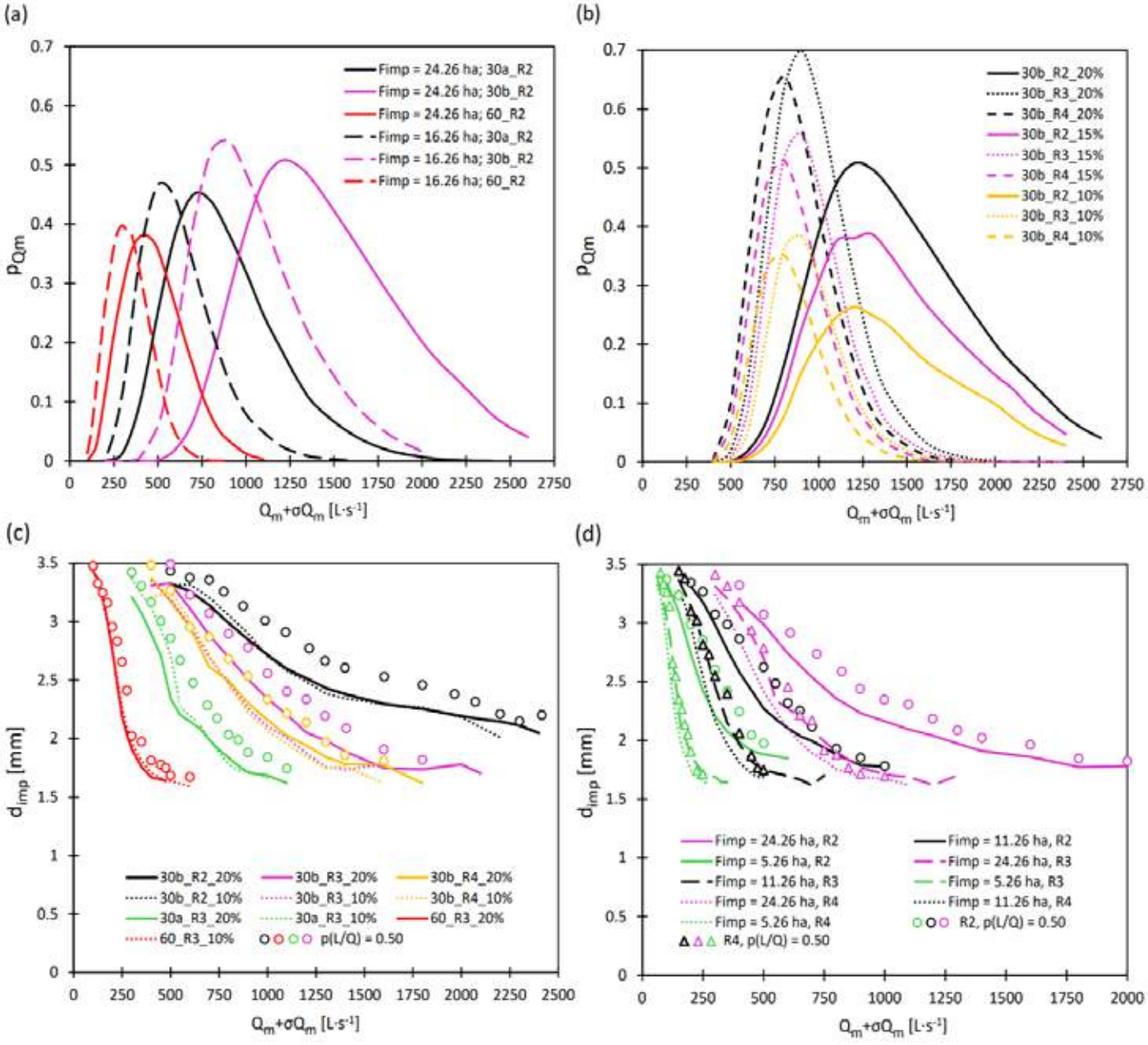

Figure 5. (a) Influence of maximum design flow (Q_m), catchment characteristics (F_{imp}), rainfall data on p_{Qm} probability; (b) Influence of maximum design flow (Q_m), rainfall distribution (type R2, R3, R4), acceptable uncertainty threshold (σ) on p_{Qm} probability; (c) Influence of maximum design flow (Q_m), rainfall data, permissible uncertainty threshold (σ) on d_{imp} with neglect and consideration of likelihood of SWMM parameters; (d) Influence of maximum design flow (Q_m), catchment characteristics (F_{imp}), temporal rainfall distribution on d_{imp} with neglect and consideration of reliability of SWMM parameters.

Discussions

Model for simulating maximum flow

The MARS method was used to simulate processes of 5 sub-catchments and identify the condition of conduits, flows, slopes, etc. To date, this method has not been applied to the calculation of maximum flows in sewer lines (Table 5), even though it has been used to simulate flows in river catchments (Fig. 1). The ML computational models presented in this study differ from those developed by other authors (She and You, 2019; Yang and Chui, 2020; Kratzert et al., 2019) in that they are expressed as analytical equations. This format allows the influence of independent variables on maximum flow simulation results to be assessed directly, without the need for additional calculations. In the present study, non-linear relationships between rainfall data and the estimated

Table 5. Review of a mechanistic machine learning model incorporating input data for predicting maxi-mum flow

Studies	Variable	Methods	Input				
			RN	SW	CT	SP	UN
Vojnovic et al. (2003)	Q(t)	ML (MLP)	1	0	0	0	0
Zhou et al. (2014)	Q	ML (SLRM)	1	1	1	1	0
Yao et al. (2016)	Qm, V	ML (MLR)	1	0	1	1	0
Gargano et al. (2015)	Q(t)	ML (SVM)	1	0	0	0	0
Yao et al. (2017)	Qm	MC (MLR)	1	0	1	1	0
Liu et al. (2017)	Qm	MC (MQR)	1	1	1	0	0
Jato-Espino et al. (2017)	Qm	ML (MQR)	0	0	0	0	1
Jato-Espino et al. (2018)	Qm	ML (MQR)	1	1	1	0	0
Kratzert et al. (2019)	Qm	ML (LSTM)	1	0	1	0	0
She and You (2019)	Q(t)	MC (RBF-NARX)	1	0	0	0	0
Yang and Chui (2020)	Q(t)	ML (XGboost)	1	0	0	0	0
Bell et al. (2020)	Qm, V	ML (logit)	0	0	1	0	0
Fatone et al. (2021)	Qm	ML (logit)	1	0	0	0	1
Palmitessa et al. (2022)	Q(t), h, Vov	ML (DNN)	1	0	0	0	0
Meierdiercks et al. (2010)	Q(t)	MC (SWMM)	1	1	1	1	1
Mejia et al. (2010)	Q(t)	MC(GUIH)	1	1	1	1	1
Cantone and Schmidt (2011)	Q(t)	MC (IUHM)	1	1	1	1	1
Zhang et al. (2014)	Q(t)	MC (GSSH)	1	1	1	1	1
Chadalawada et al. (2017)	Q(t)	MC (IUH)	1	1	1	1	1
Ichiba et al. (2018)	Q(t)	SWMM	1	1	1	1	1
Qui et al. (2020)	Q(t)	SWMM	1	1	1	1	1
Wolfs and Willems (2016)	Q(t)	MC+ML	1	1	1	1	1
this study	**Qm**	**MC (MARS)**	**1**	**1**	**1**	**1**	**1**

where: RN – rainfall; SW – sewer characteristics; CT – catchment characteristics; SP – spatial; UN – uncertainty (calibration parameter describe of the storage catchment, capacity of sewer); 1 – functional; 2 – unfunctional; SVM – support vector machines; DNN – deep neural network; XGboost – Extreme Gradient Boosting; MLR – multinomial linear regression; MQR – mulitnomial polynomial regression; RBF – radial basis function; LSTM – long short term memory; MLP – multilayer perceptron; MC – mechanistic model; GUIH – Geomorphological Unit Hydrogram Instantaneous Hydrogram; IUHM – Illinous Unit Hydrogram Model; GSSH - ; IUH – Instantaneous Unit Hydrogram.

coefficients in the MARS model were identified, as confirmed by the obtained correlation coefficients. However, it was not possible to establish generalized relationships for determining these coefficients, which means the developed model is not universal.

Similar case-study-based approaches were proposed by Fatone et al. (2021), who considered SWMM parameters (α, n_{imp}, $d_{imp,}$ n_{sew}) and rainfall data but neglected catchment and sewer network storage and topology. Yao et al. (2016) considered catchment imperviousness and, in a simplified manner, the layout of the sewer network by classifying 6 sub-catchment types. Bell (2020) included only impervious areas in his model. Among the reviewed studies, only Jato-Espino et al. (2018) developed a model for maximum flow prediction that simultaneously considers catchment imperviousness and sewer storage as a function of rainfall frequency. This model shows potential for application to other catchments, but it has not been widely studied.

Impact of catchment characteristics and sewer sewage system topology on maximum flow

It was found that the impervious area of the catchment contributes significantly to an increase in maximum flow, while other catchment characteristics were not statistically significant. This finding is consistent with the analyses of Yao et al. (2016) and Jato-Espino et al. (2018) for small urban catchments. Bell et al. (2020), based on a review of 55 publications, developed a logistic regression model to estimate the probability of exceeding the maximum flow based on the area of green infrastructure (GI) facilities in the catchment and rainfall data. However, the spatial layout of these features was not considered due to limited available data. Among drainage network characteristics, both the fractal dimension and sewer density were found to influence maximum flow, with observed correlations to rainfall depth. Yao et al. (2016) showed the influence of land use spatial layout and sewer system topology using 5 sub-catchments in Beijing. However, their study did not attempt to parameterize these spatial features using indicators such as fractal dimension or semivariogram parameters.

To date, fractal dimension has been determined through mechanistic model analyses, where its influence on sewer system performance has been confirmed (Gires et al. 2017). Ogden et al. (2011), using the GSSH model, showed that increasing sewer density leads to higher peak flows. This effect was attributed to changes in the routing of the sewer network in the catchment, but the spatial configuration of the drainage system and its effect on runoff were ignored. These findings are consistent with the results of Gironas et al. (2010), who used the advanced GIUH model to simulate sewer network outflow hydrogram. Gires et al. (2017) further demonstrated the potential of an integrated modeling tool combining MCM and fractal geometry to simulate sewer systems, impervious area, and building rooftops across 3 different networks.

Despite these advancements, no prior study has fully established a quantifiable relationship between catchment characteristics and maximum flow. The relationship identified in this study, linking fractal dimension, catchment properties, and sewer network characteristics, enhances our understanding of the interactions among these factors and their implications for urban catchment hydrology.

Impact of Rainfall Characteristics on the Relationship: SWMM parameters – maximum flow (Sensitivity Analysis)

The complex influence of rainfall load on the coefficients in the MARS model has been established. An increase in the values of SWMM parameters (d_{imp}, n_{sew}, β, etc.), depending on the range of their variability, can either increase or decrease Q_m. These results showed the influence of the spatial layout of land use and sewer network configuration on the outflow hydrogram, as different layouts generate different hydraulic conditions in the sewer network, particularly in urban catchments (Fig. 1). In many previous studies (Szeląg et al. 2016, Barco et al. 2008), the impact of calibrated parameters on sewer performance (hydrogram, flooding volumes, etc.) was analyzed using simplified approaches, which often involved a single rainfall event, limited combinations of calibrated parameters, and the neglect of temporal rainfall distribution, leading to overly generalized conclusions (Szeląg et al. 2022 b). Fatone et al. (2021) found that increases in d_{imp}, n_{imp}, n_{sew} could lead to a decrease in maximum flow, while an opposite relationship was observed for α. The difference in methodological approaches, classification models (logit) versus regression models (MARS), enabled the identification of consistent relationships across both modeling frameworks.

The results of the calculations showed that for rainfall with t_r = 30 min (type R2), the Manning roughness coefficient of sewer (n_{sew}) has the greatest influence on the maximum flow, and for rainfall with t_r = 60 min, the storage depth of impervious areas (d_{imp}) was the most influential. The influence of the temporal distribution of rainfall and catchment characteristics on the results of sensitivity analysis was confirmed by Cristiano et al. (2018), who performed analyses for 4 urban catchments (2.5 - 5.3 km^2). Similar results were obtained by Fraga et al. (2016) for a small road catchment (0.005 km^2), who found an influence of rainfall data on sensitivity coefficients and also showed the key influence of n_{imp} on the hydrogram. Fatone et al. (2021), using a logistic regression method (rainfall types R2, R3, and R4), confirmed the highest impact of n_{sew} on maximum flow (Tables 3 and 4). They found that an increase in rainfall intensity led to a reduction in sensitivity coefficients, with highest values obtained for type R1 rainfall distribution and the lowest for type R2. Krebs et al. (2014) (Imp = 86%) confirmed the key influence of sewer roughness coefficient on the catchment outflow hydrogram. On the other hand, Barco et al. (2008) (Imp = 65%), Krebs et al. (2014) (Imp = 19, 86%) found that maximum flow and runoff volume were most influenced by depression storage and catchment imperviousness; their calculations did not include rainfall data.

Risk analysis

Most current risk analysis methods (Fu and Butler 2014, Ursino et al. 2015) focus on the impact of rainfall uncertainty on the performance of the sewer networks, particularly regarding maximum flow, flood volume, and manhole overflows. , etc.). In contrast, the proposed risk analysis method considers not only rainfall uncertainty but also the characteristics of the catchment and sewer network, as well as uncertainty in depression storage and sewer capacity, as represented by SWMM parameters. The model includes a so-called acceptable uncertainty threshold for maximum flow calculations, which

can be interpreted as a reserve of canal capacity. This reserve accounts for climate change and varying catchment conditions, which is important given potential changes in catchment storage and the hydrological cycle. A similar approach was proposed by Sharifi et al. (2024), but their model was limited to analyzing the impact of climate change on sewer network design.

Soft-sensors for predicting sewer sewage system performance – field studies

Literature data (Table 6) confirm that an alternative to classical measurement methods is the used of so-called soft sensors, which operate based on ML models. This approach is gaining increasing attention, as evidenced by the growing number of studies published in this area (Guo et al. 2023). For the development of such models, it is essential to collect an sufficiently large datasets, which requires continuous monitoring of rainfall and sewer network parameters such as flow, flooding, and water depth. ML models have been successfully applied to predict catchment flow rates, overflows, water levels, flood volumes and water depths (Li et al. 2022, Guo et al. 2023). However, most of these models are case-specific and typically developed for individual catchments. As a result, their applicability is limited and dedicated models must be developed for each catchment restricting their universality. Consequently, continuous data collection is required for every application, leading to operational costs associated with maintaining high-resolution and high-quality measurement data (Kwon and Kim 2021, Al Mehedi 2023). Additionally, issues such as improper calibration or placement of flow meters can negatively affect the performance of mechanistic models and reduce the accuracy of predictions, limitations that are detailed in Table 7.

The aforementioned disadvantages - technical limitations, data quality and integration issues, and errors resulting from simplified model assumptions, have been addressed in MC models that incorporate rainfall data, land use, sewer network

Table 6. Review publications on the role of ML models in forecasting and cost reduction of measurement systems

No.	Authors and Year	Duration of Study	Measurement Devices and Measurement Resolution	Input to ML model	Measurement Issues
1	J. Liu, HS Cho (2022)	Typhoon Committee conducted urban flood monitoring projects for several years (UFRM and OSUFFIM)	LSTM Sensors (Long Short-Term Memory); automatic image monitoring based on IoT, weather radar, satellite monitoring - weather radar and satellite images providing good spatial and temporal resolution.	Rainfall data – in tropical cyclone (TC) regions, flood events in densely populated high-risk areas in the Asia-Pacific region.	Issues in real-time urban flood forecasting: low accuracy and time-consuming computations, inconsistent access to updated technology, and geographical variability in data collection leading to gaps in measurements.
2	SH Kwon, JH Kim (2021)	16 studies, including five operational UDS studies; research from the last ten years	Flow sensors, UDS system; long-term memory, LSTM - high resolution	Rainfall data, real-time data used – heavy rainfall	Discontinuous data; studies require large sample sizes (i.e., big data); challenges with generalizing ML models, data diversity, especially in the context of overflow prediction.
3	MA Al Mehedi (2023)	Five years, focusing on the rain garden in Villanova, Pennsylvania	IoT smart sensors, humidity sensors at various depths, water depth sensors, and devices monitoring air and sea temperature - high resolution due to continuous data from sensors allowed in the LSTM model.	Flow data; the LSTM model was trained on operational units such as air temperature, outlets at different depths and waters. The goal was to predict water recession rates.	0.51 ha, small catchment area with urban infrastructure for green stormwater retention.
4	G Fu, S Sun (2022)	No data	LSTM sensors; various sensors used for monitoring water, leak detection, sewer defect detection, and forecasting sewer system conditions - high, enabling continuous monitoring and forecasting based on input data.	Data includes forecasts for water demand, leak detection, forecasting sewer system conditions – synthetic data.	Lack of data synchronization; data issues; problems with data values, privacy, and trust in algorithms.
5	A Sharifi (2024)	No data	IoT, smart sensors, a series of sensors for real-time data collection - high, enabling real-time data collection and analysis.	Hydrological parameters (flow, temperature, and precipitation) of urban drainage systems.	Issues with location and inaccurate definitions of graphic concepts.

layout, and surface runoff conditions (Tabuchi 2020, Moon 2023). Guo et al. (2023) showed the predictive generalization capacity of such models to forecast sewage flooding for urban catchments, allowing their use as soft sensors. Since machine learning methods determine input - output relationships based on statistical correlations, the development of a universal model is feasible. This can be achieved by collecting data from various catchments with diverse physical and geographical characteristics, or by using mechanistic models as simulators to generate synthetic datasets for training machine learning models applicable across multiple catchments. This approach aligns with ongoing efforts to develop a low-cost soft sensors capable of predicting sewer network flow rates and identifying the volume and extent of sewage flooding.

Table 7. MC models for predicting flow intensity in sewer network catchments of different sizes

No.	Authors and Year	Catchment Size	Measurement Devices	Measurement Resolution	Measurement Data	Measurement Issues
1	Tabuchi (2020)	Paris, France; 1800 km²; 500 km of main sewage channels, modeled by 3113 nodes (23,000 computational nodes)	Flow control of the Seine in Paris, and the 5-year and 10-year wet and dry flow rates; MAGES - real-time control system in the Paris Metropolitan Region - 150 management sites (basins, valves, and pumps)	Simulation (approx. 3 minutes within 24 hours); 5-minute cycle	Real-time rainfall data; Flow data; Historical and operational data from the sanitation system, including sewer network performance, maintenance records, and real-time environmental data.	Processing rainfall data and configuring real-time data exchange platforms between SIAAP (Interdepartmental Syndicate for Sanitation in the Paris Region) and each partner: limitations related to sewage pollution and the impact of discharges on the natural environment.
2	Tao (2020)	Kentucky, USA; 385 square miles catchment, 11 Ohio River catchments	The RTC system has ~30 control facilities, including retention basins, storage, diversion controls, and pump stations.	RTC system updated based on five-minute data sampling intervals	Sewage flow data; Rainfall forecasts; Water levels; Flows; Operational data: gate positions, pump rates, treatment capacities	Data quality inconsistencies and challenges in integrating diverse data sources; Infrastructure limitations, as well as inadequate spatial and temporal resolution of data.
3	Moon (2023)	Seoul, South Korea; 42.50 km²	Weather system (https://www.kma.go.kr), rain gauge sensors; water level monitoring systems	Rainfall data collected at 1-minute resolution for 21 years (2001–2021).	Rainfall data, water levels; Additional synthetic data generated by a rainfall-runoff model	Errors in R-R simulation results (SWMM), uncertainty in catchment data for estimating parameters is relatively high.
4	Wu (2023)	Wuhan, China; 8494 km²	Pump performance; technologies for monitoring rainfall and floodwater levels	High spatial and temporal resolution	Rainfall data; Overflow data; Pump performance data	Found a nonlinear response relationship between pump performance and the area covered by LID and UFS.
5	M. Zawilski (2013)	Łódź, Poland; 335 ha catchment, sealing degree - 40%; 60 subcatchments (1.79 - 17.16 ha)	Flow sensors, rain gauges, standalone monitoring stations for Total Suspended Solids (TSS)	Continuous quantitative and qualitative monitoring from 1989–1992, pluviometric data from 2010–2012	Precipitation data, flows in the sewage system, suspended solids data	Technical limitations: Discontinuous data, Measurement accuracy issues, Calibration difficulties.
6	Nowogoński (2019)	Poland, 288 ha catchment, 72 subcatchments of 4 ha each	Simulation, rain gauge sensors (so-called pluviometers), flow sensors in channels, and water level sensors	Temporal and spatial resolution	Precipitation data, hydrological data: flow and water level measurements, spatial data - velocity, assuming uniform runoff from rainfall	Errors arise from assuming too few subcatchments, which underestimates maximum runoff and stabilizes it at a lower level.
7	M. Wawrzyniak (2023)	Szczecin, Poland; 300.55 km²	IMGW-PIB meteorological station devices in Szczecin, flow meters	Minute data for 30 years from 1986–2015	Rainfall data; Flows; Real-time ML algorithm training	Low effectiveness of the Błaszczyk formula: Major errors, poor fit to data. Better fit for R&D models (e.g., KOSTRA atlas, PANDa, PMAXTP).

Limitations and future directions

The presented model is conceptual in nature and was developed using data from a single urban catchment with an area of 63 ha. As such, it should be regarded as a case study aimed at demonstrating the potential of machine learning-based soft sensors for predicting peak flows in stormwater systems without the need for continuous flow monitoring. Although the model was calibrated for a specific location, it is designed for broader applicability, both within Poland and internationally, pending further validation with data from catchments exhibiting diverse land use patterns and sewer system configurations.

A principal limitation of the study is the reliance on precipitation data from a single pluviometer located outside the study catchment. While this approach is generally acceptable for small catchments (Del Giudice et al., 2013; Bell et al., 2020), the use of denser rain gauge networks or radar-based rainfall estimates is recommended for larger areas to more accurately capture spatial variability in rainfall.

Hydrodynamic calculations and simulations based on the studies of Barco et al. (2008) and Catone et al. (2011) demonstrated the influence of infiltration processes on surface runoff in large urban catchments. In contrast, the present study focused on a small catchment where the contribution of green areas to runoff generation was negligible. Sobol sensitivity analysis revealed a marginal impact of infiltration-related parameters, particularly d_{imp} and β (Kiczko et al., 2018), which justified their exclusion from the modeling process. These findings are consistent with those of Fatone et al. (2021), who also reported the influence of these parameters as statistically insignificant.

Additionally, uniform parameterization was applied across the catchment, which is a common practice when modeling small urban areas in Poland (Wałęga et al., 2013, Banasik et al., 2014). These studies, focusing on rainfall-runoff modeling using SCS-CN method, demonstrated that spatial variability had a limited effect on peak flow estimation in small catchments, such as the Służewiecki Stream catchment in Warsaw. Nonetheless, future research should account for spatial heterogeneity to further enhance model accuracy.

Calibration events were carefully selected to exclude sewer overflows and surface flooding, thereby ensuring mass balance consistency, as recommended in the literature (Jato-Espino et al., 2017). Consequently, the current model does not account for hydraulic overload scenarios, an important limitation that should be addressed in future work to improve model robustness.

Future research should explore the application of dimensionality reduction techniques and the development of hybrid models that integrate data-driven approaches with conceptual hydrological modeling. Despite its limitations, the proposed soft sensor offers an energy-efficient alternative to traditional flow monitoring devices and shows significant potential for integration into real-time stormwater management systems.

Conclusions

One of the currently major challenges in hydrology is the development of universal models that can be applied to model different urban catchments. Mechanistic models often fall short in this regard due to their limited flexibility.

As part of the research, an attempt was made to develop a universal model that incorporates key factors such as catchment characteristics, sewer network topology, sewer storage, and rainfall data. This process involved both model construction and sensitivity analysis. However, it was not possible to parameterize the estimated coefficients of the MARS model with rainfall data characteristics. As a result, the proposed models lack universality and cannot be directly transferred to other urban catchments. Despite this limitation, the obtained results revealed complex relationships between depression storage, sewer network, and peak flow, which were captured through the analytical structure of the MARS model. Notably, although empirical relationships for unambiguous coefficient identification could not be established, a very strong correlation was observed between the estimated coefficients and rainfall data. This finding holds significant cognitive value in understanding the behavior of the studied catchment.

Also noteworthy is the developed risk analysis method, which accounts for both the reliability of calibrated parameters and the capacity of sewers. This analysis was conducted based on the existing system conditions and incorporated a safety margin coefficient that defines the potential excess capacity. This approach enabled the estimation of the additional volume of wastewater that the network could convey under extreme conditions. The introduction of this coefficient provides a valuable metric for assessing and enhancing the adaptability of existing sewer networks to future climate change impacts.

Considering the utilitarian nature of the approach and the potential application of the obtained results to the analyzed catchment, further research is warranted. The goal of future work will be to develop universal relationships that can be applied to other catchments. Ultimately, objective is to create a tool that will enable efficient management of urban catchments using modern hydrological solutions, including zero-emission soft sensors that require no physical installation and generate zero energy consumption. This tool will be designed to adapt to evolving hydrological and climatic conditions, enabling effective monitoring of phenomena such as heavy rainfall or droughts. In turn, it will support sustainable water resource management, increase the resilience of urban infrastructure to climate change impacts, and help mitigate the risk of damage caused by extreme weather events.

References

Addison-Atkinson, W., Chen, A.S., Memon, F.A. & Chang, T.J., 2022. Modelling urban sewer flooding and quantitative microbial risk assessment: a critical review. *J. Flood Risk Mangement*. 15, e12844.

Amiri, H., Azadi, S., Javadpour, S., Naghavi, A.A. & Boczkaj, G., 2022. Selecting wells for an optimal design of groundwater monitoring network based on monitoring priority map: a Kish Island case study. *Water Resour. Ind*. 27, 100172 DOI:10.1016/j.wri.2022.100172.

Bach, P. M., Kuller, M., McCarthy, D. T. & Deletic, A. (2020). A spatial planning-support system for generating decentralised urban stormwater management schemes. *Science of The Total Environment*, 138282. DOI:10.1016/j.scitotenv.2020.138282.

Banasik, K., Krajewski, A., Sikorska-Senoner, A. E. & Hejduk, L. (2014). Curve number estimation for a small urban catchment

from recorded rainfall-runoff events. *Archives of Environmental Protection*, 40, 3, pp. 21–30. DOI:10.2478/aep-2014-0032.

Barco, J., Wong, K.M. & Stenstrom, M.K. (2008). Automatic calibration of the U.S. EPA SWMM model for a large urban catchment. *J. Hydraul. Eng*. 134, pp. 466–474. DOI:10.1061/(ASCE)0733-9429(2008)134:4(466).

Bell, C. D., Wolfand, J. M., Panos, C. L., Bhaskar, A. S., Gilliom, R. L., Hogue, T. S. & Jefferson, A. J. (2020). Stormwater control impacts on runoff volume and peak flow: A meta-analysis of watershed modeling studies. *Hydrological Processes*. DOI:10.1002/hyp.13784.

Beven, K. (2020). Deep learning, hydrological processes and the uniqueness of place. *Hydrological Processes*, 34, 16, pp. 3608–3613. DOI:10.1002/hyp.13805.

Bhaskar, A. S., Hogan, D. M., Nimmo, J. R. & Perkins, K. S. (2018). Groundwater recharge amidst focused stormwater infiltration. *Hydrological Processes,* 32, 13, pp. 2058–2068. DOI:10.1002/hyp.13137.

Birgani, Y. T., Yazdandoost, F. & Malaekepour, S. M. (2013). Urban Drainage Systems Risk Assessment under Climate Change Conditions.

Butler, D., Farmani, R., Fu, G., Ward, S., Diao, K. & Astaraie-Imani, M. (2014). A new approach to urban water management: Safe and sure. *Procedia Engineering*, 89, pp. 347-354.

Cantone, J. & Schmidt, A. (2011). Improved understanding and prediction of the hydrologic response of highly urbanized catchments through development of the Illinois Urban Hydrologic Model. *Water Resources Research*, 47, 8. DOI:10.1029/2010wr009330.

Chadalawada, J., Havlicek, V. & Babovic, V. A (2017). Genetic Programming Approach to System Identification of Rainfall-Runoff Models. *Water Resour Manage* 31, pp. 3975–3992. DOI:10.1007/s11269-017-1719-1.

Cristiano, E., ten Veldhuis, M.C., Gaitan, S., Rodriguez, S.O. & van de Giesen, N. (2018). Critical scales to explain urban hydrological response. *Hydrol. Earth Syst. Sci. Discuss.* DOI:10.5194/hess-2017-715.

Cristiano, E., ten Veldhuis, M.C., Wright, D.B., Smith, J.A. & van de Giesen, N. (2019). The influence of rainfall and catchment critical scales on urban hydrological response sensitivity. *Water Resour. Res*. 55, pp. 3375–3390. DOI:10.1029/2018WR024143.

De Paola, F. & Ranucci, A. (2012). Analysis of spatial variability for stormwater capture tank assessment. *Irrig. Drain*. 61, pp. 682–690. DOI:10.1002/ird.

Del Giudice, D., Honti, M., Scheidegger, A., Albert, C., Reichert, P. & Rieckermann, J. (2013). Improving uncertainty estimation in urban hydrological modeling by statistically describing bias. *Hydrology and Earth System Sciences*, 17, 10, pp. 4209–4225. DOI:10.5194/hess-17-4209-2013.

Duan, H., Akker, B. van den, Thwaites, B. J., Peng, L., Herman, C., Pan, Y. & Ye, L. (2020). Mitigating nitrous oxide emissions at a full-scale wastewater treatment plant. *Water Research,* 116196. DOI:10.1016/j.watres.2020.116196

DWA-A 118E, 2006. Hydraulic Dimensioning and Verification of Drain and Sewer Systems. DWA German Association for Water, Wastewater and Waste, Hennef, Germany.

Fatone, F., Szeląg, B., Kiczko, A., Majerek, D., Majewska, M., Drewnowski, J. & Łagód, G. (2021). Advanced sensitivity analysis of the impact of the temporal distribution and intensity of rainfall on hydrograph parameters in urban catchments. *Hydrol. Earth Syst. Sci*. 25, pp. 5493–5516. DOI:10.5194/hess-25-5493-2021.

Fraga, I., Cea, L., Puertas, J., Su´arez, J., Jim´enez, V. & J´acome, A. (2016). Global sensitivity and GLUE-based uncertainty analysis of a 2D–1D dual urban drainage model. *J. Hydrol. Eng*. 21, 04016004. DOI:10.1061/(ASCE)HE.1943-5584.0001335.

Friedman, J. H. & Roosen, C. B. (1995). An introduction to multivariate adaptive regression splines. *Statistical Methods in Medical Research*, 4, 3, pp. 197–217. DOI:10.1177/096228029500400303.

Fu, G. & Butler, D. (2014). Copula-based frequency analysis of overflow and flooding in urban drainage systems. *J. Hydrol*. 510, pp. 49–58. DOI:10.1016/j.jhydrol.2013.12.006.

Fu, G., Jin, Y., Sun, S., Yuan, Z. & Butler, D. (2022). The role of deep learning in urban water management: A critical review. *Water Research* 223, 1 118973, DOI:10.1016/j.watres.2022.118973.

Gargano, R., Di Palma, F., de Marinis, G., Granata, F. & Greco, R. (2015). A stochastic approach for the water demand of residential end users. *Urban Water Journal*, 13, 6, pp. 569–582. DOI:10.1080/1573062x.2015.1011.

Gires, A., Tchiguirinskaia, I., Schertzer, D., Ochoa-Rodriguez, S., Willems, P., Ichiba, A. & ten Veldhuis, M.-C. (2017). Fractal analysis of urban catchments and their representation in semi-distributed models: imperviousness and sewer system. *Hydrology and Earth System Sciences*, 21, 5, pp./ 2361–2375. DOI:10.5194/hess-21-2361-2017.

Gironás, J., Roesner, L. A., Rossman, L. A. & Davis, J. (2010). A new applications manual for the Storm Water Management Model (SWMM*), Environ. Modell. Softw*., 25, pp. 813–814. DOI:10.1016/j.envsoft.2009.11.009, 2010.

Gong, Y., Zhang, G., Hao, Y. & Nie, L., 2022. Enrichment Evaluation of Heavy Metals from Stormwater Runoff to Soil and Shrubs in Bioretention Facilities. Water, 14(4), 638. DOI:10.3390/w14040638

Guan, M., Sillanpää, N. & Koivusalo, H. (2015). Storm runoff response to rainfall pattern, magnitude and urbanization in a developing urban catchment. *Hydrological Processes*, 30, 4, 543-557. DOI:10.1002/hyp.10624.

Guo, K., Guan, M. & Yu, D. (2021). Urban surface water flood modelling – a comprehensive review of current models and future challenges. *Hydrol. Earth Syst. Sci*. 25, pp. 2843–2860. DOI:10.5194/hess-25-2843-2021.

Guo, K., Guan, M., Haochen, Y. & Xilin, X. (2023). A spatially distributed hydrodynamic model framework for urban flood hydrological and hydraulic processes involving drainage flow quantification. *Journal of Hydrology*. 625. DOI:10.1016/j.jhydrol.2023.130135.

Hauger, M. B., Mouchel, J. M. & Mikkelsen, P. S. (2006). Indicators of hazard, vulnerability and risk in urban drainage. *Water science and technology*, 54, 6-7, pp. 441-450. DOI:10.2166/wst.2006.622.

Ichiba, A., Gires, A., Tchiguirinskaia, I., Schertzer, D., Bompard, P. & Ten Veldhuis, M.-C. (2018). Scale effect challenges in urban hydrology highlighted with a distributed hydrological model. *Hydrology and Earth System Sciences*, 22, 1, pp. 331–350. DOI:10.5194/hess-22-331-2018.

Jato-Espino, D., Sillanpää, N., Andrés-Doménech, I. & Rodriguez-Hernandez, J. (2017). Flood Risk Assessment in Urban Catchments Using Multiple Regression Analysis. *Journal of Water Resources Planning and Management*, 144, 2. DOI:10.1061/(ASCE)WR.1943-5452.0000874.

Jato-Espino, D., Sillanp¨a¨a, N., Andr´es-Dom´enech, I. & Rodriguez-Hernandez, J. (2018). Flood risk assessment in urban catchments using multiple regression analysis. *J. Water Resour. Planning Manag*. 144, 04017085. DOI:10.1061/(ASCE)WR.1943-5452.0000874.

Kiczko, A., Szeląg, B., Kozioł, A. P., Krukowski, M., Kubrak, E., Kubrak, J. & Romanowicz, R. J. (2018). Optimal capacity of a stormwater reservoir for flood peak reduction. *Journal of Hydrologic Engineering*, 23, 4. DOI:10.1061/(ASCE)HE.1943-5584.0001636

Kratzert, F., Klotz, D., Herrnegger, M., Sampson, A. K., Hochreiter, S. & Nearing, G. S. (2019). Towards Improved Predictions in Ungauged Basins: Exploiting the Power of Machine Learning. *Water Resources Research*. DOI:10.1029/2019wr026065

Krebs, G., Kokkonen, T., Valtanen, M., Setälä, H. & Koivusalo, H. (2014). Spatial resolution considerations for urban hydrological modelling, *J. Hydrol*., 512, pp. 482–497. DOI:10.1016/j.jhydrol.2014.03.013.

Kumar, S., Agarwal, A., Ganapathy, A., Villuri, V.GK. Pasupuleti, S., Kumar, D., Kaushal, D.R., Gosain, A.K. & Sivakuma, B. (2022). . Impact of climate change on stormwater drainage in urban areas. *Stoch Environ Res Risk Assess* 36, pp. 77–96. DOI:10.1007/s00477-021-02105-x.

Kwon, S. H. & Kim, J. H. (2021). Machine Learning and Urban Drainage Systems: State-of-the-Art Review. *Water,* 13, 24, 3545. DOI:10.3390/w13243545.

Li, X. & Willems, P. (2020). A hybrid model for fast and probabilistic urban pluvial flood prediction. *Water Resour. Res*. 56, 6. DOI:10.1029/2019WR025128.

Li, X., Erpicum, S., Mignot, E., Archambeau, P., Pirotton, M. & Dewals, B. (2022). Laboratory modelling of urban flooding. *Sci. Data*, 9, 1. DOI:10.1038/s41597-022-01282-w.

Liu, C. Y. & Chui, T. F. M. (2017). Factors influencing stormwater mitigation in permeable pavement. *Water*, 9, 12, 988. DOI:10.3390/w9120988.

Liu ,J., Cho, H-S., Osman, S., Jeong, H-G. & Lee, K. (2022). Review of the status of urban flood monitoring and forecasting in TC region, Tropical Cyclone Research and Review 11, 2, pp.103-119.. DOI:10.1016/j.tcrr.2022.07.001.

Luiso, J. E. & Giribet, J. I. (2017). Optical flow sensor. 2017 XVII Workshop on Information Processing and Control (RPIC). DOI:10.23919/rpic.2017.8211652.

Meierdiercks, K.L., Smith, J.A., Baeck, M.L. & Miller, A.J. (2010). Analyses of urban drainage network structure and its impact on hydrologic response. *JAWRA Journal of the American Water Resources Association* 46, pp. 932–943. DOI: 10.1111/j.1752-1688.2010.00465.x.

Mejía, A. I. & Moglen, G. E. (2010). Impact of the spatial distribution of imperviousness on the hydrologic response of an urbanizing basin. *Hydrological Processes*, 24, 23, pp. 3359–3373. DOI:10.1002/hyp.7755.

Al Mehedi, M. A., Amur, A., Metcalf, J., McGauley, M., Smith, V. & Wadzuk, B. (2023). Predicting the performance of green stormwater infrastructure using multivariate long short-term memory (LSTM) neural network. *Journal of Hydrology*, 625, 130076. DOI:10.1016/j.jhydrol.2023.130076.

Mondal, K., Bandyopadhyay, S. & Karmakar, S. (2023). Framework for global sensitivity analysis in a complex 1D-2D coupled hydrodynamic model: Highlighting its importance on flood management over large data-scarce regions. *Journal of Environmental Management,* 332, 117312. DOI:10.1016/j.jenvman.2023.117312

Moon, H., Yoon, S. & Moon, M., (2023). Urban flood forecasting using a hybrid modeling approach based on a deep learning technique. *Journal of Hydroinformatics,*25, 2, pp. 593–610. DOI:10.2166/hydro.2023.203.

Mor´an-Valencia, M., Flegl, M. & Güemes-Castorena, D. (2023). A state-level analysis of the water system management efficiency in Mexico: two-stage DEA approach. *Water Resour. Ind*. 29, 100200 DOI:10.1016/j.wri.2022.100200.

Napiorkowski, J.J., Piotrowski, A.P., Karamuz, E. & Senbeta, T.B. (2023). Calibration of conceptual rainfall-runoff models by selected differential evolution and particle swarm optimization variants. *Acta Geophys*. 71, pp. 2325–2338. DOI:10.1007/s11600-022-00988-0.

Nowogoński, I. (2019). Emporal and spatial variability of rainfall in modelling of stormwater outflows. *CEER*; 29, 4, pp. 267-278. DOI: 10.2478/ceer-2019-0060.

Ogden, F.L., Pradhan, N.R., Downer, C.W. & Zahner, J.A. (2011). Relative importance of impervious area, drainage density, width function, and subsurface storm drainage on flood runoff from an urbanized catchment. *Water Resour. Res*. 47, W12503. DOI:10.1029/2011WR010550.

Palmitessa, R., Grum, M., Engsig-Karup, A.P. & Löwe, R. (2022). Accelerating hydrodynamic simulations of urban drainage systems with physics-guided machine learning. *Water Res*. 223, 118972 DOI:10.1016/j.watres.2022.118972.

Perdikaki, M., Makropoulos, C. & Kallioras, A. (2022). Participatory groundwater modelling for managed aquifer recharge as a tool for water resources management of a coastal aquifer in Greece. *Hydrgeol*. *J*. 30, 1, pp. 37–58. DOI: 10.1007/s10040-021-02427-8

Qiu, Y., da Silva Rocha Paz, I., Chen, F., Versini, P. A., Schertzer, D. & Tchiguirinskaia, I. (2020). Space variability of hydrological responses of Nature-Based Solutions and the resulting uncertainty. *Hydrology and Earth System Sciences Discussions*, 1-34. DOI:10.5194/hess-2020-468

Rosenzweig, B.R., Cantis, H., Kim, Y., Cohn, A., Grove, K., Brock, J., Yesuf, J., Mistry, P., Welty, C., McPhearson, T., Sauer, J. & Chang, H. (2021). The value of urban flood modeling. *Earth's Future* 9, e2020EF001739. DOI:10.1029/2020EF001739.

Sharifi, A., Beris, A.T., Javidi, A.S., Nouri, M., Lonbar, A.G. & Ahmadi, M. (2024). Application of artificial intelligence in digital twin models for stormwater infrastructure systems in smart cities. *Advanced Engineering Informatics*, 61, 102485. DOI:10.1016/j.aei.2024.102485.

Sharma, S., Lee, B. S., Nicholas, R. E., & Keller, K. (2021). A safety factor approach to designing urban infrastructure for dynamic conditions. *Earth's Future*, 9, 12, e2021EF002118. DOI:10.1029/2021EF002118.

She, L. & You, X.Y. (2019). A dynamic flow forecast model for urban drainage using the coupled artificial neural network. *Water Resour. Manag*. 3, pp. 3143–3153. DOI:10.1007/s11269-019-02294-9.

Shi, B., Catsamas, S., Kolotelo, P., Wang, M., Lintern, A., Jovanovic, D. & McCarthy, D. T. (2021). A Low-Cost Water Depth and Electrical Conductivity Sensor for Detecting Inputs into Urban Stormwater Networks. *Sensors,* 21, 9, 3056. DOI:10.3390/s21093056.

Szeląg, B., (2013). Influence of the Hydrogramme Shape on the Capacity and Selection of Drains of a Small Retention Reservoir. University of Technology, Kielce. PhD thesis.

Szeląg, B., Kiczko, A. & Dąbek, L. (2016). Sensitivity and uncertainty analysis of hydrodynamic model (SWMM) for storm water runoff forecating in an urban basin – A case study, *Ochr. Sr*., 38, pp. 15–22.

Szeląg, B., Majerek, D., Kiczko, A., Łagód, G., Fatone, F. & McGarity, A. (2022a). Analysis of sewer network performance in context of modernization: modeling, sensitivity, uncertainty analysis. *Journal of Water Resources Planning and Management*. 148: pp[. 1– 12. DOI:10.1061/(ASCE)WR.1943–5452.0001610.

Szeląg, B., Suligowski, R., De Paola, F., Siwicki, P., Majerek, D. & Łagód, G. (2022b). Influence of urban catchment characteristics and rainfall origins on the phenomenon of stormwater flooding: case study. *Environ. Model. Softw*. 150, 105335 DOI:10.1016/j.envsoft.2022.105335.

Tabuchi, J.-P., Blanchet, B. & Rocher, V. (2020). Integrated Smart Water Management of the sanitation system of the Greater Paris region. *Water International*, 45, 6, pp. 574–603. DOI:10.1080/02508060.2020.1830584.

Tao, D. Q., Pleau, M., Akridge, A., Fradet, O., Grondin, F., Laughlin, S. & Shoemaker, L. (2020). Analytics and Optimization Reduce Sewage Overflows to Protect Community Waterways in Kentucky. *INFORMS Journal on Applied Analytics*, 50, 1, pp. 7–20. DOI:10.1287/inte.2019.1022.

Ursino, N. (2015). Risk analysis of sustainable urban drainage and irrigation. *Advances in Water Resources,* 83, pp. 277–284. DOI:10.1016/j.advwatres.2015.06.011.

Vojinovic, Z., Kecman, V. & Babovic, V. (2003). Hybrid Approach for Modeling Wet Weather Response in Wastewater Systems. *Journal of Water Resources Planning and Management,* 129, 6. DOI:10.1061/(ASCE)0733-9496(2003)129:6(511).

Wałek, G. (2019). The influence of roads on the formation of surface runoff in the urbanized area on the example of the Silnica River catchment area in Kielce. Jan Kochanowski University Press, Kielce. (in Polish).

Wałęga, A., Cupak, A., Michalec, B. & Wachulec, K. (2013). The influence of physical and geographical catchment parameters and precipitation characteristics on the runoff time of concentration. *Journal of Civil Engineering, Environment and Architecture*, 30, 60, pp. 143–160. DOI:10.7862/rb.2013.44.

Wang X., Kvaal K. & Ratnaweera H. (2019). Explicit and interpretable nonlinear soft sensor models for influent surveillance at a full-scale wastewater treatment plant. *J. Process Control*, 77, pp. 1-6. 10.1016/j.jprocont.2019.03.005 .

Wawrzyniak, M. & Wdowikowski, M. (2023). Heavy rainfall modeling in an urban catchment area on the example of Szczecin, Gaz, Woda i Technika Sanitarna. pp.22-30. DOI:10.15199/17.2023.7.4.

Willems, P. (2013). Revision of urban drainage design rules after assessment of climate change impacts on precipitation extremes at Uccle, Belgium. *Journal of Hydrology*, 496, pp. 166–177. DOI:10.1016/j.jhydrol.2013.05.037.

Wolfs, V. & Willems, P. (2016). Modular Conceptual Modelling Approach and Software for Sewer Hydraulic Computations. *Water Resources Management*, 31, 1, pp. 283–298. DOI:10.1007/s11269-016-1524-2.

Wong B. P. & Kerkez B. (2016). Real-time environmental sensor data: an application to water quality using web services. *Environmental Modelling and Software* 84, pp. 505–517. DOI:10.1016/j.envsoft.2016.07.020.

Wu, Y., She, D., Xia, J., Song, J., Xiao, T. & Zhou, Y. (2023). The quantitative assessment of impact of pumping capacity and LID on urban flood susceptibility based on machine learning. *Journal of Hydrology*, 617, 129116. DOI:10.1016/j.jhydrol.2023.129116.

Yang, Y. & Chui, T. F. M. (2020). Modelling and interpreting hydrological responses of sustainable urban drainage systems with explainable machine learning methods, *Hydrol. And Earth Syst. Sci.*, 25,11, pp. 5839-5858. DOI:10.5194/hess-2020-460, in review, .

Yao, L., Wei, W. & Chen, L. (2016). How does imperviousness impact the urban rainfall-runoff process under various storm cases? Ecological Indicators, 60, pp. 893–905. DOI:10.1016/j.ecolind.2015.08.041 10.1016/j.ecolind.2015.08.041.

Yao, Y., Li, J., Jiang, Y. & Huang, G. (2023). Evaluating the response and adaptation of urban stormwater systems to changed rainfall with the CMIP6 projections. *Journal of Environmental Management,* 347, 1, 119135. DOI:10.1016/j.jenvman.2023.119135.

Zawilski, M. & Sakson, G. (2013). Assessment of total suspended solid emission discharged via storm sewerage system from urban areas. OCHRONA SRODOWISKA, 35, 2, pp. 33-40.

Zhang, K., Liu, Y., Deletic, A., McCarthy, D. T., Hatt, B. E., Payne, E. G. Chandrasena, G., Li, Y., Pham, T., Jamali, B., Daly, E., Fletcher, T.D. & Lintern, A. (2021). The impact of stormwater biofilter design and operational variables on nutrient removal-a statistical modelling approach. *Water Research*, 188, 116486.

Zhou, Q. (2014). A Review of Sustainable Urban Drainage Systems Considering the Climate Change and Urbanization Impacts. *Water*, 6, 4, pp. 976–992. DOI:10.3390/w6040976.

Innowacyjna metoda prognozowania maksymalnego przepływu w systemach kanalizacji deszczowej z wykorzystaniem soft-sensorów.

Streszczenie. Tworzenie uniwersalnych modeli hydrologicznych do modelowania zlewni miejskich jest jednym z największych wyzwań współczesnej hydrologii. Niniejsze badanie podejmuje próbę opracowania modelu uwzględniającego różnorodne cechy zlewni, topologię sieci kanalizacyjnej, retencję w kanałach oraz dane opadowe, a także przeprowadzenia analizy wrażliwości modelu na zmiany parametrów wejściowych. Celem było zbadanie, w jakim stopniu zastosowanie zaawansowanych metod analitycznych, takich jak modele MARS (Multivariate Adaptive Regression Splines) oraz technologia soft-sensorów, może poprawić prognozowanie przepływów szczytowych (Qm) w systemach kanalizacji deszczowej. W badaniu wykorzystano zaawansowane metody analityczne, w tym modele MARS, do prognozowania przepływów szczytowych w systemach kanalizacji deszczowej. W proces modelowania włączono technologię soft-sensorów, uwzględniającą różnorodne cechy zlewni, topologię sieci kanalizacyjnej, retencję w kanałach oraz zmienne dane opadowe. Dodatkowo przeprowadzono analizę wrażliwości w celu oceny reakcji modelu na zmiany parametrów wejściowych. Wyniki pokazały, że połączenie modeli MARS z soft-sensorami pozwala na uzyskanie wysokiej dokładności prognoz (R^2 = 0,96, RMSE = 0,038), pomimo

zmienności warunków opadowych. Jednakże, nie udało się opracować uniwersalnych zależności modelowych z powodu trudności w parametryzacji modelu w kontekście zmiennych danych opadowych. Chociaż proponowane podejście nie prowadzi do stworzenia uniwersalnych narzędzi, dostarcza cennych wskazówek do dalszych badań nad adaptacją systemów kanalizacyjnych do zmieniających się warunków hydrologicznych. Zastosowana metoda analizy ryzyka umożliwiła uwzględnienie przepustowości sieci kanalizacyjnej oraz wprowadzenie współczynnika marginesu bezpieczeństwa, który ocenia elastyczność systemu w kontekście przyszłych zmian klimatycznych. Badanie wskazuje kierunki przyszłych prac nad modelami, które mogłyby być stosowane w różnych zlewniach miejskich, szczególnie poprzez rozwój bezkosztowych, zeroemisyjnych soft-sensorów.

Section A1. GLUE (Generalized Likelihood Uncertainty)

The uncertainty analysis involves the following steps:

- Selection of SWMM model parameter ranges (determination of the prior distribution) – Table A1,
- Simulation of parameters (N=5000N = 5000 samples) using the Monte Carlo method,
- Simulation of runoff hydrographs from the catchment for rainfall-runoff events, considering uncertainty,

The transformation of the a priori distribution P(θ) to the a posteriori P(θ⁄Q) was performed by the likelihood function L(θ⁄Q) using the equations (1A) (2A):

$$P(Q/\theta) = \frac{L(Q/\theta)P(\theta)}{\int L(Q/\theta)P(\theta)} \tag{1A}$$

where: P(θ) represents the prior coefficient distribution (see Table A1), and L(θ⁄Q) is the likelihood function used to assign weights to the Monte Carlo sample based on model fit to observed basin flows Q and P(θ⁄Q), yielding the posterior distribution of model coefficient θ. The likelihood function used is from Romanowicz and Beven (2006):

$$L(Q/\theta) = exp\left(\frac{\sum_{i=1}^{N}\left(Q_i - \widehat{Q}_i\right)^2}{\kappa \cdot \sigma^2}\right) \tag{2A}$$

where: Q_i and $\widehat{Q}_i$ denote the i -values of these measurements and simulated flows; $\kappa$is a scaling factor for the variance σ^2 of model residual, used to adjust the width of the confidence intervals. The value of κ (the factor used to control the variance of the a posteriori distribution) was determined ensuring, that 95% of measured flow points is enclosed by 95% confidence intervals of the model output (Kiczko et al. 2018).

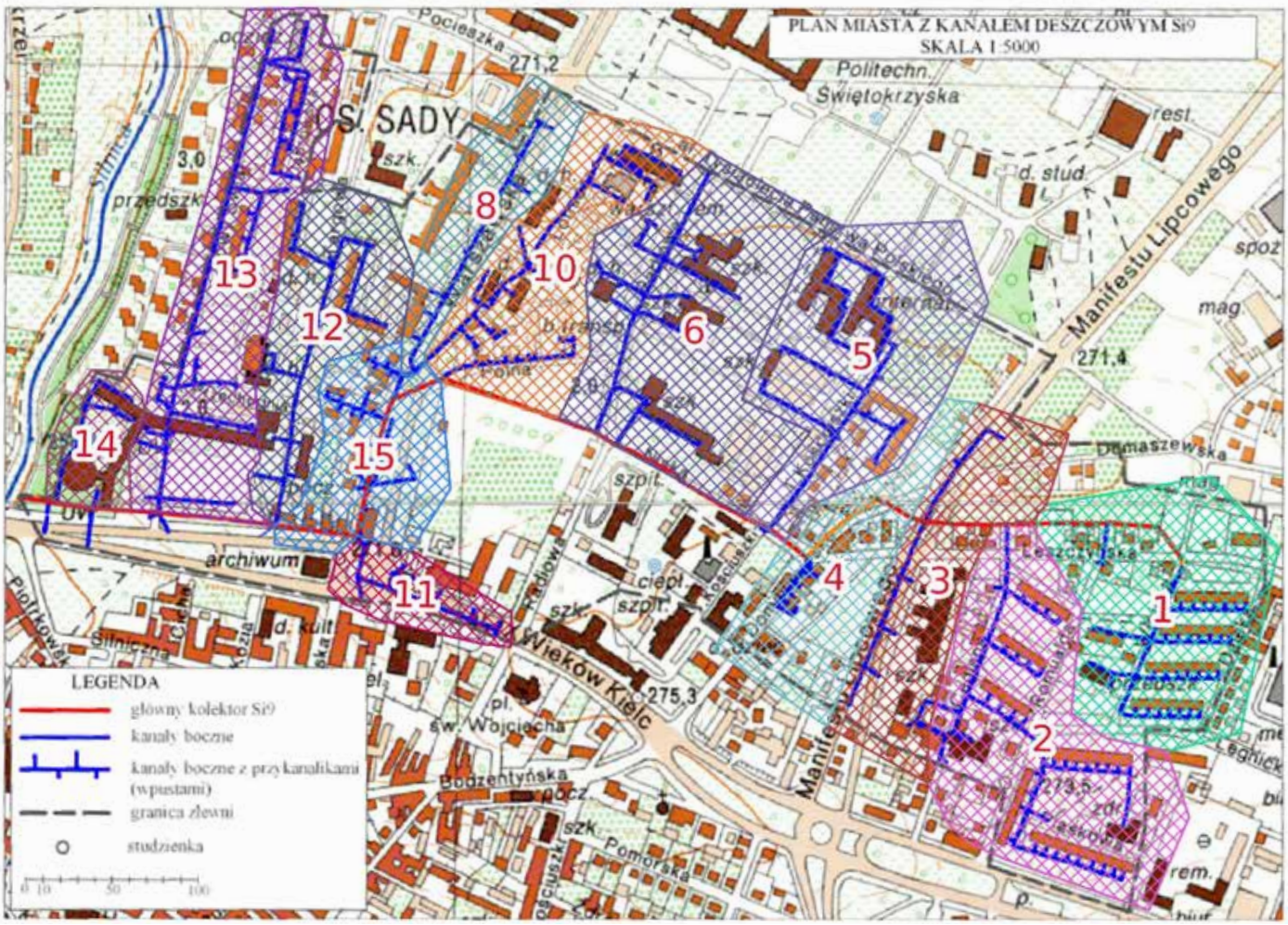

Figure A1. Map of the situational stormwater sewage network

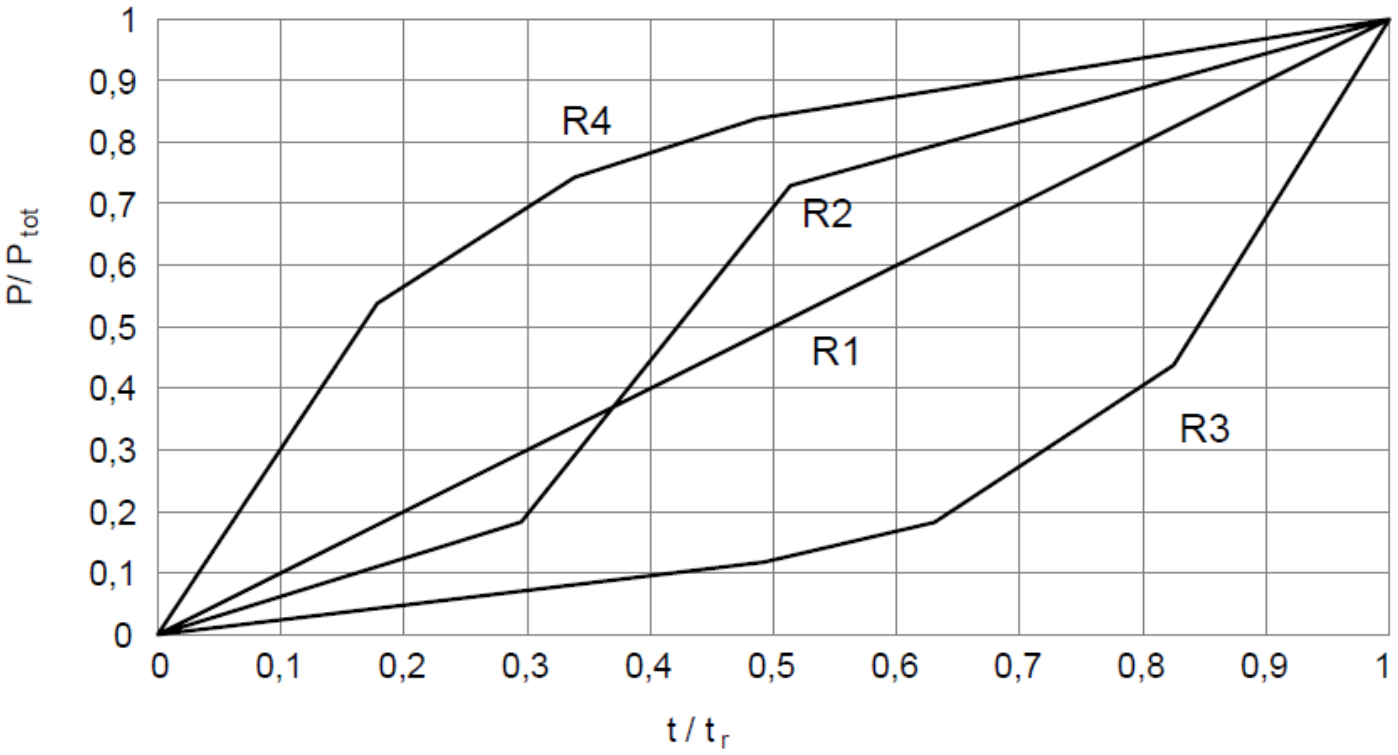

Figure A2. Temporal rainfall distributions (ξ = R1, R2, R3, R4)

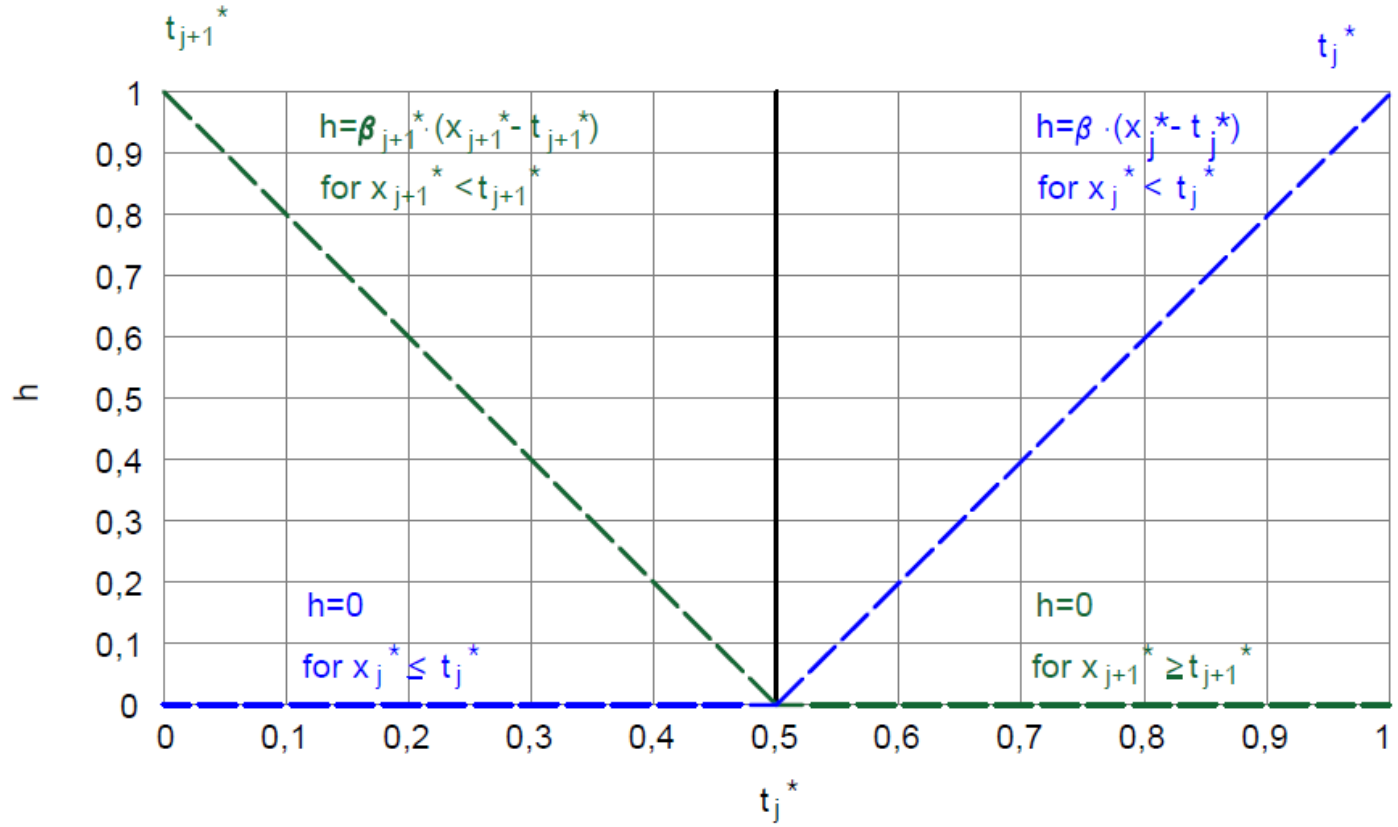

Figure A3. The base function in the MARS model